



UNIL | Université de Lausanne

Unicentre

CH-1015 Lausanne

<http://serval.unil.ch>

Year : 2018

Investigating thermal decay in K-feldspar for the application of IRSL thermochronometry on the Mont Blanc massif

Lambert Renske

Lambert Renske, 2018, Investigating thermal decay in K-feldspar for the application of IRSL thermochronometry on the Mont Blanc massif

Originally published at : Thesis, University of Lausanne

Posted at the University of Lausanne Open Archive <http://serval.unil.ch>

Document URN : urn:nbn:ch:serval-BIB_1D3A3165DE479

Droits d'auteur

L'Université de Lausanne attire expressément l'attention des utilisateurs sur le fait que tous les documents publiés dans l'Archive SERVAL sont protégés par le droit d'auteur, conformément à la loi fédérale sur le droit d'auteur et les droits voisins (LDA). A ce titre, il est indispensable d'obtenir le consentement préalable de l'auteur et/ou de l'éditeur avant toute utilisation d'une oeuvre ou d'une partie d'une oeuvre ne relevant pas d'une utilisation à des fins personnelles au sens de la LDA (art. 19, al. 1 lettre a). A défaut, tout contrevenant s'expose aux sanctions prévues par cette loi. Nous déclinons toute responsabilité en la matière.

Copyright

The University of Lausanne expressly draws the attention of users to the fact that all documents published in the SERVAL Archive are protected by copyright in accordance with federal law on copyright and similar rights (LDA). Accordingly it is indispensable to obtain prior consent from the author and/or publisher before any use of a work or part of a work for purposes other than personal use within the meaning of LDA (art. 19, para. 1 letter a). Failure to do so will expose offenders to the sanctions laid down by this law. We accept no liability in this respect.



University of Lausanne
Faculty of Geosciences and Environment
Institute of Earth Surface Dynamics

Investigating thermal decay in K-feldspar for the application of IRSL thermochronometry on the Mont Blanc massif

Ph.D. thesis

Presented at the
Faculty of Geosciences and Environment, University of Lausanne
by

RENSKE LAMBERT

M.Sc. University of Utrecht (The Netherlands)

JURY

Director:	Prof. Frédéric Herman
Examiner :	Dr. Georgina King
Examiner :	Dr. Pierre Valla
Examiner :	Dr. Sumiko Tsukamoto
Examiner :	Prof. Lukas Baumgartner
President of the jury:	Prof. Michel Jaboyedoff

Lausanne, 2018

IMPRIMATUR

Vu le rapport présenté par le jury d'examen, composé de

Président de la séance publique :	M. le Professeur Michel Jaboyedoff
Président du colloque :	M. le Professeur Michel Jaboyedoff
Directeur de thèse :	M. le Professeur Frédéric Herman
Expert interne :	M. le Professeur Lukas Baumgartner
Expert externe :	M. le Professeur Pierre Valla
Experte externe :	Mme la Docteure Sumiko Tsukamoto
Experte externe :	Mme la Docteure Georgina King

Le Doyen de la Faculté des géosciences et de l'environnement autorise l'impression de la thèse de

Madame Renske LAMBERT

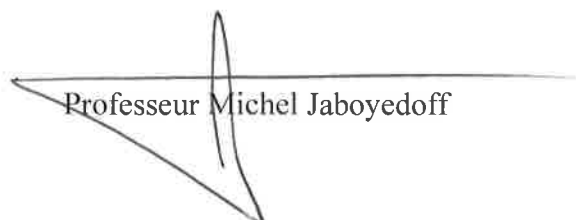
Titulaire d'un
Master en Géologie
de l'Université d'Utrecht

intitulée

Investigating thermal kinetics in K-feldspar for the application of IRSL thermochronometry on the Mont Blanc massif

Lausanne, le 28 août 2018

Pour le Doyen de la Faculté des géosciences et de
l'environnement



Professeur Michel Jaboyedoff



**Investigating thermal decay in K-feldspar for the
application of IRSL thermochronometry
on the Mont Blanc massif**



Renske Lambert

PhD research project

Institute of Earth Surface Dynamics
University of Lausanne

Committee:

Prof. Frédéric Herman (UNIL, thesis director)

Dr. Georgina King (UNIBE)

Dr. Pierre Valla (UNIBE)

Dr. Sumiko Tsukamoto (LIAG)

Prof. Lukas Baumgartner (UNIL)

TABLE OF CONTENTS

TABLE OF CONTENTS	iii
ABSTRACT	vii
RÉSUMÉ	ix
1. INTRODUCTION	1-1
1.1 Landscape evolution in mountainous settings	1-1
1.2 Luminescence thermochronometry	1-2
1.3 Principles of luminescence dating	1-3
1.4 Limitations and challenges	1-5
1.5 Thesis objectives	1-7
1.6 Approach	1-7
1.7 Thesis structure	1-8
References	1-9
2. VALIDATING MULTIPLE FIRST-ORDER KINETIC MODELS FOR FELDSPAR THERMAL DECAY IN LUMINESCENCE THERMOCHRONOMETRY	2-15
<i>Abstract</i>	2-15
2.1 Introduction	2-15
2.2 Models of feldspar charge transfer	2-19
2.2.1 Rate equation for thermochronometry	2-19
2.2.2 Thermal decay models	2-21
2.3 Numerical validation	2-25
2.4 Discussion	2-28
2.5 Conclusions	2-30
Acknowledgements	2-30
References	2-31
Tables	2-36
Appendix - Probability density function of BTS model	2-38
3. TOWARDS OSL-THERMOCHRONOMETRY OF THE MONT BLANC MASSIF: EXPERIMENTAL INVESTIGATIONS INTO CONSTRAINING FELDSPAR THERMAL DECAY	3-39
<i>Abstract</i>	3-39
3.1 Introduction	3-39
3.2 Models	3-40
3.2.1 Trapping and athermal decay	3-41
3.2.2 Thermal decay	3-42

3.2.3	Trap occupancy.....	3-44
3.3	Experimental approach	3-44
3.3.1	Overview of experiments and analyses.....	3-44
3.3.2	Sample preparation and instrumentation.....	3-45
3.3.3	Experimental procedure	3-46
3.3.4	Constraining thermal kinetic parameters.....	3-47
3.4	Results	3-47
3.4.1	Thermal decay, dose response and fading characteristics.....	3-47
3.4.2	Isothermal decay dose dependency.....	3-48
3.4.3	Isothermal decay preheat dependency.....	3-50
3.4.4	Modelling trap occupancy for a linear cooling history.....	3-53
3.5	Discussion	3-54
3.5.1	Dose response and dose dependency isothermal decay	3-54
3.5.2	Distribution of activation energies and preheat dependency isothermal decay.....	3-55
3.6	Conclusions.....	3-56
	Acknowledgements	3-57
	References.....	3-57
	Appendix.....	3-60
A.1	Additional experimental results	3-60
A.2	Kinetic parameters	3-65
4.	RAPID COOLING DURING THE LAST 10 - 100 KA IN THE MONT BLANC MASSIF; INSIGHTS FROM LUMINESCENCE THERMOCHRONOMETRY.....	4-67
	<i>Abstract</i>	4-67
4.1	Introduction.....	4-67
4.2	Geological setting	4-69
4.3	Rate equation for K-feldspar luminescence thermochronometry	4-70
4.4	Analytical procedures	4-72
4.4.1	Sample preparation and instrumentation.....	4-72
4.4.2	Experimental procedure	4-72
4.4.3	Modelling procedure	4-73
4.5	Results	4-75
4.5.1	Laboratory kinetic parameters	4-75
4.5.2	Natural signals and steady state conditions.....	4-78
4.5.3	Apparent steady state temperatures	4-79

4.5.4	Two stage linear cooling histories	4-80
4.5.5	Reconstructed past temperatures along tunnel transect	4-84
4.6	Discussion	4-85
4.6.1	Natural luminescence signal trends	4-85
4.6.2	Thermal history reconstruction	4-86
4.7	Conclusions.....	4-87
	Acknowledgements	4-88
	References	4-88
	Supplementary	4-92
5.	DISCUSSION AND CONCLUSIONS	5-99
5.1	Synthesis.....	5-99
5.2	Implications	5-100
5.3	Perspectives.....	5-102
	References	5-105
6.	ACKNOWLEDGEMENTS.....	6-109
7.	APPENDIX.....	A-111
	Contributions as co-author.....	A-111
	List of publications.....	A-112
	References	A-112
	Multi-OSL-thermochronometry of feldspar	A-113
	Thermoluminescence analysis for particle temperature sensing and thermochronometry: Principles and fundamental challenges	A-138

ABSTRACT

Luminescence thermochronometry is a dating technique, which can be used to constrain the thermal history of a rock over Late-Quaternary timescales (10-100 ka). The method is based on the balance between electron trapping, due to environmental radiation, and temperature-dependent electron detrapping in the crystal structure of minerals such as quartz or feldspar. Based on the net accumulated charge, which can be measured as a luminescence signal and derivation of the associated kinetics, this method enables the thermal history of rocks to be quantitatively investigated. For reliable extrapolation from laboratory to geological timescales, an appropriate model of thermal detrapping is required. However, the understanding of kinetic processes controlling charge transport in feldspar is presently limited. In this thesis, the thermal decay of trapped charge in infra-red (IR) sensitive traps in feldspar was studied and infra-red stimulated luminescence (IRSL) thermochronometry applied to the Mont Blanc massif to constrain its recent cooling history (~100 ka).

Constraining thermal decay of trapped charge in IR sensitive traps in feldspar is essential for thermochronometric studies, but has proven complicated because it is not a simple exponential decay process. Based on the band-tail states model proposed by Li and Li (2013), in this thesis a model with a Gaussian shaped distribution of trap depths, with and without band-tail states, is presented and all three models were validated on samples from a thermal steady-state setting (KTB borehole in Germany; Guralnik et al., 2015). Through experimental investigations the applicability of general order kinetics and three multiple first-order kinetic thermal decay models for feldspar was explored using samples from the Mont Blanc massif (western European Alps). Isothermal decay data following different doses show that the thermal decay process in IR sensitive traps in feldspar is not controlled by the initial concentration of trapped charge, suggesting first-order or low-order kinetic behaviour. The isothermal decay data could be well fitted using a multiple first-order kinetic model consisting of a distribution of thermal lifetimes, following from a distribution of activation energies based on a Gaussian shaped distribution of trap depths. More thermally stable IRSL signals were obtained following higher temperature preheats, which is in agreement with a model based on a distribution of lifetimes.

As luminescence thermochronometry can constrain the recent cooling history (~100 ka) of rocks, it may offer the possibility to quantify changes in geothermal gradient that occur over those timescales. This method was applied to bedrock samples from the Mont Blanc tunnel, for which the temperature has likely fluctuated in response to meteoric fluid infiltration in the last 12 ka. The IRSL₅₀ and post-IR IRSL₂₂₅ signals of K-feldspar extracts were measured and through dosing, fading and isothermal decay

experiments the kinetic parameters that characterize the trapping and detrapping behaviour of charge in IR sensitive traps of feldspar were constrained. By inverting the measured data using the constrained kinetic model and published apatite fission track and (U-Th-[Sm])/He data (Glotzbach et al., 2008), the most probable cooling history of each rock sample for which the final temperature was known was derived. The results suggest cooling rates in the last 100 ka of the order of 0.1 to 0.4 °C/ka. Previous modeling results (Maréchal et al., 1999) suggested significantly higher cooling rates between 0.5 and 2 °C/ka in the last 12 ka. The results imply that feldspar IRSL thermochronometry provides constraints on changes of the geothermal gradient integrated over 100 ka, but it cannot constrain changes at 1-10 ka timescales. Future interpretation of luminescence thermochronometry data should account for changes in the near surface geothermal gradient related to hydrothermal flow. An integrated approach using multiple thermochronometers leads to more comprehensive interpretations of thermal field reconstructions and may provide insights into the general understanding of these systems, applicable in the wider field of luminescence.

RÉSUMÉ

La thermochronométrie par luminescence est une technique de datation qui peut être utilisée pour contraindre l'histoire thermique d'une roche. La méthode est basée sur l'équilibre entre le piégeage d'électrons, dû au rayonnement environnemental, et l'éviction d'électrons en fonction de la température dans la structure cristalline des minéraux tels que le quartz ou le feldspath. Sur la base de la charge nette accumulée, qui peut être mesurée en tant que signal de luminescence et des contraintes obtenues en laboratoire sur la cinétique associée, cette méthode permet d'étudier quantitativement l'histoire thermique des roches. Pour obtenir une extrapolation fiable du laboratoire aux échelles de temps géologiques, un modèle approprié d'éviction thermique est requis. La compréhension des processus cinétiques contrôlant le transport de charge dans le feldspath est toutefois limitée. Dans cette thèse, l'éviction thermique de la charge piégée dans les pièges sensibles au feldspath infrarouge (IR) a été étudiée et la thermochronométrie par luminescence stimulée par infrarouge (IRSL) appliquée au massif du Mont Blanc afin de contraindre son histoire récente de refroidissement (~ 100 ka).

Contraindre l'éviction thermique de la charge piégée dans les pièges sensibles aux infrarouges dans le feldspath est essentiel pour les études thermochronométriques, mais s'est révélée compliquée car il ne s'agit pas d'un simple processus de décroissance exponentielle. Basé sur le modèle des états de 'Band-Tail states' proposé par Li et Li (2013), nous présentons dans cette thèse un modèle avec une distribution gaussienne d'énergie d'activation de pièges et ces modèles ont été validés sur des échantillons d'un régime thermique permanent (forage KTB en Allemagne, Guralnik et al., 2015). Grâce à des études expérimentales, l'applicabilité de la cinétique de l'ordre général et de trois modèles d'éviction thermique cinétique de premier ordre pour le feldspath a été explorée à partir d'échantillons du massif du Mont Blanc (Alpes de l'Ouest). Les données de décroissance isothermale après différentes doses montrent que le processus de décroissance thermique dans les pièges sensibles aux IR dans le feldspath n'est pas contrôlé par la concentration initiale de la charge piégée, suggérant un comportement cinétique de premier ordre ou de faible ordre. Les données de désintégration isotherme pourraient être ajustées avec précision en utilisant un modèle cinétique de premier ordre composé d'une distribution des durées de vie thermiques, à la suite d'une distribution des énergies d'activation basée sur une distribution gaussienne des profondeurs des pièges. Des signaux IRSL plus thermiquement stables ont été obtenus après des préchauffages à température plus élevée, ce qui est en accord avec un modèle de distribution.

La thermochronométrie par luminescence permet de contraindre l'histoire de refroidissement récente (~ 100 ka) des roches, elle offre par conséquent la possibilité de quantifier les changements

du gradient géothermique qui se produisent au cours de ces échelles de temps. Cette méthode a été appliquée à des échantillons de substratum rocheux du tunnel du Mont-Blanc, pour lesquels la température a probablement fluctué en réponse à l'infiltration de liquide au cours des 12 derniers ka. Les signaux IRSL₅₀ et IRSL₂₂₅ post-IR des extraits de feldspath potassique ont été mesurés. Grâce à des expériences de dosage, de décroissance athermale et isothermale, les paramètres cinétiques qui caractérisent le comportement de piégeage et d'éviction de la charge dans les pièges sensibles au IR du feldspath ont été limités. En inversant les données mesurées à l'aide du modèle cinétique contraint et l'histoire de refroidissement la plus probable de chaque échantillon de roche pour lequel la température finale était connue a été dérivée. Les résultats suggèrent des vitesses de refroidissement dans les 100 derniers ka de l'ordre de 0,1 à 0,4 °C/ka. Des résultats de modélisation antérieurs (Maréchal et al., 1999) suggèrent des vitesses de refroidissement significativement plus élevées entre 0,5 et 2 °C/ka au cours des 12 derniers ka. Les résultats impliquent que la thermochronométrie IRSL du feldspath fournit des contraintes sur les changements du gradient géothermique intégrés sur 100 ka, mais elle ne peut pas contraindre les changements à des échelles de temps de 1 à 10 ka. L'interprétation future des données de thermochronométrie par luminescence devrait tenir compte des changements dans le gradient géothermique proche de la surface lié à la circulation hydrothermal. Une approche intégrée utilisant plusieurs thermochronomètres conduit à des interprétations plus complètes des reconstructions de champs thermiques et peut fournir un aperçu de la compréhension générale de ces systèmes, applicable dans le domaine plus large de la luminescence.

1. INTRODUCTION

1.1 Landscape evolution in mountainous settings

The Earth's surface is constantly changing in response to tectonics, climate and earth surface processes. There is an ongoing debate on the underlying roles of these processes and the way they interact to shape topographic relief, depending on the geomorphological setting (Molnar and England, 1990; Whipple et al., 1999; Champagnac et al., 2012). Mountain ranges form as a result of converging plates, causing crustal shortening and thickening, and isostatic response (e.g. Robl et al., 2017). At the same time, erosional processes play a role in shaping the landscape, which may be induced by tectonic processes (rock fracturing or landslides triggered by earthquakes) or climate-driven (Zhang et al., 2001; Molnar et al., 2007). Through precipitation and temperature changes, climate variability impacts hill-slope processes, glacial and fluvial erosion and sediment transport (Braun and Willett, 2013). In turn, erosion may affect tectonics through modifying deformation patterns and the thermal structure of the crust (Whipple, 2009; Champagnac et al., 2012). Climate may also directly influence tectonics by loading or unloading the lithosphere whereas topography affects climate locally up to globally by altering the atmospheric circulation and orographic precipitation (Roe et al., 2002; Herman and Braun, 2006).

As all these processes occur at different timescales and there are various potential feedback mechanisms between them, a palette of methodological approaches and techniques are required to characterize an orogenic setting, decipher the states (transient or steady-state) of the processes involved and understand their relative roles (e.g. Champagnac et al., 2014; Robl et al., 2017). The timing and rates of these processes in relation to their spatial variability provide essential information. A key constraint on changes in the landscape is the quantification of erosion rates. Sedimentary records may provide useful information to this end, but can be difficult to interpret due to overlapping patterns, the Sadler effect (Sadler, 1981), or their absence in mountainous settings (Whipple 2009). Several complementary techniques are available to date bedrock directly, such as surface exposure dating based on cosmogenic isotopes, which can be used to determine erosion rates over hundred to hundred thousand year timescales (Bierman, 1994), or low-temperature thermochronometric methods, by which exhumation rates over timescales of typically one to ten million years can be quantified (Figure 1-1; e.g. Reiners and Brandon, 2006). While these methods provide direct temporal constraints, they are applicable for specific timescales and based on the availability of certain rock minerals. In addition, numerical landscape evolution modelling is a powerful tool to simulate the dynamic interplay between tectonics, climate and surface processes

and to test different hypotheses on feedback mechanisms (e.g. Van der Beek and Braun, 1998; Braun and Willett, 2013).

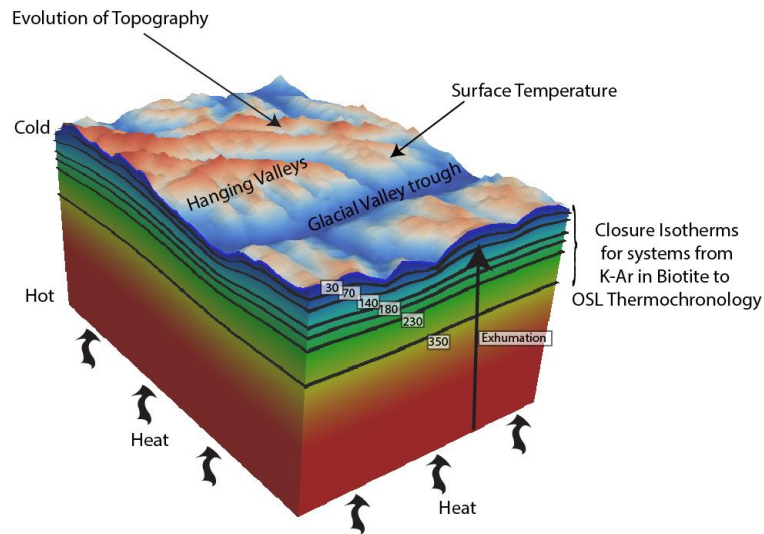


Fig. 1-1: Thermal field of mountainous setting, indicating closure isotherms for different thermochronometric systems (Braun et al, 2012).

1.2 Luminescence thermochronometry

Thermochronometric systems may be used to determine rock cooling rates, which can be converted into exhumation rates based on the local geothermal field (Figure 1-1). A wide range of thermochronometers are available that can provide information on different time-temperature windows, based on closure isotherms corresponding to different minerals and radioactive decay systems (Figure 1-2). Recently, there has been growing interest in very low temperature systems, which can be used to investigate changes in the near-surface geothermal gradient, i.e. a short timescale (10-100 ka) that corresponds to Late-Quaternary climate cycles. Over the past decade, luminescence dating, a well-known technique to date sediment burial and heating, has been developed as a thermochronometer (Herman et al, 2010; Li and Li, 2012; Guralnik et al, 2013, 2015a; King et al, 2016a; Herman and King, 2018; Biswas et al., 2018). Luminescence thermochronometry is based on trapping of electrons in defects of a mineral and may increase the temporal resolution of thermochronometric data due to the relatively low temperature window of ~30-100 °C at which the accumulation of electrons starts (Figure 1-2). A limitation is that the number of traps is finite and may all become filled, after which the thermal history is no longer recorded. This contrasts with more commonly used thermochronometers, which are based on the accumulation of daughter isotopes and which do not experience a saturation limit. The method is thus typically suitable only in rapidly exhuming settings or subsurface studies (i.e. tunnels and boreholes; Wu et al., 2015; King et al., 2016a). Furthermore, as the temperature range that this method resolves constrains changes in the

geothermal gradient close to the Earth's surface, consideration must be made that rock cooling in mountainous settings may reflect a combination of processes, such as exhumation due to surface uplift and erosion, changes in surface temperature, effects of hydrothermal flow and meteoric fluid infiltration (Figure 1-1; Whipp and Ehlers, 2007; Cox et al., 2015). This provides both opportunities and challenges which will be touched upon in this thesis.

Luminescence thermochronometry has demonstrated its potential in various studies, covering a range of geological settings. It was applied to samples from the Southern Alps of New Zealand, a tectonically active mountain belt which has experienced glacial cycles that were initiated in the Pliocene (~2.5 Ma; Suggate 1990; Herman et al., 2010). The results of Herman et al. (2010) suggest that tectonics and not climate controls the erosion rates and amplitude of relief in this setting. A validation study was done on samples from the KTB-borehole in Germany for which thermal steady-state conditions were recovered based on luminescence thermochronometry (Guralnik et al., 2015b). Application of the method on samples from the Namche Barwa massif in the eastern Himalaya yielded cooling histories and exhumation rates at sub-Quaternary timescales, providing insights in the role of erosion and tectonics (King et al., 2016b; Biswas et al., 2018).

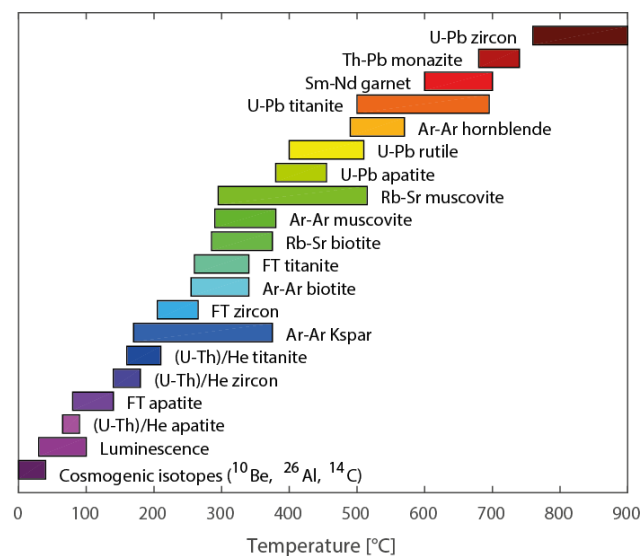


Fig. 1-2: Temperature range of thermochronometers after Pollard, 2002 (adapted from P. Fitzgerald, S. Baldwin, G. Gehrels, P. Reiners, and M. Ducea).

1.3 Principles of luminescence dating

Luminescence dating is based on measuring the light signal from electrons trapped in defects or impurities in the crystal lattice of a mineral (Aitken, 1985; Huntley et al., 1985). Electrons are trapped due to in situ radioactive decay of surrounding material (Figure 1-3 A) and detrapped due to energy

from heat or light. When electrons are detrapped, they recombine with a hole at a recombination centre, and release energy, some of which is in the form of light (Figure 1-3 B). Analyzing a sample in a laboratory is done by detrapping the trapped charges through stimulation by heat and/or light, and detection of the luminescence signal at a different wavelength. The intensity of the luminescence signal is assumed to be proportional to the number of trapped charges. Minerals have limited storage capacity; eventually all traps are filled and the crystal becomes saturated. In a mineral such as feldspar, electrons can also be detrapped athermally (Wintle, 1973). This phenomenon can be explained by quantum mechanical tunneling, by which direct recombination of an electron with a hole occurs without requiring activation energy (Huntley and Lian, 2006; Visocekas, 2002). The different detrapping mechanisms in feldspar are described by Jain and Ankjærgaard (2011) using an energy band model. However, due to the complexity of the crystal structure and charge transport, uncertainties remain regarding these processes.

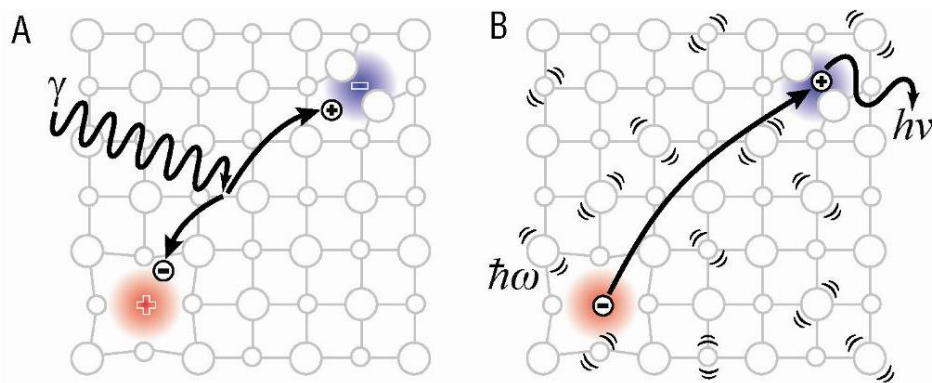


Fig. 1-3: Trapping and detrapping of charges by Guralnik (2014). (A) Excited by ionizing radiation electrons and holes may move through the crystal lattice and become trapped in crystal defects or impurities. (B) Through stimulation by heat and/or light electrons may receive sufficient energy to escape their trap and recombine with a hole, thereby releasing energy in the form of light.

When rocks are exhumed along a geothermal gradient, electrons are continuously trapped through exposure to the decay of radioactive elements in the surrounding rock. At high temperatures thermal detrapping is dominant and there is no accumulation of charge. At lower temperatures ranging from ~30-100 °C net accumulation begins to outweigh net loss due to reduced thermal detrapping: this is how the thermal history (of the last phase) of exhumation can be recorded (Li and Li, 2012; Guralnik et al., 2013). With continuous filling of traps, the number of available traps decreases, which leads to a reduction in the rate of trap filling. When all available traps have been occupied, the crystal has become saturated. Further irradiation does not result in further accumulation of electrons in the crystal and the resulting luminescence signal only gives an indication of a minimum age for the start of signal accumulation or maximum cooling rate (e.g. Guralnik et al., 2013). As rocks cool to temperatures where thermal detrapping no longer plays a dominant role, feldspar crystals may reach

a steady state where no further signal builds up as the rate at which charge recombines due to thermal and athermal detrapping equals the rate at which charge traps due to in situ radioactive decay. The crystal is said to be in field saturation, while not all traps are filled (e.g. Valla et al., 2016).

To derive a rock sample's cooling history, quartz and/or feldspar crystals are extracted and the natural luminescence signal is measured, which is the luminescence signal corresponding to the net trapped charge accumulated in nature. This can be done through several techniques: thermoluminescence (TL) is a method by which stimulation occurs through heat and optically stimulated luminescence (OSL) uses light to stimulate the trapped charges; this term is usually used when it is applied to quartz, whereas infrared stimulated luminescence (IRSL) uses light to stimulate trapped charges in feldspar (Aitken 1985; Aitken 1998). The different stimulation methods assess specific trapped charge populations, each with its own (a-)thermal stability (e.g. Johnson, 1966; Prokein and Wagner, 1994; Chen and McKeever, 1997; Bailey, 2001; Li and Li, 2011a; Brown and Rhodes, 2017). Subsequently, the rates of the different processes involved, i.e. trapping, thermal and athermal detrapping, are determined through mimicking these processes in experiments. The rate of trapping is derived in an experiment where the luminescence signal is measured in response to different radioactive doses (Murray and Wintle, 2000; Wallinga et al., 2000). To investigate the rate of thermal electron loss, samples are given a dose in the laboratory to fill the traps and then held at a constant temperature (Murray and Wintle, 1999). Finally, to constrain athermal loss, samples are given a dose and held at room temperature (e.g. Huntley and Lamothe, 2001).

1.4 Limitations and challenges

One of the major limitations of luminescence dating applied in thermochronology is the limited time scale for which the technique is applicable associated with saturation. In aiming to extend the age range, both the choice of mineral and the stability of the traps that are accessed need to be carefully considered. Feldspar is known to have a further extended age range than quartz of possibly up to 1 Myr, because it saturates at higher total radiation doses (Li and Tso, 1997; Thiel et al., 2011b). Although athermal decay complicates the use of this mineral, there are feldspar signals that show less fading, such as post-IR IRSL signals (Thomsen et al., 2008; Buylaert et al., 2009; Thiel et al., 2011a; Thomsen et al, 2011). These are IRSL signals measured at elevated temperature following IR stimulation at 50 °C (post-IR IRSL) and have been shown to be much more athermally stable than the low temperature IRSL signal. Methods have been proposed to take fading into account and correct for it (Kars et al., 2008; Huntley and Lamothe, 2001; Lamothe et al., 2003), although, through necessity these methods are based on the assumption that the fading rate on a laboratory timescale can be extrapolated to geological timescales.

Understanding kinetic properties of traps plays a key role in luminescence dating as target traps should be stable over the time scale of interest (Huntley and Lamothe, 2001; Prokein and Wagner, 1994). In the TL and OSL signal of quartz different components convey information on the different stages of the thermal history (Bailey et al., 1997; Bailey, 2004; Murray et al., 2009; Qin et al., 2015). However, due to its low luminescence sensitivity, the ubiquitous lack of the “fast component” in bedrock and signal contamination due to mineral inclusions (e.g. feldspar, zircon), quartz has not proven to be ideal for OSL thermochronometry (Herman et al., 2010; Wintle and Murray, 2006; Jeong and Choi, 2012; Guralnik et al., 2015b; Valla et al., 2016). The advantage of TL is that it may be possible to access multiple traps with different thermal stabilities, which could reveal more cooling stages, thereby giving more constraints to the exhumation history (Tang and Li, 2015; Brown et al., 2017; Tang and Li, 2017; Biswas et al., 2018).

Feldspar has several advantages over quartz in having a higher luminescence sensitivity (e.g. King et al., 2014), higher storage capacity and negligible quartz signal contamination (e.g. Sohpati et al., 2013). Although uncertainties remain regarding the kinetic processes in feldspar related to IR sensitive traps, measurement protocols are available as IRSL has been successfully applied in sedimentary dating applications (e.g. Buylaert et al., 2012). IRSL on feldspar is therefore a suitable candidate for luminescence thermochronometric applications and through different stimulations methods multiple signals can be assessed (Li and Li, 2011b), providing multiple constraints on a rock's cooling path (King et al., 2016c). A cooling history is derived by inverse modelling, i.e. the evolution of trapped charge is simulated in response to a range of possible cooling histories and the modelled final trapped charge concentrations are compared to the natural trapped charge concentration, derived from the natural luminescence signal. For this, the kinetic parameters describing the rates of trapping, thermal and athermal detrapping need to be accurately constrained for each sample. High-quality data sets thus need to be obtained through appropriate experimental protocols and validation of models describing the physical processes.

One critical aspect for the interpretation of luminescence data for application studies is the need for a robust kinetic model. Such a model enables the extrapolation of laboratory data (from seconds to days) to geological timescales (more than tens of thousands of years). A lot of research has been devoted to understanding the kinetics of feldspar (Jain et al., 2012; Li and Li, 2013; Guralnik et al., 2015b; Jain et al., 2015), but there remain some challenges. IRSL thermal decay curves deviate from simple exponential decay (e.g. Grün, 1994; Guralnik et al., 2015a; Guralnik et al., 2015b), which has been explained through various mechanisms. These include retrapping, variable distance-dependent recombination probabilities or other processes that can be described by general order kinetics behaviour (Guralnik et al., 2015b). Alternatively, a first-order kinetic model assuming a distribution of

activation energies, and thus thermal lifetimes, for a population of trapped electrons has been proposed (Poolton et al., 2002; Poolton et al., 2009; Li and Li, 2013). Localized transitions may also provide a distribution of activation energies, determined by trap depth relative to the excited state of the trap and a distribution of tunnelling distances (Jain et al., 2012; 2015). All these mechanisms may play a role in the process of thermal decay.

1.5 Thesis objectives

The general aim of this thesis is to develop and apply luminescence dating as a tool to track changes in the near surface geothermal gradient. This has been addressed by choosing a well-constrained, actively eroding geologic-geomorphic field setting, the Mont Blanc massif, and investigating different luminescence methods applied to K-feldspar aliquots, i.e. IRSL experimental protocols. The models currently proposed for interpretation of analyses have been tested and developed relative to the luminescence measurements made. Finally, the acquired IRSL data was interpreted through comparison with the results of other modelling studies in this setting.

The thesis addresses the following objectives:

- Constrain the thermal kinetics in K-feldspar through physically-based and experimentally verified modelling of the thermal decay mechanisms in K-feldspar for application in luminescence thermochronometry;
- Apply luminescence thermochronometry on the Mont Blanc massif to constrain its recent thermal history (over the last ~100 ka) and use this to improve the temporal resolution of the geologic-geomorphic evolution of the Mont Blanc massif during the Quaternary.

1.6 Approach

The thesis uses a case study approach to address the objectives of the research project: the Mont Blanc massif in the European Alps. This is a suitable site to further develop this relatively new method in several ways. Thermochronometric and modelling studies have shown that there has been a strong increase in exhumation over the last 2 Ma in this part of the Alps, which may be related to enhanced glacial erosion in response to surface uplift (Glotzbach et al, 2008; Vernon et al., 2008; Willett 2010; Glotzbach et al, 2011; Egli and Mancktelow, 2013; Fox et al, 2015). Moreover, samples could be studied from the Mont Blanc tunnel (MBT; provided by the Cantonal Museum of Geology in Lausanne), for which there is available temperature data measured when the tunnel was constructed (in 1960s). Both the available apatite fission-track and (U-Th-Sm)/He data (Glotzbach et al, 2008) and the rock temperature data provide additional thermal constraints. The possibility to take samples

from a tunnel (i.e. with relatively high ambient temperatures) in a relatively fast exhuming setting is favourable to avoid all samples being saturated. Furthermore, since the massif consists mainly of granite and schist/gneiss (Figure 1-4), abundant K-feldspar is available in the rock samples, which could be extracted to measure the trapped charge in the infra-red (IR) sensitive traps of this mineral. We stimulated using infra-red at 50 °C (IRSL₅₀) and subsequently infra-red at 225 °C (post-IR IRSL₂₂₅) (Thomsen et al., 2008). These two luminescence signals each have specific thermal and athermal characteristics, resulting in two constraints on the thermal history of each sample (Qin et al., 2015; King et al., 2016c).

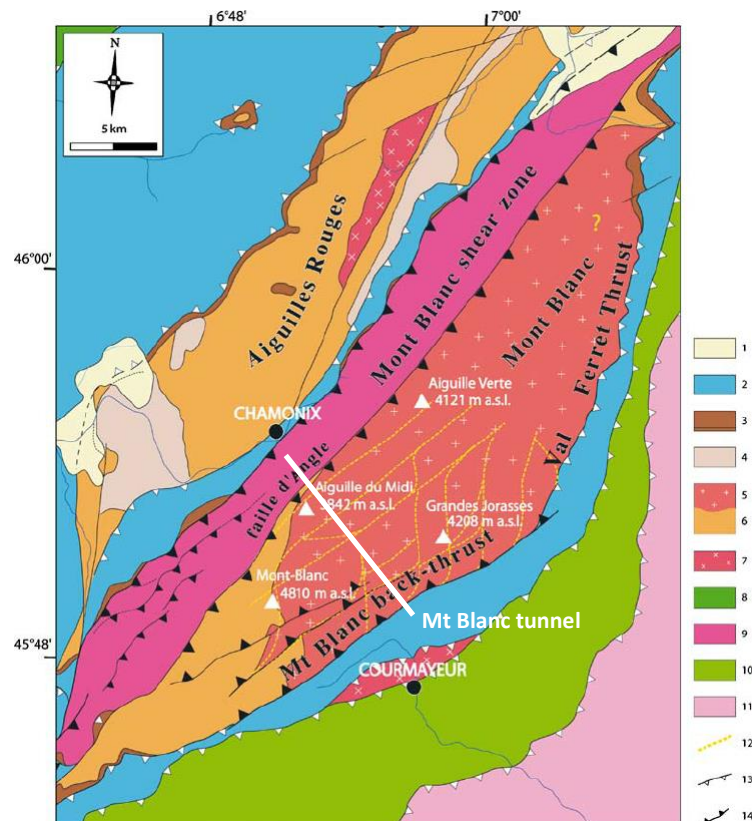


Fig. 1-4: Geological map of the Mont Blanc area (Ravel et al., 2010) and location of Mont Blanc tunnel. 1 Quaternary, 2 Dauphinois and Helvetic Mesozoic sediments, 3 Triassic, 4 carboniferous, 5 Mont Blanc granite, 6 Variscan metamorphic rocks (gneiss), 7 undifferentiated granites, 8 Penninic klippe, 9 Mont Blanc shear zone (gneiss), 10 Versoyen + Valais, 11 internal zones, 12 mapped shear zone network, 13 thrust, 14 late reverse fault.

1.7 Thesis structure

In [Chapter 2](#), we propose a multiple first-order thermal decay model based on a Gaussian distribution of trap depths and validate it on published isothermal decay data from the KTB borehole (Guralnik et al, 2015a). The development of this model type resulted from evaluation of two existing models on the MBT samples: a general order kinetics (Guralnik et al, 2015b) and band-tail states model (Li and

Li, 2013). This was done based on physical considerations and experimental verification, which are presented in [Chapter 3](#). An interpretation of the IRSL data on the samples of the Mont Blanc massif is given in [Chapter 4](#). Finally, a synthesis of the different studies and their implications are discussed in [Chapter 5](#), as well as an outlook for further research in this field. An overview of publications that I have contributed to as co-author is given in the Supplementary.

References

- Aitken, M.J., 1985. Thermoluminescence dating. Academic press.
- Aitken, M.J., 1998. An introduction to optical dating: the dating of Quaternary sediments by the use of photon-stimulated luminescence. Oxford University Press.
- Bailey, R., 2001. Towards a general kinetic model for optically and thermally stimulated luminescence of quartz. *Radiation Measurements* 33, 17-45.
- Bailey, R., 2004. Paper I—simulation of dose absorption in quartz over geological timescales and its implications for the precision and accuracy of optical dating. *Radiation Measurements* 38, 299-310.
- Bailey, R., Smith, B., Rhodes, E., 1997. Partial bleaching and the decay form characteristics of quartz OSL. *Radiation Measurements* 27, 123-136.
- Bierman, P.R., 1994. Using in situ produced cosmogenic isotopes to estimate rates of landscape evolution: A review from the geomorphic perspective. *Journal of Geophysical Research: Solid Earth* 99, 13885-13896.
- Biswas, R., Herman, F., King, G., Braun, J., 2018. Thermoluminescence of feldspar as a multi-thermochronometer to constrain the temporal variation of rock exhumation in the recent past. *Earth and Planetary Science Letters* 495, 56-68.
- Braun, J., Van der Beek, P., Batt, G., 2006. Quantitative thermochronology: numerical methods for the interpretation of thermochronological data. Cambridge University Press.
- Braun, J., Willett, S.D., 2013. A very efficient $O(n)$, implicit and parallel method to solve the stream power equation governing fluvial incision and landscape evolution. *Geomorphology* 180, 170-179.
- Brown, N., Rhodes, E., 2017. Thermoluminescence measurements of trap depth in alkali feldspars extracted from bedrock samples. *Radiation Measurements* 96, 53-61.
- Brown, N., Rhodes, E., Harrison, T.M., 2017. Using thermoluminescence signals from feldspars for low-temperature thermochronology. *Quaternary Geochronology* 42, 31-41.
- Buylaert, J.-P., Jain, M., Murray, A.S., Thomsen, K.J., Thiel, C., Sohbaty, R., 2012. A robust feldspar luminescence dating method for Middle and Late Pleistocene sediments. *Boreas* 41, 435-451.
- Buylaert, J.-P., Murray, A., Thomsen, K.J., Jain, M., 2009. Testing the potential of an elevated temperature IRSL signal from K-feldspar. *Radiation Measurements* 44, 560-565.

- Champagnac, J.-D., Valla, P.G., Herman, F., 2014. Late-Cenozoic relief evolution under evolving climate: A review. *Tectonophysics* 614, 44-65.
- Champagnac, J.D., Molnar, P., Sue, C., Herman, F., 2012. Tectonics, climate, and mountain topography. *Journal of Geophysical Research: Solid Earth (1978–2012)* 117.
- Chen, R., McKeever, S.W., 1997. *Theory of thermoluminescence and related phenomena*. World Scientific.
- Cox, S.C., Menzies, C.D., Sutherland, R., Denys, P.H., Chamberlain, C., Teagle, D.A., 2015. Changes in hot spring temperature and hydrogeology of the Alpine Fault hanging wall, New Zealand, induced by distal South Island earthquakes. *Geofluids* 15, 216-239.
- Egli, D., Mancktelow, N., 2013. The structural history of the Mont Blanc massif with regard to models for its recent exhumation. *Swiss journal of geosciences* 106, 469-489.
- Fox, M., Herman, F., Kissling, E., Willett, S.D., 2015. Rapid exhumation in the Western Alps driven by slab detachment and glacial erosion. *Geology* 43, 379-382.
- Glotzbach, C., Reinecker, J., Danišík, M., Rahn, M., Frisch, W., Spiegel, C., 2008. Neogene exhumation history of the Mont Blanc massif, western Alps. *Tectonics* 27, n/a-n/a.
- Glotzbach, C., van der Beek, P.A., Spiegel, C., 2011. Episodic exhumation and relief growth in the Mont Blanc massif, Western Alps from numerical modelling of thermochronology data. *Earth and Planetary Science Letters* 304, 417-430.
- Guralnik, B., 2014. *Low-temperature optically stimulated luminescence thermochronometry: development and applications*. ETH Zürich.
- Guralnik, B., Jain, M., Herman, F., Ankjærgaard, C., Murray, A.S., Valla, P.G., Preusser, F., King, G.E., Chen, R., Lowick, S.E., 2015a. OSL-thermochronometry of feldspar from the KTB borehole, Germany. *Earth and Planetary Science Letters* 423, 232-243.
- Guralnik, B., Jain, M., Herman, F., Paris, R.B., Harrison, T.M., Murray, A.S., Valla, P.G., Rhodes, E.J., 2013. Effective closure temperature in leaky and/or saturating thermochronometers. *Earth and Planetary Science Letters* 384, 209-218.
- Guralnik, B., Li, B., Jain, M., Chen, R., Paris, R.B., Murray, A.S., Li, S.-H., Pagonis, V., Valla, P.G., Herman, F., 2015b. Radiation-induced growth and isothermal decay of infrared-stimulated luminescence from feldspar. *Radiation Measurements* 81, 224-231.
- Herman, F., Braun, J., 2006. Fluvial response to horizontal shortening and glaciations: A study in the Southern Alps of New Zealand. *Journal of Geophysical Research: Earth Surface* 111.
- Herman F., King G.E., 2018. *Luminescence Thermochronometry: Investigating the Link between Mountain Erosion, Tectonics and Climate*. *Elements: An International Magazine of Mineralogy, Geochemistry, and Petrology* 14, 33-38.
- Herman, F., Rhodes, E.J., Braun, J., Heiniger, L., 2010. Uniform erosion rates and relief amplitude during glacial cycles in the Southern Alps of New Zealand, as revealed from OSL-thermochronology. *Earth and Planetary Science Letters* 297, 183-189.
- Huntley, D., Lian, O.B., 2006. Some observations on tunnelling of trapped electrons in feldspars and their implications for optical dating. *Quaternary Science Reviews* 25, 2503-2512.

- Huntley, D.J., Godfrey-Smith, D.I., Thewalt, M.L., 1985. Optical dating of sediments.
- Huntley, D.J., Lamothe, M., 2001. Ubiquity of anomalous fading in K-feldspars and the measurement and correction for it in optical dating. *Canadian Journal of Earth Sciences* 38, 1093-1106.
- Jain, M., Ankjærgaard, C., 2011. Towards a non-fading signal in feldspar: insight into charge transport and tunnelling from time-resolved optically stimulated luminescence. *Radiation Measurements* 46, 292-309.
- Jain, M., Guralnik, B., Andersen, M.T., 2012. Stimulated luminescence emission from localized recombination in randomly distributed defects. *Journal of Physics: Condensed Matter* 24, 385402.
- Jain, M., Sohpati, R., Guralnik, B., Murray, A. S., Kook, M., Lapp, T., Buylaert, J. P., 2015. Kinetics of infrared stimulated luminescence from feldspars. *Radiation Measurements* 81, 242-250.
- Jeong, G.Y., Choi, J.-H., 2012. Variations in quartz OSL components with lithology, weathering and transportation. *Quaternary Geochronology* 10, 320-326.
- Johnson, N.M., 1966. Geothermometry from the thermoluminescence of contact-metamorphosed limestone. *The Journal of Geology* 74, 607-619.
- Kars, R., Wallinga, J., Cohen, K., 2008. A new approach towards anomalous fading correction for feldspar IRSL dating—tests on samples in field saturation. *Radiation Measurements* 43, 786-790.
- King, G.E., Guralnik, B., Valla, P.G., Herman, F., 2016a. Trapped-charge thermochronometry and thermometry: A status review. *Chemical Geology* 446, 3-17.
- King, G.E., Herman, F., Guralnik, B., 2016b. Northward migration of the eastern Himalayan syntaxis revealed by OSL thermochronometry. *Science* 353, 800-804.
- King, G.E., Herman, F., Lambert, R., Valla, P., Guralnik, B., 2016c. Multi-OSL-thermochronometry of feldspar. *Quaternary Geochronology* 33, 76-87.
- King, G.E., Robinson, R.A.J., Finch, A.A., 2014. Towards successful OSL sampling strategies in glacial environments: deciphering the influence of depositional processes on bleaching of modern glacial sediments from Jostedal, Southern Norway. *Quaternary Science Reviews* 89, 94-107.
- Lamothe, M., Auclair, M., Hamzaoui, C., Huot, S., 2003. Towards a prediction of long-term anomalous fading of feldspar IRSL. *Radiation Measurements* 37, 493-498.
- Li, B., Li, S.-H., 2011a. Luminescence dating of K-feldspar from sediments: a protocol without anomalous fading correction. *Quaternary Geochronology* 6, 468-479.
- Li, B., Li, S.-H., 2011b. Thermal stability of infrared stimulated luminescence of sedimentary K-feldspar. *Radiation Measurements* 46, 29-36.
- Li, B., Li, S.-H., 2012. Determining the cooling age using luminescence-thermochronology. *Tectonophysics* 580, 242-248.
- Li, B., Li, S.-H., 2013. The effect of band-tail states on the thermal stability of the infrared stimulated luminescence from K-feldspar. *Journal of Luminescence* 136, 5-10.
- Li, S.-H., Tso, M.-Y.W., 1997. Lifetime determination of OSL signals from potassium feldspar. *Radiation Measurements* 27, 119-121.

- Molnar, P., Anderson, R.S., Anderson, S.P., 2007. Tectonics, fracturing of rock, and erosion. *Journal of Geophysical Research: Earth Surface* 112.
- Molnar, P., England, P., 1990. Late Cenozoic uplift of mountain ranges and global climate change: chicken or egg? *Nature* 346, 29-34.
- Murray, A., Buylaert, J.-P., Thomsen, K.J., Jain, M., 2009. The effect of preheating on the IRSL signal from feldspar. *Radiation Measurements* 44, 554-559.
- Murray, A., Wintle, A., 1999. Isothermal decay of optically stimulated luminescence in quartz. *Radiation Measurements* 30, 119-125.
- Murray, A., Wintle, A., 2000. Application of the single-aliquot regenerative-dose protocol to the 375 C quartz TL signal. *Radiation Measurements* 32, 579-583.
- Poolton, N., Kars, R., Wallinga, J., Bos, A., 2009. Direct evidence for the participation of band-tails and excited-state tunnelling in the luminescence of irradiated feldspars. *Journal of Physics: Condensed Matter* 21, 485505.
- Poolton, N., Ozanyan, K., Wallinga, J., Murray, A., Bøtter-Jensen, L., 2002. Electrons in feldspar II: a consideration of the influence of conduction band-tail states on luminescence processes. *Physics and Chemistry of Minerals* 29, 217-225.
- Prokein, J., Wagner, G.A., 1994. Analysis of thermoluminescent glow peaks in quartz derived from the KTB-drill hole. *Radiation measurements* 23, 85-94.
- Qin, J., Chen, J., Valla, P.G., Herman, F., Li, K., 2015. Estimating rock cooling rates by using multiple luminescence thermochronometers. *Radiation Measurements* 79, 13-18.
- Ravanel, L., Allignol, F., Deline, P., Gruber, S., Ravello, M., 2010. Rock falls in the Mont Blanc Massif in 2007 and 2008. *Landslides* 7, 493-501.
- Reiners, P.W., Brandon, M.T., 2006. Using thermochronology to understand orogenic erosion. *Annu. Rev. Earth Planet. Sci.* 34, 419-466.
- Robl, J., Hergarten, S., Prasicek, G., 2017. The topographic state of fluvially conditioned mountain ranges. *Earth-Science Reviews* 168, 190-217.
- Roe, G.H., Montgomery, D.R., Hallet, B., 2002. Effects of orographic precipitation variations on the concavity of steady-state river profiles. *Geology* 30, 143-146.
- Sadler, P.M., 1981. Sediment accumulation rates and the completeness of stratigraphic sections. *The Journal of Geology* 89, 569-584.
- Sohbati, R., Murray, A.S., Chapot, M.S., Jain, M., Pederson, J., 2012. Optically stimulated luminescence (OSL) as a chronometer for surface exposure dating. *Journal of Geophysical Research* 117.
- Suggate, R., 1990. Late pliocene and quaternary glaciations of New Zealand. *Quaternary science reviews* 9, 175-197.
- Tang, S.-L., Li, S.-H., 2015. Low temperature thermochronology using thermoluminescence signals from quartz. *Radiation measurements* 81, 92-97.

- Tang, S.-L., Li, S.-H., 2017. Low temperature thermochronology using thermoluminescence signals from K-feldspar. *Geochronometria* 44, 112-120.
- Thiel, C., Buylaert, J.-P., Murray, A., Terhorst, B., Hofer, I., Tsukamoto, S., Frechen, M., 2011a. Luminescence dating of the Stratzing loess profile (Austria) – Testing the potential of an elevated temperature post-IR IRSL protocol. *Quaternary International* 234, 23-31.
- Thiel, C., Buylaert, J.-P., Murray, A.S., Tsukamoto, S., 2011b. On the applicability of post-IR IRSL dating to Japanese loess. *Geochronometria* 38, 369.
- Thomsen, K.J., Murray, A.S., Jain, M., 2011. Stability of IRSL signals from sedimentary K-feldspar samples. *Geochronometria* 38, 1-13.
- Thomsen, K.J., Murray, A.S., Jain, M., Bøtter-Jensen, L., 2008. Laboratory fading rates of various luminescence signals from feldspar-rich sediment extracts. *Radiation Measurements* 43, 1474-1486.
- Valla, P.G., Lowick, S.E., Herman, F., Champagnac, J.-D., Steer, P., Guralnik, B., 2016. Exploring IRSL 50 fading variability in bedrock feldspars and implications for OSL thermochronometry. *Quaternary Geochronology* 36, 55-66.
- Van de Beek, P., Braun, J., 1998. Numerical modelling of landscape evolution on geological time-scales: A parameter analysis and comparison with the south-eastern highlands of Australia. *Basin Research* 10, 49-68.
- Vernon, A.J., van der Beek, P.A., Sinclair, H.D., Rahn, M.K., 2008. Increase in late Neogene denudation of the European Alps confirmed by analysis of a fission-track thermochronology database. *Earth and Planetary Science Letters* 270, 316-329.
- Visocekas, R., 2002. Tunnelling in Afterglow: Its coexistence and interweaving with thermally stimulated luminescence. *Radiation protection dosimetry* 100, 45-53.
- Wallinga, J., Murray, A., Wintle, A., 2000. The single-aliquot regenerative-dose (SAR) protocol applied to coarse-grain feldspar. *Radiation Measurements* 32, 529-533.
- Whipp, D.M., Ehlers, T.A., 2007. Influence of groundwater flow on thermochronometer-derived exhumation rates in the central Nepalese Himalaya. *Geology* 35, 851-854.
- Whipple, K.X., 2009. The influence of climate on the tectonic evolution of mountain belts. *Nature Geoscience* 2, 97-104.
- Whipple, K.X., Kirby, E., Brocklehurst, S.H., 1999. Geomorphic limits to climate-induced increases in topographic relief. *Nature* 401, 39.
- Willett, S.D., 2010. Late Neogene Erosion of the Alps: A Climate Driver? *Annual Review of Earth and Planetary Sciences* 38, 411-437.
- Wintle, A.G., 1973. Anomalous fading of thermo-luminescence in mineral samples. *Nature* 245, 143-144.
- Wintle, A.G., Murray, A.S., 2006. A review of quartz optically stimulated luminescence characteristics and their relevance in single-aliquot regeneration dating protocols. *Radiation Measurements* 41, 369-391.

Wu, T.-S., Jain, M., Guralnik, B., Murray, A.S., Chen, Y.-G., 2015. Luminescence characteristics of quartz from Hsuehshan Range (Central Taiwan) and implications for thermochronometry. *Radiation Measurements* 81, 104-109.

Zhang, P., Molnar, P., Downs, W.R., 2001. Increased sedimentation rates and grain sizes 2–4 Myr ago due to the influence of climate change on erosion rates. *Nature* 410, 891-897.

2. VALIDATING MULTIPLE FIRST-ORDER KINETIC MODELS FOR FELDSPAR THERMAL DECAY IN LUMINESCENCE THERMOCHRONOMETRY

Abstract

Luminescence thermochronometry is based on the balance between electron trapping due to environmental radiation and temperature-dependent electron detrapping in certain minerals, mainly quartz and feldspar. Based on the acquired luminescence signal and derivation of the associated kinetics, this method enables the thermal history of rocks to be quantitatively constrained. For reliable extrapolation from laboratory to geological timescales, an appropriate model of thermal detrapping is required. However, the kinetic processes controlling charge transport in feldspar remain a subject of discussion. A range of models describe infra-red stimulated luminescence (IRSL) laboratory decay and have been used for the application of feldspar luminescence thermochronometry: a multiple first-order kinetic model based on band-tail states, a model based on localized transitions and a general-order kinetics model. In this study, we validate the band-tail states model using published IRSL data of samples of known steady-state thermal conditions from the KTB borehole in Germany. Furthermore, we investigate thermal decay of trapped charge in IR sensitive traps in feldspar through exploring the effect of a Gaussian distribution of trap depths. Our results show that the band-tail states, a Gaussian distribution of trap depths and the combination of the two can all describe the laboratory and field data. We conclude that these models are suitable for application in IRSL-thermochronometry studies.

Keywords: thermal kinetic processes; feldspar; distribution of thermal lifetimes; luminescence thermochronometry.

2.1 Introduction

Luminescence thermochronometry is a tool capable of determining rock cooling and exhumation rates over 10-100 ka timescales (Herman et al., 2010; Li and Li, 2012; Guralnik et al., 2013, 2015a; King et al., 2016a, 2016c). It is based on the accumulation of charge in minerals such as quartz and feldspar during rock cooling (Aitken, 1985; Prokein and Wagner, 1994; Grün et al., 1999). Electrons are freed from their normal atomic sites due to ionizing radiation resulting from radioactive decay within the mineral itself and in the surrounding rock matrix. Some of these electrons become trapped in crystal defects, which may vary in thermal stability. Ambient heat causes thermally stimulated eviction of trapped electrons, which can then recombine either radiatively (i.e. producing luminescence) or non-radiatively. As the rock cools, the rate of thermally stimulated detrapping decreases, the system effectively closes and net charge accumulates. The closure temperature

corresponds to the rock's temperature at the time of the sample's apparent age (Dodson, 1973; Guralnik et al., 2013), and can be calculated using laboratory derived kinetic parameters. In luminescence thermochronometry, closure temperatures in the range of 30 - 95 °C have been suggested (Herman et al., 2010; Guralnik et al., 2013; Ankjærgaard et al., 2015; King et al., 2016b, 2016c), depending on the cooling rate and the thermal decay parameters, which themselves depend upon the mineral and the type of laboratory stimulation. The trapped charge that has accumulated during rock cooling since passing through the closure temperature can then be measured in the laboratory as a luminescence signal through stimulation by heat and/or light (Fig. 2-1). This is referred to as the natural luminescence signal and it is generally assumed that the intensity of the luminescence signal is proportional to the number of trapped electrons (Aitken, 1985). To convert the natural signal into a rock cooling rate, the kinetic processes need to be described and the sample specific kinetic parameters must be constrained in the laboratory (Guralnik et al., 2015a; King et al., 2016c).

The main limitation of luminescence thermochronometry is that over time the crystal may become saturated (i.e. all traps are filled), after which a thermal history is no longer recorded (Guralnik et al., 2015a; King et al., 2016c; Valla et al., 2016). Signal saturation thus limits its application to high temperature settings (i.e. boreholes or tunnels, e.g. Guralnik et al., 2015a; Schmidt et al., 2015) or to settings experiencing extremely rapid exhumation, i.e. > 5 mm/yr (e.g. Herman et al., 2010; King et al., 2016b), or rock cooling. The luminescence of feldspar saturates at radiation doses that are an order of magnitude greater than for quartz (Huntley and Lamothe, 2001); feldspar luminescence can thus provide information over longer timescales and may be a more suitable mineral for the application of luminescence thermochronometry (Li and Li, 2012). In addition, infra-red stimulated luminescence (IRSL) signals from feldspar are usually much brighter than the optically stimulated luminescence (OSL) signal from quartz, enabling more precise luminescence measurements (Huntley and Lamothe, 2001; King et al., 2014). A complication is that feldspar luminescence signals are known to fade due to quantum mechanical tunnelling of electrons (Wintle, 1973; Visocekas, 2002; Huntley and Lian, 2006), which is referred to as athermal signal loss or anomalous fading. Some IRSL signals have been shown to be less affected by anomalous fading, such as post-IR IRSL signals (Buylaert et al., 2009; Thomsen, 2011; Thomsen et al., 2008), or alternatively, fading must be corrected for (Huntley, 2006; Kars et al., 2008). Within this context, Guralnik et al. (2015a) used IRSL from Na-feldspar to constrain paleotemperatures in the thermally steady-state setting of the KTB borehole in Germany.

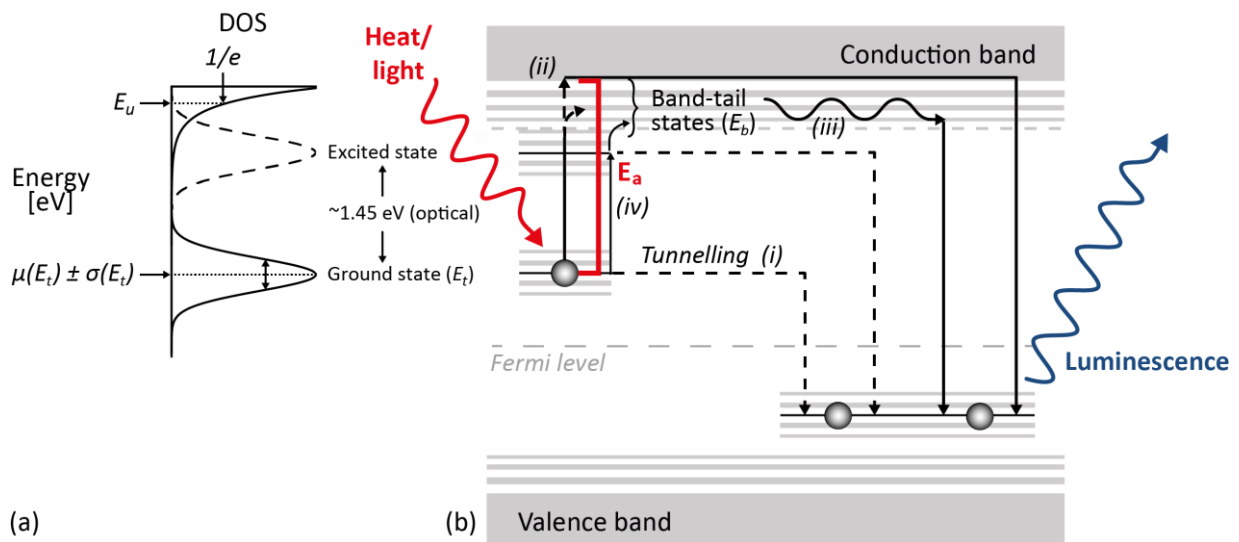


Fig. 2-1: Schematic energy diagram showing different charge detrapping routes from an infra-red (IR) sensitive trap's ground state to a recombination site in a feldspar crystal following Poolton et al. (2002a) and Jain and Ankjærgaard (2011). (a) Density of states (DOS) of the band tails and the ground and excited state of the IR trap. Here we consider an exponential distribution of band-tail states (E_b) with Urbach band-tail width E_u below the conduction band and a Gaussian distribution of trap depths denoted by a mean trap depth $\mu(E_t)$ and width $\sigma(E_t)$. (b) For thermally stimulated eviction, an electron needs activation energy (E_a), which corresponds to the difference between the trap depth, E_t , and the lowest energy level of the conduction band or band-tail state, E_b . The following recombination pathways are shown: (i) electrons may be evicted from the ground state of an IR sensitive trap without additional energy through quantum mechanical tunnelling (i.e. 'fading'); (ii) energy in the form of heat can excite trapped electrons to the conduction band or to a band-tail state below the conduction band, after which they may recombine with a hole; (iii) from a band-tail state, charge may transfer to another band-tail state through thermal assistance (i.e. band-tail state hopping) or eviction via quantum mechanical tunnelling either to another band-tail state or directly to a recombination centre; (iv) during IR stimulation electrons are excited to the excited state, from which they may be thermally assisted to a band-tail state. The 'Fermi level' lies in the middle of the band gap and is indicated here merely as a reference line (not to scale).

Despite several studies demonstrating the potential of feldspar luminescence thermochronometry (Guralnik et al., 2015a; King et al., 2016b,c), uncertainties remain on the kinetics of thermal decay in feldspar due to the complexity of the crystal structure, related defect energy levels and the multitude of charge transport mechanisms (e.g. Poolton et al., 2009; Jain and Ankjærgaard, 2011; Kars et al., 2013). Feldspar is a wide band-gap (~ 7.7 eV) aluminosilicate in the group of tectosilicates and as such has a relatively open crystal structure and a wide range of bonding angles and lengths (Putnis, 1992; Malins et al., 2004). Together with the presence of many defects in naturally occurring feldspar (e.g. impurities), these cause a large degree of disorder in the crystal (Poolton et al., 2002a). The disorder results in localized conduction band fluctuations where there is reduced electron mobility, typically

described as band-tail states (Redfield, 1963a,b; Mott and Davis, 1971; Poolton et al., 2002a). The influence of the band-tail states on feldspar luminescence was identified by Poolton et al. (1994) and Visocekas et al. (1998). During IR stimulation (~1.45 eV optical energy) at both room and elevated temperatures, it is thought that electrons are excited to an excited state of the trap (the 1.45 eV resonance; Hütt et al., 1988; Poolton et al., 1995; Poolton et al., 2002b; Kars et al., 2013), and thermally assisted to a nearby band-tail state from which the charge can recombine (Poolton et al., 2009; Jain and Ankjærgaard, 2011; Kars et al., 2013). Li and Li (2013) indicated that neglecting band-tail states may result in an underestimation of the thermal trap depth, which is the thermal energy needed to excite an electron from the ground state to the conduction band (Kars et al., 2013). Note that the thermal trap depth is lower than the trap depth measured by optical methods (Hütt et al., 1988; Chen and McKeever, 1997, Ch. 5; Poolton et al., 2009). Similarly, due to the variable structural configuration of feldspar, a distribution of trap depths for the IR sensitive trap may be expected, which is considered in this study. In general, the degree of ordering depends largely on the rate of cooling during crystallization and is therefore expected to be sample dependent (Duller, 1997; Malins et al., 2004). Apart from recombination processes via the conduction band, electrons may be thermally stimulated into an excited state from which they can recombine through tunnelling (Templer, 1986; McKeever and Chen, 1997).

Guralnik et al. (2015b) evaluated three different feldspar models for describing luminescence dose response and isothermal decay, and subsequent studies have used two of these for IRSL thermochronometric applications: a general-order kinetics model (GOK; Guralnik et al., 2015a) and a band-tail states model (BTS; King et al., 2016b). The GOK model has been validated against samples of known steady-state thermal conditions from the KTB borehole in Germany (Guralnik et al., 2015a). However, this approach may yield high kinetic orders (>2) for IRSL signals (Guralnik et al., 2015; Lambert et al., *subm.*). Moreover, the general analytical solution of a higher order kinetic differential equation implies a dependency on the initial trapped charge concentration. This effect becomes pronounced as the kinetic order increases, but experimental data for different feldspars reported in Lambert et al. (*subm.*) reveal only a weak dose dependency, a phenomenon also described by Li and Li (2013). Another approach is to describe the thermal decay of trapped charge in IR sensitive traps in feldspar through a distribution of thermal lifetimes, for instance, resulting from a distribution of activation energies. The concept of a distribution of activation energies has been introduced as a distribution of trap depths for materials other than feldspar; for amorphous semi-conductors by Grenet et al. (1973) and for quartz by Huntley et al. (1996). The localized transition model of Jain et al. (2012; 2015) describes a distribution of activation energies for feldspar, which is determined by trap depth relative to the excited state of the trap and a distribution of tunnelling distances, also

evaluated by Guralnik et al. (2015b). In this study, we test several multiple first-order thermal decay models based on delocalized thermal decay. The main purpose of this study is (1) to validate the band-tail states model using the KTB dataset, (2) to investigate the behaviour of thermal decay in feldspar through a distribution of activation energies based on a Gaussian distribution of trap depths, and (3) to study the combination of band-tail states and a distribution of trap depths.

2.2 Models of feldspar charge transfer

Different models for feldspar luminescence exist, which can be broadly grouped into three categories, assuming: (I) localized transitions (II) delocalized transitions and (III) semi-localized transitions which are a combination of (I) and (II) (see review by Pagonis et al., 2017). Halperin and Braner (1960) considered thermal decay via localized transitions, and Jain et al. (2012; 2015) have developed a comprehensive model for feldspar on this basis. The latter model proposes that the majority of the pathways involved in the decay processes in feldspar are localized transitions either directly from the ground state of the trap (tunnelling) or through thermal or optical excitation of trapped electrons to the excited state of the trap (IR resonance) from where the electrons recombine through tunnelling. In contrast, general-order kinetics models (e.g. Guralnik et al., 2015) and the band-tail states model (Li and Li, 2013) of feldspar thermal decay are based on delocalized transitions, i.e. transitions via the band-tail states or conduction band. The derivation of feldspar thermal kinetic parameters is often based on laboratory measurements of sample isothermal decay at elevated temperatures. However, as the probability of thermal decay through localized and delocalized transitions and their corresponding energy states is thermally dependent (Mandowski, 2004), the relation of laboratory measurements to environmental conditions in natural cooling settings is not inherently evident. Therefore, a model combining both transition types to describe the thermal kinetics of IR sensitive traps in feldspar crystals (Mandowski, 2004; Horowitz et al., 2016; Pagonis et al., 2017) is worthy of investigation. Here we focus on a simple model that consists of delocalized thermal decay and localized ground state tunneling.

2.2.1 Rate equation for thermochronometry

The net rate of charge trapping and detrapping in a feldspar crystal, for a specific trap during irradiation at a given temperature, can be expressed by the following differential equation (for a review see King et al., 2016a)

$$\frac{d\left(\frac{n}{N}(t, E_a, r')\right)}{dt} = p_{trapping} \cdot \left(1 - \frac{n}{N}(t, E_a, r')\right) - p_{detrapping} \cdot \frac{n}{N}(t, E_a, r') \quad (1)$$

where n/N is the ratio of trapped electrons with activation energy E_a [eV] and distance r' (dimensionless) to the nearest neighbouring hole as a function of time t [s]. The rate at which electrons are trapped is given by the probability that an electron becomes trapped ($p_{trapping}$), multiplied by the proportion of available traps $\left(1 - \frac{n}{N}\right)$. For some samples the trapping rate cannot be described by a simple saturating exponential function and a general-order kinetics model can be adopted (May and Partridge, 1964; Whitehead et al., 2009; Guralnik et al., 2015b). In this case, we have $\left(1 - \frac{n}{N}\right)^a$, where $1 \leq a \leq 2$ is the kinetic order to describe non-first order electron trapping. As the growth curve over time approaches saturation (i.e. $\frac{n}{N} \approx 1$) asymptotically and we assume a finite number of traps, we pose a maximum limit on a , while still finding a satisfactory fit to laboratory data. The electron trapping probability ($p_{trapping}$) is dependent on the environmental dose rate \dot{D} [Gy/s] and the characteristic dose of saturation D_0 [Gy], which are assumed to be constant over time (e.g. Wintle and Murray, 2006), leading to

$$p_{trapping} = \frac{\dot{D}}{D_0} \quad (2)$$

The rate at which electrons escape from traps is given by the probability of thermally stimulated detrapping ($p_{thermal}$) and the probability of eviction through quantum mechanical tunnelling ($p_{athermal}$), together represented as $p_{detrapping}$ in Eq. (1), multiplied by the proportion of trapped charge $\left(\frac{n}{N}\right)$. Athermal loss results in ‘fading’ of the luminescence signal over time without stimulation by heat or light. Its probability ($p_{athermal}$) can be expressed through the inverse of the athermal lifetime τ_{tun} [s] of a trapped electron, which is determined by the tunnelling distance r' (dimensionless) to a recombination site in a crystal, a variable ρ' (dimensionless) which relates to the density of recombination centres, and frequency factor $s_{tun} \approx 3 \cdot 10^{15} \text{ s}^{-1}$ (after Huntley, 2006)

$$\tau_{tun} = (p_{athermal})^{-1} = s_{tun}^{-1} e^{r' \cdot (\rho')^{-1/3}} \quad (3)$$

Following Huntley (2006), it is assumed that recombination centres are randomly distributed and an electron will tunnel to the nearest recombination centre. Thus, we integrate over the following probability distribution for tunnelling distance r'

$$p(r') = 3r'^2 e^{-(r')^3} \quad (4)$$

The probability of thermal loss ($p_{thermal}$) can be expressed through the inverse of the thermal lifetime τ_{th} [s] of a trapped electron, which is determined by the activation energy E_a [eV] necessary to escape, Boltzmann’s constant k_B [eV/K], temperature $T(t)$ [K] at time t and frequency factor s_{th} [s⁻¹]

$$\tau_{th} = (p_{thermal})^{-1} = s_{th}^{-1} e^{\frac{E_a}{k_B T(t)}} \quad (5)$$

Although for various solids a simple first-order exponential decay model (Eq. (5)) may sufficiently describe the thermal decay of trapped charge (e.g. Randall and Wilkins, 1945), it has been observed that IRSL signals from feldspars follow a slower thermal decay curve (e.g. Grün, 1994; Guralnik et al., 2015a; Guralnik et al., 2015b). One mechanism that has been suggested to explain this deviation from an exponential decay is electron retrapping, i.e. once an electron has been thermally evicted from its trap there is the possibility to either recombine or be retrapped, giving rise to second-order kinetic behaviour (see Aitken, 1985; Sunta et al., 1997 for reviews) or general-order kinetic behaviour; alternatively variable distance-dependent recombination probabilities may contribute to this effect (Guralnik et al., 2015b) or other processes. However, the rate of thermal decay with time is then no longer proportional to the number of remaining trapped electrons, which implies that the decay is dose dependent (Aitken, 1985; Lambert et al., *subm.*). Alternatively, a first-order kinetic model assuming a distribution of thermal lifetimes for a population of trapped electrons has been proposed (Poolton et al., 2002a; Poolton et al., 2009; Li and Li, 2013). The band-tail states (Fig. 2-1) give rise to a distribution of activation energies and thus of thermal lifetimes. This model was successfully applied in an IRSL-thermochronometry study of actively cooling samples from the Namche Barwa syntaxis (King et al., 2016b; King et al., 2016c). The localized transition model of Jain et al. (2012; 2015) also describes a distribution of activation energies, determined by trap depth relative to the excited state of the trap and a distribution of tunnelling distances. In this case, the assumption is made that there are sufficient recombination centres in the close neighbourhood of the trap. Here we restrict our investigation to multiple first-order kinetic models comprising delocalized thermal decay and ground state tunneling.

2.2.2 Thermal decay models

We seek a suitable model to constrain the thermal decay of trapped charge in IR sensitive traps of feldspar based on the results of isothermal decay experiments. Below we derive the equations that are used to fit the isothermal decay data for the multiple first-order kinetic models. We progressively build on Eq. (1).

Band-tail states

Following Poolton et al. (2002a, 2002b, 2009), Li and Li (2013) proposed a model to describe the thermal decay of charge in feldspar in the presence of band-tail states (BTS model). The band-tail states form a continuum of energy states below the conduction band that are spatially distributed throughout the crystal (Fig. 2-1a in Poolton et al., 1994). Each trapped electron can thermally escape

via a band-tail energy level, which makes eviction from the trap easier (Figs. 1 and 2a). As a first approximation, the density of band-tail states is assumed to be exponentially distributed below the conduction band edge and can be characterized by the Urbach band-tail width E_u [eV] (Urbach, 1953). However, the parameter E_u , that is derived through fitting this model to IRSL isothermal decay data, represents a measure for the band-tail states distribution that is accessible from the ground state of IR sensitive traps only and is therefore not necessarily the same as the crystal's Urbach width. Moreover, the preheat in the experimental procedure is sufficient to evict part of the trapped electron population that need low activation energies to escape (Fig. 2-2a shows the evolution towards a near linear distribution of activation energies of the remaining trapped charge when the BTS model is applied). Thus, the experimental data lack information on this part of the energy states distribution, and obtained E_u values may not reflect the full distribution of band-tail states available to electrons in the IRSL trap.

The BTS model assumes that all recombination processes following thermal stimulation occur only through the band-tail states (no recombination occurs through the excited state of the trap or the conduction band) and that retrapping is negligible (i.e. a first-order kinetic condition is assumed). For each band-tail state with energy $E_b \in [E_{b,min}, E_{b,max}]$ [eV], one can thus write

$$\tau_{th} = s_{th}^{-1} e^{\frac{E_t - E_b}{k_B T(t)}}, \quad (6)$$

where E_t [eV] is the thermal trap depth of the IR sensitive trap, and $E_{b,min}$ [eV] and $E_{b,max}$ [eV] represent the energies of the shallowest and deepest band-tail states thermally accessible (we assume $E_{b,min} > 0$ and $E_{b,max} < E_t$). The thermal decay mechanism in this model is independent of trap occupation, thus N is not relevant. For each band-tail state, the thermal decay of trapped charge can be described by the following first-order differential equation

$$\frac{dn}{dt} = -\frac{n}{\tau_{th}} \quad (7)$$

For a constant temperature, integration of Eq. (7) leads to

$$n(t, E_b) = n(0, E_b) \cdot \exp\left(-\frac{t}{\tau_{th}}\right) \quad (8)$$

To estimate the total amount of charge that escapes through the band-tail states, we integrate Eq. (8) over the full distribution of band-tail states

$$\frac{n(t)}{n(0)} = \int_{E_{b,min}}^{E_{b,max}} P_b(E_b) \cdot \exp\left(-\frac{t}{\tau_{th}}\right) dE_b, \quad (9)$$

where $P_b(E_b)$ is the probability density function of the band-tail states and $n(t)$ the number of trapped charges remaining after time t . The presence of band-tail states lowers the apparent activation energy (i.e. $E_a = E_t - E_b$) necessary for an electron to escape from a trap, and the distribution of energy states gives rise to a distribution of thermal lifetimes for one trap depth. Li and Li (2013) noted that other distributions than exponential may also be possible (e.g. linear, Gaussian or double-exponential; Chen and McKeever, 1997). For an exponential distribution of the density of band-tail states, the probability of electrons being thermally evicted into the band-tail states is given by

$$P_b(E_b)dE_b = A \exp\left(-\frac{E_b}{E_u}\right)dE_b \quad (10)$$

where A is a constant (Li and Li, 2013). Based on

$$\int_{E_{b,min}}^{E_{b,max}} P_b(E_b)dE_b = 1, \quad (11)$$

which follows from Eq. (9) for $t = 0$, the following probability density function can be derived (see Appendix)

$$P_b(E_b) = \frac{\exp\left(-\frac{E_b}{E_u}\right)}{E_u \left(\exp\left(-\frac{E_{b,min}}{E_u}\right) - \exp\left(-\frac{E_{b,max}}{E_u}\right) \right)} \quad (12)$$

Gaussian distribution of trap depths

Band-tail states are part of the density of states within a crystal and the model discussed above gives rise to a distribution of activation energies ($E_a = E_t - E_b$) for the population of trapped electrons in IR sensitive traps, and thus a distribution of thermal lifetimes. Similarly, a distribution of activation energies could be considered through the assumption of a Gaussian spatial distribution of trap depths for IR sensitive traps (GTD model; Figs. 1 and 2b). Poolton et al. (2002a) also suggested that in feldspars the defect energy states (and their excited states) accessed by IRSL may have a distribution, in addition to the distribution of band-tail states, which they illustrate but do not discuss (Fig. 2-1 in Poolton et. al, 2002a). Furthermore, such a Gaussian distribution is analogous to the symmetrically shaped distribution of activation energies E' proposed by Jain et al. (2015). Although the latter model is based on localized rather than delocalized transitions, it results in an analogous concept of a distribution of activation energies and thus a distribution of thermal lifetimes. We explore a simple

model, where we assume that thermal eviction occurs from the trap's ground state to the conduction band (no recombination occurs through the excited state of a trap or via a band-tail state), so that Eq. (9) becomes

$$\frac{n(t)}{n(0)} = \int_0^{E_{t,max}} P_t(E_t) \cdot \exp\left(-\frac{t}{\tau_{th}}\right) dE_t \quad (13)$$

where $P_t(E_t)$ is the Gaussian trap depth distribution with mean thermal trap depth $\mu(E_t)$ [eV] and width $\sigma(E_t)$ [eV] given by

$$P_t(E_t) = \frac{1}{\sigma(E_t)\sqrt{2\pi}} \exp\left(-\frac{1}{2}\left(\frac{E_t - \mu(E_t)}{\sigma(E_t)}\right)^2\right) \quad (14)$$

and $E_{t,max}$ [eV] represents the deepest thermal trap depth within the Gaussian distribution (note that in practice it is sufficient to assume $E_{t,max} < 2 \cdot E_t$).

If on the other hand one assumes that band-tail states play a role in the thermal eviction of trapped charge and the above-mentioned distributions for band-tail states and trap depths are independent, the number of trapped electrons in time can be described by the following equation

$$\frac{n(t)}{n(0)} = \int_{E_{b,min}}^{E_{b,max}} P_b(E_b) \int_0^{E_{t,max}} P_t(E_t) \cdot \exp\left(-\frac{t}{\tau_{th}}\right) dE_t dE_b \quad (15)$$

The distributions of the two models can be combined into an effective distribution $P_a(E_a)$ of activation energies $E_a = E_t - E_b$ via a convolution integral that can be efficiently calculated using a Fast Fourier Transform. Similar to Eq. (9) and (13), we then have

$$\frac{n(t)}{n(0)} = \int_0^{E_{a,max}} P_a(E_a) \cdot \exp\left(-\frac{t}{\tau_{th}}\right) dE_a \quad (16)$$

where $E_{a,max}$ [eV] is the difference between the deepest trap depth and shallowest band-tail state, or in other words the largest net activation energy needed for an electron to escape from the IR sensitive trap (BTS + GTD model; Figs. 1 and 2c). The effective distribution of activation energies is Gaussian in shape, but slightly asymmetrical towards the conduction band where relatively low activation energies are present. Combining the presence of band-tail states and a distribution of trap depths enables the assessment of their occurrence and relative contributions to electron detrapping, or simply the exploration of characteristic distributions of activation energies corresponding to the data trends.

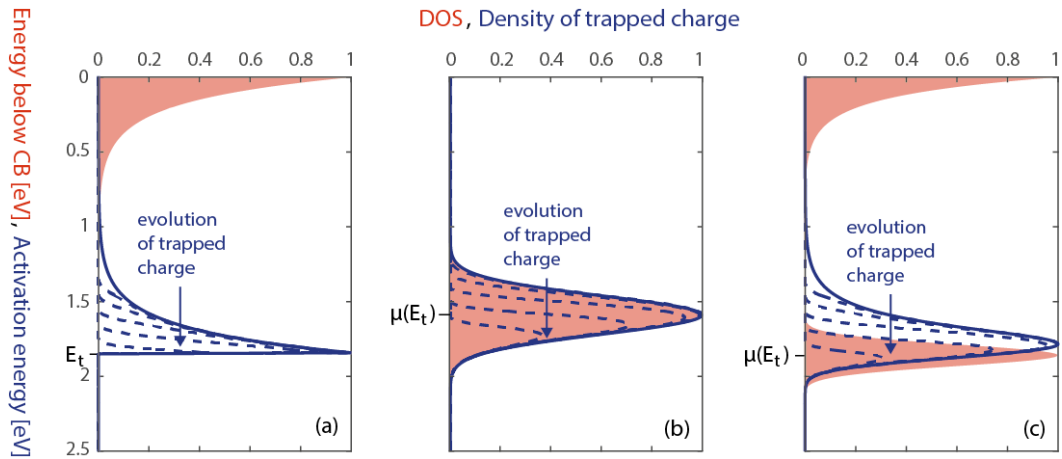


Fig. 2-2: Schematic energy diagrams illustrating the BTS, GTD and BTS + GTD model. The density of states below the conduction band (CB) for the IR sensitive trap is shown in red and the resulting distribution of activation energies necessary for trapped charge to escape is shown in blue. (a) Illustration of the BTS model, where spatially distributed band-tail states for a single trap depth are assumed. This results in an asymmetrical distribution of activation energies necessary for trapped charge to escape from the trap. (b) Illustration of the GTD model, where a Gaussian spatial distribution for trap depths is assumed. This results in a symmetrical distribution of activation energies necessary for trapped charge to escape from the trap. (c) Illustration of the combination of band-tail states and a Gaussian distribution of trap depths (BTS + GTD model). This results in a slightly asymmetrical Gaussian distribution of activation energies necessary for trapped charge to escape from the trap. The dotted lines show the evolution (in the direction of the arrow) of the remaining distribution of trapped charge with its corresponding activation energy during isothermal decay at a given temperature ($T = 250\text{ }^{\circ}\text{C}$ in this example) for different decay periods ($t = 10^i\text{ s}$ for $i = 1, \dots, 5$).

2.3 Numerical validation

We evaluate the BTS, GTD and GTD + BTS models by applying them to previously published IRSL₅₀ (infra-red stimulated luminescence at 50 °C) data measured on Na-feldspar extracts from the KTB borehole (Guralnik et al., 2015a). These twelve samples have experienced known steady-state thermal conditions (~10-70 °C) during the last ~25 Myr and therefore provide an appropriate reference data set (Coyle et al., 1997; Wolfe and Stockli, 2010).

The published isothermal decay data of Guralnik et al. (2015a; obtained through a short shine protocol with delays up to 20470 s at 190, 210 and 230 °C) were fitted using the different thermal decay models described in Section 2.2. Following King et al. (2016a,b) we accounted for anomalous fading that occurs throughout isothermal decay measurements using the localized transition model of Huntley (2006) and Kars et al. (2008). We characterized the fading of these samples based on the available fading data of Guralnik et al. (2015a). Fading times were calculated as half of the irradiation time, plus the time between irradiation and IR stimulation after Auclair et al. (2003). In the GTD and

GTD + BTS models, for which we assume a distribution of trap depths, the different trap depths may correspond to energy states with a different athermal stability. However, we do not account for this in this study and assume a single fading parameter ρ' (Eq. (3)) in all tested models (McKeever and Chen, 1997, Eq. (77); Huntley, 2006). All derived kinetic parameters are given in Tables 2-1 and 2-2. Figure 2-3 shows the isothermal decay data and model fits for sample KTB/428B.

The model fits of the BTS, GTD and combined BTS + GTD model are all statistically significant. The residual plots show that for all three models the deviation is within 0.05 of the data points. It is worth noting, however, that the residuals are homoscedastic, i.e. equally distributed, for the GTD and the combination of BTS and GTD (Fig. 2-3e,f).

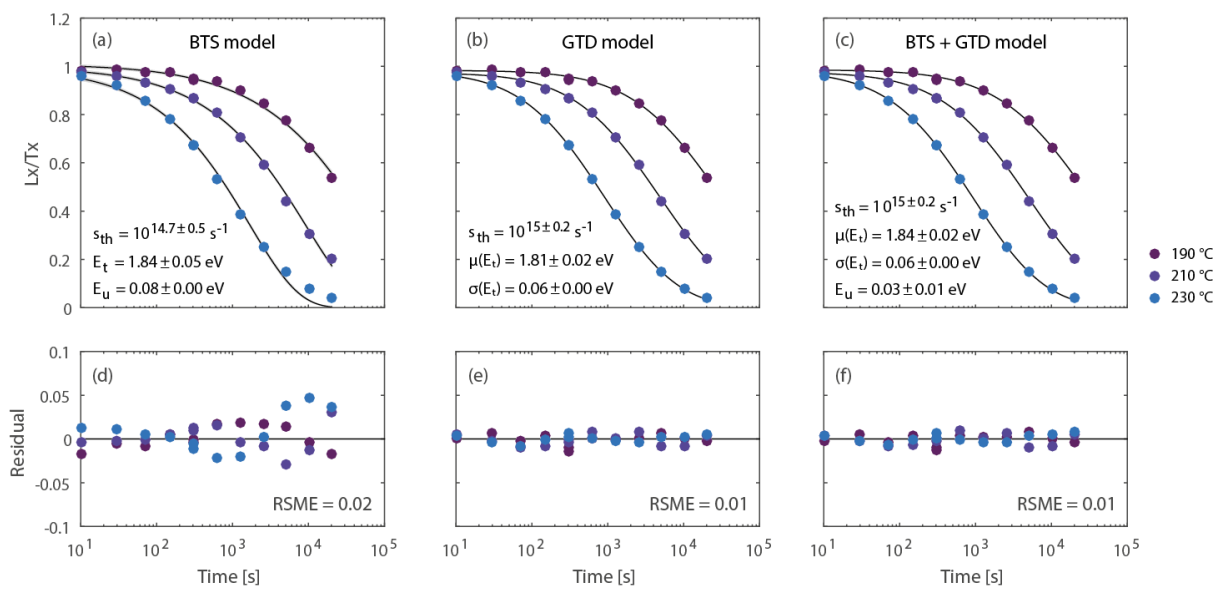


Fig. 2-3: (a)-(c) Isothermal decay data for the $IRSL_{50}$ signal of sample KTB/428B, obtained through a short shine protocol ($T = 190, 210, 230$ °C and time delays $t = 0 - 20470$ s) fitted with the BTS, GTD and BTS + GTD model respectively. (d)-(f) Residuals of the model fits to the isothermal decay data of sample KTB/428B.

To compare the thermal stability determined from the obtained thermal kinetic parameters for the BTS, GTD and BTS + GTD models, we simulate the thermal decay for a constant temperature (30 °C). Figure 2-4 shows the thermal decay trends for all KTB samples and specifically for sample KTB/428B as predicted by the three multiple first-order kinetic models. As the model fits for the GTD and BTS + GTD models overlap, they are both depicted by a blue surface area. Figure 2-4 shows that the BTS model describes a thermally less stable decay than the other two models. Such deviations may have implications for thermochronometric studies.

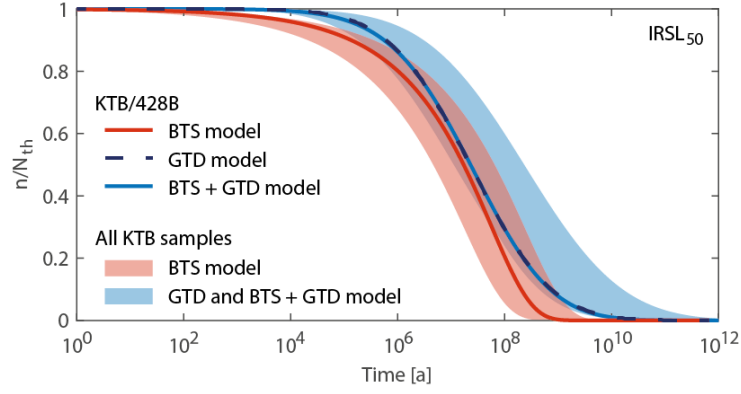


Fig. 2-4: Simulated thermal decay at 30 °C for the $IRSL_{50}$ signals of sample KTB/428B (depicted by the red and blue lines) and all KTB samples (depicted by the red and blue surface area) through application of the three multiple first-order kinetic models (BTS, GTD and BTS + GTD model).

To continue our model validation, we predicted trap occupancy levels ($n/N_{ss,th}$ values) using a forward model for the known sample-specific isothermal temperatures and compared them to trap occupancy corresponding to the natural luminescence signals for samples at each individual temperature (n/N_{nat} , Fig. 2-5 and Table 2-2; Guralnik et al., 2015a). We used the following differential equation, which is similar to Eq. (1) and comprises a trapping, thermal decay and athermal decay term

$$\frac{d\left(\frac{n}{N}(t, E_a, r')\right)}{dt} = \frac{\dot{D}}{D_0} \cdot \left(1 - \frac{n}{N}(t, E_a, r')\right)^a - \frac{n}{N}(t, E_a, r') \frac{1}{\tau_{th}} - \frac{n}{N}(t, E_a, r') \frac{1}{\tau_{tun}} \quad (17)$$

where

$$\tau_{th} = s_{th}^{-1} e^{\frac{E_a}{k_B T(t)}} \quad \text{with} \quad E_a = E_b - E_t \quad (18)$$

and

$$\tau_{tun} = s_{tun}^{-1} e^{r' \cdot (\rho')^{-1/3}} \quad (19)$$

We solve for n/N (the ratio of trapped electrons in the IR sensitive trap) numerically and integrate over the probability distributions for the activation energy E_a (described in sections 2.2.1 and 2.2.2) and the tunnelling distance r' (Eq. (4) in section 2.1).

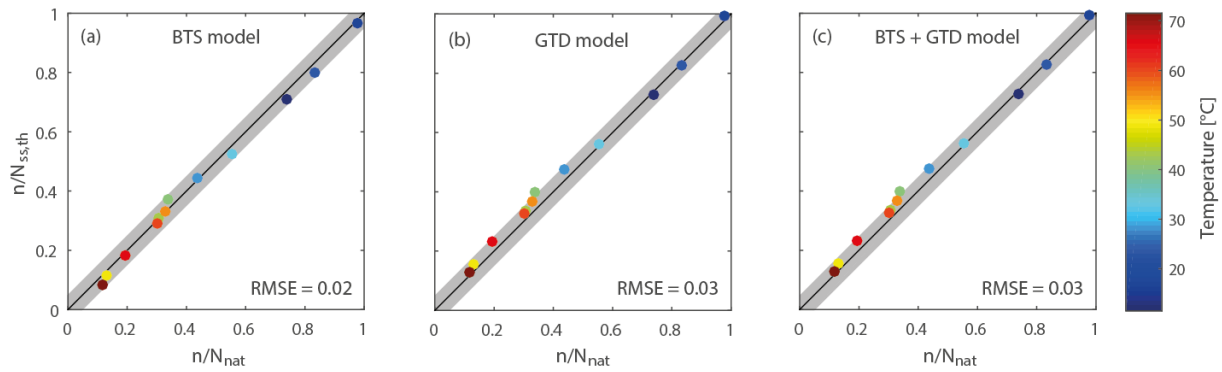


Fig. 2-5: (a)-(c) Validation of the BTS, GTD and BTS + GTD models for the suite of KTB samples. Modelled $n/N_{ss,th}$ values for known thermal steady-state conditions relative to n/N_{nat} values derived from the natural luminescence signals, obtained by applying the combined model (Eq. (1) or (17)) with the BTS, GTD and BTS + GTD model. The shaded area indicates a deviation of 0.05 from the 1:1 line and the root mean square error is given for each validation.

While the residuals of the isothermal decay model fits are reduced for the GTD and BTS + GTD models relative to the BTS model, all three models can significantly reproduce the observed data (Fig. 2-5). The three multiple first-order kinetics models predict $n/N_{ss,th}$ values within ± 0.05 of the natural n/N_{nat} values, with the exception of sample KTB/253F.

2.4 Discussion

The BTS model is able to fit the IRSL₅₀ isothermal decay data of sample KTB/428B, except for the longest delays at the highest temperature, which show a systematic deviation although residuals are within 0.05 (Fig. 2-3a,d). The application of the GTD model gives a significant fit to the data, including the data points corresponding to the last part of the decay (Fig. 2-3b,e); this part of the curve is explained by the GTD model as the decay of trapped electrons with a relatively higher activation energy, and thus longer thermal lifetime. Since Poolton et al. (2009) found direct evidence for the presence of band-tail states in feldspar crystals, we also explored the BTS + GTD model. The GTD and BTS + GTD models yield similar model fits for sample KTB/428B (Fig. 2-3b,c,e,f). The mean trap depth $\mu(E_t)$ and band-tail width E_u obtained through application of the BTS + GTD model describe a similar distribution of activation energies as the slightly lower mean trap depth $\mu(E_t)$ of the GTD model. This is because the presence of band-tail states effectively reduces the activation energy required for electrons to escape. Figure 2-4 shows that for all KTB samples, these two models give a similar thermal decay curve.

We have shown that several first-order decay models assuming a distribution of activation energies can fit the observed isothermal decay trends of the IRSL₅₀ signal of a suite of feldspar samples from the KTB borehole. Whilst values for the band-tail width are much lower than previously reported

(Table 2-2; Poolton et al., 2009; Kars et al., 2013; Prasad et al., 2016), the trap depth values obtained for the KTB samples appear to be plausible relative to previously published kinetic parameters (Aitken, 1985, Table E.1; Strickertsson, 1985; Hütt, 1988). The comparison of kinetic parameters from different studies must be done with care, as differences in values may be due to (1) sample specific thermal characteristics related to crystal structure/disorder (e.g. Malins et al., 2004), (2) the adopted experimental procedure (e.g. preheat; see measurement protocol in Lambert et al., *subm.*) and/or (3) physical and numerical model assumptions.

All of the multiple first-order kinetic thermal decay models explored in this study are able to predict trap occupancy levels comparable to measured natural values for the KTB borehole (Fig. 2-5). For this validation, using samples from a steady-state thermal setting, we have chosen to apply a general order kinetics model to describe the sample-specific trapping kinetics (following Guralnik et al., 2015b). A multiple first-order kinetic model could also be used to describe the process of electron trapping in response to constant dose rate, and may be a logical counterpart of the adopted thermal decay models, especially when the deviation from simple exponential behaviour is explained by variations in energy levels related to the mineral's crystal structure. However, the trapping process is in essence different from thermal decay (e.g. Williams, 1992) and the potential effects of laboratory artefacts associated with dose rates several orders of magnitude greater than in the natural environment (e.g. Chapot et al., 2012; Li et al., 2015) necessitate that any new model for electron trapping is thoroughly evaluated and validated, which is outside the scope of the present study.

A distribution of thermal lifetimes may be attributed to a range (or combination) of different kinetic processes. Here we have explored the possibility of a spatial distribution of trap depths in addition to band-tail states below the conduction band due to variations in the crystal structure. This leads to a distribution of activation energies and thus thermal lifetimes for the trapped charge population in the IR sensitive traps. However, neither the presence of a distribution of trap depths nor the underlying process of delocalized thermal eviction from the ground state to the conduction band or a band-tail state has been proven. A notable advantage of multiple first-order kinetic models above a general-order kinetic model is that no assumption of dose dependency is required, which is explored further in Lambert et al. (*subm.*). A limitation of the proposed models is that they only take into account delocalized transitions and no effects of higher order kinetic processes or localized transitions (e.g. via the excited state of IR resonance), except for ground state tunneling.

For the application of luminescence thermochronometry, we have to consider the remaining unknowns concerning the extent to which laboratory measurements at high temperatures and relatively short durations mimic low temperature processes from the natural environment; in the

latter, localized transitions may be expected to play a more significant role (McKeever and Chen, 1997; Prasad et al., 2017). A combination of isothermal and pulse-anneal thermal decay experiments may enable delocalized and localized transitions to be distinguished, from which the relative rates of such transitions can be derived. Kitis et al. (2016) have recently suggested that isothermal decay of TL at high temperatures can be used to differentiate between delocalized and localized recombination processes. Yet, simple multiple first-order kinetic models are able to fit the laboratory data and predict trap occupancy levels of a known thermal steady-state setting and therefore appear suitable for luminescence thermochronometric studies.

2.5 Conclusions

We have validated the applicability of three multiple first-order kinetic models for thermal decay of trapped charge in IR sensitive traps of feldspar based on a distribution of energy states below the conduction band. The first model is based on the Li and Li (2013) band-tail states model, which has already been successfully applied in luminescence thermochronometry (e.g. King et al., 2016b; King et al., 2016c). The second model assumes a Gaussian distribution around trap depth and the third model incorporates the Gaussian distribution with an exponential distribution of the band-tail states. Whilst the thermal decay component of the models is based on an assumption of delocalized transitions, they are implemented together with the localized transition model of Huntley (2006) for anomalous fading. All three models yield satisfactory fits to previously published isothermal decay data of KTB borehole samples (Guralnik et al., 2015a) and have been successfully validated using the KTB data from a thermal steady-state setting, indicating that they can be used for luminescence thermochronometry. Future studies on the physical properties of feldspar, specifically the interaction between localized and delocalized processes, will help to further refine the existing models.

Acknowledgements

This research was funded by Swiss National Science Foundation (SNSF) grant numbers PP00P2-38956 and 200021-127127. PGV was funded by grants PZ00P2_148191 and PP00P2_170559, GEK by grant PZ00P2_167960 awarded by the SNSF. We thank Reuven Chen for valuable feedback, and Benny Guralnik and Mayank Jain for their constructive reviews.

References

- Aitken, M.J., 1985. Thermoluminescence dating. Academic press.
- Ankjærgaard, C., Guralnik, B., Porat, N., Heimann, A., Jain, M., Wallinga, J., 2015. Violet stimulated luminescence: geo-or thermochronometer? *Radiation Measurements* 81, 78-84.
- Auclair, M., Lamothe, M., Huot, S., 2003. Measurement of anomalous fading for feldspar IRSL using SAR. *Radiation measurements* 37, 487-492.
- Buylaert, J.-P., Murray, A., Thomsen, K.J., Jain, M., 2009. Testing the potential of an elevated temperature IRSL signal from K-feldspar. *Radiation Measurements* 44, 560-565.
- Chapot, M., Roberts, H., Duller, G., Lai, Z., 2012. A comparison of natural-and laboratory-generated dose response curves for quartz optically stimulated luminescence signals from Chinese Loess. *Radiation Measurements* 47, 1045-1052.
- Chen, R., McKeever, S.W., 1997. Theory of thermoluminescence and related phenomena. World Scientific.
- Coyle, D., Wagner, G., Hejl, E., Brown, R., Van den Haute, P., 1997. The Cretaceous and younger thermal history of the KTB site (Germany): apatite fission-track data from the Vorbohrung. *Geologische Rundschau* 86, 203-209.
- Dodson, M.H., 1973. Closure temperature in cooling geochronological and petrological systems. *Contributions to Mineralogy and Petrology* 40, 259-274.
- Duller, G.A.T., 1997. Behavioural studies of stimulated luminescence from feldspars. *Radiation Measurements* 27, 663-694.
- Grenet, J., Vautier, C., Carles, D., Chabrier, J., 1973. Space charge conduction in presence of a gaussian distribution of localized states. *Philosophical Magazine* 28, 1265-1277.
- Grün, R., 1994. The kinetics of TL peaks and its effect on the dose versus temperature plot. *Radiation measurements* 23, 175-194.
- Grün, R., Tani, A., Gurbanov, A., Koshchug, D., Williams, I., Braun, J., 1999. A new method for the estimation of cooling and denudation rates using paramagnetic centers in quartz: a case study on the Eldzhurtinskiy Granite, Caucasus. *Journal of Geophysical Research: Solid Earth* 104, 17531-17549.
- Guralnik, B., Jain, M., Herman, F., Ankjærgaard, C., Murray, A.S., Valla, P.G., Preusser, F., King, G.E., Chen, R., Lowick, S.E., 2015a. OSL-thermochronometry of feldspar from the KTB borehole, Germany. *Earth and Planetary Science Letters* 423, 232-243.
- Guralnik, B., Jain, M., Herman, F., Paris, R.B., Harrison, T.M., Murray, A.S., Valla, P.G., Rhodes, E.J., 2013. Effective closure temperature in leaky and/or saturating thermochronometers. *Earth and Planetary Science Letters* 384, 209-218.
- Guralnik, B., Li, B., Jain, M., Chen, R., Paris, R.B., Murray, A.S., Li, S.-H., Pagonis, V., Valla, P.G., Herman, F., 2015b. Radiation-induced growth and isothermal decay of infrared-stimulated luminescence from feldspar. *Radiation Measurements* 81, 224-231.

- Halperin, A., Braner, A.A., 1960. Evaluation of thermal activation energies from glow curves. *Physical Review* 117, 408.
- Herman, F., Rhodes, E.J., Braun, J., Heiniger, L., 2010. Uniform erosion rates and relief amplitude during glacial cycles in the Southern Alps of New Zealand, as revealed from OSL-thermochronology. *Earth and Planetary Science Letters* 297, 183-189.
- Horowitz, Y., Eliyahu, I., Oster, L., 2016. Kinetic simulations of thermoluminescence dose response: long overdue confrontation with the effects of ionisation density. *Radiation protection dosimetry* 172, 524-540.
- Huntley, D., 2006. An explanation of the power-law decay of luminescence. *Journal of Physics: Condensed Matter* 18, 1359.
- Huntley, D., Lian, O.B., 2006. Some observations on tunnelling of trapped electrons in feldspars and their implications for optical dating. *Quaternary Science Reviews* 25, 2503-2512.
- Huntley, D.J., Lamothe, M., 2001. Ubiquity of anomalous fading in K-feldspars and the measurement and correction for it in optical dating. *Canadian Journal of Earth Sciences* 38, 1093-1106.
- Huntley, D., Short, M., Dunphy, K., 1996. Deep traps in quartz and their use for optical dating. *Canadian Journal of Physics* 74, 81-91.
- Hütt, G., Jaek, I., Tchonka, J., 1988. Optical dating: K-feldspars optical response stimulation spectra. *Quaternary Science Reviews* 7, 381-385.
- Jain, M., Ankjærgaard, C., 2011. Towards a non-fading signal in feldspar: insight into charge transport and tunnelling from time-resolved optically stimulated luminescence. *Radiation Measurements* 46, 292-309.
- Jain, M., Guralnik, B., Andersen, M.T., 2012. Stimulated luminescence emission from localized recombination in randomly distributed defects. *Journal of Physics: Condensed Matter* 24, 385402.
- Jain, M., Sohpati, R., Guralnik, B., Murray, A. S., Kook, M., Lapp, T., Buylaert, J. P., 2015. Kinetics of infrared stimulated luminescence from feldspars. *Radiation Measurements* 81, 242-250.
- Kars, R., Wallinga, J., Cohen, K., 2008. A new approach towards anomalous fading correction for feldspar IRSL dating—tests on samples in field saturation. *Radiation Measurements* 43, 786-790.
- Kars, R.H., Poolton, N.R., Jain, M., Ankjærgaard, C., Dorenbos, P., Wallinga, J., 2013. On the trap depth of the IR-sensitive trap in Na- and K-feldspar. *Radiation Measurements* 59, 103-113.
- King, G.E., Guralnik, B., Valla, P.G., Herman, F., 2016a. Trapped-charge thermochronometry and thermometry: A status review. *Chemical Geology* 446, 3-17.
- King, G.E., Herman, F., Guralnik, B., 2016b. Northward migration of the eastern Himalayan syntaxis revealed by OSL thermochronometry. *Science* 353, 800-804.
- King, G.E., Herman, F., Lambert, R., Valla, P., Guralnik, B., 2016c. Multi-OSL-thermochronometry of feldspar. *Quaternary Geochronology* 33, 76-87.
- King, G.E., Robinson, R.A.J., Finch, A.A., 2014. Towards successful OSL sampling strategies in glacial environments: deciphering the influence of depositional processes on bleaching of modern glacial sediments from Jostedal, Southern Norway. *Quaternary Science Reviews* 89, 94-107.

- Kitis, G., Polymeris, G.S., Sfampa, I.K., Prokic, M., Meriç, N., Pagonis, V., 2016. Prompt isothermal decay of thermoluminescence in MgB₄O₇: Dy, Na and LiB₄O₇: Cu, In dosimeters. *Radiation Measurements* 84, 15-25.
- Lambert, R., King, G.E., Valla, P.G., Herman, F., subm. Experimental investigations on thermal decay of feldspar from the Mont Blanc massif, European Alps. *Radiation Measurements*.
- Li, B., Li, S.-H., 2012. Determining the cooling age using luminescence-thermochronology. *Tectonophysics* 580, 242-248.
- Li, B., Li, S.-H., 2013. The effect of band-tail states on the thermal stability of the infrared stimulated luminescence from K-feldspar. *Journal of Luminescence* 136, 5-10.
- Li, B., Roberts, R.G., Jacobs, Z., Li, S.-H., Guo, Y.-J., 2015. Construction of a 'global standardised growth curve' (gSGC) for infrared stimulated luminescence dating of K-feldspar. *Quaternary Geochronology* 27, 119-130.
- Malins, A., Poolton, N., Quinn, F., Johnsen, O., Denby, P.M., 2004. Luminescence excitation characteristics of Ca, Na and K-aluminosilicates (feldspars) in the stimulation range 5–40 eV: determination of the band-gap energies. *Journal of Physics D: Applied Physics* 37, 1439.
- Mandowski, A., 2004. Semi-localized transitions model for thermoluminescence. *Journal of Physics D: Applied Physics* 38, 17.
- May, C., Partridge, J., 1964. Thermoluminescent Kinetics of Alpha-Irradiated Alkali Halides. *The Journal of Chemical Physics* 40, 1401-1409.
- McKeever, S.W.S., Chen, R., 1997. Luminescence models. *Radiation Measurements* 27, 625-661.
- Mott, N.F., Davis, E.A., 1971. *Electronic processes in non-crystalline materials*. Clarendon press.
- Pagonis, V., Chen, R., Kulp, C., Kitis, G., 2017. An overview of recent developments in luminescence models with a focus on localized transitions. *Radiation Measurements*.
- Poolton, N., Bøtter-Jensen, L., Johnsen, O., 1995. Thermo-optical properties of optically stimulated luminescence in feldspars. *Radiation Measurements* 24, 531-534.
- Poolton, N., Bøtter-Jensen, L., Ypma, P., Johnsen, O., 1994. Influence of crystal structure on the optically stimulated luminescence properties of feldspars. *Radiation Measurements* 23, 551-554.
- Poolton, N., Kars, R., Wallinga, J., Bos, A., 2009. Direct evidence for the participation of band-tails and excited-state tunnelling in the luminescence of irradiated feldspars. *Journal of Physics: Condensed Matter* 21, 485505.
- Poolton, N., Ozanyan, K., Wallinga, J., Murray, A., Bøtter-Jensen, L., 2002a. Electrons in feldspar II: a consideration of the influence of conduction band-tail states on luminescence processes. *Physics and Chemistry of Minerals* 29, 217-225.
- Poolton, N., Wallinga, J., Murray, A., Bulur, E., Bøtter-Jensen, L., 2002b. Electrons in feldspar I: on the wavefunction of electrons trapped at simple lattice defects. *Physics and Chemistry of Minerals* 29, 210-216.
- Prasad, A.K., Lapp, T., Kook, M., Jain, M., 2016. Probing luminescence centers in Na rich feldspar. *Radiation Measurements* 90, 292-297.

- Prasad, A.K., Poolton, N.R., Kook, M., Jain, M., 2017. Optical dating in a new light: A direct, non-destructive probe of trapped electrons. *Scientific Reports* 7, 12097.
- Prokein, J., Wagner, G.A., 1994. Analysis of thermoluminescent glow peaks in quartz derived from the KTB-drill hole. *Radiation measurements* 23, 85-94.
- Putnis, A., 1992. *An introduction to mineral sciences*. Cambridge University Press.
- Randall, J., Wilkins, M., 1945. The phosphorescence of various solids. *Proceedings of the Royal Society of London. Series A, Mathematical and Physical Sciences*, 347-364.
- Redfield, D., 1963a. Effect of defect fields on the optical absorption edge. *Physical Review* 130, 916.
- Redfield, D., 1963b. Electric fields of defects in solids. *Physical Review* 130, 914.
- Schmidt, C., Friedrich, J., Zöller, L., 2015. Thermochronometry using red TL of quartz?—Numerical simulation and observations from in-situ drill-hole samples. *Radiation Measurements* 81, 98-103.
- Strickertsson, K., 1985. The thermoluminescence of potassium feldspars—glow curve characteristics and initial rise measurements. *Nuclear Tracks and Radiation Measurements* 10, 613-617.
- Sunta, C., Ayta, W.F., Kulkarni, R., Pifers, T., Watanabe, S., 1997. General-order kinetics of thermoluminescence and its physical meaning. *Journal of Physics D: Applied Physics* 30, 1234.
- Templer, R.H., 1986. A new model for anomalous fading. Chapter 6. D.Phil. Thesis, Oxford University.
- Thomsen, K.J., 2011. Stability of IRSL signals from sedimentary K-feldspar samples. *Geochronometria* 38, 1-13.
- Thomsen, K.J., Murray, A.S., Jain, M., Bøtter-Jensen, L., 2008. Laboratory fading rates of various luminescence signals from feldspar-rich sediment extracts. *Radiation Measurements* 43, 1474-1486.
- Urbach, F., 1953. The long-wavelength edge of photographic sensitivity and of the electronic absorption of solids. *Physical Review* 92, 1324.
- Valla, P.G., Lowick, S.E., Herman, F., Champagnac, J.-D., Steer, P., Guralnik, B., 2016. Exploring IRSL50 fading variability in bedrock feldspars and implications for OSL thermochronometry. *Quaternary Geochronology* 36, 55-66.
- Visocekas, R., 2002. Tunnelling in Afterglow: Its coexistence and interweaving with thermally stimulated luminescence. *Radiation protection dosimetry* 100, 45-53.
- Visocekas, R., Tale, V., Zink, A., Tale, I., 1998. Trap spectroscopy and tunnelling luminescence in feldspars. *Radiation measurements* 29, 427-434.
- Whitehead, L., Whitehead, R., Valeur, B., Berberan-Santos, M., 2009. A simple function for the description of near-exponential decays: The stretched or compressed hyperbola. *American Journal of Physics* 77, 173-179.
- Williams, C., 1992. Kinetics of trapping, detrapping, and trap generation. *Journal of electronic materials* 21, 711-720.
- Wintle, A.G., 1973. Anomalous fading of thermo-luminescence in mineral samples. *Nature* 245, 143-144.

- Wintle, A.G., Murray, A., 2006. A review of quartz optically stimulated luminescence characteristics and their relevance in single-aliquot regeneration dating protocols. *Radiation Measurements* 41, 369-391.
- Wolfe, M.R., Stockli, D.F., 2010. Zircon (U–Th)/He thermochronometry in the KTB drill hole, Germany, and its implications for bulk He diffusion kinetics in zircon. *Earth and Planetary Science Letters* 295, 69-82.

Tables

Sample	Lithology	T_{ss} [°C]	\dot{D}_{nat} [Gy/ka]	g_{2days} [%/decade]	ρ' [10^{-6}]	D_0 [Gy]	a
KTB/19B	ttn amphibolite	11.5	1.50 ± 0.23	1.69 ± 2.09	1.13 ± 1.40	172 ± 11	1.75 ± 0.14
KTB/48B	cpx amphibolite	16.7	1.03 ± 0.15	0.00 ± 0.21	0.01 ± 0.15	78 ± 14	1.43 ± 0.43
KTB/105B	ky-sil-grt-bt gneiss	23.1	2.92 ± 0.44	1.05 ± 1.23	0.68 ± 0.86	181 ± 9	1.44 ± 0.13
KTB/146A	ky-sil-grt-bt gneiss	27.5	2.84 ± 0.43	3.66 ± 0.47	2.47 ± 0.31	276 ± 11	2.00 ± 0.24
KTB/218A	grt-sil-bt gneiss	32.6	2.96 ± 0.44	2.83 ± 1.95	1.94 ± 1.30	250 ± 14	1.42 ± 0.14
KTB/253F	grt amphibolite	39.8	1.58 ± 0.24	3.57 ± 1.73	2.41 ± 1.14	248 ± 15	1.60 ± 0.26
KTB/273G	grt amphibolite	43.3	1.07 ± 0.16	3.84 ± 0.77	2.60 ± 0.50	213 ± 14	1.71 ± 0.29
KTB/314B	grt amphibolite	48.7	1.07 ± 0.16	5.87 ± 1.39	3.86 ± 0.86	321 ± 34	1.84 ± 0.60
KTB/383C	sil-ms-bt gneiss	55.1	3.02 ± 0.45	1.77 ± 0.48	1.24 ± 0.33	207 ± 12	1.68 ± 0.24
KTB/428B	grt-sil-bt gneiss	59.5	3.44 ± 0.52	1.82 ± 0.64	1.27 ± 0.44	232 ± 13	1.63 ± 0.25
KTB/481B	grt-sil-bt gneiss	65.2	3.58 ± 0.54	2.03 ± 0.69	1.38 ± 0.47	236 ± 11	1.67 ± 0.21
KTB/564A	grt-sil-bt gneiss	71.5	3.30 ± 0.50	2.30 ± 0.53	1.58 ± 0.36	246 ± 14	1.96 ± 0.34

Table 2-1: Natural dose rate and athermal detrapping and trapping parameters for the $IRSL_{50}$ signal of Na-feldspar extracts from KTB samples (Guralnik et al., 2015a). Athermal stability is also expressed as g_{2days} [%/decade] (Aitken, 1985; Huntley and Lamothe, 2001). Mineral abbreviations: bt = biotite, cpx = clinopyroxene, grt = garnet, ky = kyanite, ms = muscovite, sil = sillimanite, ttn = titanite.

Band-tail states model

Sample	$\log_{10}(S_{th})$	E_t [eV]	E_u [eV]*	n/N_{nat}	n/N_{mod}
KTB/19B	14.1 ± 1.1	1.84 ± 0.11	0.08 ± 0.01	0.74	0.71
KTB/48B	14.1 ± 1.1	1.84 ± 0.11	0.08 ± 0.01	0.98	0.96
KTB/105B	15.6 ± 0.9	1.92 ± 0.09	0.07 ± 0.01	0.83	0.80
KTB/146A	14.5 ± 0.8	1.85 ± 0.08	0.08 ± 0.01	0.44	0.44
KTB/218A	14.7 ± 0.6	1.85 ± 0.06	0.08 ± 0.01	0.55	0.52
KTB/253F	14.7 ± 0.7	1.83 ± 0.07	0.08 ± 0.01	0.34	0.37
KTB/273G	14.8 ± 0.7	1.85 ± 0.06	0.08 ± 0.01	0.30	0.31
KTB/314B	13.3 ± 1.0	1.73 ± 0.10	0.09 ± 0.01	0.13	0.12
KTB/383C	14.5 ± 0.5	1.82 ± 0.05	0.07 ± 0.00	0.33	0.33
KTB/428B	14.7 ± 0.5	1.84 ± 0.05	0.08 ± 0.00	0.30	0.29
KTB/481B	14.5 ± 0.6	1.83 ± 0.06	0.08 ± 0.01	0.19	0.18
KTB/564A	14.6 ± 0.6	1.84 ± 0.06	0.08 ± 0.01	0.12	0.09

Gaussian trap depth distribution model

Sample	$\log_{10}(s_{th})$	$\mu(E_t)$ [eV]	$\sigma(E_t)$ [eV]	n/N_{nat}	n/N_{mod}
KTB/19B	15.1 ± 0.5	1.88 ± 0.05	0.08 ± 0.00	0.74	0.73
KTB/48B	15.0 ± 0.6	1.86 ± 0.05	0.08 ± 0.00	0.98	0.99
KTB/105B	15.9 ± 0.6	1.88 ± 0.06	0.06 ± 0.00	0.83	0.83
KTB/146A	15.1 ± 0.3	1.84 ± 0.03	0.07 ± 0.00	0.44	0.47
KTB/218A	15.2 ± 0.2	1.83 ± 0.20	0.07 ± 0.00	0.55	0.56
KTB/253F	15.0 ± 0.4	1.80 ± 0.04	0.07 ± 0.00	0.34	0.40
KTB/273G	15.2 ± 0.3	1.82 ± 0.03	0.06 ± 0.00	0.30	0.33
KTB/314B	14.1 ± 0.5	1.74 ± 0.05	0.08 ± 0.00	0.13	0.15
KTB/383C	14.9 ± 0.2	1.79 ± 0.02	0.06 ± 0.00	0.33	0.37
KTB/428B	15.0 ± 0.2	1.81 ± 0.02	0.06 ± 0.00	0.30	0.33
KTB/481B	14.9 ± 0.2	1.80 ± 0.02	0.07 ± 0.00	0.19	0.23
KTB/564A	15.1 ± 0.2	1.82 ± 0.02	0.07 ± 0.00	0.12	0.13

Band-tail states + Gaussian trap depth distribution model

Sample	$\log_{10}(s_{th})$	$\mu(E_t)$ [eV]	$\sigma(E_t)$ [eV]	E_u [eV]*	n/N_{nat}	n/N_{mod}
KTB/19B	15.1 ± 0.5	1.88 ± 0.05	0.08 ± 0.00	0.00	0.74	0.73
KTB/48B	15.0 ± 0.6	1.86 ± 0.05	0.08 ± 0.00	0.08	0.98	0.99
KTB/105B	15.9 ± 0.6	1.88 ± 0.06	0.06 ± 0.00	0.00	0.83	0.83
KTB/146A	15.1 ± 0.3	1.84 ± 0.03	0.07 ± 0.00	0.00	0.44	0.47
KTB/218A	15.2 ± 0.2	1.84 ± 0.20	0.07 ± 0.01	0.01 ± 0.20	0.55	0.56
KTB/253F	15.0 ± 0.4	1.80 ± 0.04	0.07 ± 0.00	0.00	0.34	0.40
KTB/273G	15.2 ± 0.3	1.82 ± 0.03	0.06 ± 0.00	0.00	0.30	0.33
KTB/314B	14.1 ± 0.5	1.74 ± 0.05	0.08 ± 0.00	0.00	0.13	0.15
KTB/383C	14.9 ± 0.2	1.82 ± 0.02	0.06 ± 0.00	0.03 ± 0.01	0.33	0.37
KTB/428B	15.0 ± 0.2	1.84 ± 0.02	0.06 ± 0.00	0.03 ± 0.01	0.30	0.33
KTB/481B	14.9 ± 0.2	1.81 ± 0.13	0.07 ± 0.01	0.01 ± 0.13	0.19	0.23
KTB/564A	15.1 ± 0.2	1.82 ± 0.26	0.07 ± 0.02	0.01 ± 0.26	0.12	0.13

Table 2-2: Thermal detrapping parameters derived through application of the BTS, GTD and BTS + GTD model on the isothermal decay data of the IRSL₅₀ signal of Na-feldspar extracts from KTB samples. * For some cases, large uncertainties were found for $\mu(E_t)$ and E_u , which may originate from a numerical correlation between these two parameters; subsequently, E_u was fixed to the best-fit value to evaluate the uncertainties of the other parameters. This did not have an effect on the parameter values.

Appendix - Probability density function of BTS model

The BTS model assumes that all recombination processes during thermal stimulation occur through the band-tail states (no recombination occurs through the excited state of a trap or the conduction band), from which it follows that for any assumed distribution of the band-tail states accessible from the ground state of IR sensitive traps, the integral of the probability density function is equal to one. To fulfill this criterion, the distribution can be scaled, i.e. divided by its integral. Li and Li (2013) introduce a constant A , which represents this scaling factor under this condition. We thus have

$$P(E_b)dE_b = A \exp\left(-\frac{E_b}{E_u}\right)dE_b \quad (\text{A.1})$$

Since

$$\int_{E_{b,min}}^{E_{b,max}} P(E_b)dE_b = 1 \quad (\text{A.2})$$

$$\begin{aligned} \int_{E_{b,min}}^{E_{b,max}} A \exp\left(-\frac{E_b}{E_u}\right)dE_b &= A \left[-E_u \exp\left(-\frac{E_b}{E_u}\right) \right]_{E_{b,min}}^{E_{b,max}} \\ &= AE_u \left(\exp\left(-\frac{E_{b,min}}{E_u}\right) - \exp\left(-\frac{E_{b,max}}{E_u}\right) \right) = 1 \end{aligned} \quad (\text{A.3})$$

It follows that

$$A = \frac{1}{E_u \left(\exp\left(-\frac{E_{b,min}}{E_u}\right) - \exp\left(-\frac{E_{b,max}}{E_u}\right) \right)} \quad (\text{A.4})$$

Where $E_{b,min}$ and $E_{b,max}$ represent the energies of the shallowest and deepest band-tail states thermally accessible. When integrating from $E_{b,min} \rightarrow 0$ to infinity

$$A = \frac{1}{E_u} \quad (\text{A.5})$$

and this also holds for $E_{b,max} \approx E_t$ (sufficiently in the tail of the exponential function). This has been verified through numerical calculations.

3. TOWARDS OSL-THERMOCHRONOMETRY OF THE MONT BLANC MASSIF: EXPERIMENTAL INVESTIGATIONS INTO CONSTRAINING FELDSPAR THERMAL DECAY

Abstract

Constraining thermal decay of trapped charge in infra-red (IR) sensitive traps in feldspar is essential for thermochronometric studies, but has proven complicated because it is not a simple exponential decay process. In this study we (1) investigate the thermal decay process in feldspar experimentally and (2) explore the applicability of general order kinetics and three related multiple first-order kinetic thermal decay models for feldspar relevant for infra-red stimulated luminescence (IRSL) thermochronometry on samples from the Mont Blanc massif. Isothermal decay data following different doses show that the thermal decay process in IR sensitive traps in feldspar is not controlled by the initial concentration of trapped charge, suggesting first-order or low-order kinetic behaviour. More thermally stable IRSL signals were obtained following higher temperature preheats, indicating a more thermally stable subpopulation of trapped charge with respect to the total trapped charge population obtained after the lower preheat. We show that our isothermal decay data can be well fitted using a multiple first-order kinetic model consisting of a distribution of thermal lifetimes, following from a distribution of activation energies based on a Gaussian shaped distribution of trap depths. Finally, we model trap occupancy levels to investigate the implication of multiple first-order kinetic thermal decay models for thermochronometric application.

3.1 Introduction

Luminescence thermochronometry uses charge trapping due to ionizing radiation and charge detrapping in response to ambient heat to quantitatively constrain rock cooling histories. It has been rapidly extended from conventional optically stimulated luminescence (OSL) quartz measurements (Herman et al., 2010; De Sarkar et al., 2013) to single (Guralnik et al., 2015a) and then multiple feldspar infra-red stimulated luminescence (IRSL; Li and Li, 2012; King et al., 2016a; King et al., 2016b), as well as thermoluminescence (TL; Brown et al., 2015; Biswas et al., 2018) signals. The versatility of luminescence dating and its capacity as a multi-thermochronometer (Li and Li, 2012; King et al., 2016b; Biswas et al., 2018) has enabled the derivation of cooling histories over previously inaccessible temporal scales and resolution (e.g. King et al., 2016a; Herman and King, 2018).

Constraining the thermal kinetic processes of the trapped electron population related to the mineral and the luminescence signal under investigation is central for the successful application of luminescence thermochronometry. This is done by assuming that the kinetics derived under laboratory conditions (at high temperatures, generally ≥ 170 °C, and over short timescales from

seconds to hours) describe the physical processes that occur in nature over geological timescales (ka-Ma), i.e. thermal decay at much lower temperatures (10 - 100 °C) and at a much lower rate (e.g. Yukihiro et al., 2018). Besides this assumption, there remain uncertainties on the thermally-driven processes of charge transport in naturally occurring feldspar crystals due to the complex crystal structure and defect energy levels (e.g. Poolton et al., 2009; Jain and Ankjærgaard, 2011). To characterize thermal decay in infra-red (IR) sensitive traps, isothermal decay experiments are performed by measuring IRSL signals following sample heating at a constant temperature for different durations. Isothermal decay patterns in this mineral do not follow simple exponential decay, but instead a slower thermal decay curve (e.g. Grün, 1994; Guralnik et al., 2015a; Guralnik et al., 2015b). The observed deviation may follow from a dependence on the trapped charge concentration (general order kinetics) and/or from a temporal variation through assuming a trapped charge population with a distribution of thermal lifetimes (multi first-order kinetics).

In the present study, we investigate how to constrain the thermal kinetic parameters of samples from the Mont Blanc massif. The crystalline massif has experienced fast exhumation rates (up to ~ 2 km/Myr) over the last 2 Ma (Glotzbach et al., 2011) and in addition, the thermal field appears to have changed rapidly due to fluid infiltration over the last 12,000 years (Maréchal et al., 1999). Luminescence thermochronometry can be used to constrain temporal variations in the upper crustal thermal field over the Late Quaternary. We investigate the thermal stability of two luminescence signals (IRSL₅₀ and post-IR IRSL₂₂₅), which are expected to have different thermal stabilities (Li and Li, 2011) and could therefore provide two complementary thermal constraints in a thermochronometric study (e.g. King et al., 2016b). Through a series of different isothermal decay experiments, we investigate the dependency of thermal decay in feldspar on the initial trapped charge concentration and preheat treatment. The experimental results are used to evaluate general order kinetics and multi first-order decay models for application of luminescence thermochronometry on samples from the Mont Blanc massif.

3.2 Models

To investigate thermal decay and assess the implications of this process during rock cooling, both the trapping and athermal detrapping processes in feldspar need to be characterized. Here, we give an overview of the models that are used to describe all three processes and how the kinetic parameters can be constrained from isothermal decay experiments.

3.2.1 Trapping and athermal decay

The process of trapping in IR sensitive traps during irradiation can be described as (Guralnik et al. 2015b)

$$\frac{d\left(\frac{n}{N}\right)}{dt} = \frac{\dot{D}}{D_0} \left(1 - \frac{n}{N}\right)^a \quad (1)$$

where n/N is the concentration of trapped charge, \dot{D} [Gy/s] is the radiation dose rate and D_0 [Gy] is the characteristic dose of saturation. The power a gives the order of kinetics to describe non-first order electron trapping which we limit to $a \leq 2$. After Guralnik et al. (2015b), we use the following analytical solution to fit laboratory dose response curves

$$\frac{n}{N}(t) = 1 - \left[1 - (1 - a) \frac{\dot{D}}{D_0} t\right]^{\frac{1}{1-a}} \quad (2)$$

To characterize athermal detrapping from the ground-state of the IR sensitive trap, we use the model proposed by Huntley (2006), so that

$$\frac{d\left(\frac{n}{N}\right)}{dt} = -\frac{n}{N} \tau_{tun}^{-1} \quad (3)$$

with

$$\tau_{tun} = s_{tun}^{-1} e^{r' \cdot (\rho')^{-1/3}} \quad (4)$$

where τ_{tun} [s] is the athermal lifetime of a trapped electron, which is determined by the tunnelling distance r' (dimensionless) to a recombination site in a crystal, a variable ρ' (dimensionless) which relates to the density of recombination centres, and frequency factor $s_{tun} \approx 3 \cdot 10^{15} \text{ s}^{-1}$ (after Huntley, 2006). It is assumed that recombination centres are randomly distributed and an electron will tunnel to the nearest recombination centre. Therefore, we integrate over the following probability distribution for tunnelling distance r'

$$p(r') = 3r'^2 \exp(-r'^3) \quad (5)$$

After Huntley (2006) and Kars et al. (2008), we use the following expression to fit laboratory athermal decay data

$$\frac{n(t)}{n(0)} = e^{(-\rho' \cdot (\log(1.8 \cdot s_{tun} \cdot t))^3)} \quad (6)$$

Athermal stability is also expressed as g_{2days} [%/decade] (Aitken, 1985; Huntley and Lamothe, 2001)

$$\frac{n(t)}{n(0)} = 1 - \frac{g_{2days}}{100} \cdot \log_{10} \left(\frac{t}{t_{2days}} \right) \quad (7)$$

3.2.2 Thermal decay

The isothermal decay data were fitted with two different thermal decay model types, firstly a general order kinetic model (Guralnik et al., 2015b) and secondly a range of different multiple first-order kinetic models which are based on a distribution of activation energies (Li and Li, 2013; Lambert et al., *subm.*). We outline the principles and assumptions of the models below and give the equations used to fit our experimental data.

General-order kinetics

When thermal decay follows general order kinetics, the change in the population of trapped electrons over time can be described by the following ordinary differential equation with $b > 1$

$$\frac{d\left(\frac{n}{N}\right)}{dt} = -\frac{1}{\tau_{th}} \left(\frac{n}{N}\right)^b \quad (8)$$

where $\frac{n}{N}$ is the proportion of trapped charge and τ_{th} [s] the thermal lifetime, determined by the trap depth E_t [eV], Boltzmann's constant k_B [eV/K], temperature $T(t)$ [K] at time t and frequency factor s_{th} [s⁻¹], given by

$$\tau_{th} = s_{th}^{-1} e^{\frac{E_t}{k_B T(t)}} \quad (9)$$

Since we are interested in fitting isothermal decay experiments, Eq. (8) is integrated for a constant temperature

$$\frac{n}{N}(t) = \left[\left(\frac{n_0}{N}\right)^{1-b} - (1-b) \frac{t}{\tau_{th}} \right]^{\frac{1}{1-b}} \quad (10)$$

From Eq. (10), it follows that the initial population of trapped charges n_0/N (where $n_0 = n(t=0)$), and thus the initial dose given to the sample, should affect the rate of thermal decay. This effect becomes more significant as the kinetic order b increases.

Multiple first-order kinetics

The multiple first-order kinetic models assume a distribution of thermal lifetimes through a distribution of activation energies (Lambert et al., *subm.*). These distributions follow from different assumptions: (1) the presence of an exponentially distributed density of band-tail states beneath the conduction band (BTS model; Li and Li, 2013), (2) a Gaussian distribution of trap depths (GTD model)

or (3) a combination of a distribution of band-tails states and a Gaussian distribution of trap depths (BTS + GTD model). In these models, the activation energy ($E_a = E_t - E_b$) represents the energy needed to be thermally evicted from the ground state of a trap (E_t) to a band-tail state (E_b) or the conduction band. The models are all based on delocalized thermal decay and localized ground state tunnelling (see details in Lambert et al., subm.). Since in the multiple first-order kinetic models the thermal decay rate does not depend on the initial population of trapped charge, N does not need to be considered.

The evolution of trapped charge for a constant temperature assuming a distribution of band-tail states can be described by the following equation

$$\frac{n(t)}{n(0)} = \int_0^{E_{b,max}} P_b(E_b) \cdot \exp\left(-\frac{t}{\tau_{th}}\right) dE_b \quad (11)$$

with

$$P_b(E_b) = \frac{1}{E_u} \cdot \exp\left(-\frac{E_b}{E_u}\right) \quad (12)$$

and

$$\tau_{th} = s_{th}^{-1} e^{\frac{E_t - E_b}{k_B T(t)}} \quad (13)$$

where $n(t)$ represents the number of trapped electrons, E_b [eV] is the energy of a band-tail state, E_u [eV] represents the width of the distribution of band-tail states accessible from the ground state of IR sensitive traps and E_t [eV] is the trap depth.

When considering a Gaussian distribution of trap depths E_t [eV] with a mean thermal trap depth $\mu(E_t)$ [eV] and width $\sigma(E_t)$ [eV] the evolution of trapped charge for a constant temperature can be described by

$$\frac{n(t)}{n(0)} = \int_0^{E_{t,max}} P_t(E_t) \cdot \exp\left(-\frac{t}{\tau_{th}}\right) dE_t \quad (14)$$

with

$$P_t(E_t) = \frac{1}{\sigma(E_t)\sqrt{2\pi}} \exp\left(-\frac{1}{2}\left(\frac{E_t - \mu(E_t)}{\sigma(E_t)}\right)^2\right) \quad (15)$$

Assuming that the above-mentioned distributions for band-tail states and trap depths are independent and both play a role in the thermal eviction of trapped electrons in IR sensitive traps,

the evolution of a trapped electron population with time for a constant temperature can be described by the following equation

$$\frac{n(t)}{n(0)} = \int_{E_{b,min}}^{E_{b,max}} P_b(E_b) \int_0^{E_t,max} P_t(E_t) \cdot \exp\left(-\frac{t}{\tau_{th}}\right) dE_t dE_b \quad (16)$$

3.2.3 Trap occupancy

We assume that for an IR sensitive trap with activation energy E_a and tunneling distance r' to a recombination site in a crystal, the process of charge trapping and detrapping during irradiation at a given temperature can be described by the following equation (Herman et al. 2010; Li and Li 2012; Guralnik et al. 2015b; King et al., 2016b; Herman and King, 2018)

$$\frac{d\left(\frac{n}{N}(t, E_a, r')\right)}{dt} = \frac{\dot{D}}{D_0} \cdot \left(1 - \frac{n}{N}(t, E_a, r')\right)^a - \frac{n}{N}(t, E_a, r') \frac{1}{\tau_{th}} - \frac{n}{N}(t, E_a, r') \frac{1}{\tau_{tun}} \quad (17)$$

where

$$\tau_{th} = s_{th}^{-1} e^{\frac{E_a}{k_B T(t)}} \quad \text{with} \quad E_a = E_b - E_t \quad (18)$$

and

$$\tau_{tun} = s_{tun}^{-1} e^{r' \cdot (\rho')^{-1/3}} \quad (19)$$

We solve for n/N (the ratio of trapped electrons in the IR sensitive trap) numerically and integrate over the probability distributions for the activation energy E_a (described in section 2.2.2) and the tunnelling distance r' (Eq. (14) in section 2.1).

3.3 Experimental approach

3.3.1 Overview of experiments and analyses

In this study, feldspar thermal decay of bedrock samples from the Mont Blanc massif is characterized through several isothermal decay experiments. These consist of giving an aliquot a known dose and measuring the infra-red stimulated luminescence (IRSL) signal loss following holding at a constant temperature, for different durations over laboratory timescales (Murray and Wintle, 1999). We consider the general order kinetic and multi first-order kinetic models described in the previous section (Section 2.2) and evaluate their performance based on the experimental data.

First, we explore the dose dependency of isothermal decay trends by doing the experiments for different given doses ranging over several orders of magnitude. Based on these results, we assess

whether thermal decay follows general order kinetics behaviour (Eq. (9)). For this, we derive the initial ratio of trapped charge for each given dose from the dose response curve obtained in a dosing experiment which characterizes the trapping process. Throughout laboratory measurements some athermal decay is expected, which is characterized in a fading experiment and accounted for when fitting the other luminescence data (e.g. King et al., 2016b).

Second, we investigate the applicability of multi first-order kinetic decay models based on a distribution of activation energies, and thus of thermal lifetimes, for the Mont Blanc samples. Besides evaluating the model fits of isothermal decay data following a preheat of 250 °C, we explore the effect of a higher preheat temperature (325 °C) on the thermal stability of the measured IRSL signals, which provides an indication of the applicability of this model concept. Fading experiments for both preheats were done to be able to take into account the effect of athermal decay when fitting the isothermal decay data. To distinguish amongst the distributions and assess the extent of thermal transfer during isothermal decay from non-IR sensitive traps, the latter effect was measured through recuperation experiments for both preheats.

Finally, we simulate the effect of linear cooling histories on trap occupancies to investigate the implications of multi first-order kinetic decay models for application in thermochronometry (Eq. (17)). In this analysis we use the fitting results of dosing, fading and isothermal decay experiments to describe trapping and detrapping of charge in IR sensitive traps during irradiation and rock cooling.

3.3.2 Sample preparation and instrumentation

Two granitic samples from the Mont Blanc tunnel (MBT; UNIL/MBTF4700, UNIL/MBTI4250) were prepared for analysis under subdued red light conditions. The outer 1 cm of the rock samples was removed using a diamond saw to ensure that only the light safe interior was prepared for luminescence analysis (Sohbati et al., 2012). By crushing and sieving the samples, a 180-212 μm fraction was obtained and subsequently treated with hydrochloric acid (HCl) and hydrogen peroxide (H_2O_2) to obtain a pure mineral extract. K-feldspar fractions were separated using sodium polytungstate ($\rho_{\text{K-fs}} < 2.58 \text{ g cm}^{-3}$). The purity of the K-feldspar extracts was tested using X-ray diffraction and scanning electron microscopy. Aliquots of 2 mm in diameter, consisting of a single layer of grains, were mounted on stainless steel discs (10 mm in diameter), using silicon spray as an adhesive and a mask to regulate the aliquot size.

Luminescence measurements were done at the Institute of Earth Surface Dynamics at the University of Lausanne using Risø TL-DA-20 luminescence readers (Bøtter-Jensen et al., 2010), equipped with $^{90}\text{Sr}/^{90}\text{Y}$ beta-sources with dose rates of 0.1-0.2 Gy s^{-1} . Instrument measurement reproducibility was between 1.14 and 1.26 %. Optical stimulation of feldspar was done with IR light emitting diodes

(LEDs, 870 ± 20 nm) and a filter combination of a Schott BG-3 and Schott BG-39 was used to restrict detection to the blue spectrum and UV. The luminescence signal intensity of the studied samples was very high ($> 10^6$ counts), which caused saturation of the photomultiplier tube. Therefore an aperture filter was used to reduce the signal for the dose response experiments. Preheats or stimulations at temperatures higher than 200 °C were done in a nitrogen atmosphere.

3.3.3 Experimental procedure

Luminescence measurements were made using the single aliquot regenerative dose (SAR) protocol (Murray and Wintle, 2000; Wallinga et al., 2000), which comprised preheating at 250 °C for 60 s followed by an IRSL₅₀ stimulation (at 50 °C) for 100 s and a post-IR IRSL₂₂₅ stimulation (at 225 °C) for 100 s (Buylaert et al., 2009; Thomsen et al., 2008). The applicability of the protocol was confirmed by a successful preheat plateau dose recovery test (Fig. A.2 in the Appendix). Rates of athermal decay were measured following irradiation of three aliquots of each sample with 54 Gy and preheating prior to storage for different delay times (see also Auclair et al., 2003), ranging from 5 minutes to 2 days. The test dose was kept equal to the given dose. Luminescence dose response curves were obtained through dosing experiments using the same aliquots, where the luminescence response to increasing radiation dose was measured, using a test dose of 54 Gy and a maximum dose of 4.5 kGy.

To test whether the thermal decay rates in our feldspar samples are dependent on the initial concentration of trapped charge (i.e. n/N at $t = 0$ s), isothermal decay experiments on sample UNIL/MBTI4250 were done for three regenerative doses (54, 136 and 4352 Gy) and the same test dose. Because of the magnitude of the highest dose, to make these experiments practical over laboratory timescales, they were done for the IRSL₅₀ signal only, using a short optical stimulation protocol (for experimental details, see Table 3-1; Huntley and Lamothe, 2001; Auclair et al., 2003; Guralnik et al., 2015a). We assume that the isothermal decay results using this protocol are comparable to those obtained using a long optical stimulation protocol, given that Valla et al. (2016) found similar results from athermal decay experiments using both protocols.

To investigate the effect of preheat on thermal decay rates, isothermal decay experiments on sample UNIL/MBTF4700 were done for two preheats (250 and 325 °C). Athermal decay following a 325 °C preheat was measured in a similar manner as following a 250 °C preheat. To measure isothermal decay, a previously measured aliquot was given a dose of 136 Gy and held at a constant temperature in the range of 170 - 250 °C for different periods of time ($t = 0 - 10240$ s) before measurement using the SAR protocol outlined above, including a test dose equal to the given dose (for experimental details, see Table 3-1). In the experiment with a preheat of 325°C thermal loss was also measured after holding the sample at 270 and 290 °C.

Finally, thermal transfer recuperation experiments were done on sample UNIL/MBTF4700 for the different preheats. The experiment comprised a given dose of 132 Gy, preheat (250 or 325 °C) and measuring the luminescence signal during an IRSL₅₀ (100 s) and a post-IR IRSL₂₂₅ (100 s) stimulation, after which recuperation was measured following different thermal treatments (170, 250 and 290 °C for 5120 s), again through measuring the luminescence signal during an IRSL₅₀ (100 s) and a post-IR IRSL₂₂₅ (100 s) stimulation. This sequence was followed by a test cycle during which the same dose and preheat were given, but no thermal treatment was applied before measurement of the luminescence and recuperation signals.

Isothermal decay procedure	Isothermal decay procedure (shortshine)
Regenerative dose	IRSL bleaching at 290 °C for 100 s
Preheat at 250 °C for 60 s	Regenerative dose
Heat to T_{iso} for t (0, ..., 10240 s)	Preheat at 250 °C for 60 s
IRSL at 50 °C for 100 s (L_x)	Heat to T_{iso} (170 - 230 °C) for t (0, ..., 10240 s) } *
post-IR IRSL at 225 °C for 100 s (L_x)	IRSL at 50 °C for 0.77 s (L_x)
Test dose	IRSL at 290 °C for 100 s
Preheat at 250 °C for 60 s	Test dose
IRSL at 50 °C for 100 s (T_x)	Preheat at 250 °C for 60 s
post-IR IRSL at 225 °C for 100 s (T_x)	IRSL at 50 °C for 0.77 s (T_x ; x 12)

* These two steps are alternated so that signal loss is measured after progressive decay (x 12)

Table 3-1: Procedure for SAR isothermal decay experiments, performed for $T_{iso} = 170, 190, 210, 230, 250$ °C (left) and procedure for short shine isothermal decay experiments, performed for $T_{iso} = 170, 190, 210, 230$ °C (right).

3.3.4 Constraining thermal kinetic parameters

Thermal kinetic parameters were derived through simultaneous fitting of the isothermal decay data for the different elevated temperatures (T_{iso}) specific to each experiment. We accounted for athermal decay (i.e. ground-state tunnelling) when fitting the isothermal decay data using Eq. (6), following a similar approach as King et al. (2016a). Fading times were computed as half of the irradiation time plus the time between irradiation and IR stimulation after Auclair et al. (2003). We assume a single fading parameter ρ' (Eq. (4)) in all models. In the fitting procedure, no restrictions were imposed on the thermal kinetic parameters.

3.4 Results

3.4.1 Thermal decay, dose response and fading characteristics

The MBT samples have very bright luminescence signals ($\sim 10^4$ counts/s for the IRSL₅₀ signal and $\sim 10^3$ counts/s for the post-IR IRSL₂₂₅ signal following a preheat of 250 °C), which enables precise

measurements as shown in Figure 3-1. Athermal decay rates are smaller for post-IR IRSL₂₂₅ signals than IR₅₀ signals, with g_{2days} values calculated following Huntley and Lamothe (2001) ranging from 3.5 to 3.7 %/decade for the IRSL₅₀ signal and from 1.5 to 1.8 %/decade for the post-IR IRSL₂₂₅ signal. Dose response curves do not saturate and continue to grow despite irradiation up to 4.5 kGy. Fitting them with a general order kinetics model and correcting for fading yields a kinetic order of $a \cong 2$ (i.e. the maximum limit imposed) for the IRSL₅₀ signal and $a \cong 1.7$ for the post-IR IRSL₂₂₅ signal. Figure 3-1 shows the athermal decay, dose response curve and the fading corrected and normalized trapping curve of the IRSL₅₀ signal of sample UNIL/MBTI4250. The MBT samples exhibit a similar isothermal decay pattern, which is more gradual than a simple exponential decay, both following a short shine protocol (Fig. 3-2; UNIL/MBTI4250) and a SAR protocol (Fig. 3-3, UNIL/MBTF4700).

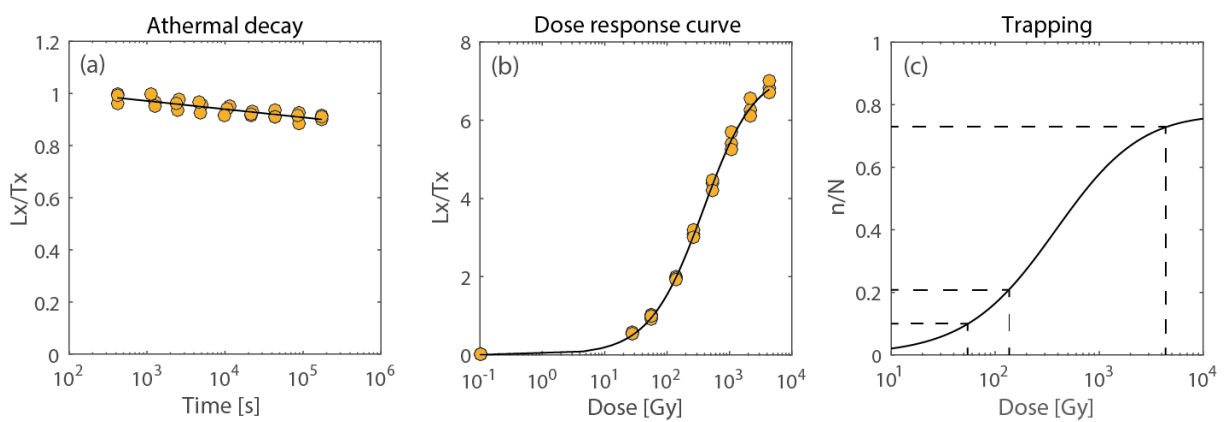


Fig. 3-1: Measured IRSL₅₀ data after a preheat of 250 °C for sample UNIL/MBTI4250. (a) Athermal decay data following a short shine protocol and model curve following Huntley (2006) and Kars et al. (2008) from which $\rho' = (2.36 \pm 0.28) \cdot 10^{-6}$ was derived, equal to $g_{2days} = 3.51 \pm 0.42$ %/decade following Huntley and Lamothe (2001). (b) Dose response curve following a SAR protocol fitted with the general order kinetics model following Guralnik et al. (2015b) from which kinetic parameters $D_0 = 405 \pm 5$ Gy and $a = 2.00 \pm 0.07$ were derived. (c) Fading corrected and normalized trapping curve; the dashed lines indicate initial populations of trapped charge ($n_0/N = 0.10, 0.21$ and 0.73) corresponding to given doses of 54, 136 and 4352 Gy in the isothermal decay dose dependency experiment (Section 4.2).

3.4.2 Isothermal decay dose dependency

Figure 3-2 shows the isothermal decay data of the IRSL₅₀ signal of sample UNIL/MBTI4250 for doses of 54, 136 and 4352 Gy, which were obtained after a preheat of 250 °C using a short shine protocol. Corresponding ratios of initially trapped electrons of $n_0/N = 0.10, 0.21$ and 0.73 were derived from fitting the sample dose response curve with the general order kinetic model and correcting for fading (Section 2.1; Fig. 3-1 c; Table A.2 in the Appendix for the derived trapping parameters). The isothermal decay data are similar despite the different regenerative doses used (Fig. 3-2a,b,c),

although the ratio between the data corresponding to the lowest and highest dose shows a slight increase for longer time delays, which is more pronounced at higher temperatures (Fig. 3-2d).

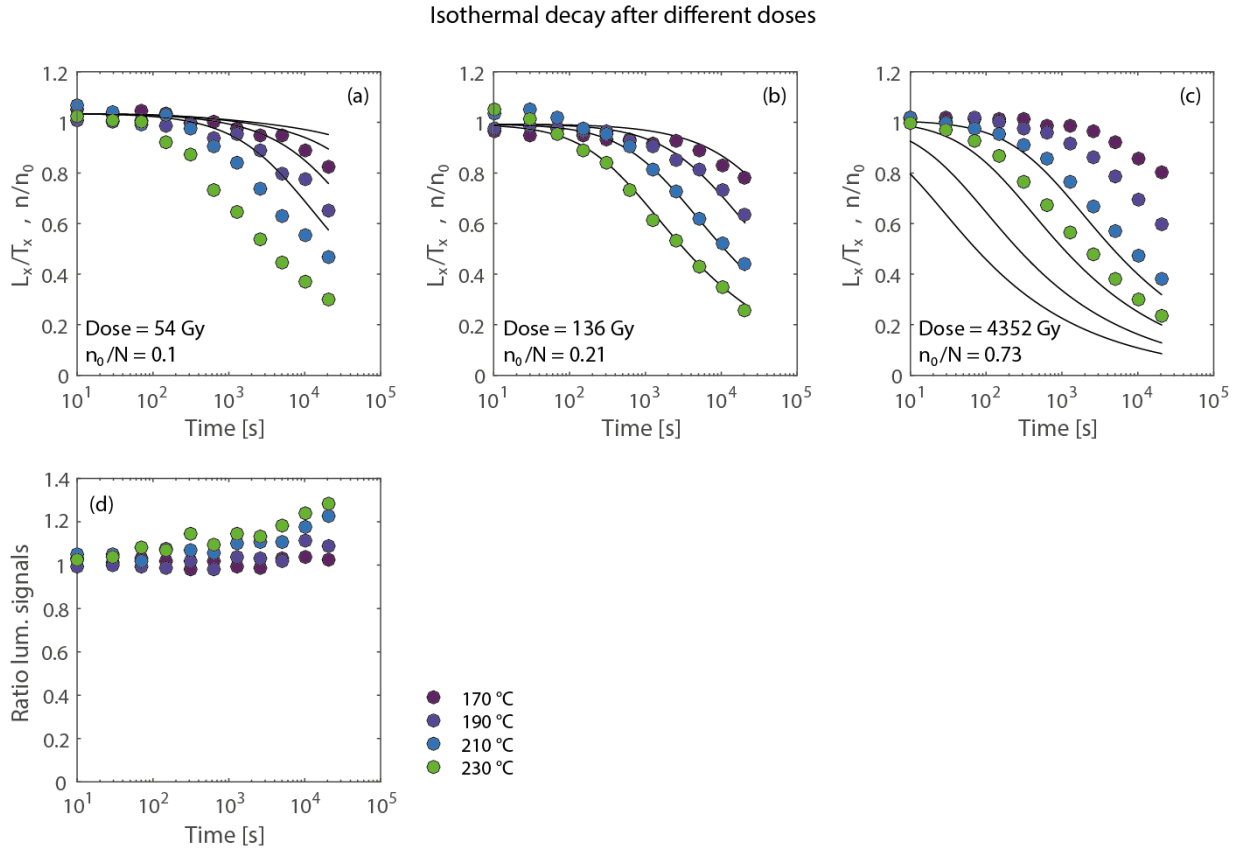


Fig. 3-2: (a-c) Isothermal decay data for the IRSL₅₀ signal after a preheat of 250 °C of sample UNIL/MBTI4250 in response to different given doses ($T = 170, 190, 210, 230$ °C and time delays $t = 0 - 20470$ s) following a short shine protocol. The isothermal decay data are fitted using a general order kinetics model (including dose dependency, see section 2.1.1 for details). L_x/T_x values are the sensitivity corrected and normalized luminescence responses, and modeled lines show the ratio of the remaining trapped charge population (n) relative to the initial trapped charge population (n_0). (d) Ratio between luminescence signal responses shown in (a) and (c).

A general order kinetic model, including a dependence on the initial ratio of trapped electrons (Eq. (9)), was fitted to the 136 Gy experiment isothermal decay data (Fig. 3-2b; $n_0/N = 0.21$). The derived thermal kinetic parameters are $s_{th} = 10^{12.4 \pm 0.9} \text{ s}^{-1}$, $E_t = 1.34 \pm 0.07 \text{ eV}$ and $b = 4.15 \pm 0.34$. This model is able to fit the shape of the thermal decay trend (Fig. 3-2b), but the same parameter set cannot describe the other two experimental data sets when their specific initial conditions are used to calculate the model curve (Fig. 3-2a,c; $n_0/N = 0.10$ and 0.73 , respectively). When fitting the individual data sets per initial dose, the resulting thermal kinetic parameters vary considerably: s_{th} values vary by more than 2 orders of magnitude, while E_t and b values vary by approximately 10 % (see Table A.2 in the Appendix). When we apply a general order kinetics model assuming $n_0/N = 1$,

following Guralnik et al. (2015b), we obtain a similar high kinetic order $b > 4$. It is not possible to fit the data if b is fixed to ≤ 2 , i.e. assuming second order kinetics.

3.4.3 Isothermal decay preheat dependency

The isothermal decay data for sample UNIL/MBTF4700 in Figure 3-3, obtained after a preheat at 250 °C using a SAR protocol, indicate that the IRSL₅₀ signal is thermally less stable than the post-IR IRSL₂₂₅ signal. When an exponential distribution of band-tail states is assumed (BTS model; Fig. 3-3a,c), the model fit approximates the observed data trend, i.e. within 15 % uncertainty for the IRSL₅₀ signal and within 10 % uncertainty for the post-IR IRSL₂₂₅ signal, but there are systematic mismatches that are visible in the residuals per individual temperature (Fig. 3-3b,d). Deviation from the measurements is more pronounced for the longer delays and high temperatures (note the log-timescale). A model based on a Gaussian distribution of trap depths enables an improved fit to the data of sample UNIL/MBTF4700 (GTD model; Fig. 3-3e,g). Residuals are reduced to within ~5 % and show less scatter when compared to those of the BTS model, although a low-amplitude wavelike systematic error is observed (Fig. 3-3f,h). Fitting this data set with a model combining a distribution for band-tail states and trap depths (BTS + GTD model) yields a very similar fit with nearly identical model parameters as for the GTD model; it appears that the band-tail states distribution has become practically redundant for both signals, yielding a width of 0 eV for the IRSL₅₀ signal and 0.01 eV for the post-IR IRSL₂₂₅ signal (Fig. A.3 in the Appendix).

Preheat [°C]	Signal	Model	$\log_{10}(s_{th})$	E_t or $\mu(E_t)$ [eV]*	$\sigma(E_t)$ [eV]	E_u [eV]**	τ_{th} [y]***
250	IRSL ₅₀	BTS	12.4 ± 0.8	1.67 ± 0.08	-	0.09 ± 0.01	2.04E+09
	post-IR IRSL ₂₂₅		11.5 ± 0.8	1.65 ± 0.08	-	0.12 ± 0.01	7.24E+09
325	IRSL ₅₀	BTS	11.3 ± 0.3	1.68 ± 0.03	-	0.07 ± 0.00	3.84E+10
	post-IR IRSL ₂₂₅		10.6 ± 0.3	1.65 ± 0.03	-	0.07 ± 0.00	5.75E+10
250	IRSL ₅₀	GTD	13.1 ± 0.3	1.66 ± 0.03	0.10 ± 0.00	-	2.72E+08
	post-IR IRSL ₂₂₅		12.1 ± 0.3	1.61 ± 0.03	0.13 ± 0.00	-	3.63E+08
325	IRSL ₅₀	GTD	11.5 ± 0.2	1.64 ± 0.02	0.07 ± 0.00	-	4.84E+09
	post-IR IRSL ₂₂₅		10.9 ± 0.2	1.62 ± 0.02	0.08 ± 0.00	-	8.61E+09
250	IRSL ₅₀	BTS + GTD	13.1 ± 0.3	1.66 ± 0.03	0.10 ± 0.00	0.00	2.72E+08
	post-IR IRSL ₂₂₅		12.1 ± 0.3	1.62 ± 0.03	0.13 ± 0.00	0.01	5.43E+08
325	IRSL ₅₀	BTS + GTD	11.5 ± 0.2	1.68 ± 0.02	0.06 ± 0.00	0.04 ± 0.01	2.42E+10
	post-IR IRSL ₂₂₅		10.9 ± 0.2	1.65 ± 0.02	0.08 ± 0.01	0.03 ± 0.01	2.88E+10

Table 3-2: Thermal detrapping parameters derived through application of the BTS, GTD and BTS + GTD model on IRSL₅₀ and post-IR IRSL₂₂₅ isothermal decay data of sample UNIL/MBTF4700 after different preheats (250 and 325 °C). Fitting was done using the least squares method, parameter uncertainties are reported at the 68 %

confidence interval. E_t corresponds to the BTS model, whereas $\mu(E_t)$ is used in the GTD and BTS + GTD model. **When fitting the BTS + GTD model to the isothermal decay data obtained after a preheat of 250 °C, large uncertainties were found for $\mu(E_t)$ and E_u , which may originate from a numerical correlation between these two parameters; subsequently, E_u was fixed to the best-fit value to evaluate the uncertainties of the other parameters. This did not have an effect on the parameter values. ***Thermal lifetimes were calculated for s_{th} and E_t or $\mu(E_t)$ at an ambient temperature of 15 °C. As these values do not represent the full distributions, they are only indicative for the order of magnitude.

The isothermal decay trend of sample UNIL/MBTF4700 following a preheat of 325 °C is more stable and slightly steeper (Fig. A.4 in the Appendix) compared to the thermal decay trends following a preheat of 250 °C (Figs. 3-3 and A.3 in the Appendix). Athermal decay parameters indicate that the IRSL₅₀ signal after the preheat of 325 °C is also slightly athermally more stable than after the preheat of 250 °C, with g_{2days} values of 3.35 ± 0.55 and 3.74 ± 0.12 %/decade, respectively. The post-IR IRSL₂₂₅ signal after the higher preheat shows a slight decrease in athermal stability with g_{2days} values of 1.77 ± 0.93 and 1.48 ± 0.26 %/decade, respectively. Although the BTS model fit to the isothermal decay data of the 325 °C preheat (Fig. A.4a-d) shows less deviation from the data in comparison with the model fit to the 250 °C preheat data, an exponential distribution cannot fully explain the observed trend. An improved fit to these data is obtained by the GTD model (Fig. A.4e-h) and comparable results are found when the model assuming a combination of a distribution for band-tail states and trap depths (BTS + GTD model) is applied (Fig. A.4i-l). The thermal transfer recuperation experimental results are similar for both preheats, recuperation was less than 6 % and the results do not show a clear trend with temperature (Fig. A.5 in the Appendix).

Best-fit parameter values derived through application of the multiple first-order kinetic models on the isothermal thermal decay data sets after the different preheat treatments are given in Table 3-2. While E_t or $\mu(E_t)$ values are similar or within uncertainty for the different preheat temperatures, the s_{th} values are consistently lower for the preheat of 325 °C compared to those for the preheat of 250 °C. To compare the thermal stability of the two luminescence signals after both preheats, we show thermal decay curves as predicted by these models at 70 °C (Fig. 3-4), a temperature within the temperature window (~30-100 °C) for which luminescence thermochronometry may provide information on a rock sample's cooling history. The IRSL₅₀ and post-IR IRSL₂₂₅ model curves for the 250 °C preheat are thermally less stable than for the 325 °C preheat, except at the end of the decay where the GTD and BTS + GTD curves overlap. The difference in thermal stability between the two luminescence signals is less pronounced for the 325 °C preheat than it is for the 250 °C preheat. The IRSL₅₀ signal is typically less stable than the post-IR IRSL₂₂₅ signal following either preheat, except for the first part of the decay curves (note the log-timescale).

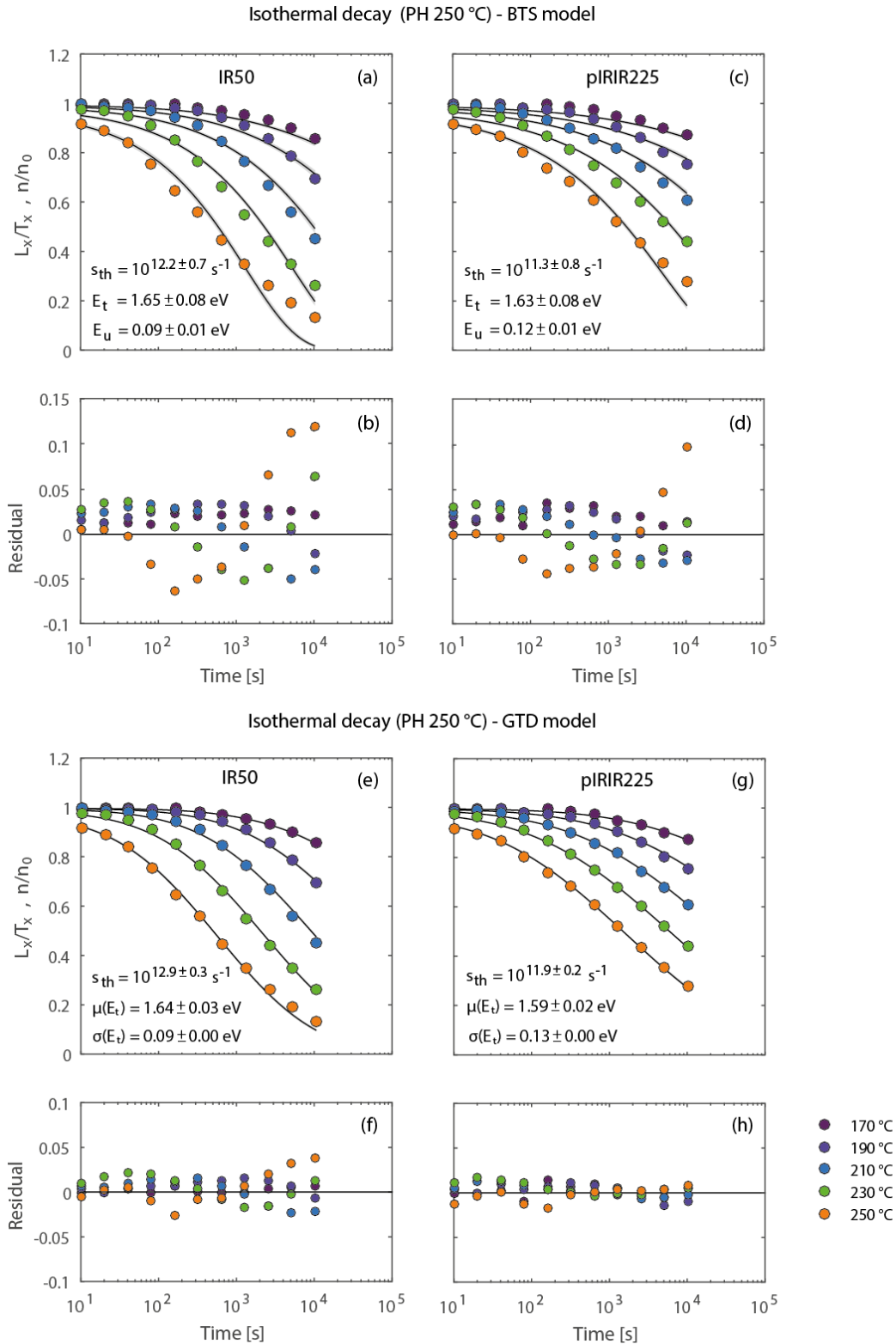


Fig. 3-3: Isothermal decay data for sample UNIL/MBTF4700 after a preheat of 250 °C ($T = 170, 190, 210, 230, 250$ °C and time delays $t = 0 - 10240$ s), fitted with the band-tail states model (Li and Li, 2013) for the $IRSL_{50}$ signal (a) and post-IR $IRSL_{225}$ signal (c). Model residuals are shown in (b) and (d). The same data is fitted with the model based on a distribution of activation energies due to the presence of band-tail states and a Gaussian trap distribution for the $IRSL_{50}$ signal (e) and post-IR $IRSL_{225}$ signal (g). Model residuals are shown in (f) and (h).

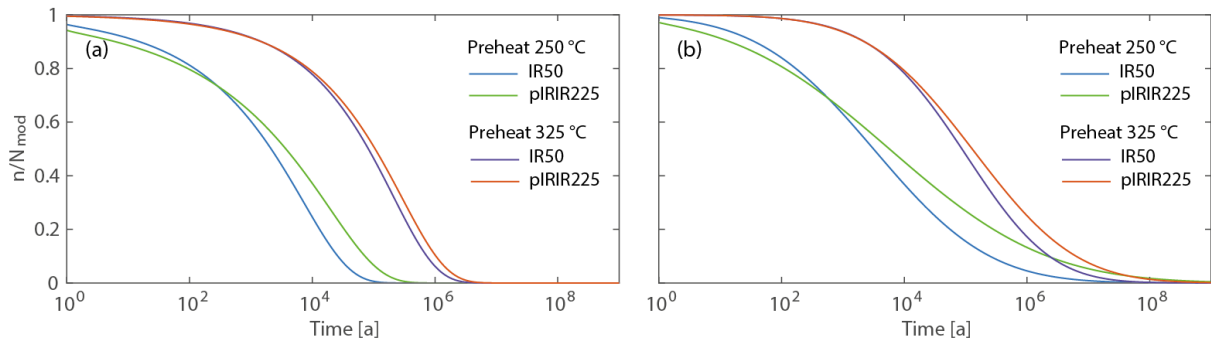


Fig. 3-4: Modelled thermal decay at 70 °C for the $IRSL_{50}$ and post-IR $IRSL_{225}$ signals of sample MBT-F 4700 using the (a) BTS and (b) GTD and BTS + GTD model. Athermal decay was included during the fitting procedure (see Table A.1 in the Appendix for parameters), but not in the calculation of the model curves to enable the direct comparison of the different preheat treatments on the thermal stability. Decay curves are expressed by the trap occupancy level (n/N_{mod}) at time t [a]. To show the full decay, we applied an initial condition of $n/N_{mod}(t = 0) = 1$.

3.4.4 Modelling trap occupancy for a linear cooling history

To test the implications of the multi first-order decay models for thermochronometric applications, trap occupancy levels (n/N_{lin} values) following three different linear cooling scenarios (150, 450 and 900 °C/Myr) were calculated for sample UNIL/MBF4700 based on the 250 °C preheat best-fit kinetic parameters (Table 3-2) and the trapping and athermal decay parameters given in Table A.1 of the Appendix (Fig. 3-5). The obtained n/N_{lin} values show distinct clusters for each of the linear cooling scenarios. In agreement with the difference in thermal stability between the models following from fitting the isothermal decay data, the BTS model consistently yields lower n/N_{lin} values than the GTD and BTS + GTD model.

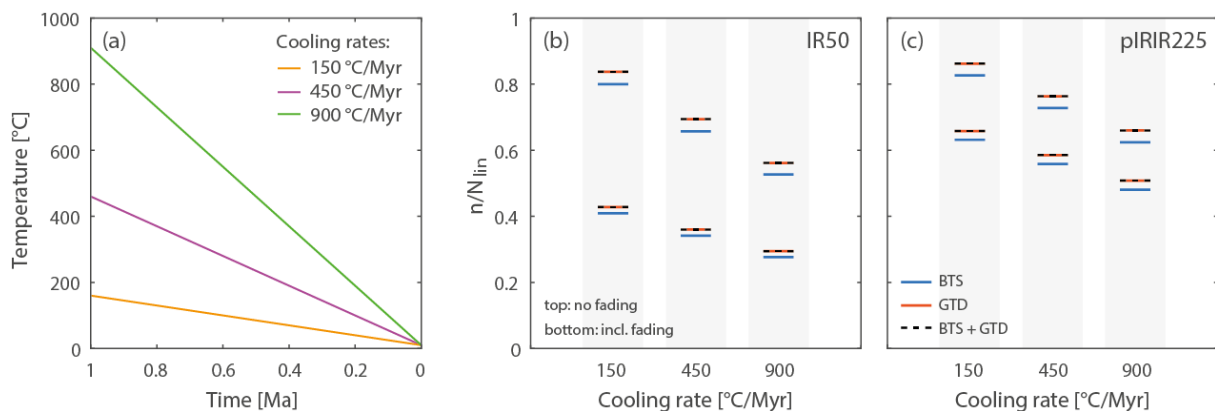


Fig. 3-5: Modelled n/N_{lin} values for three different linear cooling scenarios: 150, 450 and 900 °C/Myr for the (b) $IRSL_{50}$ and (c) post-IR $IRSL_{225}$ signal of sample UNIL/MBF4700 after a preheat of 250 °C, without the effect of athermal decay (top) and including the effect of athermal decay (bottom). A characteristic environmental dose rate $\dot{D} = 10$ Gy/ka was assumed and a (final) sample temperature of 10 °C.

3.5 Discussion

3.5.1 Dose response and dose dependency isothermal decay

The charge trapping behaviour measured using IRSL₅₀ and post-IR IRSL₂₂₅ stimulation in feldspar crystals from the MBT samples does not follow simple saturating exponential growth (e.g. IRSL₅₀ of sample UNIL/MBTI4250 in Fig. 3-1). The continuously increasing luminescence signals in response to high laboratory doses could be explained by the samples having a maximum trapped charge capacity greater than reached in this experiment, or alternatively may reflect increasing trapping capacity with dosing, although the latter is subject to debate (e.g. Lowick et al., 2010; Chapot et al., 2012).

Similarly, the trend in thermal decay is more gradual than simple exponential decay as is illustrated for sample UNIL/MBTI4250 in Fig. 3-2a-c. The comparable isothermal decay patterns following different doses (Fig. 3-2) show that there is only a slight dependence of thermal decay on the initial population of trapped electrons for the studied feldspar crystals. This is not commensurate with a general order kinetic model including a dependency on the initial population of trapped charge, which predicts that the rate of signal loss should be strongly dependent on the initial trapped charge population. The observed decay implies that the net effect of mechanisms associated with general order kinetics (e.g. retrapping of electrons, which is dependent on the fraction of available traps) is subordinate in the isothermal decay process. The low recuperation signals measured (Fig. A.5 in the Appendix) also indicate a limited effect of retrapping from non IR sensitive traps.

Pronounced dose dependency is not observed for sample UNIL/MBTI4250, which deviates strongly from simple first-order decay (Fig. 3-2). The same investigation was done for a sample that exhibits near simple first-order isothermal decay behaviour (UNIL/NB123, see Section 1.1 in the Appendix) and the outcome is similar, i.e. no pronounced dose dependency is observed (Fig. A.1 in the Appendix). Li and Li (2013) have reported similar findings for a different sedimentary K-feldspar sample. The results suggest that in all of these samples the thermal decay process is of relatively low kinetic order and may be sufficiently approximated by a model based on (multi) first-order kinetics. The observed behaviour explains why assuming an initial condition of $n_0/N = 1$ results in a satisfactory fit to the data, irrespective of the given dose before isothermal holding. However, where this assumption is made, the model fit for the MBT samples requires a remarkably high kinetic order of $b > 4$. In addition, the initial condition n_0/N is assumed to be 1 (i.e. a fully saturated crystal), which is commonly not the case in laboratory experiments and not valid in naturally exhuming settings, where the ratio of trapped charge is initially 0 and accumulates as the rock travels towards the surface and cools progressively.

3.5.2 Distribution of activation energies and preheat dependency isothermal decay

The multi first-order kinetic model fits shown in Figure 3-3 illustrate that a distribution of activation energies, and thus of thermal lifetimes, can give rise to a slower than simple exponential isothermal decay curve as is observed for sample UNIL/MBTF4700. The presence of band-tail states facilitates electron escape, i.e. for part of the trapped electron population relatively low activation energy is needed for detrapping to occur, which corresponds to the first part of the isothermal decay curve. However, the assumption of an exponential distribution of the density of band-tail states (BTS model) results in an asymmetric thermal decay path, i.e. from gradual to more rapid decay, which does not match the more symmetrical and overall gradual experimental decay trend observed for this sample (Fig. 3-3a-d). A Gaussian distribution of trap depths introduces a range of both shallow and deep energy states and forms a symmetrically shaped, smooth distribution of activation energies, in accordance with the data trend of sample UNIL/MBTF4700 (Fig. 3-3e-h). For this sample, fitting the data with a combination of distributions for both band-tail states and trap depths (BTS + GTD model) yields negligible advantages over the GTD model. The minor effect of thermal transfer from non IR sensitive traps (Fig. A.5 in the Appendix) is not sufficient to explain the deviation of the band-tail states model from the isothermal decay data.

The thermally more stable signals after the 325 °C preheat (Fig. A.3 in the Appendix) indicates the importance of using the same measurement conditions for all the luminescence experiments in a thermochronometric study (i.e. dosing, fading and isothermal decay experiments). These results are in agreement with the assumption of a distribution of activation energies, or more generally a distribution of thermal lifetimes, for trapped charge in the IR sensitive traps. The resulting trapped charge after the higher preheat can be regarded as a sub-population of the trapped charge in the IRSL sensitive traps after the lower preheat, as is consistent with the modelled thermal decay curves for both preheats shown in Figure 3-4; the population of trapped charge following the 250 °C preheat includes a thermally less stable sub-population that was evicted during the 325 °C preheat, but they share the thermally more stable portion as illustrated by the coinciding curves at the end of the modelled decay. Similarly, an increase in athermal stability may be expected, which we observed for the IRSL₅₀ signal, although this is not significant (within uncertainty) and was also found by Murray et al. (2009, Fig. 3-3b). Based on these results, this effect is minor for the investigated MBT sample.

A multi first-order kinetic decay model based on a distribution of activation energies, following from the assumption of a Gaussian trap depth distribution, fits the isothermal decay data of the MBT samples and yields plausible thermal kinetic parameters. The dose dependency experimental results indicate low-order kinetic behaviour and preheat dependent thermal stability corresponds with a trapped electron population with different thermal lifetimes, possibly due to a variety of activation

energies. We do not exclude the role of other charge transfer mechanisms, such as localized transitions via the excited state in IR sensitive traps (Mandowski, 2004; Jain et al. 2015; Pagonis et al., 2017), in contributing to the distributed character of thermal decay. Although it is not possible to specify the exact nature of charge transport following from the analyses done in this study, a distribution-based model can be used to explore thermal decay in feldspar and to reconstruct cooling histories in thermochronometric applications (Fig. 3-5; see also Lambert et al., *subm.*).

3.6 Conclusions

Constraining thermal decay of trapped charge in IR sensitive traps in feldspar is essential for thermochronometric studies, but not straightforward as isothermal decay patterns in this mineral do not follow simple exponential decay. The series of experimental IRSL results on mineral extracts of Mont Blanc bedrock samples provide further insights into the thermal decay processes of feldspars. Similar isothermal decay patterns in experiments with varying doses indicate that these processes are not governed by the initial amount of trapped charge; the results show only minor dose dependency. We conclude that thermal decay of trapped charge IR sensitive traps in our samples is controlled by first-order or low-order kinetic processes and that the net effect of mechanisms associated with general order kinetics does not play a dominant role.

A multiple first-order kinetic decay model, comprised of a sum of thermal decay rates, can successfully fit deviation from a simple exponential decay. Such decay may be attributed to a distribution of activation energies associated with band-tail states below the conduction band. However, isothermal decay data of samples from the Mont Blanc massif do not exhibit the asymmetrical decay trend that the band-tail states model predicts. A Gaussian shaped distribution of activation energies, following from a Gaussian trap depth distribution, provides a better fit to these data. Isothermal decay data after a higher preheat temperature indicates increased thermal stability, which is in agreement with the assumption of a distribution of activation energies, or more generally, a distribution of thermal lifetimes. Thus, experimental design may affect the IRSL response and associated kinetic parameters which characterize sample thermal stability. This emphasizes the importance of consistency throughout all experiments. While further experiments are needed to discriminate between and quantify charge transport mechanisms that play a role during thermal decay, a first-order kinetic decay model based on a Gaussian distribution such as presented in this study can be used to characterize thermal detrapping to derive recent cooling histories. Following the validation of this model in a known thermal steady-state setting (Lambert et al., *subm.*), we regard it as appropriate for samples from the Mont Blanc massif.

Acknowledgements

We thank the Cantonal Museum of Geology in Lausanne (Switzerland) for providing the MBT samples and Sally Lowick for access to the Bern luminescence laboratory for sample chemical treatment whilst the luminescence laboratory at the University of Lausanne was being constructed. This research was funded by Swiss National Fund (SNF) grant numbers PP00P2-38956 and 200021-127127 awarded to FH, PZ00P2_148191 and PP00P2_170559 awarded to PGV, and PZ00P2-167960 awarded to GEK. We are grateful to Rabiul Haque Biswas for useful discussions and to Benny Guralnik and Mayank Jain for their constructive reviews.

References

- Aitken, M.J., 1985. Thermoluminescence dating. Academic press.
- Auclair, M., Lamothe, M., Huot, S., 2003. Measurement of anomalous fading for feldspar IRSL using SAR. *Radiation measurements* 37, 487-492.
- Biswas, R.H., Herman, F., King, G.E., Braun, J., in revision. Thermoluminescence of feldspar as a multi-thermochronometer to constrain the temporal variation of rock exhumation in the recent past. *Earth and Planetary Science Letters*.
- Bøtter-Jensen, L., Thomsen, K.J., Jain, M., 2010. Review of optically stimulated luminescence (OSL) instrumental developments for retrospective dosimetry. *Radiation Measurements* 45, 253-257.
- Brown, N., Rhodes, E., Harrison, T.M., 2017. Using thermoluminescence signals from feldspars for low-temperature thermochronology. *Quaternary Geochronology* 42, 31-41.
- Buylaert, J.-P., Murray, A., Thomsen, K.J., Jain, M., 2009. Testing the potential of an elevated temperature IRSL signal from K-feldspar. *Radiation Measurements* 44, 560-565.
- Chapot, M., Roberts, H., Duller, G., Lai, Z., 2012. A comparison of natural-and laboratory-generated dose response curves for quartz optically stimulated luminescence signals from Chinese Loess. *Radiation Measurements* 47, 1045-1052.
- De Sarkar, S., Mathew, G., Pande, K., Chauhan, N., Singhvi, A.K., 2013. Rapid denudation of Higher Himalaya during late Pliocene, evidence from OSL thermochronology. *Geochronometria* 40, 304-310.
- Guralnik, B., Jain, M., Herman, F., Ankjær, C., Murray, A.S., Valla, P.G., Preusser, F., King, G.E., Chen, R., Lowick, S.E., 2015a. OSL-thermochronometry of feldspar from the KTB borehole, Germany. *Earth and Planetary Science Letters* 423, 232-243.
- Guralnik, B., Li, B., Jain, M., Chen, R., Paris, R.B., Murray, A.S., Li, S.-H., Pagonis, V., Valla, P.G., Herman, F., 2015b. Radiation-induced growth and isothermal decay of infrared-stimulated luminescence from feldspar. *Radiation Measurements* 81, 224-231.
- Herman F., King G.E., 2018. Luminescence Thermochronometry: Investigating the Link between Mountain Erosion, Tectonics and Climate. *Elements: An International Magazine of Mineralogy, Geochemistry, and Petrology* 14, 33-38.

- Herman, F., Rhodes, E.J., Braun, J., Heiniger, L., 2010. Uniform erosion rates and relief amplitude during glacial cycles in the Southern Alps of New Zealand, as revealed from OSL-thermochronology. *Earth and Planetary Science Letters* 297, 183-189.
- Huntley, D., 2006. An explanation of the power-law decay of luminescence. *Journal of Physics: Condensed Matter* 18, 1359.
- Huntley, D.J., Lamothe, M., 2001. Ubiquity of anomalous fading in K-feldspars and the measurement and correction for it in optical dating. *Canadian Journal of Earth Sciences* 38, 1093-1106.
- Jain, M., Ankjærgaard, C., 2011. Towards a non-fading signal in feldspar: insight into charge transport and tunnelling from time-resolved optically stimulated luminescence. *Radiation Measurements* 46, 292-309.
- Jain, M., Sohbati, R., Guralnik, B., Murray, A. S., Kook, M., Lapp, T., Buylaert, J. P., 2015. Kinetics of infrared stimulated luminescence from feldspars. *Radiation Measurements* 81, 242-250.
- Kars, R., Wallinga, J., Cohen, K., 2008. A new approach towards anomalous fading correction for feldspar IRSL dating—tests on samples in field saturation. *Radiation Measurements* 43, 786-790.
- King, G.E., Herman, F., Guralnik, B., 2016a. Northward migration of the eastern Himalayan syntaxis revealed by OSL thermochronometry. *Science* 353, 800-804.
- King, G.E., Herman, F., Lambert, R., Valla, P., Guralnik, B., 2016b. Multi-OSL-thermochronometry of feldspar. *Quaternary Geochronology* 33, 76-87.
- Lambert, R., King, G.E., Valla, P.G., Herman, F., *subm.* Validating multiple first-order kinetic models for feldspar thermal decay in luminescence thermochronometry. *Radiation Measurements*.
- Li, B., Li, S.-H., 2011. Luminescence dating of K-feldspar from sediments: a protocol without anomalous fading correction. *Quaternary Geochronology* 6, 468-479.
- Li, B., Li, S.-H., 2012. Determining the cooling age using luminescence-thermochronology. *Tectonophysics* 580, 242-248.
- Li, B., Li, S.-H., 2013. The effect of band-tail states on the thermal stability of the infrared stimulated luminescence from K-feldspar. *Journal of Luminescence* 136, 5-10.
- Lowick, S.E., Preusser, F., Wintle, A.G., 2010. Investigating quartz optically stimulated luminescence dose–response curves at high doses. *Radiation Measurements* 45, 975-984.
- Mandowski, A., 2004. Semi-localized transitions model for thermoluminescence. *Journal of Physics D: Applied Physics* 38, 17.
- Murray, A., Buylaert, J.-P., Thomsen, K.J., Jain, M., 2009. The effect of preheating on the IRSL signal from feldspar. *Radiation Measurements* 44, 554-559.
- Murray, A., Wintle, A., 1999. Isothermal decay of optically stimulated luminescence in quartz. *Radiation Measurements* 30, 119-125.
- Murray, A., Wintle, A., 2000. Application of the single-aliquot regenerative-dose protocol to the 375 C quartz TL signal. *Radiation Measurements* 32, 579-583.
- Pagonis, V., Chen, R., Kulp, C., Kitis, G., 2017. An overview of recent developments in luminescence models with a focus on localized transitions. *Radiation Measurements*.

- Poolton, N., Kars, R., Wallinga, J., Bos, A., 2009. Direct evidence for the participation of band-tails and excited-state tunnelling in the luminescence of irradiated feldspars. *Journal of Physics: Condensed Matter* 21, 485505.
- Sohbati, R., Murray, A.S., Chapot, M.S., Jain, M., Pederson, J., 2012. Optically stimulated luminescence (OSL) as a chronometer for surface exposure dating. *Journal of Geophysical Research* 117.
- Thomsen, K.J., Murray, A.S., Jain, M., Bøtter-Jensen, L., 2008. Laboratory fading rates of various luminescence signals from feldspar-rich sediment extracts. *Radiation Measurements* 43, 1474-1486.
- Wallinga, J., Murray, A., Wintle, A., 2000. The single-aliquot regenerative-dose (SAR) protocol applied to coarse-grain feldspar. *Radiation Measurements* 32, 529-533.
- Yukihara, E., Coleman, A., Biswas, R., Lambert, R., Herman, F., King, G., *subm.* Thermoluminescence Analysis for Particle Temperature Sensing and Thermochronometry: Principles and Fundamental Challenges. *Radiation Measurements*.

Appendix

A.1 Additional experimental results

Dose dependency isothermal decay

An additional sample from Namche Barwa (UNIL/NB123) was analyzed (further analytical details are given in King et al., 2016b), because of its near first-order kinetic behaviour. The thermal decay behaviour of sample UNIL/NB123 shows only a slight dose dependency in comparison to what is predicted by application of a general order kinetics model (without making an assumption on the initial condition), similar to the MBT sample, although it is thermally less stable (i.e. it decays more rapidly) and the order of kinetics is lower (see Fig. A.1 and Tables A.2 and A.3 in the Appendix). When these isothermal decay data sets corresponding to varying doses are fitted using the approach of Guralnik et al. (2015b), b values of 2.5-3 were obtained.

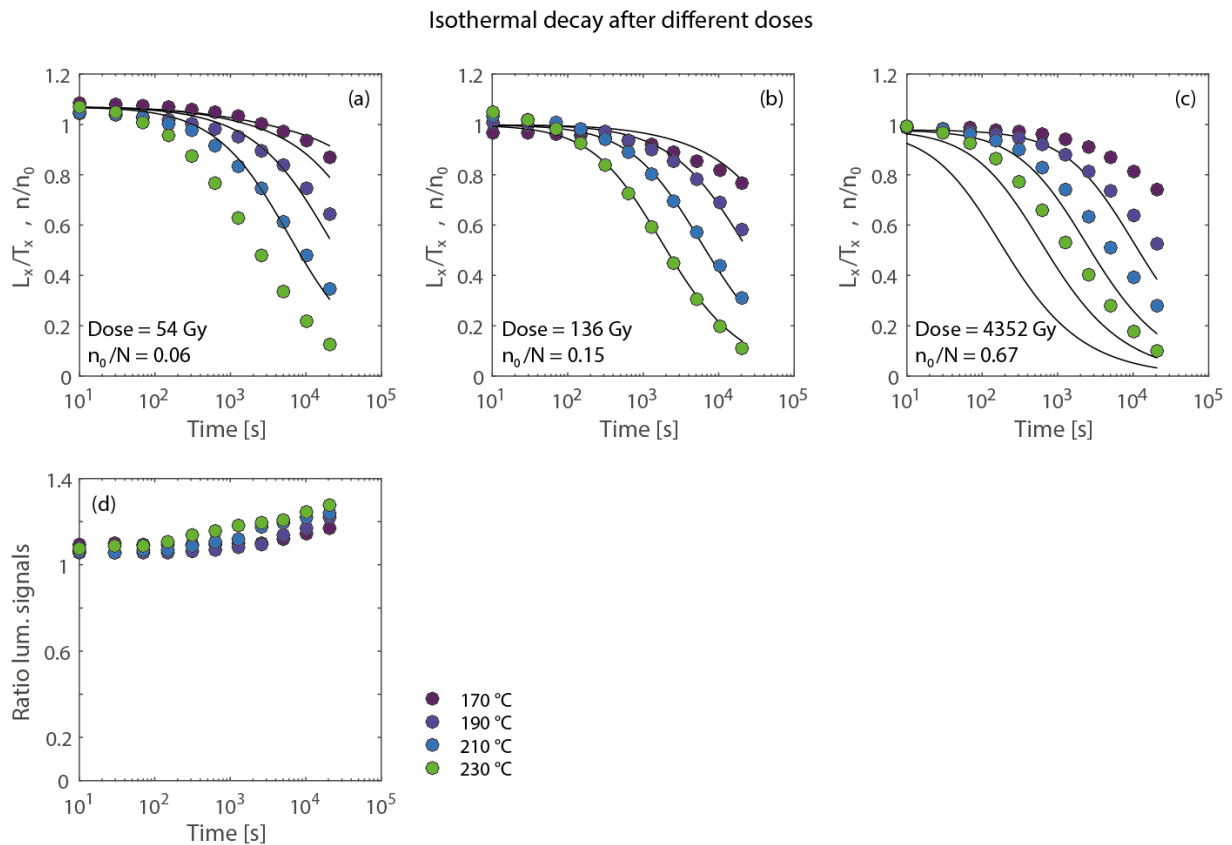


Fig. A.1: (a-c) Isothermal decay data for the IRSL₅₀ signal after a preheat of 250 °C of sample UNIL/NB123 in response to different doses ($T = 170, 190, 210, 230$ °C and time delays $t = 0 - 20470$ s) following a short shine protocol. The isothermal decay data are fitted using a general order kinetics model (including dose dependency, see section 2.1 for details). L_x/T_x values are the sensitivity corrected and normalized luminescence responses and modeled lines show the ratio of the remaining trapped charge population (n) relative to the initial trapped charge population (n_0). (d) Ratio of luminescence signal responses shown in (a) and those shown in (c).

Dose recovery preheat plateau data

Figure A.2 shows the results of the dose recovery preheat plateau test. Doses are well recovered for both the IRSL₅₀ and post-IR IRSL₂₂₅ signal, confirming that preheats from 250 to 325 °C can be used in the experiments. Since fading is not included, the values for the IRSL₅₀ signal are expected to be slightly lower than 1.

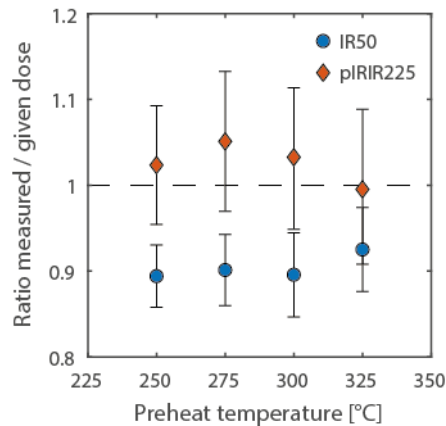


Fig. A.2: Results of dose recovery preheat plateau experiment for the IRSL₅₀ and post-IR IRSL₂₂₅ signals of sample UNIL/MBTF4700 for a given dose of 455 Gy and preheats of 250, 275, 300 and 325 °C. All aliquots were thermally bleached by heating them to 450 °C at a heating rate of 5 °C/s. Residuals were measured in response to sunlight bleaching and comprised <1 % of the given dose. Where residuals measured after a thermal bleach are expected to be smaller, they are considered to be negligible.

Isothermal decay data preheat 250 °C and 325 °C

Figure A.3 shows the isothermal decay data of sample UNIL/MBTF4700 following a preheat of 250 °C, fitted with the BTS + GTD model. The model yields a very similar fit with nearly identical model parameters as for the GTD model.

The isothermal decay data of sample UNIL/MBTF4700 following a preheat of 325 °C are shown in Figure A.4. The decay trend for both luminescence signals is more stable and slightly steeper compared to the decay trends following a preheat of 250 °C (Fig. 3-3 and A.3). These data exhibit less deviation from what is predicted by the BTS model, although an exponential distribution still cannot fully explain the data and the GTD and BTS + GTD models provide an improved fit to the data. Best-fit parameter values are given in Table 3-2.

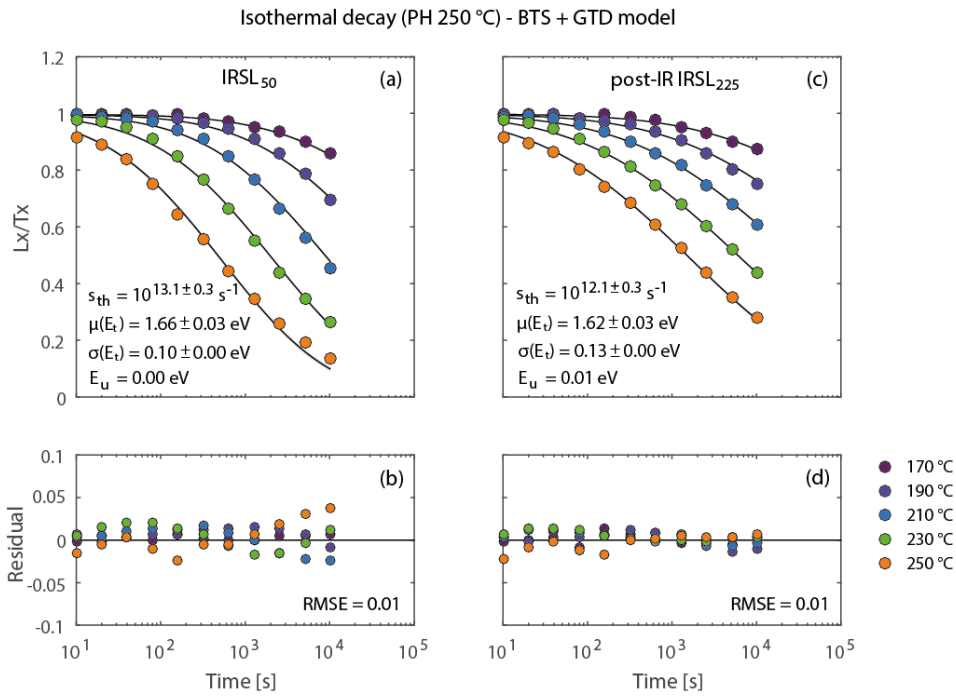
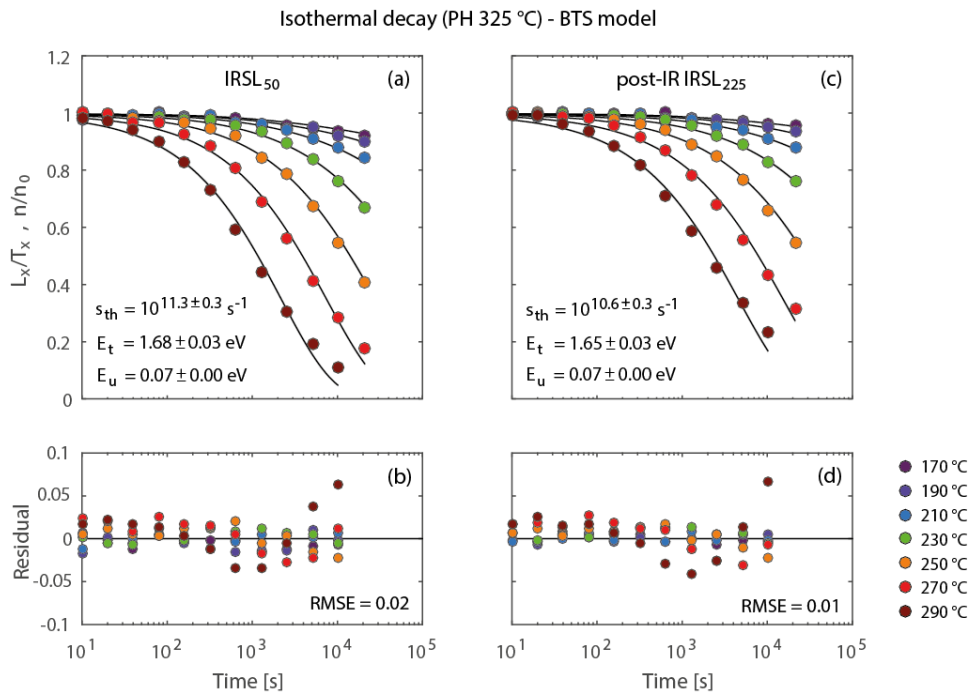


Fig. A.3: Isothermal decay data for sample UNIL/MBTF4700 after a preheat of 250 °C ($T = 170, 190, 210, 230, 250$ °C and time delays $t = 0 - 10240$ s), fitted with the BTS + GTD model for the IRSL₅₀ signal (a) and post-IR IRSL₂₂₅ signal (c). Model residuals are shown in (b) and (d).



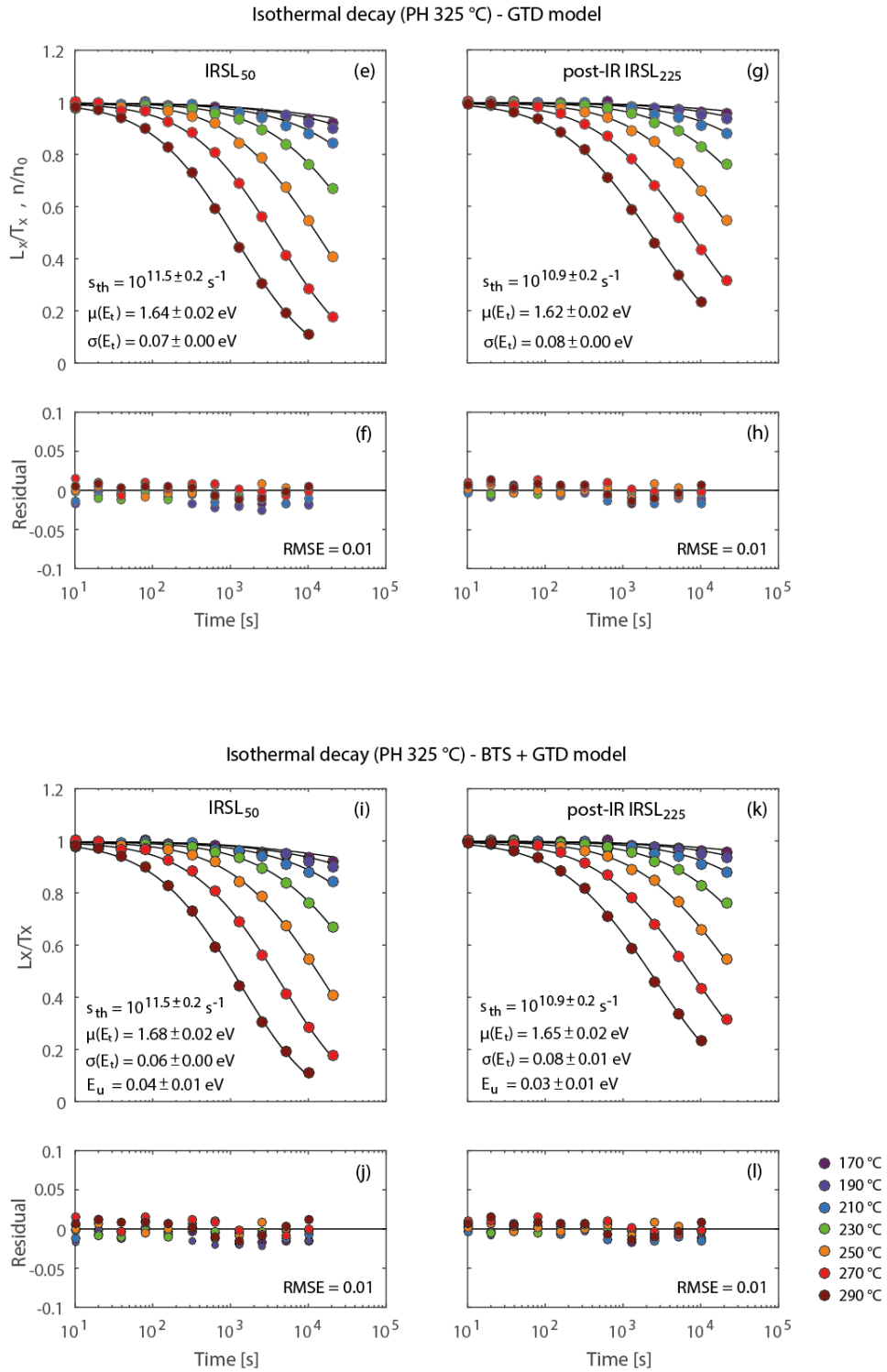


Fig. A.4: Isothermal decay data for sample UNIL/MBTF4700 after a preheat of 325 °C ($T = 170, 190, 210, 230, 250, 270, 290$ °C and time delays $t = 0 - 10240$ s), fitted with the band-tail states model (BTS model; Li and Li, 2013) for the $IRSL_{50}$ signal (a) and post-IR $IRSL_{225}$ signal (c). Model residuals are shown in (b) and (d). The same data is fitted with the model based on a distribution of activation energies due to a Gaussian trap distribution (GTD model) for the $IRSL_{50}$ signal (e) and post-IR $IRSL_{225}$ signal (g). Model residuals are shown in (f) and (h) and with the model based on the presence of band-tail states and a Gaussian trap distribution (BTS + GTD model) as shown in (i)-(l).

Recuperation after temperature treatments

Figure A.5 shows results of both the isothermal decay and recuperation experiments done after two different preheats (250 and 325 °C) for sample UNIL/MBTF4700. All data points are plotted relative to the test dose measurement of the corresponding experiment. The diamond shaped data points represent prompt measurements, i.e. luminescence signal response directly after the given dose of 136 Gy and preheat (no further temperature treatment). The circles represent measurements after the given dose of 136 Gy, preheat and sample holding at elevated temperature ($T= 170, 250$ and 290 °C for 5120 s). Finally, the triangles represent the recuperation measurements after the given dose of 132 Gy, preheat, luminescence measurement and sample holding at elevated temperature ($T= 170, 250$ and 290 °C for 5120 s). Recuperation was less than 6 % and similar for both preheats. Recuperation does not show a clear trend with temperature.

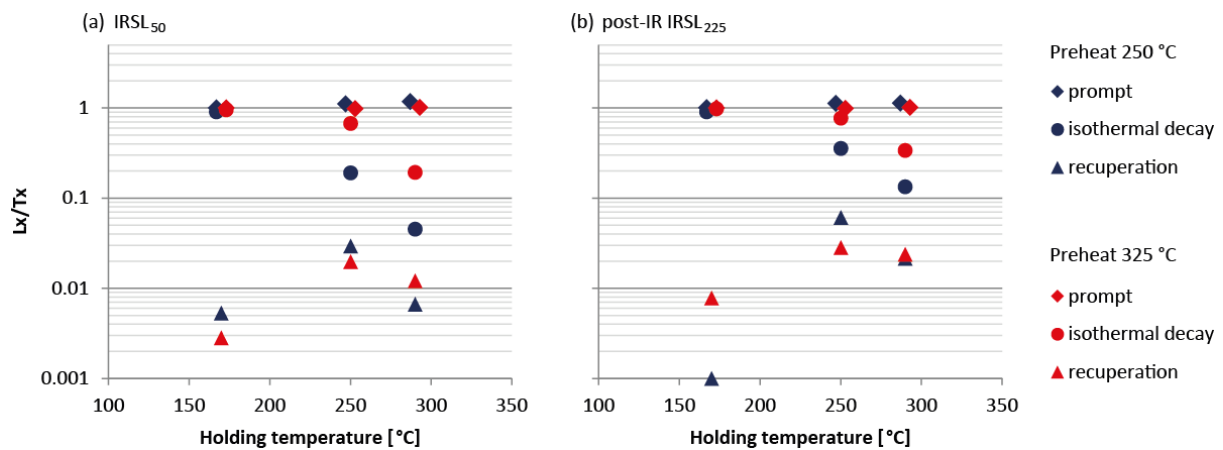


Fig. A.5: Isothermal decay and recuperation data for sample UNIL/MBTF4700: L_x/T_x of (a) IRSL₅₀ signal and (b) post-IR IRSL₂₂₅ signal after a dose (136 or 132 Gy respectively), preheat (of 250 °C or 325 °C for 60 s) and holding aliquot at $T= 170, 250$ and 290 °C for 5120 s. (Partially) overlapping data points have been plotted with a slight off-set to enhance visibility.

A.2 Kinetic parameters

Fitting was done using the least squares method, parameter uncertainties reported at the 68 % confidence interval.

Sample	Preheat [°C]	Signal	g_{2days} [%/decade]	ρ' [10^{-6}]	D_0 [Gy]	a
UNIL/MBTI4250	250	IRSL ₅₀	3.51 ± 0.42	2.36 ± 0.28	405 ± 5	2.00 ± 0.07
UNIL/NB123	250	IRSL ₅₀	6.01 ± 0.45	3.92 ± 0.26	589 ± 12	1.23 ± 0.06
UNIL/MBTF4700	250	IRSL ₅₀	3.74 ± 0.12	2.58 ± 0.07	413 ± 11	2.00 ± 0.15
		post-IR IRSL ₂₂₅	1.48 ± 0.26	1.05 ± 0.18	252 ± 9	2.00 ± 0.16
	325	IRSL ₅₀	3.35 ± 0.55	2.32 ± 0.37	312 ± 6	2.00 ± 0.11
		post-IR IRSL ₂₂₅	1.77 ± 0.93	1.27 ± 0.65	185 ± 3	1.71 ± 0.06

Table A.1: Athermal detrapping and trapping parameters for the IRSL₅₀ signal of samples UNIL/MBTI4250 and UNIL/NB123 and for the IRSL₅₀ and post-IR IRSL₂₂₅ signals of sample UNIL/MBTF4700 after different preheats (250 and 325 °C).

Sample	Preheat [°C]	Signal	D [Gy]	n_0/N	b	$\log_{10}(s_{th})$	E_t [eV]
UNIL/MBTI4250	250	IRSL ₅₀	54	0.1	4.60 ± 0.24	14.7 ± 0.7	1.42 ± 0.05
		IRSL ₅₀	136	0.21	4.15 ± 0.34	12.4 ± 0.9	1.34 ± 0.07
		IRSL ₅₀	4352	0.73	4.34 ± 0.09	12.1 ± 0.2	1.44 ± 0.02
UNIL/NB123	250	IRSL ₅₀	54	0.06	2.78 ± 0.13	13.9 ± 0.5	1.49 ± 0.04
		IRSL ₅₀	136	0.15	2.55 ± 0.19	11.2 ± 0.7	1.32 ± 0.06
		IRSL ₅₀	4352	0.67	2.89 ± 0.11	10.3 ± 0.3	1.3 ± 0.03

Table A.2: Thermal detrapping parameters derived through application of the GOK model, including the initial condition, on isothermal decay data of the IRSL₅₀ signal of samples UNIL/MBTI4250 and UNIL/NB123.

4. RAPID COOLING DURING THE LAST 10 - 100 KA IN THE MONT BLANC MASSIF; INSIGHTS FROM LUMINESCENCE THERMOCHRONOMETRY

Abstract

Luminescence thermochronometry can constrain the recent cooling history (~100 ka) of rocks, and thus offers the possibility to quantify changes in geothermal gradient that occur over those timescales. The method is based on the accumulation of charge in minerals such as quartz and feldspar during rock cooling. Here we apply this method to the Mont Blanc massif (western European Alps). Bedrock samples from the Mont Blanc tunnel were collected, for which the temperature has likely fluctuated in response to fluid infiltration in the last 12 ka. We measured the IRSL₅₀ and post-IR IRSL₂₂₅ signals of K-feldspar extracts. Through dosing, fading and isothermal decay experiments we constrained the kinetic parameters that characterize the trapping and detrapping behaviour of charge in IR sensitive traps of feldspar. By inverting the measured data using the constrained kinetic model and published apatite fission track and (U-Th-[Sm])/He data we then derive the most probable cooling history of each rock sample. The results suggest cooling rates in the last 100 ka of the order of 1 to 4 °C/ 10 ka. Previous modeling results (Maréchal et al., 1999) suggested significantly higher cooling rates between 5 and 21 °C/ 10 ka in the last 12 ka. The results imply that feldspar IRSL thermochronometry provides constraints on changes of the geothermal gradient integrated over 100 ka, but it cannot constrain changes at 1-10 ka timescales. More importantly, future interpretation of luminescence thermochronometry data should account for changes in the near surface geothermal gradient related to hydrothermal flow.

Keywords: low-temperature thermochronometry, luminescence, paleo-geothermal gradient reconstruction

4.1 Introduction

Luminescence thermochronometry is a technique that can be used to quantify rock cooling rates over Quaternary timescales (Herman et al., 2010; Li and Li, 2012; Guralnik et al., 2013, 2015a; King et al., 2016a, 2016c; Herman and King, 2018). In previous studies, past temperatures have been reconstructed (e.g. in a thermal steady-state setting, the KTB borehole in Germany; Guralnik et al., 2015b) and exhumation rates derived (e.g. for the Namche Barwa syntaxis in the Himalaya; King et al., 2016b). The method is based on charge trapping in defects or impurities in the crystal lattice of a mineral due to in situ radioactive decay of the surrounding rock matrix (Aitken, 1985; Huntley et al., 1985). Ambient heat causes electrons to detrapp, and in feldspar crystals electrons may also escape from a trap due to an athermal process, quantum mechanical tunnelling (Wintle, 1973; Visocekas,

2002; Huntley and Lian, 2006). During rock exhumation, trapped charge accumulates as a result of these processes and the net accumulated trapped charge can be measured as the natural luminescence signal in the laboratory through stimulation with heat and/or light. After charge has been evicted from a trap, energy is released, some of which is in the form of luminescence, which can be measured in the laboratory. The intensity of the luminescence signal is assumed to be proportional to the number of trapped charges. Minerals have limited storage capacity; eventually all traps are filled and the crystal becomes saturated, which limits the typical timescale of application: ~100 ka.

The subsurface thermal field, and in particular the thermal conductivity, may be strongly affected by fluid circulations, such as hydrothermal flows and the percolation of meteoric fluids (e.g. Russell, 1935; Clauser and Huenges, 1995). It has been shown previously that such fluid circulations, and their influence on the thermal conductivity of rocks, should be accounted for when interpreting thermochronometric data (Whipp et al., 2007; Braun et al., 2016). However, how the thermal conductivity varies over geological timescales remains poorly known. Given its sensitivity to low temperatures, i.e. 30-100 °C, luminescence thermochronometry may provide a means to constrain variations of the thermal conductivity over ~100 ka timescales. The objective of this study is to apply infra-red stimulated luminescence (IRSL) thermochronometry to the Mont Blanc massif (west European Alps; Fig.1), more specifically to K-feldspar extracts from samples collected from the Mont Blanc tunnel, where the subsurface thermal regime has been influenced by infiltration of water from the glaciated area above, over the last 12 ka as modelled by Maréchal et al. (1999). We test the sensitivity of the method to changes in temperature related to this fluid flow.

For a suite of nine samples we measured the natural luminescence signals and performed experiments from which the kinetic parameters that describe charge trapping and detrapping were derived. The thermal kinetic behaviour of charge in IR sensitive traps of K-feldspar extracts from samples of the Mont Blanc tunnel has been tested in a previous study (Lambert et al, in review-a). Following these experimental results, we applied a thermal decay model based on a distribution of activation energies to describe the thermal kinetic processes in these samples (Lambert et al, in review-b). Based on a kinetic model, which integrates the charge trapping and detrapping processes, we simulate the evolution of trapped charge in IR sensitive traps in response to different cooling scenarios. Potential thermal histories were evaluated through comparison of the resulting modelled trapped charge concentration values with those derived from the natural luminescence signals. Finally, we interpreted our reconstructed past temperatures in comparison with the simulation results of Maréchal et al. (1999).

4.2 Geological setting

The geological setting of the Mont Blanc massif is well-constrained as its lithology and geological history are well-known through previous studies (e.g. Von Raumer and Neubauer, 1993; Leloup et al., 2005; Glotzbach et al., 2008; Glotzbach et al., 2011; Egli and Mancktelow, 2013; Fox et al., 2015). It is mainly composed of granite, which has intruded Variscan metamorphic rocks and is bounded by Mesozoic sediments in the northwest and southeast. Modelling of thermochronology data indicates a strong increase in exhumation in the last 2 Ma in the western European Alps, locally up to ~ 2 mm/a (Glotzbach et al., 2008; Glotzbach et al., 2011; Fox et al., 2015). Egli and Mancktelow (2013) found no evidence for local tectonic uplift of the Mont Blanc massif and suggest enhanced erosion during a more regional uplift, which may be related to glaciation.

The Mont Blanc tunnel (MBT) has enabled us to study samples taken at temperatures closer to the temperature at which the accumulation of electrons starts, which is advantageous in luminescence thermochronometric studies: less time has elapsed since the onset of signal accumulation, reducing the risk of signal saturation. Nine samples along the tunnel were analyzed, obtained at temperatures ranging from ~ 12 to 32 °C (Fig. 4-1). The rock samples were provided by the Cantonal Museum of Geology in Lausanne and the rock temperature curve along the tunnel transect was taken from a geological study (1959-1962) by the Office of Geological and Mining Research (BRGM) when the tunnel was constructed in the 1960s (archive of the Cantonal Museum of Geology in Lausanne). The thermal profile of rock temperature data provides both final constraints on the thermal history for each sample, as well as a general context of the modern (1960s) temperature variability throughout the tunnel.

In a study by Glotzbach et al. (2008), apatite fission track (AFT) and apatite (U-Th-[Sm])/He (AHe) data of (other) samples from the Mont Blanc tunnel are presented, which provide additional constraints on the thermal history of this part of the massif (Fig. 4-1). Table 4-1 gives an overview of these data and the average values which we have used in our calculations (more details such as sample locations are given in Glotzbach et al. (2008)). At present cold water penetrates through the tectonic zone located at ~ 8 km from the NW-portal of the tunnel, resulting in a decrease in rock temperature near this zone (Baggio and Malaroda, 1962). Maréchal et al. (1999), have performed hydro-thermal simulations and concluded that infiltration has occurred since the end of the last glacial period (12 ka) following glacial retreat.

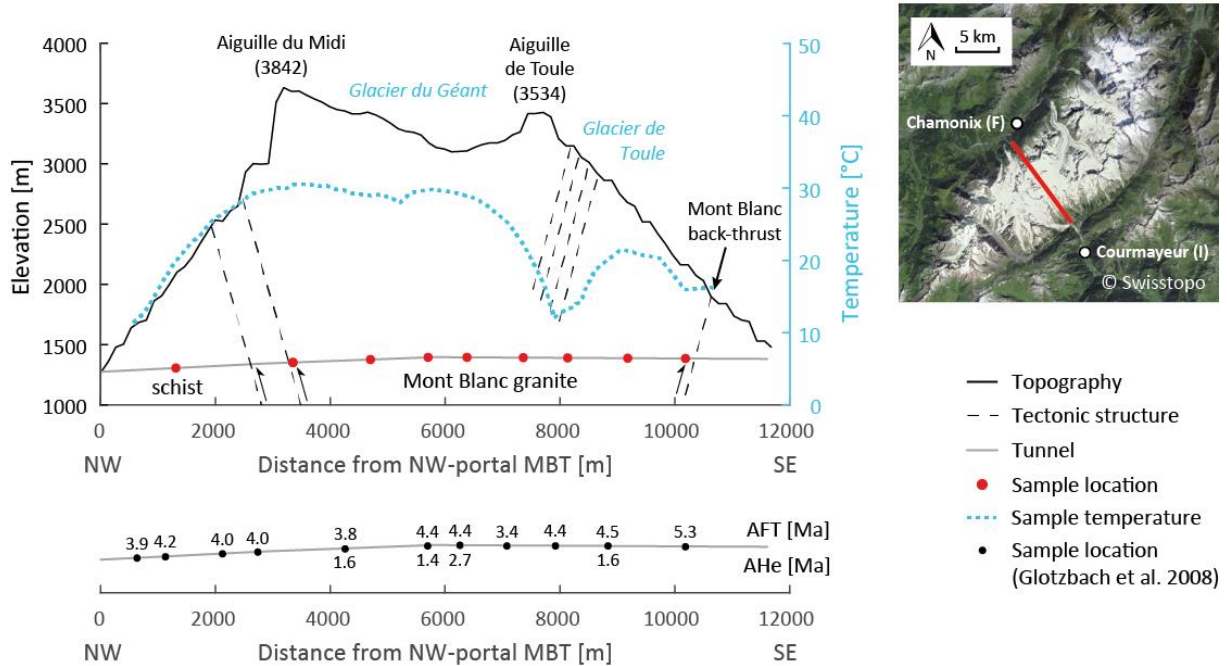


Fig 4-1: Mont Blanc tunnel transect from NW to SE, showing an elevation profile of the massif (black line) and the road tunnel (grey line), along which sample locations are indicated by the red dots (rock samples were provided by the Cantonal Museum of Geology in Lausanne). The light-blue dotted line represents rock temperature data provided by a geological study (1959-1962) by the Office of Geological and Mining Research (BRGM) when the tunnel was constructed in the 1960s. Sample locations for which apatite fission track and/or (U-Th-[Sm])/He ages have been determined by Glotzbach et al. (2008) are indicated by the black dots.

AFT age $\pm 1\sigma$ [Ma]	AHe age $\pm 1\sigma$ [Ma]
3.9 ± 0.2	1.6 ± 0.1
4.2 ± 0.4	1.4 ± 0.6
4.0 ± 0.2	2.7* ± 0.2
4.0 ± 0.4	1.6 ± 0.2
3.8 ± 0.7	$\mu_{max} = 1.825$
4.4 ± 1.1	$\mu_{min}^{**} = 1.533$
4.4 ± 0.8	
3.4 ± 0.7	* regarded as outlier
4.4 ± 0.7	** mean value
4.5 ± 0.6	excluding outlier
5.3 ± 0.7	
$\mu = 4.21 \pm 0.3$	

Table 4-1: Apatite fission track and (U-Th-[Sm])/He data from Glotzbach et al. (2008) and mean ages (μ) for both thermochronometric systems.

4.3 Rate equation for K-feldspar luminescence thermochronometry

The process of charge trapping and escape during irradiation at a given temperature can be described by the following equation, which consists of a trapping, thermal detrapping and athermal

detrapping term. For a trap with activation energy E_a and tunneling distance r' to a recombination site in a crystal we have:

$$\frac{d\left(\frac{n}{N}\right)}{dt} = \frac{\dot{D}}{D_0} \left(1 - \frac{n}{N}\right)^a - \frac{\left(\frac{n}{N}\right)}{\tau_{th}} - \frac{\left(\frac{n}{N}\right)}{\tau_{tun}}, \quad (1)$$

with $\tau_{th} = s_{th}^{-1} e^{\frac{E_a}{k_B T}}$ and $\tau_{tun} = s_{tun}^{-1} e^{r' \cdot (\rho')^{-1/3}}$,

where n is the number of trapped charges at time t , N is the total number of charges that can be trapped and n/N is the saturation ratio at time t (Herman et al., 2010; Li and Li, 2012; Guralnik et al., 2015c; Lambert et al., in review-b). The rate of trapping is determined by the dose rate of radiation \dot{D} (Gy/ka), the characteristic dose of saturation D_0 (Gy) and the order of kinetics a , which we restrict to ≤ 2 following Biswas et al. (2018). The rate of thermal detrapping is determined by the thermal lifetime τ_{th} (s), which is dependent on s_{th} (s^{-1}), the frequency factor or the number of attempts to escape per second, the activation energy E_a (eV), Boltzmann's constant k_B (eV/K) and temperature T (K) (Randall and Wilkins 1945). For the total population of IR-sensitive traps, we assume a distribution of activation energies with $E_a = E_t - E_b$, where E_t [eV] is the trap depth and E_b [eV] a band-tail state energy level. We assume a Gaussian distribution of trap depths, characterized by the mean trap depth $\mu(E_t)$ [eV] and width $\sigma(E_t)$ [eV], and an exponential distribution of band-tail states, characterized by the Urbach band-tail width E_U . Assuming that these distributions are independent, they can be given by the following probability density functions:

$$P_t(E_t) = \frac{1}{\sigma(E_t)\sqrt{2\pi}} \exp\left(-\frac{1}{2}\left(\frac{E_t - \mu(E_t)}{\sigma(E_t)}\right)^2\right) \quad (2)$$

for trap depth and

$$P_b(E_b) = \frac{\exp\left(-\frac{E_b}{E_U}\right)}{E_U \left(\exp\left(-\frac{E_{b,min}}{E_U}\right) - \exp\left(-\frac{E_{b,max}}{E_U}\right)\right)} \quad (3)$$

for the band-tail states, where $E_{b,min}$ and $E_{b,max}$ represent the energies of the shallowest and deepest band-tail states thermally accessible. The rate of athermal detrapping is determined by the athermal lifetime τ_{tun} (s), which is dependent on $s_{tun} = 3.0 \cdot 10^{15}$ (s^{-1}), the frequency factor or the number of attempts to escape per second, the density of recombination centres ρ' , and r' , a dimensionless variable for the tunneling distance for an electron-recombination pair (Huntley, 2006; Kars et al., 2008). It is assumed that recombination centres are randomly distributed and an electron will tunnel to the nearest recombination centre (Huntley 2006). Accordingly, we integrate over the following probability distribution for tunnelling distance r'

$$p(r') = 3r'^2 e^{-(r')^3} \quad (4)$$

By adding the terms corresponding to the different processes, the assumption is made that thermal and athermal detrapping probabilities are independent of each other (Kars et al., 2009).

4.4 Analytical procedures

4.4.1 Sample preparation and instrumentation

Nine bedrock samples were selected from the Mont Blanc tunnel, provided by the Cantonal Museum of Geology (see Figure 4-1). Most samples are Mont Blanc granites, except for sample MBT-F 1311 which is a schist. All sample preparation was done under subdued red light conditions. The outer 1 cm of the rock samples was removed using a diamond saw to ensure that only the light safe interior was prepared for luminescence analysis (Sohbati et al., 2012). By crushing and sieving the samples, a 180-212 μm fraction was obtained and subsequently treated with hydrochloric acid (HCl) and hydrogen peroxide (H_2O_2) to obtain a pure mineral extract. K-feldspars were separated using heavy liquids based on sodium polytungstate (2.58 g cm^{-3}). To ensure that the mineral fraction used to measure the IRSL signal consists of K-feldspar, samples were examined using X-ray diffraction and scanning electron microscopy. Aliquots of 2 mm in diameter, consisting of a single layer of grains, were mounted on stainless steel discs (10 mm in diameter), using silicon spray as an adhesive and a mask to regulate the aliquot size.

The experiments were carried out in the Institute of Earth Surface Dynamics at the University of Lausanne using Risø TL-DA-20 luminescence readers (Bøtter-Jensen et al., 2010), equipped with $^{90}\text{Sr}/^{90}\text{Y}$ beta-sources. The readers have dose rates of $0.1\text{-}0.2 \text{ Gy s}^{-1}$, and measurement reproducibility between 1.14 and 1.26 %. Optical stimulation of feldspar was done with infrared (IR) light emitting diodes (LEDs, $870 \pm 20 \text{ nm}$) and a filter combination of a Schott BG-3 and Schott BG-39 was used to restrict detection to the blue spectrum and UV. The luminescence signal intensity of the samples studied was very high ($>10^6 \text{ cts/s}$ during the preheat). To prevent saturation of the photomultiplier tube, an aperture filter was used to reduce the signal for the dose response experiments. Preheats or stimulations at temperatures higher than $200 \text{ }^\circ\text{C}$ were done in a nitrogen atmosphere.

4.4.2 Experimental procedure

All luminescence measurements were performed using a single aliquot regenerative dose (SAR) protocol (Murray and Wintle, 2000; Wallinga et al., 2000) that comprised preheating at $250 \text{ }^\circ\text{C}$ for 60 s followed by an IRSL_{50} stimulation (at $50 \text{ }^\circ\text{C}$) for 100 s and a post-IR IRSL_{225} stimulation (at $225 \text{ }^\circ\text{C}$) for 100 s. The protocol was validated using a dose recovery preheat plateau test (Buylaert et al., 2012; Thomsen et al., 2008). As the two signals (IRSL_{50} and post-IR IRSL_{225}) are expected to have different

thermal stabilities (Li and Li, 2011), they could provide two thermal constraints on a cooling history (e.g. Qin et al., 2015; King et al., 2016c). After measuring the natural luminescence signals, several experiments were done to constrain the rates of the processes of trapping, thermal detrapping and athermal detrapping for each sample.

Dose response curves were obtained using a maximum dose of 4.5 kGy and a test dose of 54 Gy. Luminescence signals were measured using the SAR protocol mentioned above for three aliquots per sample. Athermal decay was characterized for each sample through a fading experiment on three aliquots, whereby luminescence signal loss was measured following different delays between aliquot dosing (54 Gy) and luminescence measurement; aliquots were preheated prior to storage (see also Auclair et al., 2003) and delay times ranged from 5 minutes to 2 days. The same SAR protocol outlined above was used and a test dose given equal to the initial dose. Feldspar thermal decay was measured through isothermal decay experiments on one aliquot per sample, which consisted of giving an aliquot a known dose and measuring luminescence signal loss following holding at a constant temperature, for different durations over laboratory timescales. In the isothermal decay experiments, a dose of 136 Gy was given and the same test dose. Following dosing and preheating, a single aliquot of each sample was held at a constant temperature in the range of 170 - 250 °C for a given period of time ($t = 0 - 10240$ s). The remaining luminescence signal was then measured using the SAR protocol outlined above. During both the dosing experiment and isothermal decay experiments some athermal decay is expected; an effect that is taken into account when fitting the data (King et al., 2016c).

In the natural environment, the rate of trapping is dependent on the environmental dose rate \dot{D}_{env} [Gy/ka], which depends on the concentrations of U, Th, K and Rb from the rock matrix and the mineral that is investigated. Sample specific \dot{D}_{env} values were calculated based on an estimated grain size distribution (see Table S-1 and S-2 in the Supplementary materials) and following the same method outlined by Durcan et al. (2015).

4.4.3 Modelling procedure

Kinetic parameters

The sample kinetic parameters were derived from the experimental data trends, based on the model described above (Eq. (1)) and are summarized in Table 4-2. Following the validation study of OSL thermochronometry in a steady-state setting (Guralnik et al., 2015b) and recent geological applications (King et al., 2016b; Biswas et al., 2018) we assume that the obtained laboratory kinetic parameters can be extrapolated over geological timescales and simulate the processes of trapping

and detrapping of charge in IR sensitive traps under steady-state and linear cooling conditions which may occur within a natural geological setting.

Steady-state simulations

To screen the natural luminescence signals measured in the laboratory for a thermal signal, for all samples and both luminescence signals, trapped charge concentrations corresponding to field saturation (n/N_{ss}) were simulated based on Eq. (1) assuming thermal (and athermal) steady-state at the sampling temperature (Guralnik et al, 2015a; Valla et al., 2016). These were compared to the natural signals, expressed as ratio of trapped charge (n/N_{nat}), and the difference between them ($n/N_{nat} < n/N_{ss}$) considered to be indicative of a thermal signal, which contains information on a sample's thermal history. An area where n/N_{nat} values are within 15% of the predicted n/N_{ss} values is indicated, which may be used as an acceptance criterion (Guralnik et al., 2015a; King et al., 2016b). Samples with $n/N_{nat} = n/N_{ss}$ are in steady-state, and their thermal evolution cannot be derived without additional thermal constraints. Similarly, an apparent steady-state temperature based on both luminescence signals was found for each sample by doing several thermal steady-state simulations, covering a range of temperatures and minimizing the misfit between the obtained modelled n/N_{ss} values and the n/N_{nat} values, using the following misfit function:

$$\text{misfit} = \left(\sum_i \left| \frac{n/N_{mod} - n/N_{nat}}{\max(\sigma(n/N_{nat}), 0.1 \cdot n/N_{nat})} \right|^2 \right) \quad (5)$$

where i is summing over the number of luminescence signals. Any off-set of this apparent steady-state temperature from the sampling temperature, is indicative of the luminescence signals containing information on a cooling history.

Linear cooling scenarios

Two different cooling scenarios were computed. First, using the same misfit function (Eq. (5)), apparent linear cooling rates based on both luminescence signals were determined for the MBT samples. Secondly, two-stage linear cooling rates were computed, where the earliest cooling rate is calculated from the apatite fission track (AFT) and apatite (U-Th-[Sm])/He (AHe) data of the other samples from the Mont Blanc tunnel (Figure 4-1; Table 4-1; Glotzbach et al., 2008). We used the mean value $\mu = 4.21$ Ma of the AFT ages and assumed an uncertainty of ± 0.30 Ma. We also used the mean value $\mu_{max} = 1.83$ Ma of the AHe ages and used $\mu_{min} = 1.53$ Ma as a minimum age (the mean value of this data set excluding the outlier value of 2.7 Ma). Furthermore, we considered a minimum and maximum closure temperature for the apatite fission track system of 110 and 140 °C respectively (Dodson, 1973; Reiners and Brandon, 2006). For the apatite (U-Th-[Sm])/He system we assumed a

minimum and maximum closure temperature of 70 and 90 °C respectively. To meet the AFT and AHe constraints, the earliest cooling rates were defined between 10-30 °C/Ma.

The second part of the two-stage cooling histories was defined based on a variable starting date in a time window from 5 ka to 400 ka and temperature window from the measured sample temperature during tunnel construction (T_{sample}) to 80 °C (i.e. the closure temperature of the apatite (U-Th-[Sm])/He data (Farley, 2000), Table 4-1). For each sample, the resulting trapped charge for both luminescence signals was calculated for each prescribed cooling history using equation (1) and expressed as saturation ratio (n/N_{mod}), which was compared to the saturation ratio derived from the natural luminescence signal (n/N_{nat}). The likelihood of each cooling path is evaluated with the following function:

$$L = \exp\left(-0.5 \cdot \sum_i \left| \frac{n/N_{mod} - n/N_{nat}}{\max(\sigma(n/N_{nat}), 0.1 \cdot n/N_{nat})} \right|^2\right) \quad (6)$$

where i is a trap type or luminescence signal. The uncertainty of n/N_{nat} is taken into account by taking the maximum of the measured uncertainty of n/N_{nat} , $\sigma(n/N_{nat})$, and 10 % of n/N_{nat} . This approach is followed considering that there is not only an uncertainty on the measured natural signal, but also on the determination of the saturation level (Guralnik et al., 2015a; Guralnik et al., 2015c; Li et al., 2018). Scores close to 1 indicate a small deviation of n/N_{mod} from n/N_{nat} , while scores close to 0 indicate a larger misfit. These scores were compared to a random number between 0 and 1 and only those cooling paths with $L > \text{random}(0,1)$ were accepted. Through this approach, cooling paths of all kinds are retained, but those with smaller misfit have a higher probability of being accepted. Subsequently, the accepted cooling paths were projected onto a time-temperature grid and counted in each grid point to obtain a probability density function at each time step (King et al., 2016b). For each of these probability density functions, the mean and 68 % and 95 % confidence intervals were calculated. Finally, for the cooling paths defined through connecting the points of these percentiles over time, the corresponding n/N_{mod} values were calculated for both luminescence signals and contrasted with the n/N_{nat} values.

4.5 Results

4.5.1 Laboratory kinetic parameters

Figure 4-2 shows the kinetic parameters derived from equation (1) for all MBT samples and both the IRSL₅₀ and post-IR IRSL₂₂₅ luminescence signals. On average, the environmental dose rates are $\sim 11 \pm 0.55$ Gy/ka and similar for the samples taken from the Mont Blanc granite (Fig. 4-1). Sample MBT-F

1311, a schist in the Mont Blanc shear zone, has a slightly lower environmental dose rate of 8 Gy/ka. D_0 values vary throughout the tunnel, ranging from 360 to 580 Gy for the IRSL₅₀ signals and from 250 to 410 Gy for the post-IR IRSL₂₂₅ signal. The majority of the MBT samples are characterized by a relatively high kinetic order ($a = 2$ for both the IRSL₅₀ and post-IR IRSL₂₂₅ signal), except for two samples MBT-F 1311 and MBT-I 2430 which have kinetic orders closer to 1; these samples differ from the remainder of the sample suite, by containing relatively small feldspar crystals (see Fig. S-1 and

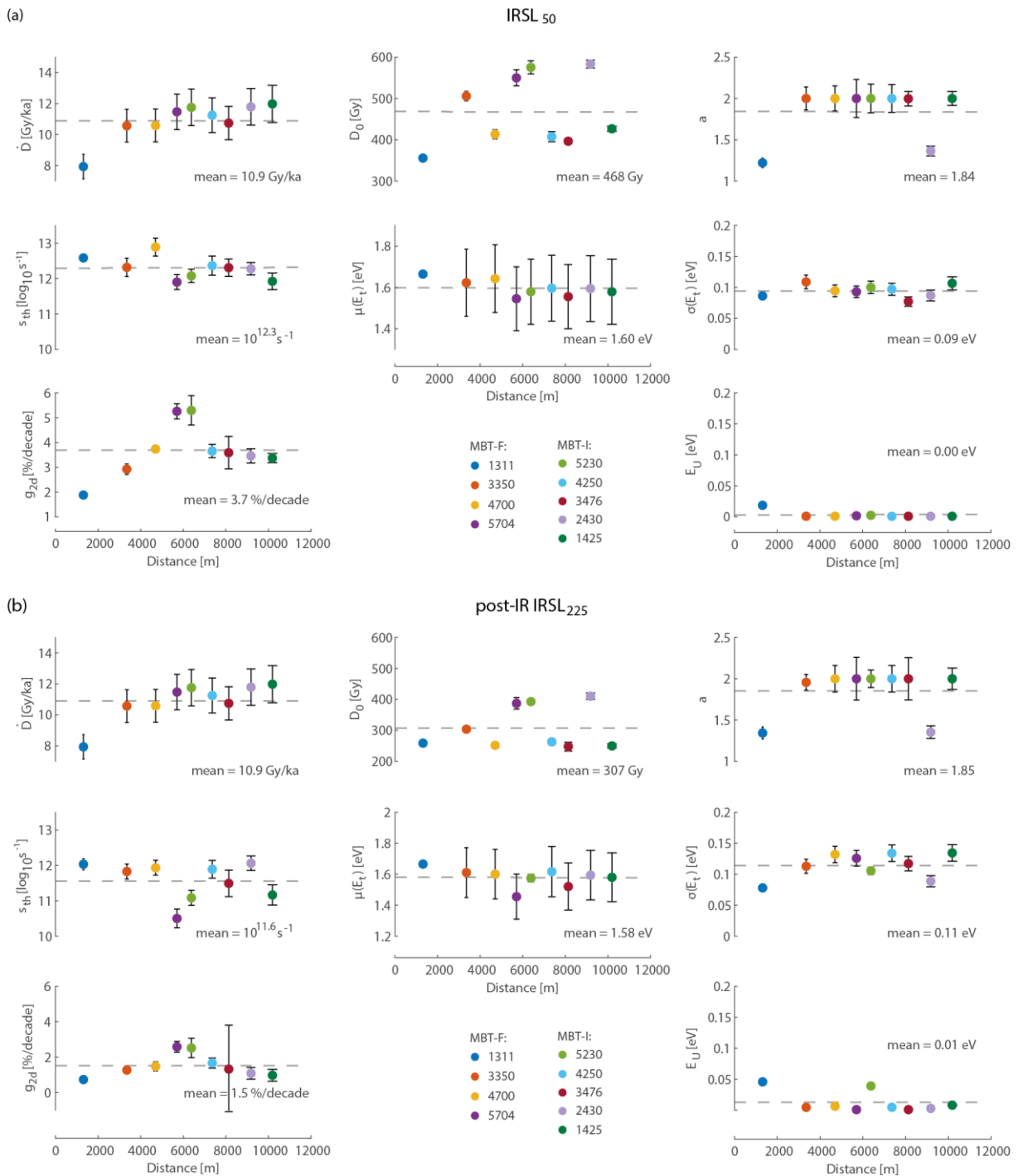


Fig. 4-2: Kinetic parameters displayed along Mont Blanc tunnel transect for the (a) IRSL₅₀ and (b) post-IR IRSL₂₂₅ signal.

IRSL₅₀

	Sample	n/N_{nat}	\dot{D} [Gy/ka]	D_0 [Gy]	a	$\log_{10}(s_{th})$ [s ⁻¹]	$\mu(E_t)$ [eV]	$\sigma(E_t)$ [eV]	E_U [eV]*	g_{2d} [%/decade]	ρ' [$\cdot 10^{-6}$]
MBT-F	1311	0.72 ±0.01	7.94 ±0.40	356 ±9	1.22 ±0.06	12.6 ±0.1	1.66 ±0.02	0.09 ±0.00	0.02 ±0.02	1.88 ±0.13	1.34 ±0.09
	3350	0.38 ±0.01	10.57 ±0.53	506 ±11	2.00 ±0.14	12.3 ±0.3	1.62 ±0.03	0.11 ±0.00	0.00	2.92 ±0.21	2.04 ±0.15
	4700	0.31 ±0.01	10.59 ±0.53	413 ±11	2.00 ±0.15	12.9 ±0.3	1.64 ±0.03	0.09 ±0.00	0.00	3.74 ±0.12	2.58 ±0.07
	5704	0.23 ±0.00	11.47 ±0.57	550 ±20	2.00 ±0.23	11.9 ±0.2	1.55 ±0.02	0.09 ±0.00	0.00	5.26 ±0.31	3.54 ±0.19
MBT-I	5230	0.25 ±0.01	11.76 ±0.59	575 ±16	2.00 ±0.17	12.1 ±0.2	1.58 ±0.02	0.10 ±0.00	0.00	5.30 ±0.59	3.57 ±0.38
	4250	0.32 ±0.00	11.25 ±0.56	407 ±12	2.00 ±0.17	12.4 ±0.3	1.60 ±0.03	0.10 ±0.00	0.00	3.66 ±0.27	2.51 ±0.18
	3476	0.38 ±0.02	10.74 ±0.54	396 ±6	2.00 ±0.09	12.3 ±0.2	1.56 ±0.02	0.08 ±0.00	0.00	3.59 ±0.66	2.47 ±0.44
	2430	0.45 ±0.00	11.79 ±0.59	583 ±10	1.36 ±0.06	12.3 ±0.2	1.59 ±0.02	0.09 ±0.00	0.00	3.46 ±0.29	2.40 ±0.19
	1425	0.39 ±0.00	11.98 ±0.60	427 ±6	2.00 ±0.08	11.9 ±0.2	1.58 ±0.02	0.11 ±0.00	0.00	3.37 ±0.19	2.33 ±0.13

post-IR IRSL₂₂₅

	Sample	n/N_{nat}	\dot{D} [Gy/ka]	D_0 [Gy]	a	$\log_{10}(s_{th})$ [s ⁻¹]	$\mu(E_t)$ [eV]	$\sigma(E_t)$ [eV]	E_U [eV]*	g_{2d} [%/decade]	ρ' [$\cdot 10^{-6}$]
MBT-F	1311	0.87 ±0.01	7.94 ±0.40	259 ±8	1.34 ±0.07	12.0 ±0.2	1.67 ±0.02	0.08 ±0.00	0.05 ±0.01	0.73 ±0.12	0.52 ±0.09
	3350	0.63 ±0.01	10.57 ±0.53	304 ±6	1.96 ±0.10	11.8 ±0.2	1.61 ±0.02	0.11 ±0.00	0.00	1.27 ±0.18	0.90 ±0.13
	4700	0.53 ±0.02	10.59 ±0.53	252 ±9	2.00 ±0.16	11.9 ±0.2	1.60 ±0.02	0.13 ±0.00	0.01	1.48 ±0.26	1.05 ±0.18
	5704	0.40 ±0.01	11.47 ±0.57	387 ±18	2.00 ±0.26	10.5 ±0.3	1.46 ±0.03	0.13 ±0.00	0.00	2.58 ±0.31	1.77 ±0.20
MBT-I	5230	0.44 ±0.01	11.76 ±0.59	393 ±8	2.00 ±0.11	11.1 ±0.2	1.58 ±0.02	0.11 ±0.01	0.04 ±0.01	2.52 ±0.55	1.75 ±0.38
	4250	0.52 ±0.03	11.25 ±0.56	263 ±9	2.00 ±0.16	11.9 ±0.2	1.62 ±0.03	0.13 ±0.00	0.00	1.66 ±0.28	1.17 ±0.20
	3476	0.61 ±0.06	10.74 ±0.54	248 ±15	2.00 ±0.26	11.5 ±0.4	1.52 ±0.04	0.12 ±0.00	0.00	1.32 ±2.48	0.97 ±1.77
	2430	0.75 ±0.01	11.79 ±0.59	410 ±11	1.35 ±0.08	12.1 ±0.2	1.59 ±0.02	0.09 ±0.00	0.00	1.09 ±0.33	0.77 ±0.24
	1425	0.59 ±0.01	11.98 ±0.60	250 ±7	2.00 ±0.13	11.2 ±0.3	1.58 ±0.03	0.13 ±0.00	0.01	0.98 ±0.33	0.70 ±0.24

Table 4-2: Kinetic parameters of the Mont Blanc tunnel samples for the IRSL₅₀ signal (top) and post-IR IRSL₂₂₅ signal (bottom). For n/N_{nat} one standard deviation is given, $\dot{D}_{env} \pm 5\%$, and for the other parameters two standard deviations are given. *When fitting the thermal decay model to the isothermal decay data, large uncertainties were found for $\mu(E_t)$ and E_U , which may originate from a numerical correlation between these two parameters; subsequently, E_U was fixed to the best-fit value to evaluate the uncertainties of the other parameters. This did not have an effect on the parameter values.

Table S-1 in the Supplementary materials). The MBT samples vary slightly in thermal stability with s_{th} values of between 10^{12} and 10^{13} s^{-1} for the IRSL₅₀ signal and between $10^{10.5}$ and 10^{12} s^{-1} for the post-IR IRSL₂₂₅ signal. For the IRSL₅₀ signal we found $\mu(E_t)$ values with a mean of $1.60 \pm 0.04 \text{ eV}$, mean $\sigma(E_t)$ values of $0.09 \pm 0.01 \text{ eV}$ and E_U values that are negligible. For the post-IR IRSL₂₂₅ signal we derived $\mu(E_t)$ values with a mean of $1.58 \pm 0.06 \text{ eV}$, mean $\sigma(E_t)$ values of $0.11 \pm 0.02 \text{ eV}$ and very small E_U values with a mean of $0.01 \pm 0.02 \text{ eV}$. Finally, athermal decay increases for rock samples deeper into the mountain massif and is more prominent for IRSL₅₀ signal with a mean of $3.7 \pm 1.1 \text{ \%/decade}$, than for the post-IR IRSL₂₂₅ signal with mean of $1.5 \pm 0.6 \text{ \%/decade}$. An overview of the kinetic parameter values is given in Table 4-2.

4.5.2 Natural signals and steady state conditions

In Figure 4-3a, the n/N_{nat} values for both the IRSL₅₀ signal (red circles) and post-IR IRSL₂₂₅ signal (blue circles) are plotted along the tunnel transect (see also Table 4-2). For both signals, the values decrease with increasing depth into the mountain range, except for sample MBT-I 1425, closest to the SE-portal of the tunnel (right). The black dotted line represents the rock temperature in the tunnel at the time it was constructed in the 1960s. Although broadly speaking, the n/N_{nat} trend shows an anti-correlation with the rock temperature curve, it does not show a relation with the rock temperature anomaly at 8000 m from the NW-portal of the tunnel. Predicted n/N_{ss} values, which were calculated under the assumption of steady-state conditions at the rock sample temperature, are shown as crosses in Figure 4-3a (in red for the IRSL₅₀ signal and in blue for the post-IR IRSL₂₂₅ signal). The n/N_{ss} values show a trend similar to the n/N_{nat} values, although the off-set with the n/N_{nat} values varies per sample along the tunnel transect. No deviation between the n/N_{nat} and n/N_{ss} values is observed for sample MBT-F 1311, which is located closest to the NW-portal of the tunnel (left). In Figure 4-3b, the n/N_{nat} and n/N_{ss} values are plotted for the IRSL₅₀ signal (left) and post-IR IRSL₂₂₅ signal (right) and compared to the 1:1 line and the grey area which indicates 15 % deviation from the 1:1 line. The value of 15% has been suggested as a threshold for signal saturation in thermochronometric applications previously (Guralnik et al., 2015; King et al., 2016). For the IRSL₅₀ signal, n/N_{nat} values of two samples plot within this area (MBT-F 1311 and MBT-I 2430), while for the post-IR IRSL₂₂₅ signal, for several more samples the n/N_{nat} values are within 15 % of the n/N_{ss} values (also MBT-F 3350, MBT-F 5704 and MBT-I 3476) or error bars are within this area (MBT-F 4700 and MBT-I 5230).

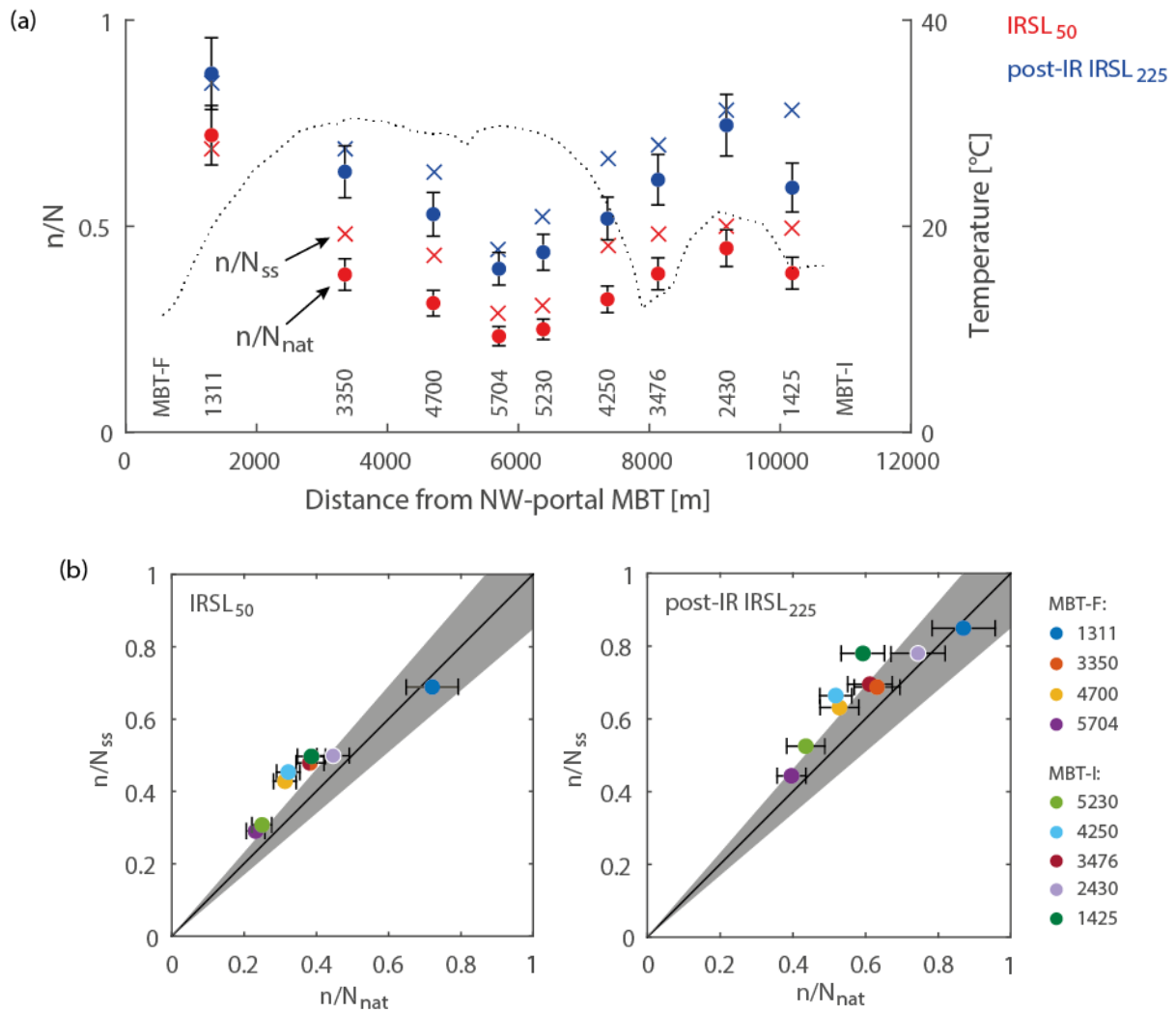


Fig. 4-3: (a) Calculated n/N_{nat} and n/N_{ss} values for the IRSL₅₀ and post-IR IRSL₂₂₅ signal. The grey shaded area represents 15 % deviation from the 1:1 line. (b) n/N_{nat} and n/N_{ss} values for the IRSL₅₀ and post-IR IRSL₂₂₅ signal along the MBT transect with rock sample temperatures measured when tunnel was constructed in the 1960s indicated by the black dotted line.

4.5.3 Apparent steady state temperatures

Figure 4-4 shows the apparent steady state temperatures for each MBT sample, found by simulating a range of thermal steady state conditions and minimizing the misfit between n/N_{mod} and n/N_{nat} for both luminescence signals. The results are displayed together with the rock temperature data and with one exception (sample MBT-F 1311) the apparent steady state temperatures are all higher than the measured rock temperature when the samples were taken in the 1960s. Two samples close to the temperature anomaly (MBT-I 3476 and MBT-I 2430) have apparent steady state temperatures that are ~ 10 °C lower than those of the other samples.

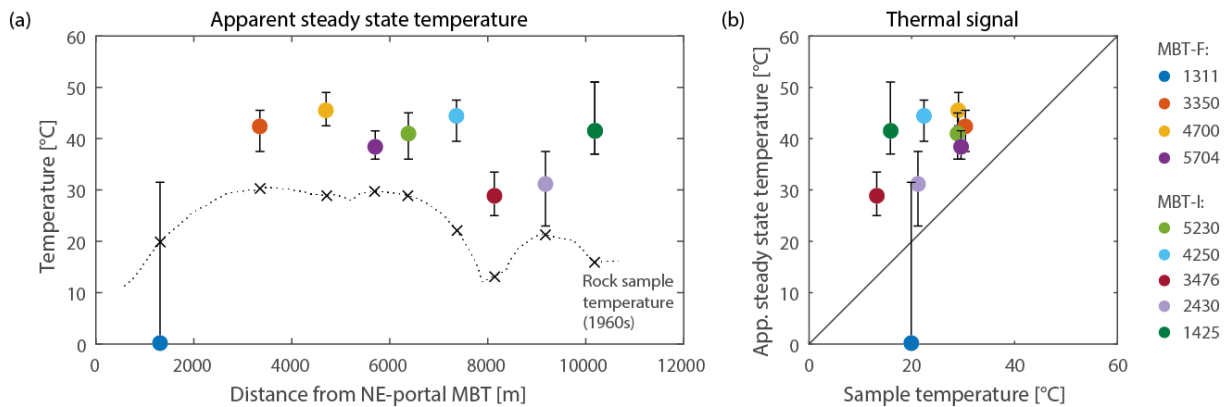


Fig. 4-4: Apparent steady state temperatures and rock sample temperatures (a) along the tunnel transect and (b) presented relative to sample temperature. Error bars represent the common error of both luminescence signals.

4.5.4 Two stage linear cooling histories

In Figure 4-5, for each sample, the apparent linear cooling path is indicated by a white dotted line and apparent linear cooling rates are listed in Table 4-3. Sample MBT-F 1311 shows a steady state condition at sample temperature (i.e. 0 °C/ Ma). In contrast, the apparent linear cooling rates of samples MBT-F 4700, MBT-I 4250 and MBT-I 1425 are extremely high, 380, 545 and 545 °C/ Ma respectively. For the other samples they are between 160 and 265 °C/ Ma. The accepted two stage linear cooling paths, based on apatite fission track and (U-Th-[Sm])/He data (Glotzbach et al., 2008) and the luminescence data from this study, are also displayed for each sample in Figure 4-5.

Figure 4-6 shows probability density functions calculated for the two-stage cooling histories; the median (red) and 68 % (green) and 95 % (black) confidence intervals are shown. The derivatives of the median curves are given in Figure 4-7 and show the extreme cooling of up to ~350-640 °C/ Ma needed to obtain n/N_{mod} values that are close to the n/N_{nat} for samples MBT-F 4700, MBT-I 4250 and MBT-I 1425. For the other samples, the median cooling paths show cooling of up to ~110-240 °C/ Ma. For each of the percentile curves, the evolution of trapped charge was calculated for both luminescence signals and most of the predicted final n/N_{mod} values were within 5 % of the n/N_{nat} values (Figure 4-8). The grey area indicates a deviation of 10 %, in which all values plot, except the n/N_{mod} value of the post-IR IRSL₂₂₅ signal of sample MBT-I 1425 which is 14 % higher than the corresponding n/N_{nat} value.

	Sample	n/N_{nat} IRSL ₅₀	n/N_{ss} IRSL ₅₀	n/N_{mod} IRSL ₅₀	n/N_{nat} pIRIR ₂₂₅	n/N_{ss} pIRIR ₂₂₅	n/N_{mod} pIRIR ₂₂₅	T_{sample} [°C]	$T_{app ss}$ [°C]	$\dot{T}_{app lin}$ [°C/Ma]
MBT-F	1311	0.72 ±0.01	0.69	0.66	0.87 ±0.01	0.85	0.83	19.9	0	0
	3350	0.38 ±0.01	0.48	0.41	0.63 ±0.01	0.69	0.62	30.4	42.5	185
	4700	0.31 ±0.01	0.43	0.33	0.53 ±0.02	0.63	0.53	29.0	45.5	380
	5704	0.23 ±0.00	0.29	0.24	0.40 ±0.01	0.44	0.39	29.7	38.5	170
MBT-I	5230	0.25 ±0.01	0.31	0.25	0.44 ±0.01	0.52	0.46	28.9	41.0	210
	4250	0.32 ±0.00	0.45	0.33	0.52 ±0.03	0.66	0.55	22.2	44.5	545
	3476	0.38 ±0.02	0.48	0.40	0.61 ±0.06	0.70	0.62	13.2	29.0	265
	2430	0.45 ±0.00	0.50	0.46	0.75 ±0.01	0.78	0.74	21.2	31.0	160
	1425	0.39 ±0.00	0.50	0.38	0.59 ±0.01	0.78	0.67	15.9	41.5	545

Table 4-3: Characteristic values based on thermochronometric analysis.

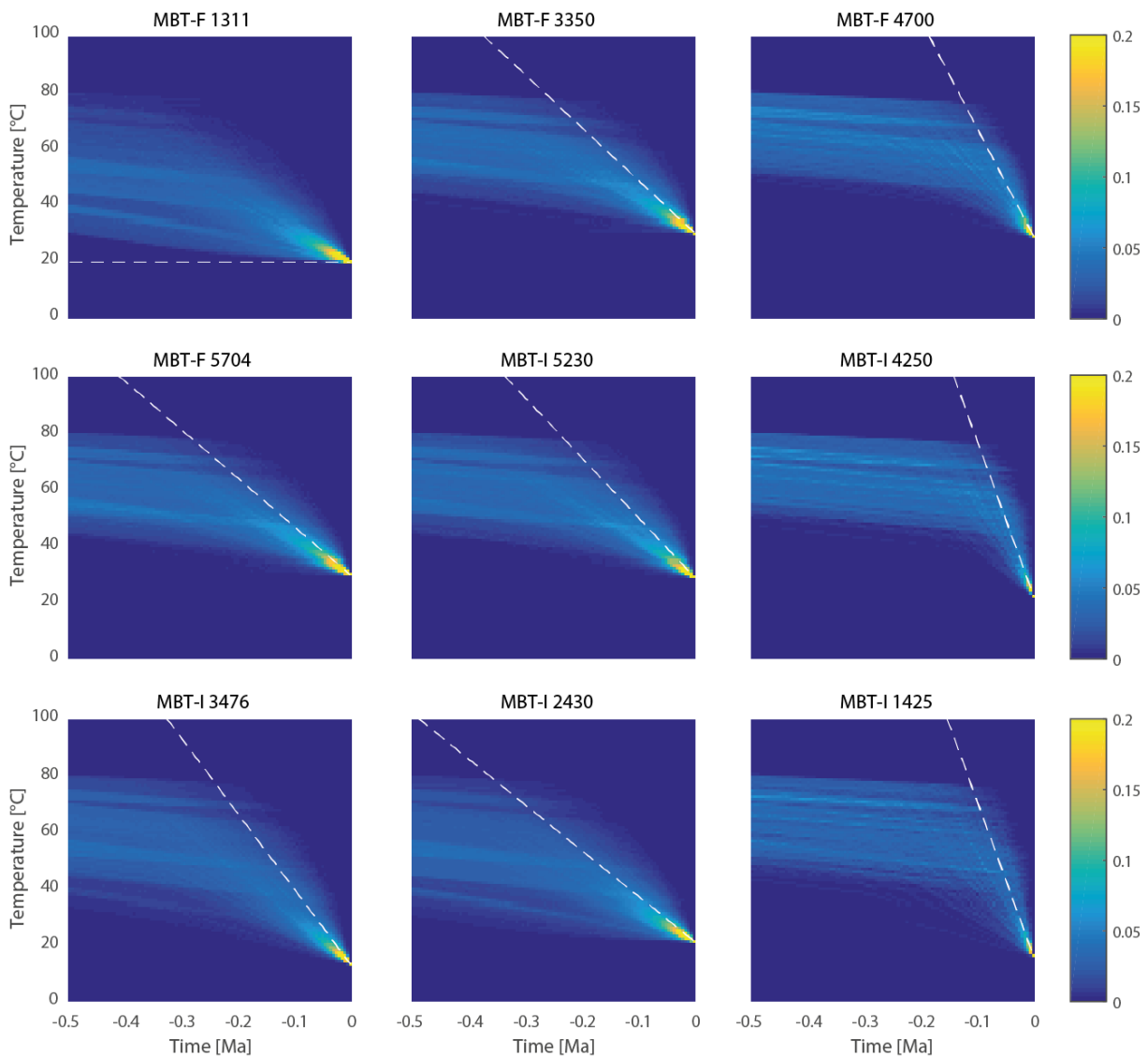


Fig. 4-5: Accepted two stage linear cooling paths (based on apatite fission track, apatite (U-Th-[Sm])/He and luminescence data) following a standard rejection algorithm (section 4.3.2). The occurrence of a path is counted in each grid point as indicated by the colors from the color bar on the right, i.e. yellow where 20-100 % of the paths pass and a color from the color gradient where fewer paths pass.

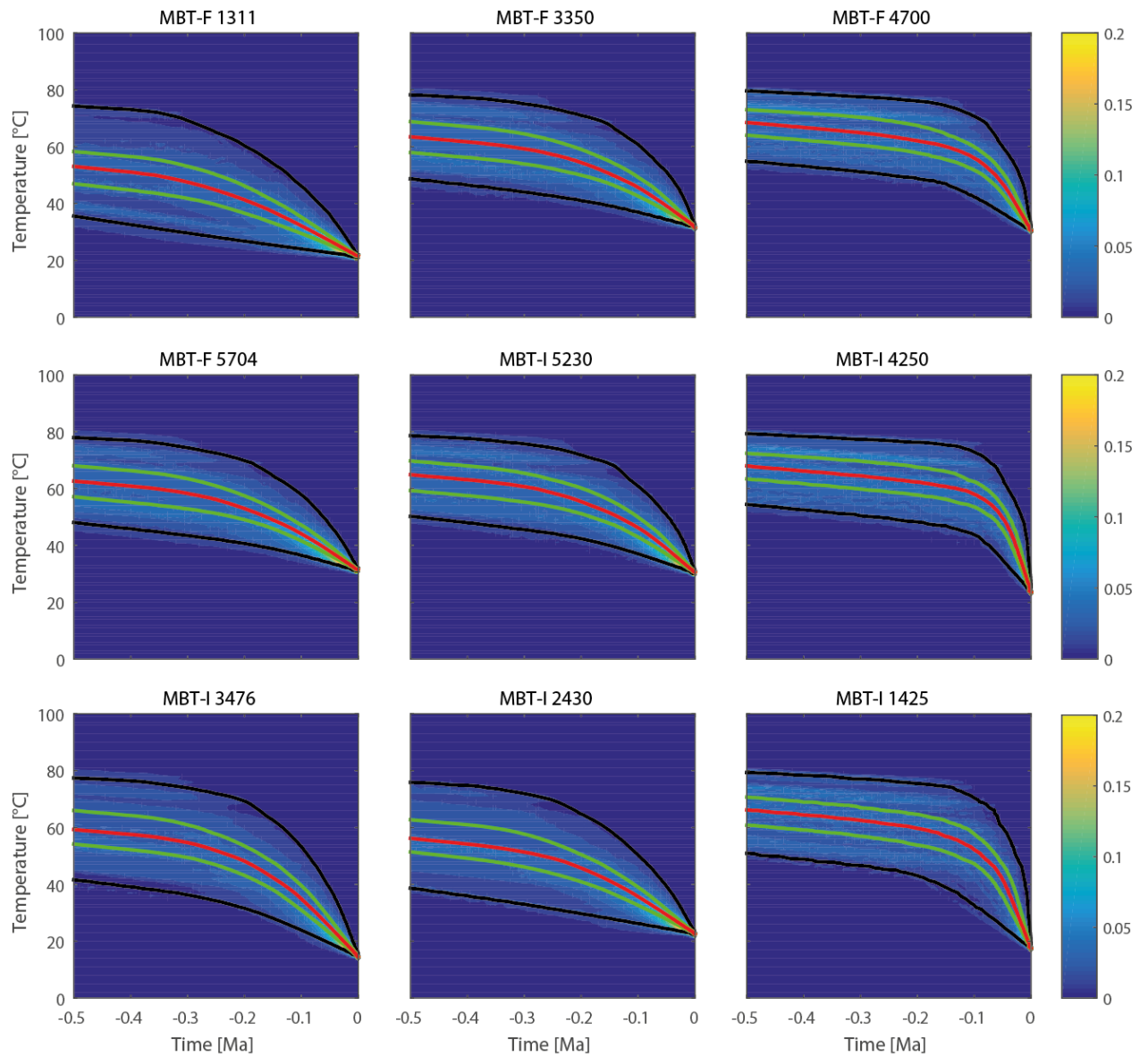


Fig. 4-6: Probability density functions calculated from the data shown in Figure 4-5 per time slice with the median in red, the 68 % confidence interval lines in green and the 95 % confidence intervals in black.

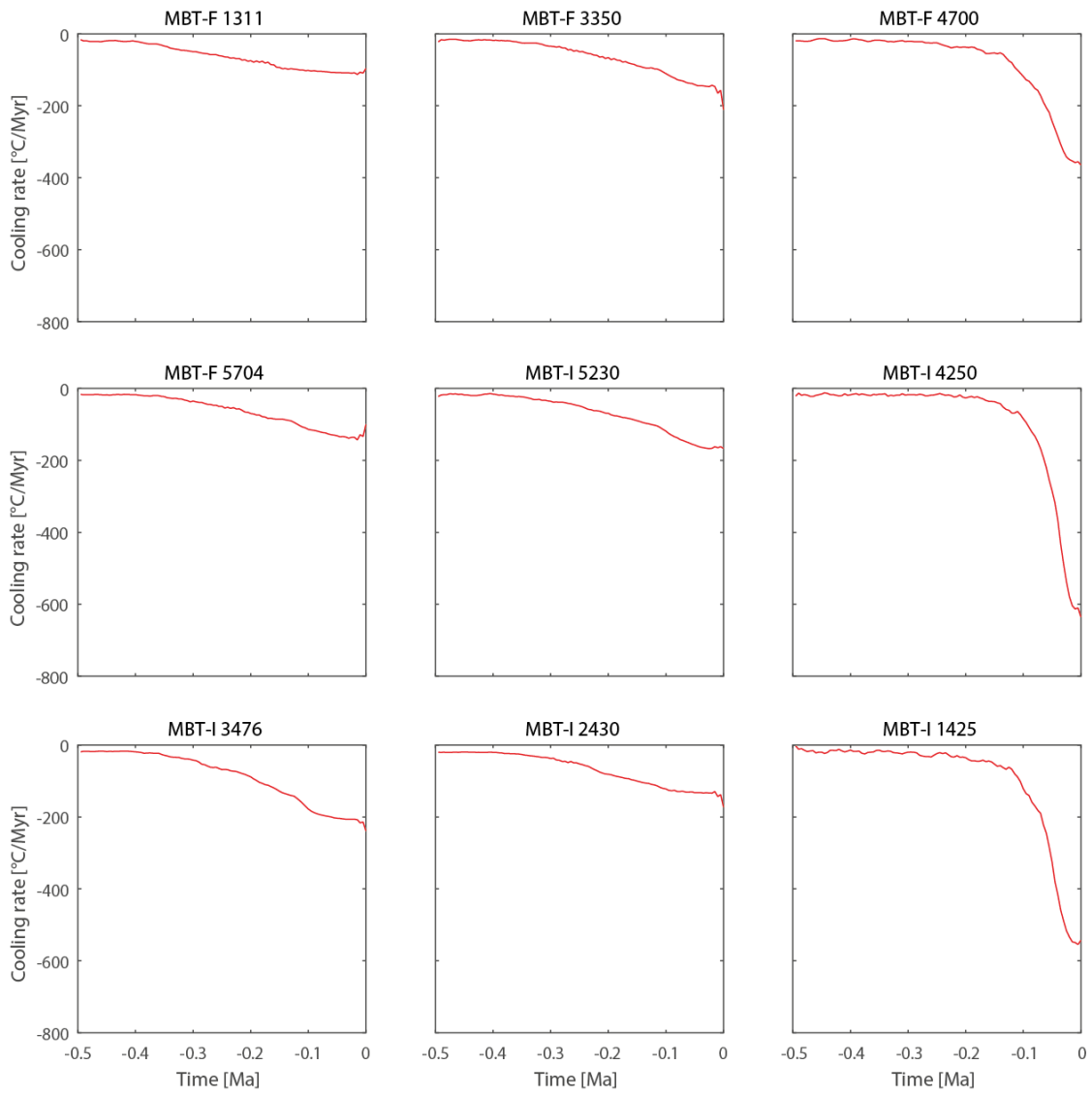


Fig. 4-7: Derivatives of cooling paths based on the median of each probability density function per time slice for each sample.

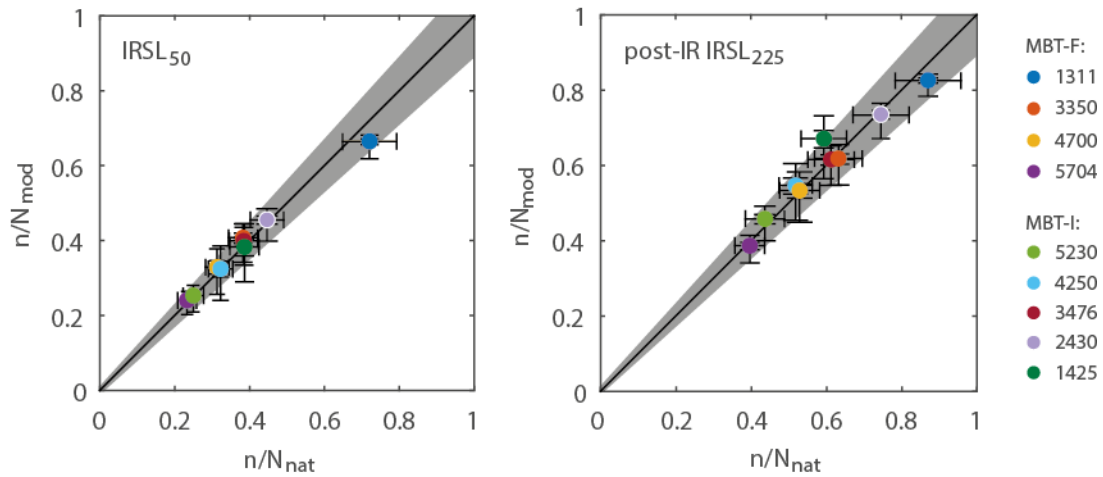


Fig. 4-8: n/N_{mod} values for the $IRSL_{50}$ and post-IR $IRSL_{225}$ signal resulting from a simulation of the evolution of the trapped charge concentration following the cooling path described by the median of each probability density function per time slice. The grey shaded area represents 10 % deviation from the 1:1 line.

4.5.5 Reconstructed past temperatures along tunnel transect

In Figure 4-9, reconstructed past temperatures extracted from the median temperature paths (red dots) are plotted along the tunnel transect for ten time slices ranging from 10 to 100 ka. Temperatures per time slice are connected by a black dotted line (only indicative) and the rock sample temperature curve (measured during tunnel construction in 1960s) is represented by the green dotted line. The modelled temperature curve at 12 ka following the simulations of Maréchal et al. (1999) is also displayed by the green solid line. For most samples, the past temperatures show a constant decrease over this time period. Relative to sample MBT-I 2430 the temperature anomaly, indicated by the past temperatures of sample MBT-I 3476, becomes gradually more apparent from 100 to 10 ka. Samples MBT-F 4700, MBT-I 4250 and MBT-I 1425 show a strong increase in cooling over the last 100 ka and have much higher (about 15 °C) past temperatures at 100 ka compared to the other samples. Whereas Maréchal et al. (1999) simulated a decrease in rock temperature at tunnel elevation of 0-25 °C over 12 ka, equating to a cooling rate of ~0-21 °C/ 10 ka, the luminescence results indicate cooling of 10-37 °C over 100 ka, thus an average cooling rate of ~1-4 °C/ 10 ka.

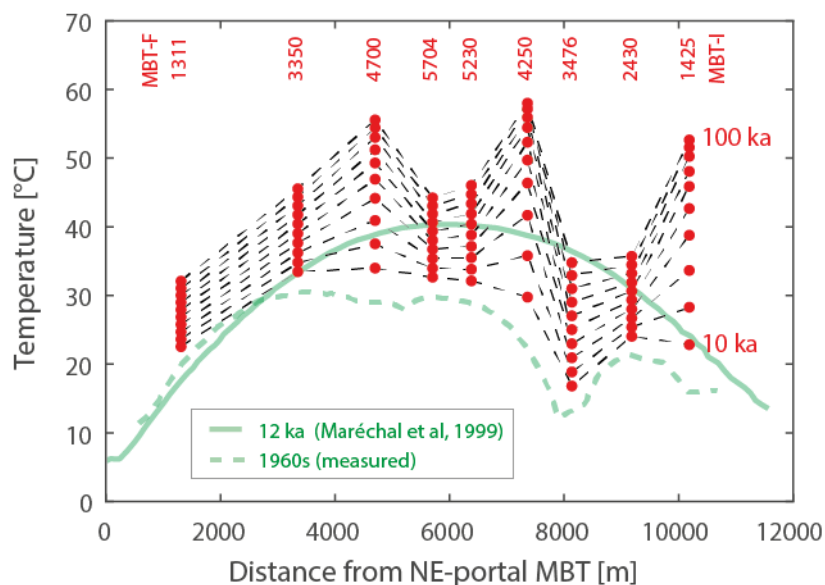


Fig. 4-9: Reconstructed past temperatures extracted from the median temperature paths along the tunnel transect for ten time slices ranging from 10 to 100 ka (red dots). Measured rock sample temperature data (1960s) is displayed by the green dotted line and modelled rock temperature 12 ka at tunnel elevation (Maréchal et al., 1999) is indicated by the green solid line.

4.6 Discussion

4.6.1 Natural luminescence signal trends

The observed trend of n/N_{nat} values with sample location is generally consistent, with that anticipated: for samples that are relatively close to the surface (located close to the tunnel openings), where ambient temperatures and thermal detrapping rates are relatively low, the n/N_{nat} values are higher than for samples deeper in the mountain massif (located in the middle of the tunnel). Sample MBT-I 1425 is an exception to this observed trend with relatively low n/N_{nat} values for both luminescence signals. No anti-correlation between n/N_{nat} values and sample rock temperatures is found (Figure 4-3a). Several studies use the criterion that natural n/N_{nat} values should be at least 15 % from the steady-state n/N_{ss} values to be able to provide reliable information on its cooling history (Guralnik et al., 2015a; King et al., 2016b). This approach has been proposed to deal with the last part of the dose response curve, where the slope becomes more shallow but it is not clear when saturation is reached, both in laboratory and natural settings (Li et al., 2018). While the n/N_{nat} values are lower than the steady-state n/N_{ss} values for the other samples, Figure 4-3b shows that the luminescence signals are all close to saturation and some fall within the grey area. Although the obtained values appear thus critical, we consider the complete data set in our analyses, assuming one sample, MBT-F 1311, being in field saturation. This sample is located near one of the tunnel openings and has natural n/N_{nat} values for both the IRSL₅₀ and the post-IRSL₂₂₅ signal that are

similar to or even slightly higher than the predicted steady-state n/N_{ss} values for these luminescence signals.

The apparent steady-state temperatures along the tunnel transect are higher than the final rock sample temperatures, except for sample MBT-F 1311, closest to the NW-portal of the tunnel, which has already been identified as being in thermal steady-state. Although not consistent with all samples, the trend appears similar to the rock sample temperature trend, including a negative anomaly. For samples MBT-I 1425 and MBT-I 4250, the deviation between apparent steady-state temperature and rock sample temperature is largest. One explanation for these similar temperature trends could be that the n/N_{nat} values are structurally too low, relative to the n/N_{ss} values, and falsely indicate a cooling history (i.e. no thermal steady-state). This could be due to an overestimation of the luminescence level of saturation derived from laboratory experiments. We have tested this option by fitting the dose response data with a single exponential growth curve (kinetic parameter $a = 1$) and obtained slightly higher n/N_{nat} values, but simulations have shown that a deviation between n/N_{nat} and n/N_{ss} values remains.

An alternative explanation may be that since the calculation of the apparent steady-state temperatures is independent of the rock sample temperature, some of the kinetic parameters may be temperature dependent. There is a clear trend of g_{2d} values along the tunnel transect, which increase towards the center of the tunnel. We speculate that this may be indicative of a changing structure of electron energy levels available to the electrons in IR sensitive traps as the crystals cool, associated with increasing crystal order, even when the temperature window is very low (10 - 40 °C). Regarding the other kinetic parameters, no systematic trends were found and we note that such trends were not recorded in the OSL-thermochronometry validation study of Guralnik et al. (2015).

The 1960s tunnel rock temperature trend generally follows the topography of the massif (Figure 4-1) with a negative anomaly where fluid infiltration via a tectonic structure at about 8000 m from the NW-portal has occurred. This anomaly is not apparent in the n/N_{nat} values at this location, which one would anticipate to be elevated relative to adjacent samples. Considering the natural luminescence signals only, it seems that the system was not sensitive to the rock temperature changes due to the process of fluid infiltration. One could argue that fluid infiltration has only been recent or sporadic and that the IRSL thermochronometric system is not sensitive enough to pick up changes in the geothermal gradient due this process.

4.6.2 Thermal history reconstruction

The inversion of the two stage linear cooling paths suggests that most samples have experienced relatively fast cooling of the order of 10 to 35 °C/ 100 ka. These cooling rates are difficult to explain

by exhumation only. Assuming a geothermal gradient of 25-30 °C/km, a cooling rate of about 20 °C/100 ka would be indicative of an exhumation rate of 7 to 8 mm/a, which is unlikely in this setting where erosion rates have been estimated to be > 1 mm/a and locally up to 2 mm/a (Glotzbach et al., 2011). Cooling due to erosion would thus only explain 10-20 % of the total cooling rate. Other processes than exhumation, such as fluid infiltration via the tectonic structure at around 8000 m from the NW-portal (Fig. 4-1; Baggio and Malaroda, 1962), have likely contributed to cooling in this setting.

Within this context, the high cooling rate of sample MBT-I 3476, which is situated within the thermal anomaly zone might be plausible. Particularly high cooling rates were obtained for samples MBT-F 4700, MBT-I 4250 and MBT-I 1425 and may have different underlying origins. For sample MBT-I 1425, the relatively low n/N_{nat} values for both luminescence signals may be indicative of the system having been (partially) re-set by a heating event, perhaps related to the nearby Mont Blanc back-thrust (Figure 4-1), although no indications for recent local tectonic activity were found by Egli and Mancktelow (2013). For samples MBT-F 4700 and MBT-I 4250, given that their n/N_{nat} values do not deviate from the observed trend, the relatively high apparent steady-state temperatures and (two-stage) linear cooling rates seem to follow from kinetic parameter values, although there is nothing remarkable about their data sets. In addition, the imposed relatively low final rock sample temperature of sample MBT-I 4250 contributes to obtaining an extremely high cooling rate.

Although the derived cooling rates are high with respect to plausible exhumation rates in this setting, the average cooling rates, 1-4 °C/10 ka, are lower than the short term fluid infiltration cooling rates modelled by Maréchal et al. (1999). The obtained cooling rates may thus partly be explained by exhumation, but may also reflect the limit in temporal resolution for which IRSL thermochronometry can resolve changes in rock temperature (King et al., 2016c). We note that some of the kinetic parameters appear to be sensitive to changes in temperature, something that needs further investigation. We conclude that trapped charge evolution in IR sensitive traps may not be sensitive to changes in the geothermal gradient at timescales < 100 ka. Our results suggest rapid cooling in the massif over the last 100 ka. However, to be able to resolve temperature changes over this timescale, one may assess a shallower (set of) trap(s). Application of thermoluminescence (TL) enables the assessment of a range of traps in feldspar and may thus offer that possibility (Biswas et al., 2018).

4.7 Conclusions

We applied IRSL luminescence thermochronometry to samples taken from the Mont Blanc tunnel (west European Alps) and tested the sensitivity of this method to changes in the thermal field related to meteoric fluid infiltration in the massif via a tectonic structure. Together with existing apatite

fission track and (U-Th-[Sm])/He data, our new data provide constraints on the thermal history of the Mont Blanc massif, suggesting there has been rapid cooling during the last 100 ka of the order of 1 to 4 °C/ 10 ka. Previous hydro-thermal modeling results (Maréchal et al., 1999) suggested significantly higher cooling rates between 5 and 20 °C/ 10 ka, but over a shorter timescale of 12 ka. Cooling due to erosion can only explain 10-20 % of the total cooling rate and our results imply that feldspar IRSL thermochronometry provides constraints on changes of the geotherm integrated over 100 ka, but may not constrain changes at 1-10 ka timescales as previously suggested by King et al. (2016a). Thus, changes in the geotherm due to these processes could be relevant to take into account in luminescence thermochronometry studies in a rock cooling setting. Moreover, luminescence techniques could provide constraints in a setting dominated by hydrothermal flow, with potential for geothermal energy applications.

Acknowledgements

We thank the Cantonal Museum of Geology in Lausanne (Switzerland) for providing the MBT samples, giving access to their archives and their kind support for this study. We are thankful to Sally Lowick for use of the Bern luminescence laboratory for sample chemical treatment whilst the luminescence laboratory at the University of Lausanne was being constructed. This research was funded by Swiss National Fund (SNF) grant numbers PP00P2-38956 and 200021-127127 awarded to FH, PZ00P2_148191 and PP00P2_170559 awarded to PGV, and PZ00P2-167960 awarded to GEK.

References

- Aitken, M.J., 1985. Thermoluminescence dating. Academic press.
- Auclair, M., Lamothe, M., Huot, S., 2003. Measurement of anomalous fading for feldspar IRSL using SAR. *Radiation measurements* 37, 487-492.
- Baggio, P., Malaroda, R. (1962). Il traforo del Monte Bianco; prime osservazioni geologiche sul tratto dalla progressiva 2500 alla progressiva 3700. *Parte Italiana. Accad Naz Lincei Sc Fis Mat Nat* 33, 149-153.
- Biswas, R., Herman, F., King, G., Braun, J., 2018. Thermoluminescence of feldspar as a multi-thermochronometer to constrain the temporal variation of rock exhumation in the recent past. *Earth and Planetary Science Letters* 495, 56-68.
- Bøtter-Jensen, L., Thomsen, K.J., Jain, M., 2010. Review of optically stimulated luminescence (OSL) instrumental developments for retrospective dosimetry. *Radiation Measurements* 45, 253-257.
- Braun, J., Van Der Beek, P., Batt, G., 2006. *Quantitative thermochronology: numerical methods for the interpretation of thermochronological data.* Cambridge University Press.
- Buylaert, J.-P., Jain, M., Murray, A.S., Thomsen, K.J., Thiel, C., Sohbati, R., 2012. A robust feldspar luminescence dating method for Middle and Late Pleistocene sediments. *Boreas* 41, 435-451.

- Clauser, C., Huenges, E., 1995. Thermal conductivity of rocks and minerals. *Rock physics & phase relations: a handbook of physical constants*, 105-126.
- Dodson, M.H., 1973. Closure temperature in cooling geochronological and petrological systems. *Contributions to Mineralogy and Petrology* 40, 259-274.
- Durcan, J.A., King, G.E., Duller, G.A., 2015. DRAC: Dose Rate and Age Calculator for trapped charge dating. *Quaternary Geochronology* 28, 54-61.
- Egli, D., Mancktelow, N., 2013. The structural history of the Mont Blanc massif with regard to models for its recent exhumation. *Swiss journal of geosciences* 106, 469-489.
- Farley, K., 2000. Helium diffusion from apatite: General behavior as illustrated by Durango fluorapatite. *Journal of Geophysical Research: Solid Earth* 105, 2903-2914.
- Fox, M., Herman, F., Kissling, E., Willett, S.D., 2015. Rapid exhumation in the Western Alps driven by slab detachment and glacial erosion. *Geology* 43, 379-382.
- Glotzbach, C., Reinecker, J., Danišić, M., Rahn, M., Frisch, W., Spiegel, C., 2008. Neogene exhumation history of the Mont Blanc massif, western Alps. *Tectonics* 27 (4).
- Glotzbach, C., van der Beek, P.A., Spiegel, C., 2011. Episodic exhumation and relief growth in the Mont Blanc massif, Western Alps from numerical modelling of thermochronology data. *Earth and Planetary Science Letters* 304, 417-430.
- Guralnik, B., Ankjærgaard, C., Jain, M., Murray, A.S., Müller, A., Wälle, M., Lowick, S.E., Preusser, F., Rhodes, E.J., Wu, T.-S., 2015a. OSL-thermochronometry using bedrock quartz: A note of caution. *Quaternary geochronology* 25, 37-48.
- Guralnik, B., Jain, M., Herman, F., Ankjærgaard, C., Murray, A.S., Valla, P.G., Preusser, F., King, G.E., Chen, R., Lowick, S.E., 2015b. OSL-thermochronometry of feldspar from the KTB borehole, Germany. *Earth and Planetary Science Letters* 423, 232-243.
- Guralnik, B., Jain, M., Herman, F., Paris, R.B., Harrison, T.M., Murray, A.S., Valla, P.G., Rhodes, E.J., 2013. Effective closure temperature in leaky and/or saturating thermochronometers. *Earth and Planetary Science Letters* 384, 209-218.
- Guralnik, B., Li, B., Jain, M., Chen, R., Paris, R.B., Murray, A.S., Li, S.-H., Pagonis, V., Valla, P.G., Herman, F., 2015c. Radiation-induced growth and isothermal decay of infrared-stimulated luminescence from feldspar. *Radiation Measurements* 81, 224-231.
- Herman F., King G.E., 2018. Luminescence Thermochronometry: Investigating the Link between Mountain Erosion, Tectonics and Climate. *Elements: An International Magazine of Mineralogy, Geochemistry, and Petrology* 14, 33-38.
- Herman, F., Rhodes, E.J., Braun, J., Heiniger, L., 2010. Uniform erosion rates and relief amplitude during glacial cycles in the Southern Alps of New Zealand, as revealed from OSL-thermochronology. *Earth and Planetary Science Letters* 297, 183-189.
- Huntley, D., 2006. An explanation of the power-law decay of luminescence. *Journal of Physics: Condensed Matter* 18, 1359.
- Huntley, D.J., Godfrey-Smith, D.I., Thewalt, M.L., 1985. Optical dating of sediments.

- Huntley, D., Lian, O.B., 2006. Some observations on tunnelling of trapped electrons in feldspars and their implications for optical dating. *Quaternary Science Reviews* 25, 2503-2512.
- Kars, R.H., Wallinga, J., 2009. IRSL dating of K-feldspars: Modelling natural dose response curves to deal with anomalous fading and trap competition. *Radiation Measurements* 44, 594-599.
- Kars, R.H., Wallinga, J., Cohen, K., 2008. A new approach towards anomalous fading correction for feldspar IRSL dating—tests on samples in field saturation. *Radiation Measurements* 43, 786-790.
- King, G.E., Guralnik, B., Valla, P.G., Herman, F., 2016a. Trapped-charge thermochronometry and thermometry: A status review. *Chemical Geology* 446, 3-17.
- King, G.E., Herman, F., Guralnik, B., 2016b. Northward migration of the eastern Himalayan syntaxis revealed by OSL thermochronometry. *Science* 353, 800-804.
- King, G.E., Herman, F., Lambert, R., Valla, P.G., Guralnik, B., 2016c. Multi-OSL-thermochronometry of feldspar. *Quaternary Geochronology* 33, 76-87.
- Lambert, R., King, G.E., Valla, P.G., Herman, F., in review. Towards OSL-thermochronometry of the Mont Blanc massif: Experimental investigations into constraining feldspar thermal decay. *Radiation Measurements*.
- Leloup, P.H., Arnaud, N., Sobel, E.R., Lacassin, R., 2005. Alpine thermal and structural evolution of the highest external crystalline massif: The Mont Blanc. *Tectonics* 24 (4).
- Li, B., Li, S.-H., 2011. Luminescence dating of K-feldspar from sediments: a protocol without anomalous fading correction. *Quaternary Geochronology* 6, 468-479.
- Li, B., Li, S.-H., 2012. Determining the cooling age using luminescence-thermochronology. *Tectonophysics* 580, 242-248.
- Li, Y., Tsukamoto, S., Long, H., Zhang, J., Yang, L., He, Z., Frechen, M., 2018. Testing the reliability of fading correction methods for feldspar IRSL dating: A comparison between natural and simulated-natural dose response curves. *Radiation Measurements*.
- Maréchal, J.-C., Perrochet, P., Tacher, L., 1999. Long-term simulations of thermal and hydraulic characteristics in a mountain massif: The Mont Blanc case study, French and Italian Alps. *Hydrogeology Journal* 7, 341-354.
- Murray, A., Wintle, A., 2000. Application of the single-aliquot regenerative-dose protocol to the 375 C quartz TL signal. *Radiation Measurements* 32, 579-583.
- Qin, J., Chen, J., Valla, P.G., Herman, F., Li, K., 2015. Estimating rock cooling rates by using multiple luminescence thermochronometers. *Radiation Measurements* 79, 13-18.
- Reiners, P.W., Brandon, M.T., 2006. Using thermochronology to understand orogenic erosion. *Annu. Rev. Earth Planet. Sci.* 34, 419-466.
- Russell, H., 1935. Principles of heat flow in porous insulators. *Journal of the American Ceramic Society* 18, 1-5.
- Sohbati, R., Murray, A.S., Chapot, M.S., Jain, M., Pederson, J., 2012. Optically stimulated luminescence (OSL) as a chronometer for surface exposure dating. *Journal of Geophysical Research* 117.

- Thomsen, K.J., Murray, A.S., Jain, M., Bøtter-Jensen, L., 2008. Laboratory fading rates of various luminescence signals from feldspar-rich sediment extracts. *Radiation Measurements* 43, 1474-1486.
- Valla, P.G., Lowick, S.E., Herman, F., Champagnac, J.-D., Steer, P., Guralnik, B., 2016. Exploring IRSL 50 fading variability in bedrock feldspars and implications for OSL thermochronometry. *Quaternary Geochronology* 36, 55-66.
- Visocekas, R., 2002. Tunnelling in Afterglow: Its coexistence and interweaving with thermally stimulated luminescence. *Radiation protection dosimetry* 100, 45-53.
- Von Raumer, J., Neubauer, F., 1993. Late Precambrian and Palaeozoic evolution of the Alpine basement—an overview, *Pre-Mesozoic geology in the Alps*. Springer, pp. 625-639.
- Wallinga, J., Murray, A., Wintle, A., 2000. The single-aliquot regenerative-dose (SAR) protocol applied to coarse-grain feldspar. *Radiation Measurements* 32, 529-533.
- Whipp, D.M., Ehlers, T.A., 2007. Influence of groundwater flow on thermochronometer-derived exhumation rates in the central Nepalese Himalaya. *Geology* 35, 851-854.
- Wintle, A.G., 1973. Anomalous fading of thermo-luminescence in mineral samples. *Nature* 245, 143-144.

Supplementary

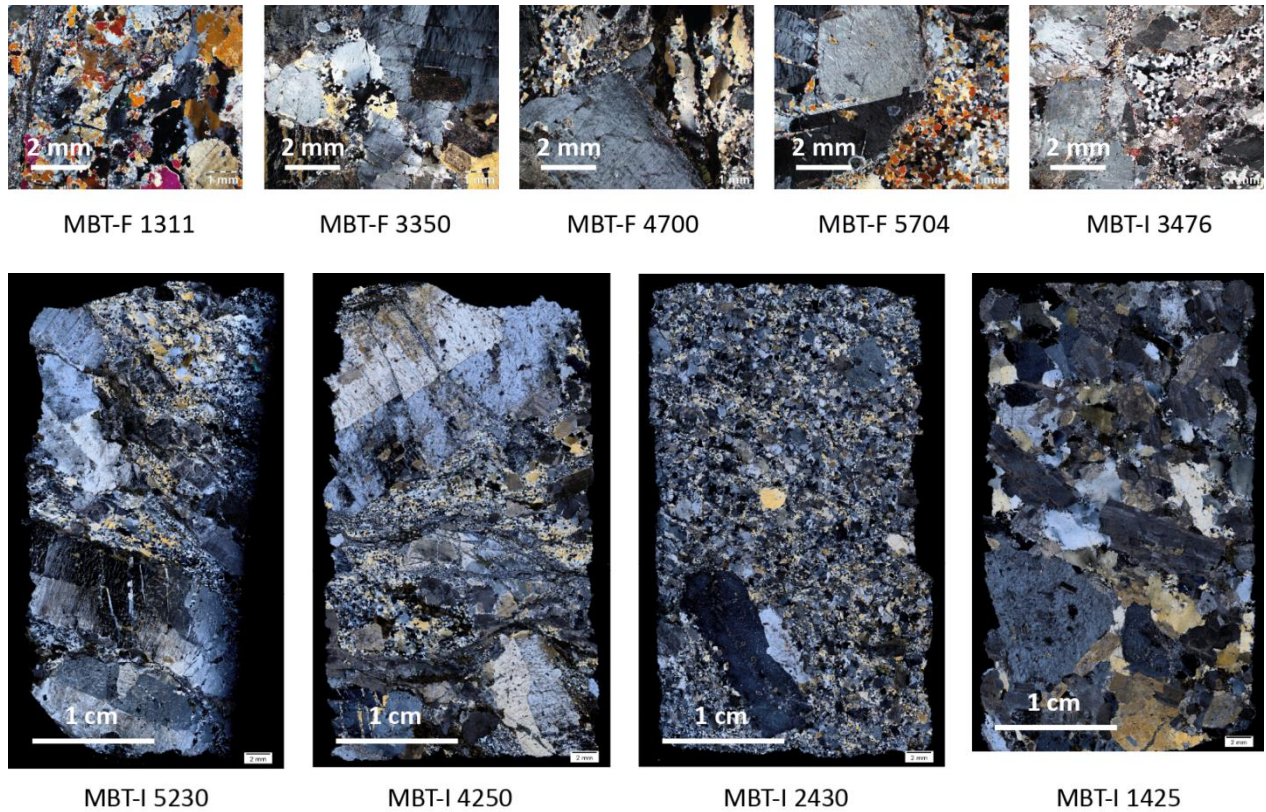


Fig. S-1: Thin sections of MBT samples in cross polarized light (XPL).

	Sample	180 μm	0.5 mm	1 mm	2 mm	5 mm	1 cm	Total
MBT-F	1311	0.25	0.25	0.25	0.25			1
	3350	0.2		0.5	0.1	0.1	0.1	1
	4700	0.3		0.4	0.1	0.1	0.1	1
	5704	0.2	0.1	0.2	0.2	0.2	0.1	1
MBT-I	5230	0.25		0.1	0.05		0.6	1
	4250	0.2		0.2	0.1	0.1	0.4	1
	3476	0.3	0.2	0.2	0.1	0.1	0.1	1
	2430	0.45		0.45	0.05		0.05	1
	1425	0.05	0.2	0.2	0.3	0.2	0.05	1

Table S-1: Feldspar grain size distributions for MBT samples based on thin sections.

Environmental dose rates \dot{D}_{env} [Gy/ka] were calculated for all MBT samples following an approach similar to that described in Durcan et al. (2015) and taking into account the variety in sample grain size (Table S-2). Dose rate conversion factors were based on Liritzis et al. (2013). Alpha attenuation factors were calculated for feldspar based on those given in Bell (1980) for quartz by considering smaller attenuation of the dose (7% was added to the attenuation factors for grain sizes $> 100 \mu\text{m}$). Beta attenuation factors were based on Guérin et al. (2012). Both alpha and beta attenuation factors were extrapolated for grain sizes up to 1 cm. Environmental dose rates \dot{D}_{env} [Gy/ka] were calculated for a range of grain sizes and weighted using the grain size distribution estimates given in Table S-1.

Sample		\dot{D}_{env} [Gy/ka]						
		180 μ m	0.5 mm	1 mm	2 mm	5 mm	1 cm	Total
MBT-F	1311	6.66	7.18	8.21	9.69	12.15	12.06	7.94
	3350	9.03	9.15	9.98	11.25	13.35	13.17	10.57
	4700	9.18	9.20	10.04	11.36	13.52	13.28	10.59
	5704	9.90	9.90	10.60	11.71	13.54	13.33	11.47
MBT-I	5230	8.93	8.89	9.79	11.25	13.62	13.31	11.76
	4250	11.14	10.71	11.47	12.81	14.98	14.59	13.14*
	3476	9.54	9.42	10.30	11.70	13.99	13.69	10.74
	2430	11.50	11.16	11.73	12.74	14.38	14.04	11.79
	1425	10.61	10.55	11.18	12.19	13.84	13.66	11.98

Table S-2: Environmental dose rates \dot{D}_{env} [Gy/ka] based on grain size distributions for each MBT sample (Table S-1). * For sample MBT-I 4250, a value of $\dot{D}_{env} = 11.25$ Gy/ka was assumed, the average of the environmental dose rates of samples MBT-I 5230 and MBT-I 3476.

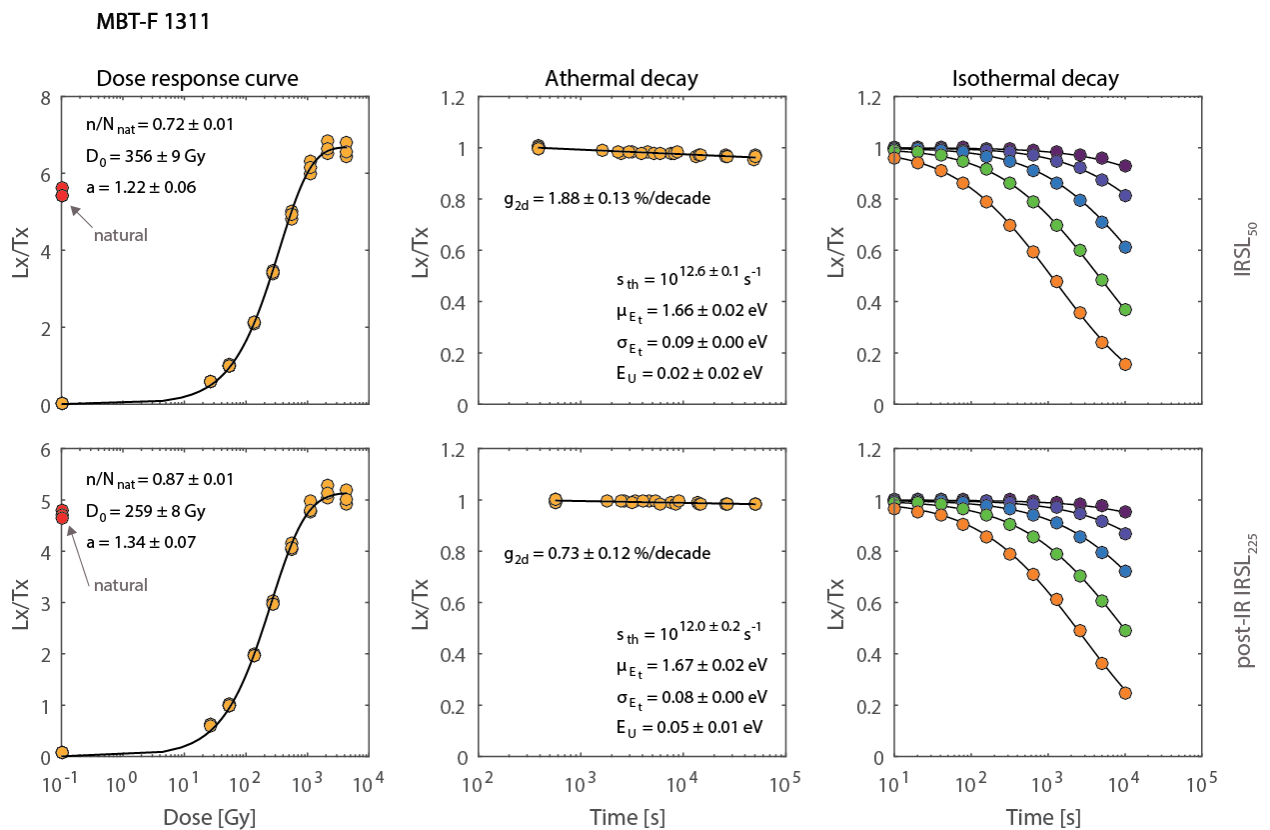
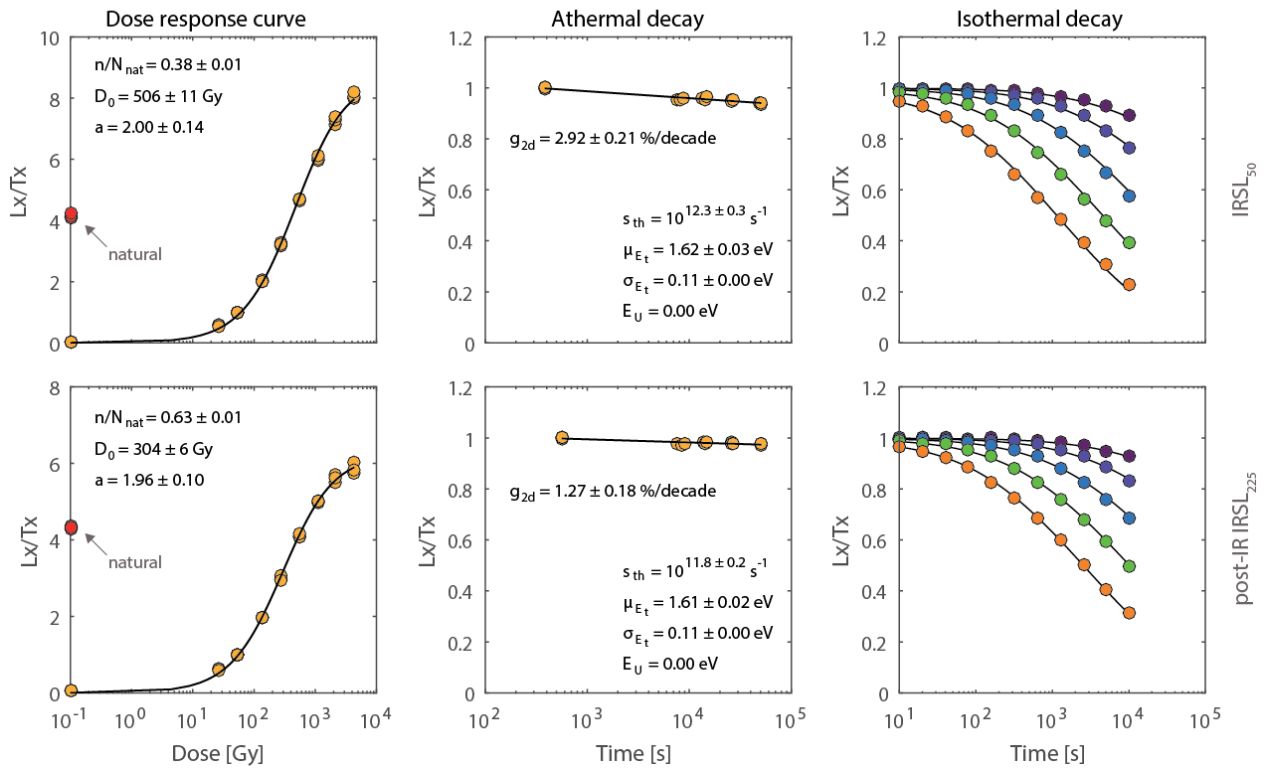
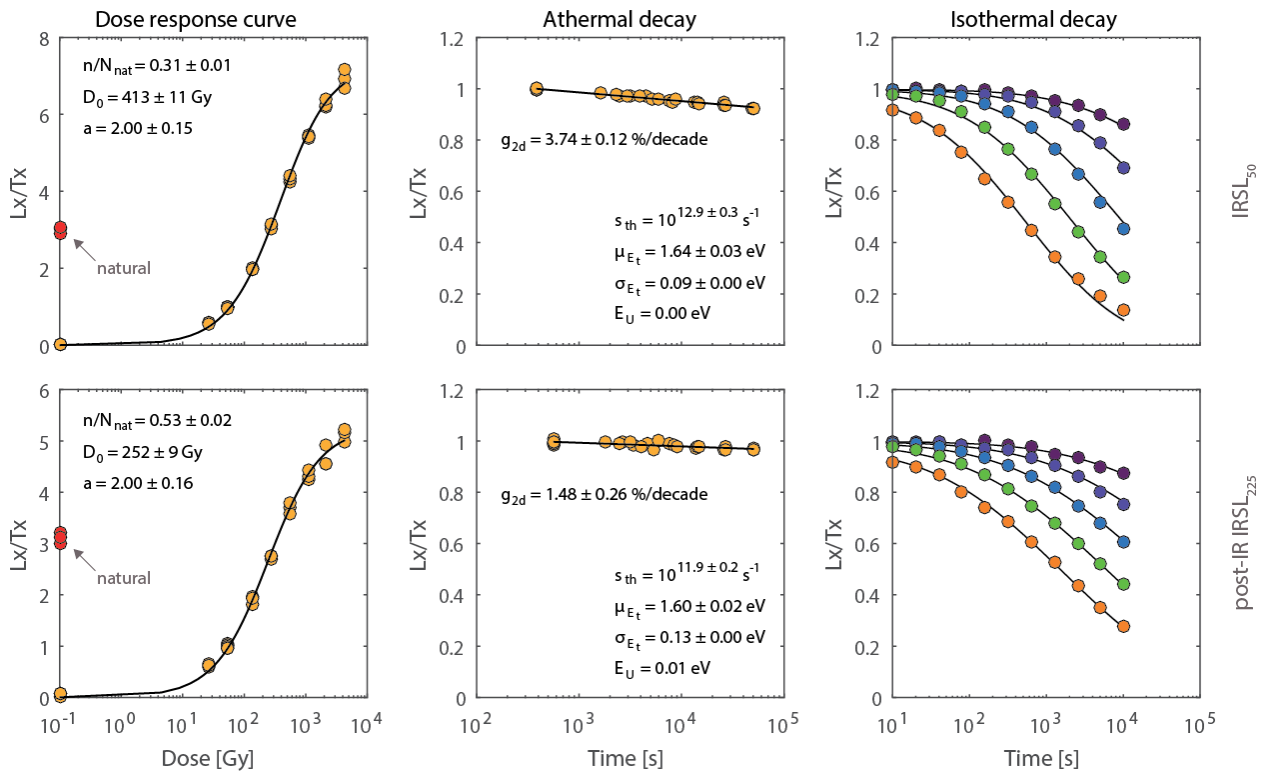


Fig. S-2: Measured IRSL₅₀ (top) and post-IR IRSL₂₂₅ (bottom) data of K-feldspar extracts from each of the MBT samples taken along the tunnel transect. The natural signal (L_n/T_n) is displayed by the red dots, measurements at room temperature, i.e. dose response curve and athermal decay data, are represented by yellow dots and measurements at elevated temperatures, i.e. isothermal decay data, are indicated by coloured dots: 170 °C = dark purple, 190 °C = dark blue, 210 °C = light blue, 230 °C = green, 250 °C = orange. From these experimental data the n/N_{nat} and kinetic parameters describing trapping, athermal and thermal detrapping were derived using equation (1).

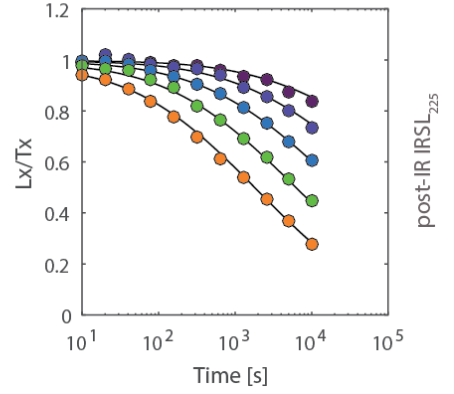
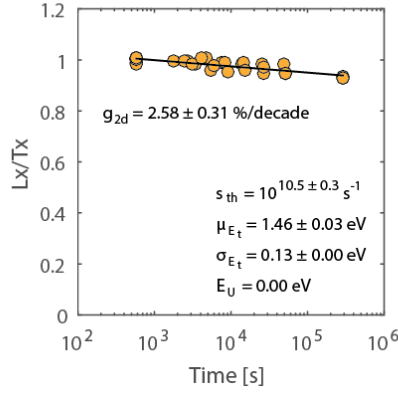
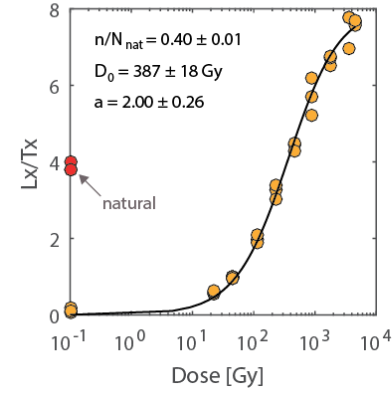
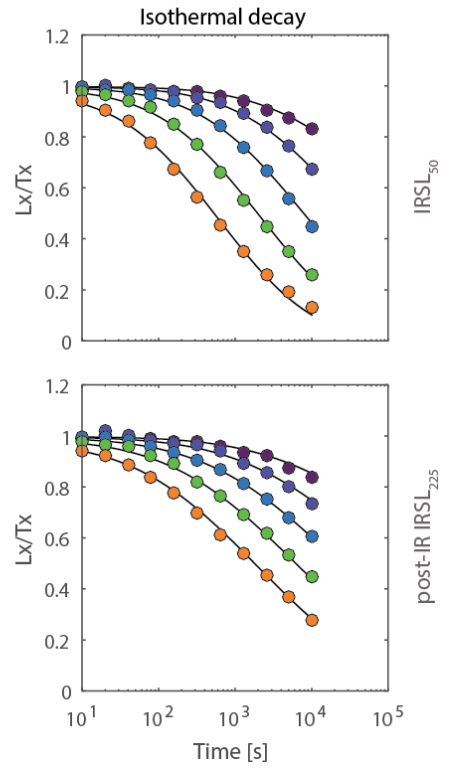
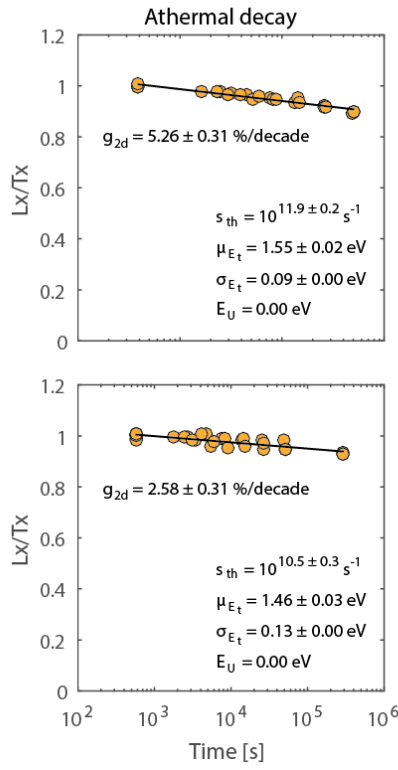
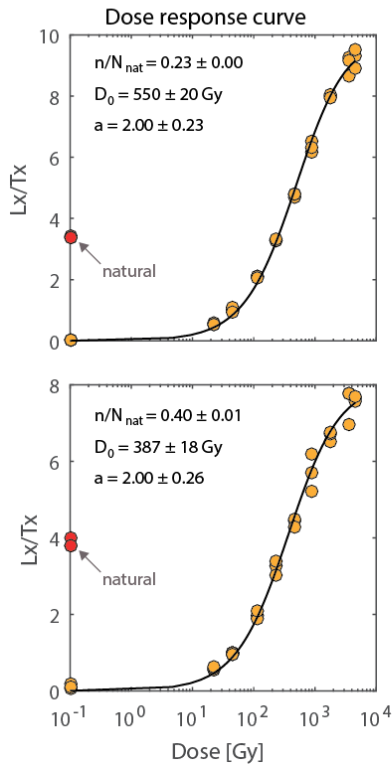
MBT-F 3350



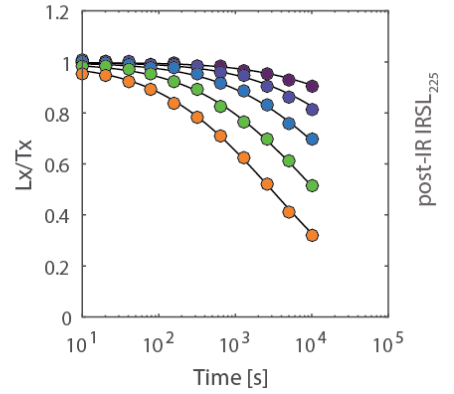
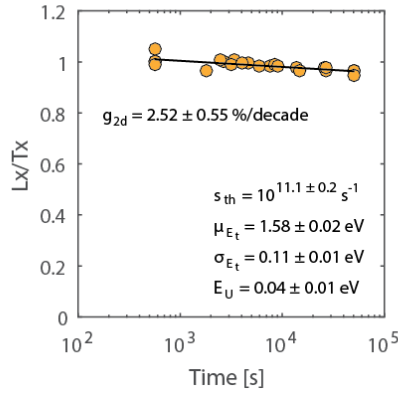
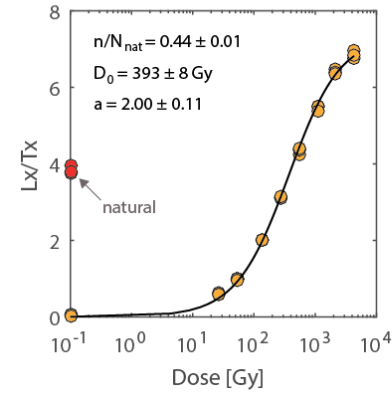
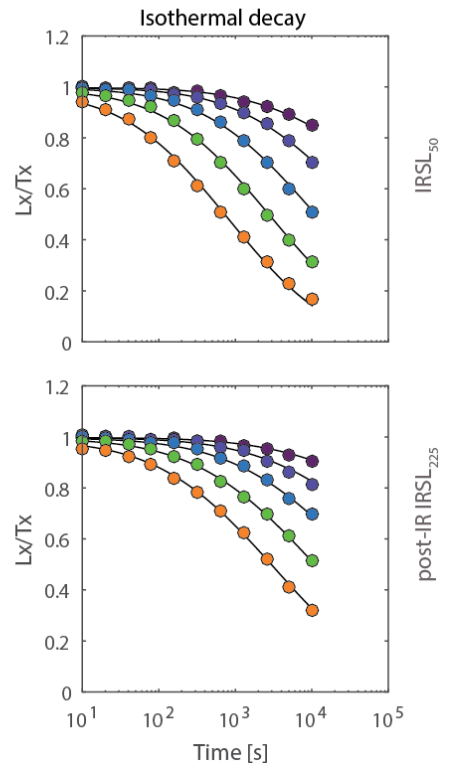
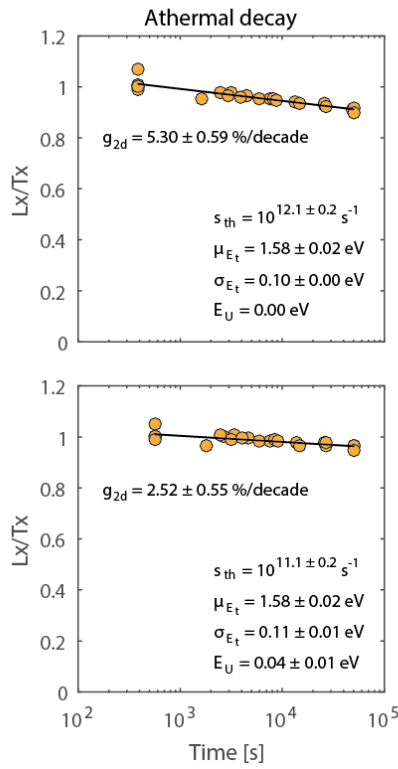
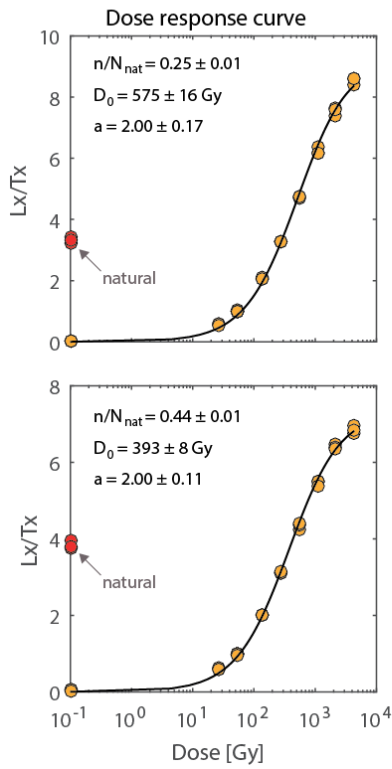
MBT-F 4700



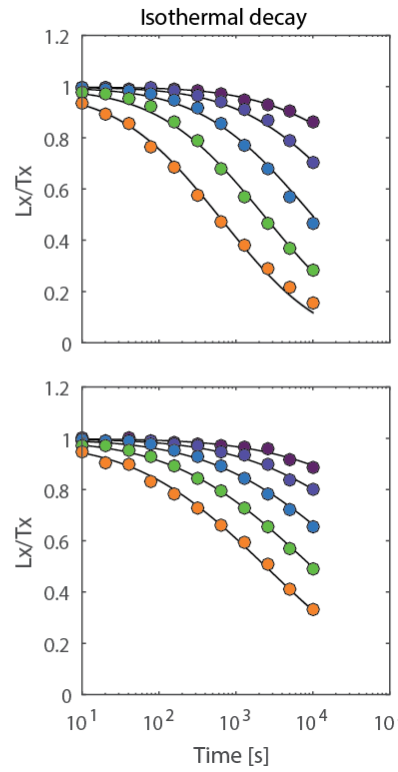
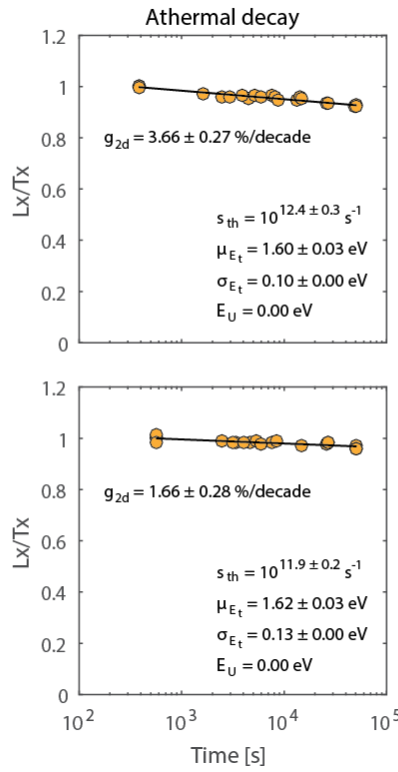
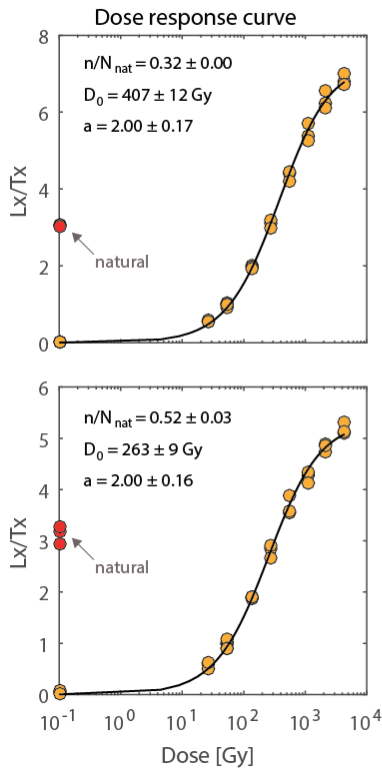
MBT-F 5704



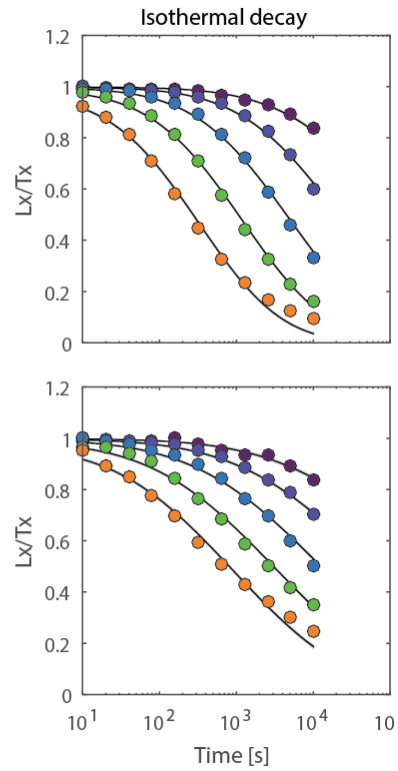
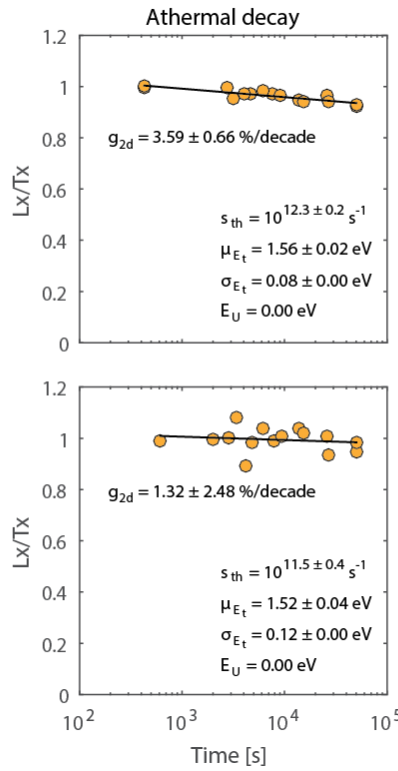
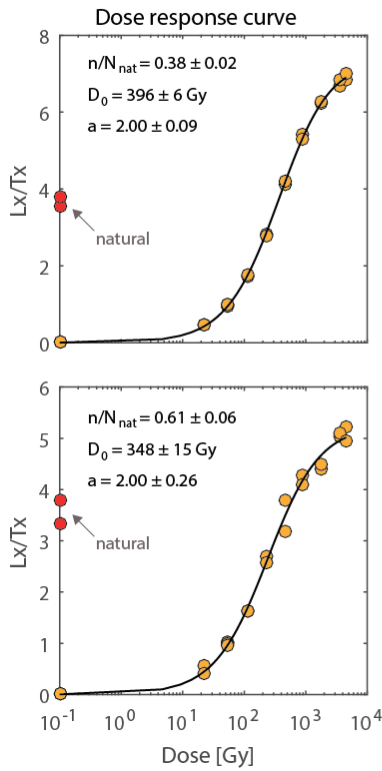
MBT-I 5230



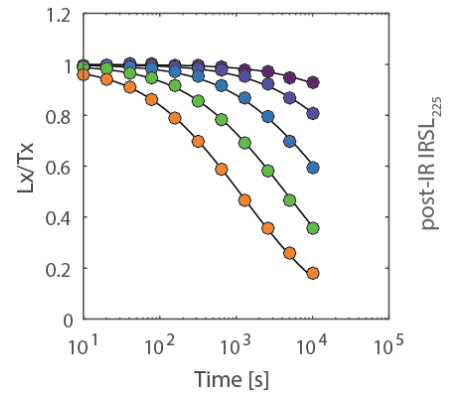
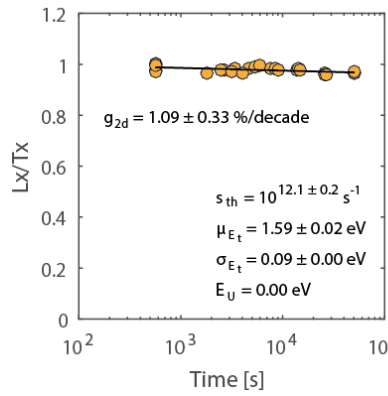
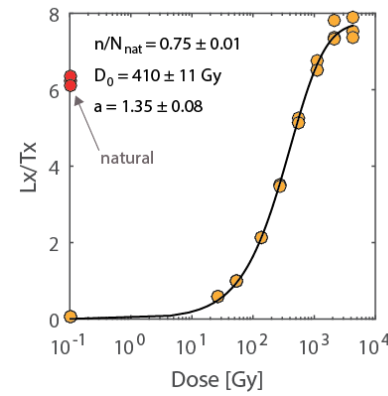
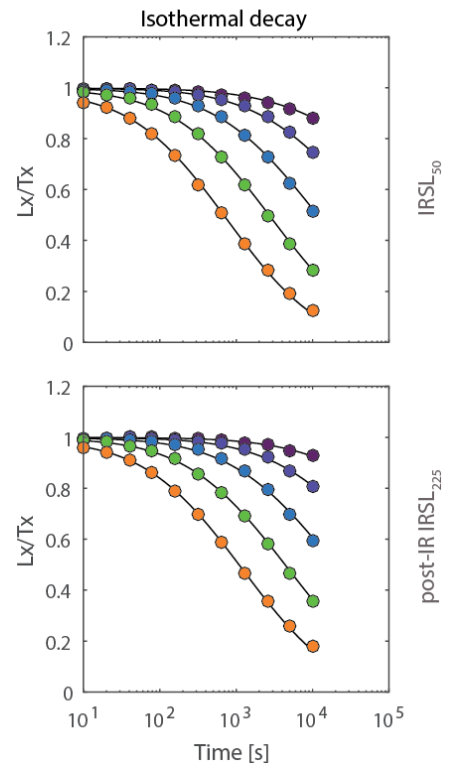
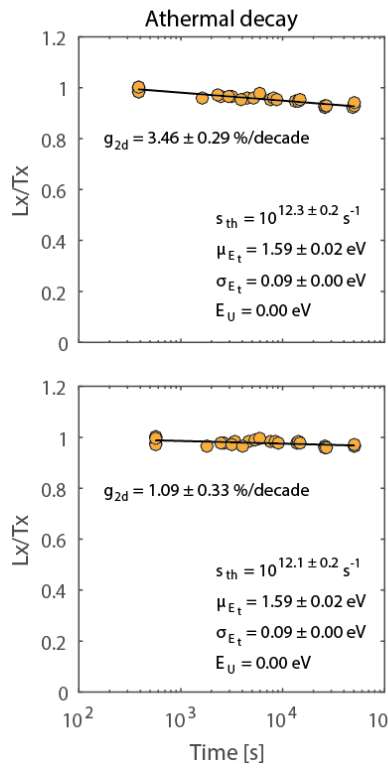
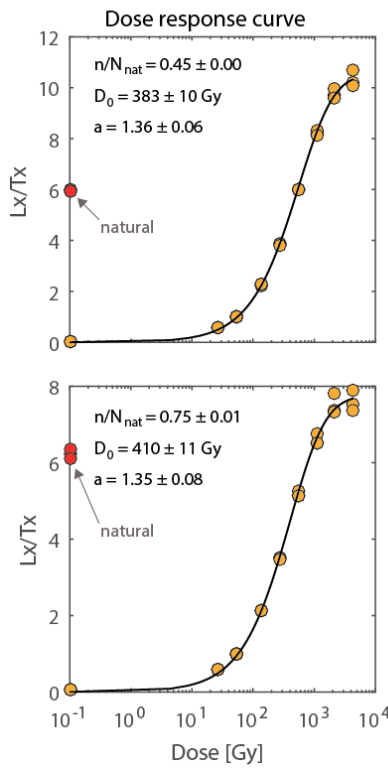
MBT-I 4250



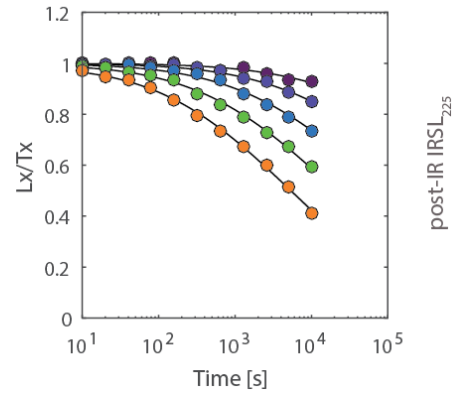
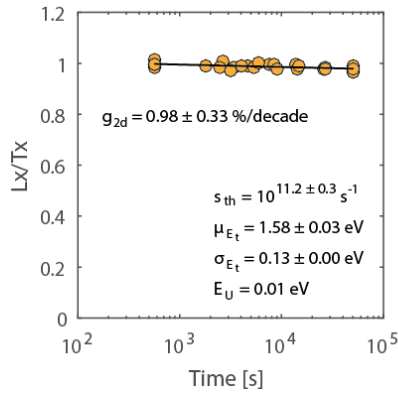
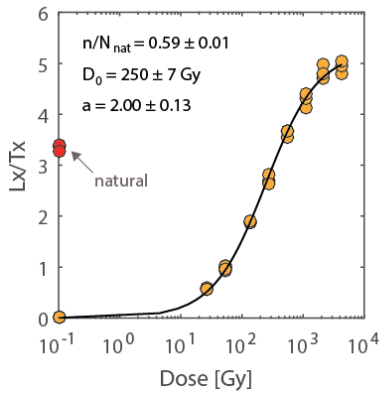
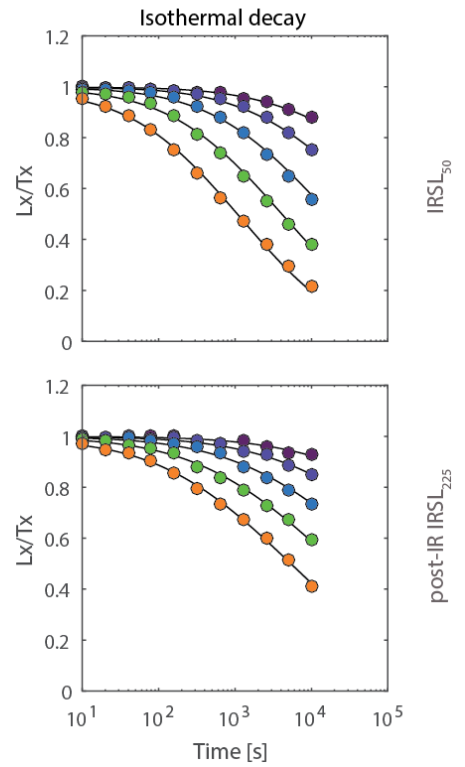
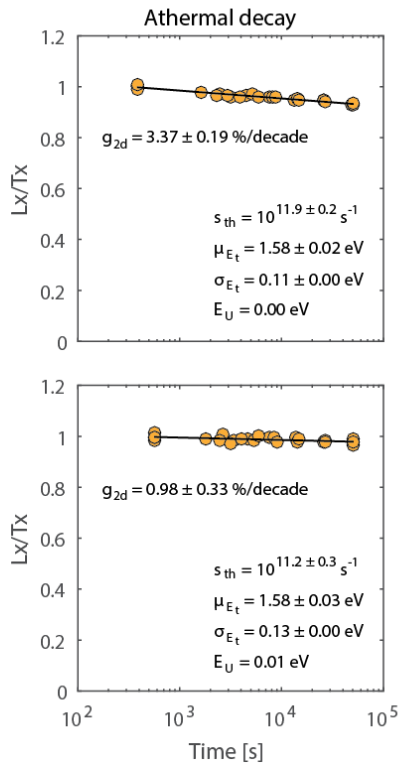
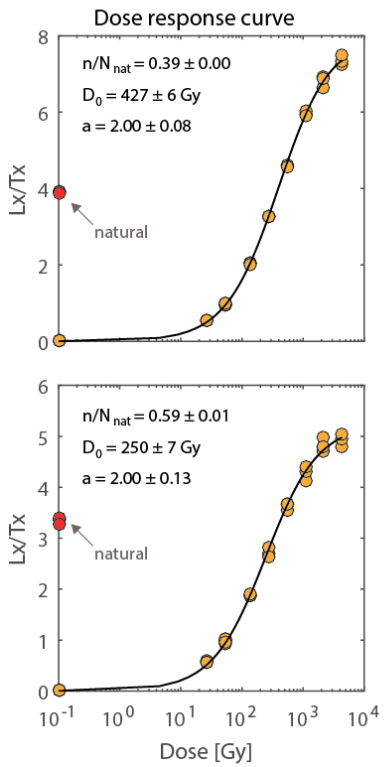
MBT-I 3476



MBT-I 2430



MBT-I 1425



References

- Bell, W., 1980. Alpha dose attenuation in quartz grains for thermoluminescence dating. *Ancient TL* 12, 8.
- Durcan, J.A., King, G.E., Duller, G.A., 2015. DRAC: Dose Rate and Age Calculator for trapped charge dating. *Quaternary Geochronology* 28, 54-61.
- Guérin, G., Mercier, N., Nathan, R., Adamiec, G., Lefrais, Y., 2012. On the use of the infinite matrix assumption and associated concepts: A critical review. *Radiation Measurements* 47, 778-785.
- Liritzis, I., Stamoulis, K., Papachristodoulou, C., Ioannides, K., 2013. A re-evaluation of radiation dose-rate conversion factors. *Mediterranean Archaeology & Archaeometry* 13, 1-15.

5. DISCUSSION AND CONCLUSIONS

In this chapter a synthesis is given of the three main chapters of the thesis. The implications of the main findings are discussed by putting them within the context of the wider field of luminescence. Finally, the major issues that need to be addressed for this work to be taken forward are considered in the section 'Perspectives'.

5.1 Synthesis

In Chapter 2, three related multiple first-order kinetic models were validated on published isothermal decay data from the KTB borehole (Guralnik et al, 2015). Based on the band-tail states model proposed by Li and Li (2013), a newly developed thermal decay model was introduced assuming a Gaussian distribution of activation energies. Although this study could not provide a direct proof of this decay mechanism, application showed improved data fit and all three multiple first-order decay models (based on band-tail states, a Gaussian distribution of trap depth and the combination) were validated in the specific thermal steady-state setting of the KTB borehole by predicting trapped charge concentrations similar to the trapped charge concentrations derived from the natural luminescence signals.

Chapter 3 presented experimental investigations to constrain the thermal decay of feldspar from Mont Blanc tunnel (MBT) samples, based on two thermal decay model types: a general order kinetics decay model and the three multiple first-order kinetic models discussed in Chapter 2. It was shown that the assumption of a general order decay system implies a dependence on the initial trapped charge. Isothermal decay experiments with varying doses showed that thermal decay in the investigated MBT sample is only slightly dose dependent in comparison to what is predicted by application of a general order kinetics model without making an assumption on the initial condition and thus does not follow purely general order kinetic behaviour. Isothermal decay experiments with varying preheat temperatures revealed a thermally more stable luminescence signal after the higher preheat. The data could be well fitted with a multiple first-order kinetic decay model based on a Gaussian distribution of trap depths and this model type is in agreement with a population of trapped electrons with a distribution of thermal lifetimes, as the experimental results suggest.

In Chapter 4, IRSL thermochronometry was applied to nine samples from the MBT, an actively eroding setting which experiences meteoric fluid infiltration. The thermal constraints following from these analyses were combined with thermal constraints from other low-temperature thermochronometric data (apatite fission track and (U-Th-[Sm])/He data) that were applied in this setting (Glotzbach et al., 2008). Through inverse modelling, most probable cooling paths were

derived for each sample, which suggest rock cooling of the order of 10 to 20 °C in the massif over the last 100 ka. Cooling due to erosion can only explain 10-20 % of the total cooling rate. The reconstructed past temperatures during the last 100 ka and corresponding cooling rates were compared with the results from a hydro-thermal modelling study by Maréchal et al. (1999), which suggested similar cooling but over a shorter timescale of 12 ka. The results indicate that IRSL thermochronometry can provide constraints on changes of the geotherm integrated over 100 ka, but may not be able to resolve changes in the geothermal gradient < 1-10 ka as found in a previous IRSL thermochronometry study by King et al. (2016b). Yet, future interpretation of luminescence thermochronometry data should account for changes in the near surface geothermal gradient related to hydrothermal flow.

5.2 Implications

Experimental analyses of the MBT samples indicated the necessity for the development of a thermal decay model that could explain the strong deviation from simple exponential decay. The experimental outcome of isothermal decay curves, being only slightly dependent on the initial given dose (Chapter 3), have shifted the concept of charge transport mechanisms based on trap competition and/or retrapping (general order kinetics behaviour) to spatially distributed energy levels and thermal lifetimes (multiple first-order kinetic decay). A distribution of thermal lifetimes based on a distribution of activation energies may reflect varying energy levels corresponding to both trap depth of IR sensitive traps and the conduction band due to a variation of bonding angles and defects in feldspar minerals (Chapter 2; Poolton et al., 2002; Poolton et al., 2009). This type of model had been proposed earlier to describe thermal decay in quartz by Huntley et al. (1996), but had not yet been developed for feldspar despite its plausibility given the open crystal structure of feldspar which allows the inclusion of many accessory elements (Fig. 5-1; Putnis, 1992; Malins et al., 2004). Through application, insight may be gained in the exact origin of the typical decay trends. This model concept is complementary to the localized model for feldspar charge transport by Jain et al. (2012; 2015) and provides a base for further research on charge transport mechanisms in feldspar with potential for wider applications, i.e. other luminescence techniques and minerals.

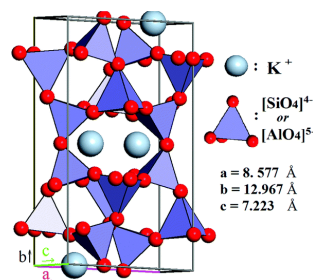


Fig. 5-1: K-feldspar chemical structure (KAlSi_3O_8) taken from <https://criticalzone.org>.

The focus on the concept of spatially distributed energy levels in feldspar crystals in this thesis and King et al. (2016b) has led to further investigations regarding band-tail states. In a study by Riedesel et al. (submitted), the excited and ground state of the principal IRSL trap and the width of the band-tail states of compositionally different feldspar samples have been optically probed. They found consistent values for trap depth and excited state, but varying band-tail widths. The model based on a Gaussian distribution of activation energies (Chapter 2) has been applied to experimental data using other luminescence techniques, i.e. blue light optically stimulated luminescence (OSL), thermally-transferred OSL (TT-OSL) and electron spin resonance (ESR) dating on quartz. Mineli et al. (in prep.) have applied the Gaussian trap depth model to OSL data of quartz from rocks and sediments and related the width to varying luminescence sensitivity and characteristic dose. In a study by Faershtein et al. (in review) the thermal stability of the TT-OSL main source trap was investigated through different experimental and modelling approaches. While the isothermal decay data was well fitted by the Gauss model, after extrapolation over geological timescales it significantly underestimated the TT-OSL thermal stability. Yukihiro et al. (2018) have described the challenges concerning the determination of thermal trap parameters and bridging laboratory (50-500 °C, 10^0 - 10^4 s) and application temperatures and timescales in both the fields of particle temperature sensing (300-1000 °C, μ s-s) and thermochronometry (~30-100 °C, ~ka-Ma). These studies reflect the growing interest and need for accurate thermal decay models and estimation of trapping parameters in the broader field of luminescence. A copy of the published studies is provided in the appendix, as well as a short description of my contribution.

The case study of IRSL thermochronometry applied to nine samples taken along the Mont Blanc tunnel transect has provided a new luminescence data set in a well-known and well-constrained setting in the European Alps (Chapter 4). Previous IRSL thermochronometry studies concerned a thermal steady-state setting (KTB borehole in Germany; Guralnik et al., 2015) and an extremely fast exhuming setting (Namche Barwe syntaxis in the Himalaya; King et al., 2016a). In this study, the method is applied to a setting with moderately fast exhumation and where meteoric fluid infiltration has played a role in rock cooling. Uncertainties remain on the kinetics of the system (e.g. possible temperature dependence of the rate of athermal decay), however, the study has demonstrated the strength of a combination of approaches (i.e. the luminescence data being complementary to other low-temperature data (Glotzbach et al., 2008) and hydro-thermal simulations based on present-day (1960s) temperature data (Maréchal et al., 1999)). No correlation was observed between the general trend of increased trapped charge concentrations with increased tunnel depth and the present-day rock sample temperature data, including a negative thermal anomaly due to fluid infiltration. Simulations of the evolution of trapped charge indicate rapid cooling during the last 100 ka. Much

faster cooling rates but over a shorter timescale of 12 ka were modelled by Maréchal et al. (1999). Whether cooling has actually occurred over 100 ka or over a shorter timescale corresponding to what has been suggested by Maréchal et al. (1999) needs further investigation, as IRSL thermochronometry may not be able to resolve changes in the geothermal gradient $< 1\text{-}10$ ka, as found by King et al. (2016b). Future interpretation of luminescence thermochronometry data should account for changes in the near surface geothermal gradient related to hydrothermal flow. The results have indicated the need of: (1) an increased temporal resolution for thermal constraints, and (2) validation through an independent method, which could both be provided by thermoluminescence (TL; Biswas et al., 2018). Moreover, luminescence techniques could provide constraints in a setting dominated by hydrothermal flow, with potential for applications in geothermal energy.

5.3 Perspectives

Luminescence thermochronometry is a recent field that has developed over the last 10 years. The charge transfer processes that are considered to play a role, i.e. trapping, thermal detrapping and athermal detrapping, are all subject to ongoing studies. Both fundamental research and applications may contribute to the advancement of this field, which is in line with this thesis.

The set of Mont Blanc tunnel samples that were analyzed are characteristic for their high sensitivity of their luminescence signals ($> 10^6$ cts/s during the preheat at 250 °C). Furthermore, both the dose response curves and the thermal decay curves show trends of a strong deviation from simple exponential growth and decay. A better understanding of the origin of this behaviour appears fundamental to our understanding of the kinetic processes and the role of the crystal energy structure. In Chapter 2, we proposed a thermal decay model based on a distribution of IR sensitive trap depths due to a strong variability in bonding angles within the crystal (Poolton et al., 2002; Poolton et al., 2009). A wide distribution suggests strong variability; however, an underlying mechanism of this form may only partly explain the observed data trend and needs experimental verification. In addition, it has not been fully explored which implications the assumption of a variability in crystal structure may have for the trapping process. It seems essential to characterize thermal eviction at the temperatures that we are interested in for IRSL thermochronometry. This could be done by doing isothermal decay experiments at relatively low temperatures (~ 100 °C) for longer durations (days-months), i.e. heating them in a separate oven after which signal loss could be measured in a Risø luminescence reader. Deviations from expected trends based on regular isothermal decay experiments (high temperatures, ~ 200 °C) and fading experiments (room

temperature), could be indicative of a lower energy state (an excited state or the IR resonance excited state) playing a role during thermal decay.

As the luminescence signals resulting from IR stimulations at 50 °C and subsequently at 225 °C are not direct measurements of the electron population(s) under investigation, this adds some uncertainty to the method. It is still being debated whether the above-mentioned luminescence signals have their origin from a single trap or multiple traps (Andersen et al., 2012; Jain et al., 2012). Despite extensive mineralogical studies on the luminescence properties of minerals relevant in luminescence dating (e.g. Krbetschek et al. 1997), there is still ongoing research to address the particular lattice defects contributing to IRSL signals (Thomsen et al., in review). Furthermore, we cannot exclude charge transfer during the experiments based on a SAR procedure (Murray and Wintle, 2000; Wallinga et al., 2000; Colarossi et al, 2017), which may need to be taken into account. Some samples may be more prone to this effect than others and protocols may thus be sample dependent.

The aim of luminescence thermochronometry is to reconstruct past thermal histories at Quaternary timescales. It remains challenging to validate our final results when there are no other independent constraints for cooling rates. Therefore, well-constrained sites have been chosen to apply the method on, such as the KTB borehole in Germany, with a known temperature data record and thermal steady-state conditions (Guralnik et al., 2015), and samples from tunnels, e.g. the Mont Blanc tunnel. Besides application in a fast exhuming setting, e.g. the Namche Barwa syntaxis in the Himalaya (King et al., 2016a), it would be useful to verify the developed methodology through applications in a variety of settings.

The method may play a crucial role in addressing key questions on the roles of tectonics, climate and earth surface processes in various geomorphological settings. Several studies have investigated the role that climate has on erosion and the subsequent influence that erosional processes have on tectonics (Whipple et al., 1999; Zeitler et al., 2001; Blisniuk et al., 2006). The potential effects of a cooling climate during the Cenozoic on erosion however remain subject of debate. Glacial erosion is thought to play an important role in modifying the distribution of the surface elevation and limiting the topography of mountain ranges (Isacks, 1992; Egholm et al., 2009; Herman et al., 2010; Herman and Champagnac, 2016). It has been argued that cooler climatic conditions may cause increased erosion and, ultimately, be responsible for an apparent enhancement in rock uplift (Molnar and England, 1990; Champagnac et al., 2014), although some studies contradict this (Koppes and Montgomery, 2009; Willenbring and Von Blanckenburg, 2010). To address such questions, erosion

rates at glacial cycles need to be resolved. This requires the temporal resolution of luminescence thermochronometry to be increased, which may be achieved by applying thermoluminescence.

In addition, this newly established technique may benefit from applications in the field of geothermal energy, thermal energy generated and stored in the Earth, which can be exploited in the form of warm water, acting as a sustainable energy resource. To predict or model the potential geothermal energy of a system, rock properties need to be determined, such as a rock's porosity, permeability and thermal conductivity (k). Luminescence thermochronometry and modelling the thermal field evolution by solving the heat equation could possibly provide additional constraints on the last-mentioned parameter. In this application predictions may actually be verified when such a socially relevant system is put into place and actual measurements can be done inside a borehole.

Luminescence techniques may potentially also be used to provide complementary information for other thermochronometric systems by serving as a proxy for radiation damage in minerals such as apatite, monazite and zircon. This is relevant for (U-Th-Sm)/He dating techniques applied to these minerals, where interpretation of the ages strongly depend on knowledge of the He diffusion kinetics (Flowers et al., 2009; Gautheron et al., 2009; Recanati et al., 2017). Several studies indicate that the He diffusion coefficients are not constant and are a function of grain chemistry and the damage created during U-Th-Sm decay (Farley 2000; Green et al., 2006; Shuster et al., 2006). In particular, the role of recoil damage in increasing He retentivity needs to be understood (Gautheron et al., 2013). Annealing of alpha-damage effects may be similar to the annealing of fission tracks (Shuster and Farley, 2009). Amin and Durrani (1985) observed differences in the shape of thermoluminescence spectra of zircons, sphenes and apatites, dependent on the degree of radiation damage. Kasuya et al. (1992) have applied electron spin resonance (ESR) to single zircon crystals and compared the results with fission tracks (they found a correlation up to a certain fission track density, after that a strong drop in ESR signal intensity to zero). Nasdala et al. (2018) found that Raman and photoluminescence allow the quantification of irradiation effects in monazite and zircon. These insights indicate that there may be several promising techniques to characterize radiation damage, but more experimental investigations are needed to ensure the reliability of these methods and more development is needed to integrate the results into a He diffusion model.

References

- Andersen, M.T., Jain, M., Tidemand-Lichtenberg, P., 2012. Red-IR stimulated luminescence in K-feldspar: Single or multiple trap origin? *Journal of Applied Physics* 112, 043507.
- Biswas, R., Herman, F., King, G., Braun, J., 2018. Thermoluminescence of feldspar as a multi-thermochronometer to constrain the temporal variation of rock exhumation in the recent past. *Earth and Planetary Science Letters* 495, 56-68.
- Colarossi, D., Duller, G., Roberts, H., 2017. Exploring the behaviour of luminescence signals from feldspars: Implications for the single aliquot regenerative dose protocol. *Radiation Measurements*.
- Durrani, S., Amin, Y., Alves, J., 1984. Studies of radiation damage in crystals using nuclear-track and thermoluminescence methods. *Nuclear Tracks and Radiation Measurements* (1982) 8, 79-84.
- Faershtein, G., Guralnik, B., Lambert, R., Matmon, A., Porat, N., in review. Investigating the thermal stability of TT-OSL main source trap. *Radiation Measurements*.
- Farley, K., 2000. Helium diffusion from apatite: General behavior as illustrated by Durango fluorapatite. *Journal of Geophysical Research: Solid Earth* 105, 2903-2914.
- Flowers, R.M., Ketcham, R.A., Shuster, D.L., Farley, K.A., 2009. Apatite (U–Th)/He thermochronometry using a radiation damage accumulation and annealing model. *Geochimica et Cosmochimica acta* 73, 2347-2365.
- Gautheron, C., Barbarand, J., Ketcham, R.A., Tassan-Got, L., van der Beek, P., Pagel, M., Pinna-Jamme, R., Couffignal, F., Fialin, M., 2013. Chemical influence on α -recoil damage annealing in apatite: Implications for (U–Th)/He dating. *Chemical Geology* 351, 257-267.
- Gautheron, C., Tassan-Got, L., Barbarand, J., Pagel, M., 2009. Effect of alpha-damage annealing on apatite (U–Th)/He thermochronology. *Chemical Geology* 266, 157-170.
- Glotzbach, C., Reinecker, J., Danišík, M., Rahn, M., Frisch, W., Spiegel, C., 2008. Neogene exhumation history of the Mont Blanc massif, western Alps. *Tectonics* 27, n/a-n/a.
- Green, P., Duddy, I., 2006. Interpretation of apatite (U–Th)/He ages and fission track ages from cratons. *Earth and Planetary Science Letters* 244, 541-547.
- Guralnik, B., Jain, M., Herman, F., Ankjærsgaard, C., Murray, A.S., Valla, P.G., Preusser, F., King, G.E., Chen, R., Lowick, S.E., 2015. OSL-thermochronometry of feldspar from the KTB borehole, Germany. *Earth and Planetary Science Letters* 423, 232-243.
- Huntley, D., Short, M., Dunphy, K., 1996. Deep traps in quartz and their use for optical dating. *Canadian Journal of Physics* 74, 81-91.
- Jain, M., Guralnik, B., Andersen, M.T., 2012. Stimulated luminescence emission from localized recombination in randomly distributed defects. *Journal of Physics: Condensed Matter* 24, 385402.
- Jain, M., Sohbaty, R., Guralnik, B., Murray, A. S., Kook, M., Lapp, T., Buylaert, J. P., 2015. Kinetics of infrared stimulated luminescence from feldspars. *Radiation Measurements* 81, 242-250.

- Kasuya, M., Motoji, I., Danhara, T., 1992. Single grain ESR analysis of zircon: comparison with fission-tracks. *Quaternary International* 13, 131-134.
- King, G.E., Herman, F., Guralnik, B., 2016a. Northward migration of the eastern Himalayan syntaxis revealed by OSL thermochronometry. *Science* 353, 800-804.
- King, G.E., Herman, F., Lambert, R., Valla, P., Guralnik, B., 2016b. Multi-OSL-thermochronometry of feldspar. *Quaternary Geochronology* 33, 76-87.
- Koppes, M.N., Montgomery, D.R., 2009. The relative efficacy of fluvial and glacial erosion over modern to orogenic timescales. *Nature Geoscience* 2, 644.
- Krbetschek, M., Götze, J., Dietrich, A., Trautmann, T., 1997. Spectral information from minerals relevant for luminescence dating. *Radiation Measurements* 27, 695-748.
- Li, B., Li, S.-H., 2013. The effect of band-tail states on the thermal stability of the infrared stimulated luminescence from K-feldspar. *Journal of Luminescence* 136, 5-10.
- Malins, A., Poolton, N., Quinn, F., Johnsen, O., Denby, P.M., 2004. Luminescence excitation characteristics of Ca, Na and K-aluminosilicates (feldspars) in the stimulation range 5–40 eV: determination of the band-gap energies. *Journal of Physics D: Applied Physics* 37, 1439.
- Maréchal, J.-C., Perrochet, P., Tacher, L., 1999. Long-term simulations of thermal and hydraulic characteristics in a mountain massif: The Mont Blanc case study, French and Italian Alps. *Hydrogeology Journal* 7, 341-354.
- Mineli, T.D., Sawakuchi, A.O., Guralnik, B., Lambert, R., Jain, M., Pupim, F.N., Del Río, I., Guedes, C.C.F., Nogueira, L., in preparation. Variation of luminescence sensitivity and characteristic dose of quartz from rocks and sediments.
- Murray, A., Wintle, A., 2000. Application of the single-aliquot regenerative-dose protocol to the 375 C quartz TL signal. *Radiation Measurements* 32, 579-583.
- Nasdala, L., Akhmadaliev, S., Artac, A., Habler, G., Lenz, C., Irradiation effects in monazite–(Ce) and zircon: Raman and photoluminescence study of Au-irradiated FIB foils. *Physics and Chemistry of Minerals*, 1-17.
- Poolton, N., Kars, R., Wallinga, J., Bos, A., 2009. Direct evidence for the participation of band-tails and excited-state tunnelling in the luminescence of irradiated feldspars. *Journal of Physics: Condensed Matter* 21, 485505.
- Poolton, N., Ozanyan, K., Wallinga, J., Murray, A., Bøtter-Jensen, L., 2002. Electrons in feldspar II: a consideration of the influence of conduction band-tail states on luminescence processes. *Physics and Chemistry of Minerals* 29, 217-225.
- Putnis, A., 1992. *An introduction to mineral sciences*. Cambridge University Press.
- Recanati, A., Gautheron, C., Barbarand, J., Missenard, Y., Pinna-Jamme, R., Tassan-Got, L., Carter, A., Douville, É., Bordier, L., Pagel, M., 2017. Helium trapping in apatite damage: Insights from (U-Th-Sm)/He dating of different granitoid lithologies. *Chemical Geology* 470, 116-131.
- Riedesel, S., King, G. E., Prasad, A. K., Kumar, R., Finch, A. A., Jain, M., submitted. Optical determination of band-tail width, depth and excited state of the IRSL trap in feldspar. *Radiation Measurements*.

- Shuster, D.L., Farley, K.A., 2009. The influence of artificial radiation damage and thermal annealing on helium diffusion kinetics in apatite. *Geochimica et cosmochimica acta* 73, 183-196.
- Shuster, D.L., Flowers, R.M., Farley, K.A., 2006. The influence of natural radiation damage on helium diffusion kinetics in apatite. *Earth and Planetary Science Letters* 249, 148-161.
- Thomsen, K.J., Kook, M., Murray, A.S., Jain, M., in review. Resolving luminescence in spatial and compositional domains. *Radiation Measurements*.
- Yukihara, E.G., Coleman, A.C., Biswas, R.H., Lambert, R., Herman, F., King, G., 2018. Thermoluminescence analysis for particle temperature sensing and thermochronometry: Principles and fundamental challenges. *Radiation Measurements*.
- Wallinga, J., Murray, A., Wintle, A., 2000. The single-aliquot regenerative-dose (SAR) protocol applied to coarse-grain feldspar. *Radiation Measurements* 32, 529-533.

6. ACKNOWLEDGEMENTS

I am grateful to have worked with a lot of nice people from various backgrounds, who have directly or indirectly contributed to this thesis.

First of all, I want to thank Frédéric for giving me the opportunity to do this research project. Thanks for your enthusiasm and giving me guidance in the research topic and the scientific world. Georgina, you have introduced me not only to luminescence dating, but also to its community. You are a great ambassador of the field and I am curious of what is more to come. Pierre, thanks for the in-depth discussions and your friendly support along the way. I have enjoyed working together with all of you and learnt a lot from each of you in a complementary manner. David Sanderson, thank you for your warm hospitality at the SUERC laboratory and stimulating discussions.

Thanks to the thesis committee members for providing feedback and evaluating this thesis.

I am grateful to have worked at this university with inspiring people working at IDyST and ISTE in particular, in a beautiful surrounding... (I will miss the lake and view on the mountains wherever I go next). At UNIL, I would like to thank my colleagues for both the scientific and non-scientific discussions. In particular, a big thanks goes to my group and room mates Alexander, Benjamin, Vjeran, Nadja, Joanne, Rabiul and Günther. You have been a great support in good and bad times – THANKS! The IDyST community has developed itself over the years and became a very social group of people that made all the difference in living life as a PhD student. I enjoyed our office neighbours Alexis, Giulia and Jürg and their musical talents and widespread positivity! Thanks Mary-Alix for providing support, Mélina for going on skitouring adventures, Deirdre for your insightfulness and lovely runs during lunch breaks, and Annegret, Josh & Jasper for chilling on weekends.

We have been lucky to have had many friends and family from the Netherlands coming to visit us during our stay here, giving indispensable moments of re-setting and enjoying good times. Both my parents and parents in law were a great support, particularly the discussions on physics with Niek at the beginning of this project, providing extra hands at our place and relaxing moments during the nice holiday breaks.

Lastly, thanks to Maarten, Lise and Espen! You are a big inspiration and irreplaceable support in my life. Let's experience many more nice moments together!

APPENDIX

Contributions as co-author

The individual chapters in this PhD thesis have been written as individual papers that are to be published in scientific journals. Some parts of the research in this thesis have contributed to closely related research that has resulted in several publications where I am co-author. In King et al. (2016), I have contributed to the inclusion of the fading correction in the analysis of isothermal decay experiments and the choice of a multiple first-order kinetics model (the band-tail states model by Li and Li, 2013). The different processes that play a role in luminescence thermochronometry, i.e. trapping, thermal detrapping and athermal detrapping, are characterized through experiments which are designed to isolate these processes as much as possible. However, under the assumption that athermal decay is thermally independent, this process always takes place and needs to be taken into account in the analyses of all experiments. This can be done by applying a multiplying factor, including the fading time (starting half-way irradiation; Auclair et al., 2003), based on the model proposed by Huntley (2006) and Kars et al. (2008), when fitting the isothermal decay data. The choice of the thermal kinetic decay model used in King et al. (2016) followed from the study and experimental results presented in Chapter 3 of this thesis. In Yukihiro et al. (2018), I have contributed in scientific discussions on thermal decay models for K-feldspar. Lastly, I have contributed to the application of the Gaussian trap depth kinetic decay model (Chapter 2) to thermally-transferred OSL (Faershtein et al., in review) and blue light optically stimulated luminescence (Mineli et al., in preparation) on quartz. The thermal decay data in these studies also show a strong deviation from single exponential decay, thus requiring an appropriate model taking this into account. This led to the application and testing of both a general order decay model (Guralnik et al., 2015) and Gaussian trap depth kinetic decay model on the data sets obtained in these studies.

List of publications

Published

King, G., Herman, F., Lambert, R., Valla, P., Guralnik, B., 2016. Multi-OSL-thermochronometry of feldspar. *Quaternary Geochronology* 33, 76-87.

Yukihara, E., Coleman, A., Biswas, R., Lambert, R., Herman, F., King, G., 2018. Thermoluminescence Analysis for Particle Temperature Sensing and Thermochronometry: Principles and Fundamental Challenges. *Radiation Measurements*.

In review

Lambert, R., King, G., Valla, P., Herman, F.: Validating multiple first-order kinetic models for feldspar thermal decay in luminescence thermochronometry. Submitted to *Radiation Measurements*.

Lambert, R., King, G., Valla, P., Herman, F.: Towards OSL-thermochronometry of the Mont Blanc massif: Experimental investigations into constraining feldspar thermal decay. Submitted to *Radiation Measurements*.

Faershtein, G., Guralnik, B., Lambert, R., Matmon, A., Porat, N.: Investigating the thermal stability of TT-OSL main source trap. *Radiation Measurements* (minor revisions).

In preparation

Lambert, R., King, G., Valla, P., Herman, F.: Rapid cooling during the last 10 - 100 ka in the Mont Blanc massif; insights from luminescence thermochronometry.

Mineli, T.D., Sawakuchi, A.O., Guralnik, B., Lambert, R., Jain, M., Pupim, F.N., Del Río, I., Guedes, C.C.F., Nogueira, L.: Variation of luminescence sensitivity and characteristic dose of quartz from rocks and sediments.

References

Auclair, M., Lamothe, M., Huot, S., 2003. Measurement of anomalous fading for feldspar IRSL using SAR. *Radiation measurements* 37, 487-492.

Guralnik, B., Li, B., Jain, M., Chen, R., Paris, R.B., Murray, A.S., Li, S.-H., Pagonis, V., Valla, P.G., Herman, F., 2015. Radiation-induced growth and isothermal decay of infrared-stimulated luminescence from feldspar. *Radiation Measurements* 81, 224-231.

Huntley, D., 2006. An explanation of the power-law decay of luminescence. *Journal of Physics: Condensed Matter* 18, 1359.

Kars, R.H., Wallinga, J., Cohen, K., 2008. A new approach towards anomalous fading correction for feldspar IRSL dating—tests on samples in field saturation. *Radiation Measurements* 43, 786-790.

Li, B., Li, S.-H., 2013. The effect of band-tail states on the thermal stability of the infrared stimulated luminescence from K-feldspar. *Journal of Luminescence* 136, 5-10.

Multi-OSL-thermochronometry of feldspar

G.E. King^{1*}, F. Herman¹, R. Lambert¹, P.G. Valla¹, B. Guralnik^{2,3}

¹Institute of Earth Surface Dynamics, University of Lausanne, Geopolis, 1015 Lausanne, Switzerland.

²Department of Earth Sciences, ETH, 8092 Zürich, Switzerland

³Soil Geography and Landscape group and the Netherlands Centre for Luminescence Dating, Wageningen University, Droevendaalsesteeg 3, 6708PB Wageningen, The Netherlands

*Corresponding author: georgina.king@gmail.com

A version of this manuscript was published in *Quaternary Geochronology* 33 (2016) 76-87:

<http://dx.doi.org/10.1016/j.quageo.2016.01.004>

The text below may deviate slightly from the published version.

Abstract

Optically stimulated luminescence (OSL)-thermochronometry has recently been proposed as a tool capable of resolving cooling histories from the top 1-2 km of the Earth's crust. This is beyond the resolution of most low-temperature thermochronometric systems, and it offers a new opportunity to investigate the interactions between climate, tectonics and surface processes over Quaternary timescales. Here we present a multi-OSL-thermochronometer which exploits the different thermal stabilities of different temperature infra-red stimulated luminescence (IRSL) signals from K- and Na-rich K-feldspar extracts, utilising the established multi-elevated-temperature (MET) measurement protocol (Li, B. and Li, S-H., 2011. Luminescence dating of K-feldspar from sediments: A protocol without anomalous fading correction. *Quaternary Geochronology* 6, 468-479). The theoretical aspects of multi-OSL-thermochronometry are discussed, prior to validation with an example from the eastern Himalayan syntax, one of the most rapidly exhuming settings on Earth. Our results show multi-OSL-thermochronometry of feldspar is able to resolve rock cooling histories over timescales ≤ 0.2 Ma and provides much tighter constraint on late-stage cooling histories than single-system OSL-thermochronometry.

Keywords: Multi-OSL-thermochronometry, feldspar, luminescence, MET, IRSL

1. Introduction

Thermochronometry has traditionally exploited the thermal dependence of the products of radioactive daughter-parent relationships within minerals, enabling the quantification of bedrock cooling histories over Ma to sub-Ma timescales (e.g. McDougall and Harrison, 1999; Reiners and Brandon, 2006; Braun et al., 2006). Thermochronometric data can enable exploration of the key

drivers of exhumation (e.g. Braun et al., 2006) and/or geothermal or hydrothermal histories (e.g. Gorynski et al., 2014; McInnes et al., 2005). However, established low-temperature (i.e. <100°C) thermochronometers such as apatite (U-Th)/He (AHe), have closure temperatures too high to either resolve changes affecting the top 1-2 km of the Earth's crust or changes in hydrothermal flow at the near-surface. Only the recently-proposed apatite $^4\text{He}/^3\text{He}$ system is sensitive to temperatures of ~30-90 °C (Shuster and Farley, 2005). Understanding the rock cooling history of the near-surface region is important because it will provide insights, for example, into the impact of Quaternary glaciation on exhumation/erosion rates, which remains a highly debated topic in geomorphology (e.g. Herman et al., 2013; Molnar, 2004; Willenbring and von Blanckenburg, 2010; Zhang et al., 2001).

Previous research has led to the electron spin resonance (Grün et al., 1999) or thermoluminescence of quartz (Prokein and Wagner, 1994) being proposed as thermochronometric systems that could span this spatial and temporal gap (see Guralnik et al. (2015b) for a review). More recently, single-system optically stimulated luminescence (OSL)-thermochronometry has been suggested (e.g. De Sarkar et al., 2013; Guralnik et al., 2015a; Guralnik et al., 2015b; Guralnik et al., 2013; Herman et al., 2010; Li and Li, 2012). OSL-thermochronometry exploits the thermal dependence of OSL signal accumulation within minerals such as quartz and feldspar, because OSL signals are the product of competition between radiation induced charge trapping, and thermally stimulated charge detrapping. Thus at high temperatures (e.g. ~100 °C) because of thermal stimulation, charge detrapping is dominant and the OSL signal is effectively zero; but at low temperatures (e.g. ~10 °C) thermal detrapping is negligible and radiation induced charge trapping is dominant. The effective closure temperature (T_c , Dodson, 1973), which can be thought of as the temperature at which thermal detrapping becomes negligible (see Guralnik et al., 2013 for its formal definition), of the quartz OSL-thermochronometric system has recently been suggested to be around 30-40 °C (Herman et al., 2010; Guralnik et al. 2013), and ~25 °C for the Na-feldspar infra-red stimulated luminescence signal measured at 50 °C (IRSL₅₀) OSL-thermochronometric system (Guralnik et al., 2015b). It is the relatively low T_c of OSL in comparison to other thermochronometric systems that makes it a potential candidate for resolving recent (Quaternary timescale) changes in rock cooling histories. However, OSL-thermochronometry is unlikely to be a panacea because despite the advantages offered by its relatively low T_c , OSL signals reach saturation as all available traps become populated, limiting the application of OSL-thermochronometry to either very rapidly exhuming settings, or elevated temperature settings (e.g. boreholes or tunnels; Guralnik et al., 2015b). Furthermore quartz OSL signals from bedrock often have very low luminescence sensitivity and can exhibit anomalous luminescence characteristics, which make some quartz unsuitable for use in OSL-thermochronometry studies (e.g. Guralnik et al., 2015a). Nevertheless in contrast to quartz, feldspar has both higher

luminescence sensitivity, enabling precise OSL measurements, and also saturates later, which has facilitated the successful application of OSL-thermochronometry in the KTB-borehole using the IRSL₅₀ signal of Na-feldspar (Guralnik et al., 2015b).

Recently, the multiple elevated temperature (MET) measurement protocol for feldspar has been proposed (Li and Li, 2011a), which was initially developed to circumvent the challenges associated with feldspar athermal charge detrapping (called anomalous fading), that is thought to be ubiquitous for the IRSL₅₀ signal of feldspars (Huntley and Lamothe, 2001). Much recent research has sought to develop measurement protocols which access more athermally stable feldspar signals (e.g. Buylaert et al., 2012; Li and Li, 2011a; Thomsen et al., 2011; Thomsen et al., 2008). Amongst these, the MET-protocol has the particularity of comprising a series of sequentially measured IRSL signals, at increasing temperatures, for example at 50 °C, 100 °C, 150 °C, 200 °C etc. Both the athermal (Li and Li, 2011a) and thermal (Li and Li, 2011b) stability of the different signals of K-feldspar have been experimentally shown to increase with stimulation temperature. This represents a clear advantage for luminescence thermochronometry because it offers the potential for a range of thermal kinetic parameters to be accessed between signals (e.g. Li and Li, 2012a; Qin et al., 2015). Therefore, the different MET signals measured for a single mineral extract (e.g. K-, or Na-feldspar) of a single sample have different closure temperatures, and thus provide multiple constraints on recent cooling histories. This paper explores the theoretical premises of using a MET protocol to develop a multi-OSL-thermochronometer, prior to validation with an example of two samples collected from the Namche Barwa syntaxis (eastern Himalaya, Tibet). Our data show that multi-OSL-thermochronometry using signals from both K-feldspar (<2.58 g cm⁻³) and Na-rich K-feldspar (2.58-2.62 g cm⁻³) extracts, results in cooling rates which are broadly consistent with those obtained from apatite (AFT) and zircon fission-track (ZFT) ages (Seward and Burg, 2008), and zircon (U-Th)/He ages (Zeitler et al., 2014) from the same area, but which offer the clear advantage of providing more precise resolution of cooling histories over the past 0.2 Ma.

2. Theoretical basis of OSL-thermochronometry

In the following sections, we discuss the theoretical basis of OSL-thermochronometry, firstly through discussing our selected model, before considering how the athermal and thermal loss parameters can be constrained.

2.1 The kinetic model

Following the first application of quartz OSL-thermochronometry by Herman et al. (2010), Li and Li (2012a) proposed a model for extracting cooling histories from quartz OSL signals, which was subsequently modified for feldspar (Guralnik et al., 2015b). In the latter work, a general order kinetic

model for OSL signal growth and thermal decay (Guralnik et al., 2015c) was coupled with the athermal detrapping model of Huntley (2006). For the dataset presented and discussed in this paper, a simpler first-order charge trapping has been adopted, alongside the band-tail states model of Li and Li (2013) which accounts for thermal loss. The main rate equation, describing the change of trapped electrons with time, is thus:

$$\frac{d\left[\frac{n}{N}(r', E_b, t)\right]}{dt} = \frac{\dot{D}}{D_0} \left[1 - \frac{n}{N}(r', E_b, t)\right] - s e^{-\frac{E_t - E_b}{k_B T}} \left[\frac{n}{N}(r', E_b, t)\right] - \tilde{s} e^{-\rho' r'^{\frac{1}{3}}} \left[\frac{n}{N}(r', E_b, t)\right] \quad [1]$$

where (n/N) is the saturation ratio, i.e. the fraction of occupied electron traps (possessing the nearest neighbouring hole at r' and a band-tail at E_b) as a function of time (t , Ma). Luminescence signal accumulation (i.e. charge trapping), first term on the right hand side of the equation, is described by a first-order process (Christodoulides et al., 1971) dependent on the environmental radiation dose rate (\dot{D} , Gy Ma⁻¹) and the fading corrected characteristic dose of saturation (D_0 , Gy). The thermal loss (charge detrapping) is described by the band-tail states model of Li and Li (2013; second term on the right), and depends on the thermal kinetic parameters of the frequency factor (s , Ma⁻¹), activation energy or trap depth (E_t , eV), the band-tail state energy level (E_b , eV), the Boltzmann constant (k_B , eV K⁻¹) and temperature (T , K). Athermal signal loss (i.e. another competing charge detrapping pathway) is described by the quantum mechanical tunnelling model of Huntley (2006; third term on the right), and is dependent on the distance between trapped electrons and their nearest neighbouring recombination centres (r' , dimensionless), the density of the recombination centres (ρ' , dimensionless) and the athermal frequency factor ($\tilde{s} = 3 \times 10^{15} \text{ s}^{-1}$ after Huntley, 2006). In turn, the total accumulation of charge with time for a given cooling history (i.e. $\frac{n}{N}(t)$) is obtained by integrating $\frac{n}{N}(r', E_b, t)$ over the range of the band-tail states, E_b , and an infinite range of dimensionless distances:

$$\frac{n}{N}(t) = \int_{r'=0}^{\infty} \int_{E_b=0}^{E_t} p(r') P(E_b) \frac{n}{N}(r', E_b, t) dE_b dr' \quad [2]$$

where $p(r')$ and $P(E_b)$ are the probability density distributions of the nearest recombination centres and of the band-tail states, respectively, further discussed below.

The key principle is to quantify the saturation ratio (n/N) of a sample, through consideration of how much signal has accumulated (first term), after accounting for thermal (second term) and athermal (third term) losses using equation [1]. In order to determine a cooling history for an OSL-thermochronometry sample, it is essential that we are able to discriminate between thermal and athermal signal loss, which is achieved using a combination of laboratory measurements and kinetic

models. The constraint of athermal loss (third term), signal accumulation (first term) and thermal loss (second term) are considered in the following sections.

2.2 Constraining athermal kinetic parameters

Athermal signal loss can be measured over laboratory time scales using a fading test (e.g. Huntley and Lamothe, 2001), which consists of giving the sample a laboratory radiation dose and then holding it at room temperature for a range of different durations before measurement ($t = 0$ to $> 10,000$ s). Athermal signal loss mimics a power-law decay, and is slower than the (semi-) exponential thermal losses at elevated temperatures (see discussion of isothermal holding experiments in Section 2.4). Athermal loss is thus more difficult to measure precisely and it is therefore important to characterise athermal losses over long timescales, although these are still practical within the laboratory.

Faded trapped charge $n(t^*)$ can be related to its initial quantity $n(0)$ using a range of models, but here we use the approach of Huntley (2006):

$$n(t^*) = n(0) \cdot \varphi(t^*), \quad [3]$$

where

$$\varphi(t^*) = e^{-\rho' \ln(1.85 t^*)^3} \quad [4]$$

in which t^* is the fading time (starting from the mid-irradiation point; Auclair et al., 2003) and $\rho' \equiv \frac{4\pi\rho}{3\alpha^3}$, where α is a constant (Huntley, 2006; Kars et al., 2008). The model of Huntley (2006) operates on the premise that recombination centres within a feldspar mineral are randomly distributed with density ρ , and that the rate of fading is controlled by the tunnelling distance (r) of charge to its nearest recombination centre.

Previous studies have recorded an increase in fading rate with increasing laboratory dose, which may reflect a changing density of recombination centres i.e. a dependence of ρ' on time (Huntley and Lian, 2006; Li and Li, 2008). However, despite this potential limitation, many studies have been able to successfully predict field saturation values for a suite of samples with independent age or temperature controls (Li and Li, 2008; Kars and Wallinga, 2008; Guralnik et al., 2015b). To further address this issue, Li and Li (2008) and Kars and Wallinga (2009) have also explored the potential effects of a reduced availability of stable trapping centres, due to competition effects with increasing dose, which may result in an increased rate of athermal detrapping at high doses (e.g. Huntley and Lian, 2006). Kars and Wallinga (2009) observed that incorporating charge-trapping competition effects into their model resulted in greater age overestimations relative to independent age controls,

than when such effects were ignored. Consequently in this work we have assumed a dose-invariant density of recombination centres ρ' and do not account for potential changes in charge trapping with changing dose, although this effect should be the subject of further research.

Laboratory measurements are also affected by athermal detrapping, and to ensure that measured (n/N) values are comparable to modelled values, laboratory responses can be fitted by incorporating factor φ to account for fading as defined in equation [4].

2.3 Constraining signal accumulation

The IRSL signal accumulation of feldspar can be fitted in a variety of ways including with a single saturating exponential function (see Guralnik et al., 2015c for a discussion of alternative approaches). Here, we use:

$$\frac{n}{N}(t) = \varphi(t^*) \cdot A \left(1 - e^{-\frac{\dot{D}_{lab} t}{D_0}} \right) \quad [5]$$

where $n(t)$ is the amount of trapped electrons at time (t) , N is the finite number of trapping sites, φ is a time-dependent factor to account for athermal detrapping (Eq. 4), A is a pre-exponential multiplier, \dot{D}_{lab} is the laboratory dose rate, and D_0 the characteristic dose of saturation.

The rate at which the signal accumulates in the natural environment is dependent upon \dot{D} , which is calculated from the concentration of U, Th, K and Rb from the rock matrix, and also from within the minerals under investigation (Durcan et al., 2015). An important assumption of this model is homogeneous trap filling, i.e. the probability that a trap is filled is independent of the nearest hole at r' or the band-tail states E_b associated with that particular trap.

2.4 Constraining thermal kinetic parameters

The kinetic model outlined in section 2.1 is sensitive to changes in the thermal kinetic parameters of different samples. In comparison to other thermochronometric techniques (such as (U-Th)/He or AFT), luminescence offers the potential to constrain these parameters for each individual sample within a reasonable time period in the laboratory. This is done using an isothermal holding experiment, whereby the sample is given a known dose before being held at a range of temperatures (e.g. $T = 170$ to 300 °C) for a range of different durations (e.g. $t = 0$ to $10,000$ s). Experiments typically take between 4-5 days for each sample, and the experimental data can then be fitted using equation [6], which is derived from equations [1] and [2] by assuming $\dot{D} = 0$:

$$\frac{n(t)}{n(0)} = \varphi(t^*) \cdot \int_0^{E_t} P(E_b) e^{\left(-ste \frac{E_t - E_b}{k_B T}\right)} dE_b \quad [6]$$

where $n(t)$ is the number of trapped electrons at time t and $n(0)$ is the initial number of trapped electrons. Following Poolton et al. (2009) and Li and Li (2013), we assume the probability of thermally evicting electrons into the band-tail states of energy in the range of $E_b + dE_b$, $P(E_b)dE_b$, is given by:

$$P(E_b)dE_b = B e^{\left(\frac{E_b}{E_u}\right)} dE_b \quad [7]$$

where B is a pre-exponential multiplier and E_u is the width of the Urbach tail (eV).

2.5 Screening for thermal signals in feldspars: accounting for athermal detrapping

Athermal signal losses can be significant. It is therefore essential for OSL-thermochronometry samples to determine whether the measured (n/N) is due only to athermal losses, or if it also reflects thermal signal loss. An athermally stable (non-fading) IRSL signal for a feldspar in saturation (i.e. where all available traps are populated and (n/N) does not continue to grow with time) well below the T_c should have an (n/N) ratio of unity. However, athermal detrapping of charge can result in low (n/N) values for samples which have been at $T < T_c$ even for long periods of time. Consequently, a sample in field-saturation may exhibit $\left(\frac{n}{N}\right) < 1$. To determine whether feldspar OSL-thermochronometry samples are in disequilibrium (i.e. contain a thermal signal), rather than exhibiting a steady-state between rates of signal accumulation and athermal signal loss (field saturation), the model of athermal detrapping proposed by Huntley (2006), can be used to estimate sample specific field saturation values: $(n/N)_{SS}$ where \dot{D} is known (Kars et al., 2008):

$$(n/N)_{SS} = \int_{r'=0}^{\infty} \frac{3r'^2 e^{-r'^3}}{1 + \frac{D_0}{\dot{D}} \tilde{s} e^{-\rho'^{1/3} r'}} dr' \quad [8]$$

where dimensionless distance $r' \equiv \left\{\frac{4\pi\rho}{3}\right\}^{\frac{1}{3}} r$, and the probability that the nearest recombination centre is at a distance between r' and $r' + dr'$ is given by $p(r')dr' = 3r'^2 e^{-r'^3} dr'$ (Huntley, 2006). Equation [8] is equivalent to equation 15 of Li and Li (2008), and one can see that the field saturation value $(n/N)_{SS}$ is strongly dependent on ρ' , but also weakly dependent on D_0 , \dot{D} and \tilde{s} .

Figure 1 shows a bi-plot between (n/N) and $(n/N)_{SS}$ calculated from four synthetic (n/N) values and kinetic parameters from Table 1 using equation [8], for measurement temperatures of 50, 100, 150, 225 °C. As the IRSL temperature increases, so too does the athermal stability of the signals, which is aided by their measurement after the IRSL₅₀ signal (c.f. Thomsen et al., 2008). If data points

plot on the 1:1 line, as illustrated by the open symbols in Figure 1, they are in steady-state and do not contain any chronometric information beyond a minimum cooling age. Because the synthetic data are offset from the 1:1 line as illustrated by the red arrow, these data do contain a thermal signal, which for these samples relates to the time that has elapsed since cooling below the closure temperature (c.f. Guralnik et al., 2013) and can be considered viable for thermochronometric investigation.

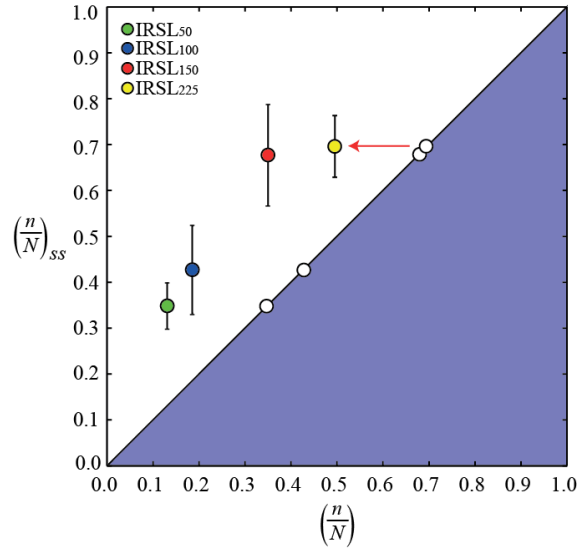


Figure 1: Four arbitrary (n/N) values determined from cooling scenario (i) described in the caption of Figure 2, contrasted with $(n/N)_{SS}$ calculated using the Huntley (2006) model, as modified by Kars et al. (2008). $(n/N)_{SS}$ values were calculated using kinetic values (D_0, ρ', \dot{D}) summarised in Tables 1 and 2 and equation [8]. Open symbols which lie on the 1:1 line are illustrative of samples which do not contain a thermal signal.

		Best-fit parameters						Modelled values	Sample properties (values not-included in modelling)			
		IRSL	E_i (eV)	E_u (eV)	$\log_{10} s$ (s^{-1})	D_0 (Gy)	$\log_{10} (\rho')$	$(\frac{n}{N})$	$(\frac{n}{N})_{SS}$	$\frac{g_{2days}}{\%/\text{decade}}$	Faded D_0 (Gy)	Faded D_e (Gy)
UNIL/NB123	K-feldspar	50	1.45 ± 0.02	0.072 ± 0.004	10.38 ± 0.20	620 ± 14	-5.41 ± 0.03	0.15 ± 0.01	0.35 ± 0.05	5.24 ± 0.36	571 ± 12	137 ± 3
		100	1.45 ± 0.02	0.070 ± 0.003	10.00 ± 0.17	681 ± 18	-5.50 ± 0.06	0.20 ± 0.01	0.43 ± 0.10	4.36 ± 0.56	639 ± 15	199 ± 5
		150	1.49 ± 0.02	0.074 ± 0.003	9.83 ± 0.17	767 ± 27	-5.84 ± 0.08	0.29 ± 0.02	0.68 ± 0.11	2.09 ± 0.38	745 ± 24	296 ± 9
		225	1.57 ± 0.03	0.093 ± 0.003	9.75 ± 0.22	669 ± 23	-5.87 ± 0.05	0.42 ± 0.02	0.70 ± 0.07	1.88 ± 0.23	650 ± 20	417 ± 13
	Na-rich K-feldspar	50	1.48 ± 0.02	0.077 ± 0.004	10.73 ± 0.23	653 ± 19	-5.33 ± 0.02	0.13 ± 0.02	0.28 ± 0.04	6.07 ± 0.33	590 ± 16	138 ± 4
		100	1.47 ± 0.02	0.080 ± 0.004	10.04 ± 0.22	711 ± 22	-5.60 ± 0.08	0.22 ± 0.01	0.51 ± 0.13	3.42 ± 0.59	674 ± 19	226 ± 6
		150	1.50 ± 0.03	0.082 ± 0.004	9.74 ± 0.22	788 ± 24	-5.82 ± 0.05	0.30 ± 0.01	0.66 ± 0.06	2.12 ± 0.23	763 ± 21	321 ± 9
		225	1.62 ± 0.03	0.105 ± 0.004	10.04 ± 0.23	671 ± 25	-5.94 ± 0.05	0.44 ± 0.01	0.73 ± 0.05	1.64 ± 0.17	654 ± 21	442 ± 14
UNIL/NB124	K-feldspar	50	1.46 ± 0.02	0.060 ± 0.003	10.85 ± 0.19	640 ± 25	-5.42 ± 0.02	0.20 ± 0.00	0.36 ± 0.03	5.14 ± 0.19	589 ± 21	198 ± 7
		100	1.43 ± 0.02	0.079 ± 0.003	9.78 ± 0.17	764 ± 28	-5.67 ± 0.03	0.29 ± 0.00	0.56 ± 0.04	3.04 ± 0.21	731 ± 24	320 ± 11
		150	1.53 ± 0.02	0.083 ± 0.003	9.95 ± 0.17	867 ± 33	-5.82 ± 0.03	0.33 ± 0.01	0.66 ± 0.04	2.26 ± 0.15	841 ± 29	402 ± 14
		225	1.59 ± 0.01	0.102 ± 0.003	9.71 ± 0.12	703 ± 31	-6.03 ± 0.04	0.48 ± 0.01	0.77 ± 0.04	1.41 ± 0.13	689 ± 27	508 ± 20
	Na-rich K-feldspar	50	1.48 ± 0.02	0.068 ± 0.003	10.93 ± 0.21	487 ± 31	-5.64 ± 0.02	0.27 ± 0.01	0.54 ± 0.04	3.17 ± 0.15	462 ± 27	192 ± 11
		100	1.41 ± 0.02	0.072 ± 0.004	9.61 ± 0.19	739 ± 43	-5.82 ± 0.02	0.33 ± 0.05	0.66 ± 0.03	2.18 ± 0.11	717 ± 37	342 ± 18
		150	1.46 ± 0.02	0.082 ± 0.003	9.40 ± 0.17	806 ± 35	-6.01 ± 0.04	0.37 ± 0.01	0.77 ± 0.04	1.46 ± 0.11	790 ± 31	410 ± 16
		225	1.51 ± 0.02	0.103 ± 0.003	9.04 ± 0.18	710 ± 31	-6.27 ± 0.06	0.50 ± 0.00	0.86 ± 0.04	0.83 ± 0.10	702 ± 27	528 ± 20

Table 1: Summary of kinetic and fitted parameters for samples UNIL/NB123 and UNIL/NB124. Uncertainties are cited at 1σ .

3. Applying the kinetic model to MET data

The preceding section has described the model and how the thermal and athermal loss terms can be derived from laboratory measurements. We now utilise this model to explore the potential of MET luminescence signals, which are measured at different temperatures and which have different athermal and thermal stabilities, for OSL-thermochronometry. Their differing stabilities are reflected in the derivation of different values of E_t , E_w , s and ρ' , and thus MET signals for the same mineral extract of the same sample, have different (n/N) ratios for common cooling histories. It is these differences in the measured (n/N) ratios for the different MET signals that enables the use of a single sample as a multi-thermochronometer, as their different kinetic parameters (E_t , E_w , s) result in differing signal closure temperatures. IRSL signals stimulated at the highest temperatures, start accumulating signal at temperatures greater than the lower temperature IRSL signals. This new development in the field of OSL-thermochronometry will enable better constraint of recent cooling histories, beyond those offered by a single thermochronometry system (e.g. IRSL₅₀ OSL-thermochronometry, Guralnik et al., 2015b).

3.1 Forward modelling: predicting (n/N) for different MET signals and different cooling histories

Six different end-member cooling histories were used to model IRSL signal accumulation for MET data using an arbitrary set of kinetic parameters for a K-feldspar fraction from Table 1, i.e. for four different IRSL signals. The cooling histories were chosen arbitrarily to explore the sensitivity of the method. Equation [1] was solved using the finite difference method, with a semi-implicit Euler method (Press, 2007, p. 727).

Cooling history (i) comprises a series of four ~ 20 °C stepped temperature reductions from 120 °C to 10 °C, history (ii) comprises only two cooling steps of ~ 50 °C from 130 °C to 10 °C. Cooling history (iii) starts at 80 °C before dropping to 10 °C at 0.1 Ma, whereas histories (iv) and (v) are isothermal at 50 °C and 10 °C respectively. The final cooling history (vi) holds a temperature of 100 °C before dropping monotonically to 10 °C from just after 0.2 Ma. The synthetic cooling histories are shown in Figure 2a and the signal accumulation of four signals of two selected cooling histories are shown in Figure 2b. It is clear that the different temperature IRSL signals result in different modelled (n/N) values, which is a consequence of their different kinetic parameters. Note that some of these cooling histories represent extreme cases, which are only used for illustrative purposes.

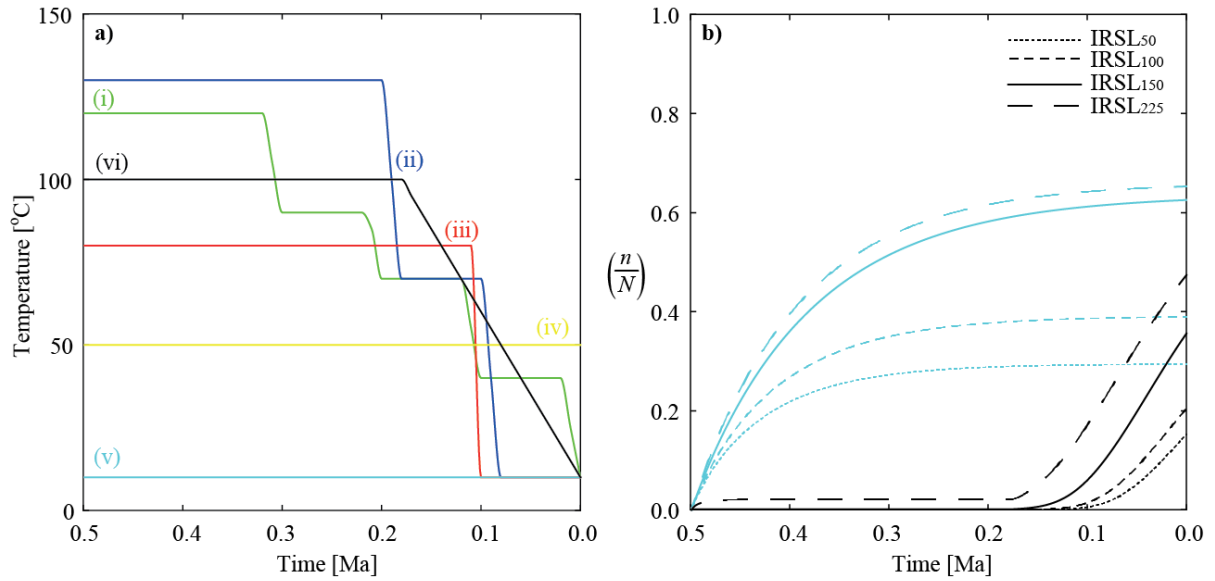


Figure 2: (a) Six different prescribed cooling histories and (b) modelled (n/N) signal accumulations for four signals from cooling scenarios (v) and (vi) using parameters (E_t, E_u, s, D_0, ρ' and \dot{D}) reported in Tables 1 and 2. Line colours reflect the cooling history used to generate (n/N) signal accumulation in the forward model. The different lines in (b) depict the time evolution of (n/N) for the different kinetic parameters of the different temperature IRSL signals for cooling scenarios (v) and (vi).

3.2 Inverse modelling: deriving cooling histories from (n/N) values

The computed (n/N) values derived for the different cooling histories were then inverted to test whether it is possible to recover the cooling scenarios shown in Figure 2a. A Bayesian approach was used to construct a probability density function for the cooling history, given the observed data, which is commonly done in thermochronometric studies (e.g. Braun et al., 2012; Gallagher, 1995, 2012). This first step includes a Monte Carlo (MC) search in which we randomly prescribed a range of different time-temperature histories, which assume monotonic cooling from temperatures of 150 to <60 °C, over a time period of 0.5 Ma. The number of steps in each cooling history is random, and the MC search enables the full time-temperature space to be explored. The second step consists of constructing the probability density function of the thermal history using a rejection method (e.g. Tarantola, 2005, p. 49). Modelled trap occupancy values, $(n/N)_{mod}$, are calculated for each of the cooling histories from the MC search using the kinetic values for each IRSL signal, these are then contrasted with the computed (n/N) values and a likelihood score calculated from:

$$L = \exp\left(-0.5 \sum_1^m \frac{(n/N_{mod} - n/N)^2}{\sigma^2}\right) \quad [9]$$

where L is the likelihood score calculated for m traps and σ is the uncertainty on (n/N) , in this case arbitrarily set to 10% of (n/N) . Likelihood scores close to 1 indicate a very low degree of misfit, whereas values close to 0 indicate a higher deviation from the measured values. The likelihood score

is then tested against a random number between 0 and 1, and where the likelihood score is larger, the result (in this case, the cooling history) is accepted (Tarantola, 2005, p.49). Through using this approach, instances of all possible cooling histories can be retained, although because the probability of accepting poorly fitting histories is smaller, fewer such histories are accepted. The dataset of accepted individual cooling histories is then transformed into a time-temperature probability density function as follows. The time and temperature axes are divided into 50 intervals, and then the number of accepted time-temperature paths that pass through each time-temperature cell are summed. From this, a contour map of the median model value, and its 60% and 90% quantiles are drawn.

Where the prescribed cooling histories are contrasted with those modelled, and the 90% quantiles (black lines) and median models (red lines) are considered, it is clear that it is possible to recover the general features of the six different cooling scenarios (Figure 3). The luminescence signals are unable to constrain cooling history temperatures greater than ~ 75 °C, which is a consequence of the low closure temperature of this system. For the three stepped cooling histories (Figures 3a, 3b and 3c), the model is able to accurately constrain the general reduction in temperature, but not the abruptness of the temperature steps. This is because although the rate of signal accumulation accelerates as thermal detrapping reduces with cooling temperature, the temperature transitions in these cooling histories are too abrupt to be fully resolved by the technique. The model is able to recover final temperature accurately, as shown for the isothermal cooling scenarios (Figure 3d), and accurately constrains 50 °C for isothermal scenario (iv) where thermal detrapping is significant. However the 10 °C isothermal scenario (v) is too far below the T_c of the system, for accurate thermal constraint (Figure 3e). Furthermore the forward modelled (n/N) values from cooling scenario (v) are approaching saturation, as all available electron traps become populated, precluding thermal inferences from being made. The rapidly cooling scenario (vi) shown in Figure 3f (500 °C Ma^{-1}) is also accurately constrained, with modelled cooling rates of ~ 500 °C Ma^{-1} . These results are significant because they demonstrate that multi-OSL-thermochronometry can resolve changes in cooling histories at ~ 0.1 - 0.2 Ma timescales, which is usually beyond the resolution of other thermochronometric systems.

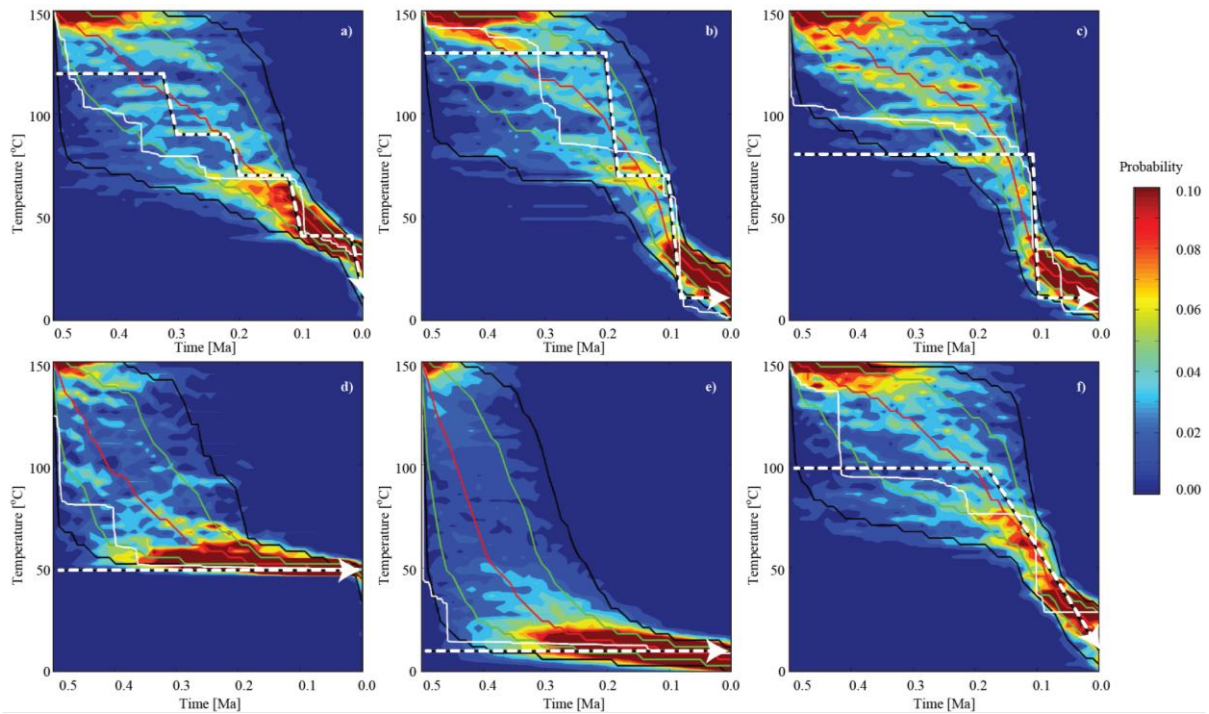


Figure 3: (a), (b), (c), (d), (e) and (f) show probability density functions of the inverted cooling histories for the different (n/N) values determined from the forward models of cooling histories (i), (ii), (iii), (iv), (v) and (vi) respectively (Figure 2). The calculation of the probability is described in section 3.2. The 60% quantile is shown in green, the 90% quantile is shown in black, the median model is shown in red and the fit with the highest likelihood is shown in white.

4. Proof of concept

The preceding sections have explored the potential of multi-OSL-thermochronometry using the MET protocol. The remainder of this paper presents an application of multi-OSL-thermochronometry to two samples from Namche Barwa (eastern Himalaya, Tibet), which is one of the most rapidly exhuming places on Earth.

4.1 Case study: Himalaya

The Namche Barwa syntaxis in the eastern Himalaya is dominated by a north plunging crustal scale antiform at the plate boundary between India and Asia (Burg et al., 1997). Zircon fission-track data show that exhumation rates outside of the fault bounds are $0.2\text{-}0.3 \text{ km Ma}^{-1}$, whereas AFT ages from within the syntaxis core are as young as $0.4 \pm 0.2 \text{ Ma}$ representing very high rates of exhumation (Seward and Burg, 2008) of $\sim 10 \text{ km Ma}^{-1}$ (Burg et al., 1998; Zeitler et al., 2014). The different ages equate to a cooling rate of the order of $500 \text{ }^\circ\text{C Ma}^{-1}$. The high rates of exhumation within this region make it an appropriate test environment for OSL-thermochronometry, as the challenges of signal saturation which are problematic in slowly exhuming regions are circumvented (see discussions in Herman et al., 2010; Li and Li, 2012; Guralnik et al., 2013).

Two samples of gneiss were selected for analysis from the rapidly exhuming zone: UNIL/NB123 and UNIL/NB124. The samples were taken 500 m apart (from a site at around 30.085N, 95.118E) and from similar elevations: UNIL/NB123, 2170 m and UNIL/NB124, 2220-2240 m.

4.2 Analytical procedures

4.2.1 Sample preparation

The two bedrock samples were prepared at the University of Lausanne under subdued red light conditions. Sample dimensions were greater than 10 cm x 10 cm x 10 cm and at least 1 cm of material was removed from the outer edges of the rocks using a diamond saw to isolate the light safe component of the samples. The light safe section was hand crushed using a pestle and mortar and care was taken not to grind the samples, to avoid potential resetting of luminescence signals via triboluminescence (e.g. Bateman et al., 2012). Crushed samples were sieved to isolate the 180-212 μm grain size, which was then treated with H_2O_2 and HCl to remove any organic material and potential surface carbonates respectively. Density separations were done using sodium polytungstate to isolate two feldspar fractions with densities of 2.58-2.62 g cm^{-3} and $<2.58 \text{ g cm}^{-3}$. The feldspar fractions were not etched (Duller, 1992).

4.2.2 Environmental dose rate (\dot{D}) determination

The light exposed portion of the samples was sent to ActLabs (Canada) for inductively coupled plasma mass spectrometry analysis to determine U, Th and K concentrations for \dot{D} determination. The \dot{D} must be adjusted for grain size attenuation effects, however as these bedrock samples have been crushed to facilitate the extraction of different mineral fractions, the original grain size was estimated from thin section images using software developed by Buscombe et al. (2013; Supplementary Figure S.5). A grain size of $700 \pm 200 \mu\text{m}$ was used for sample UNIL/NB123 and $2,500 \pm 500 \mu\text{m}$ for sample UNIL/NB124. Perfect grain sphericity has been assumed in the calculation of the \dot{D} and a water content of $2 \pm 2\%$ has been estimated for both samples. Theory predicts that while the dependence of luminescence age on dose rate is linear (Eq. A.4 in Guralnik et al., 2013, with $K = 0$), dose rate exerts only a logarithmic control on luminescence palaeo-temperatures (Eq. A.10b in Guralnik et al., 2013). For cooling histories, corresponding to intermediate scenarios between the “age” and “palaeotemperature” end-members (Guralnik et al., 2013), the effect of dose rate can thus vary between logarithmic and linear, depending on the specific cooling history. For fast cooling, the effect should be closer to linear, thus placing more weight on proper dosimetry than in OSL-palaeothermometry (Guralnik et al., 2015b and references therein). To support this notion, we show that a change in \dot{D} of $\sim 3 \text{ Gy ka}^{-1}$ results in a shift in cooling rate of $\sim 300 \text{ }^\circ\text{C/Myr}$ (Supplementary

Figure S.6). Since dose rate depends on grainsize, it is therefore important that grain sizes are appropriately constrained through thin-section analysis.

The \dot{D} values calculated for both samples were cross checked against DRAC v.1.1 (Durcan et al., 2015). The radionuclide conversion factors of Liritzis et al. (2013) were used together with the beta attenuation factors of Brennan (2003) and the alpha attenuation factors of Bell (1980). Internal K contents were measured using wavelength dispersive spectrometry on a JEOL 8200 superprobe within the Institute of Earth Sciences at the University of Lausanne, and range from 9-10% for the 2.58-2.62 g cm⁻³ fraction, hereafter referred to as Na-rich K-feldspar and 14-15% for the <2.58 g cm⁻³ fraction, hereafter referred to as the K-rich feldspar fraction (Table 2). An a-value of 0.15 ±0.05 was used after Balescu and Lamothe (1994), although as noted above, because the measured grain sizes ranged from 500 to 3000 μm, this value is also an approximation. Because these samples have been shielded from cosmic rays for the majority of their signal accumulation period, no cosmic dose rate component has been incorporated. The data used to calculate \dot{D} are summarised in Table 2.

		U (ppm)	Th (ppm)	K (%)	Internal K (%)	Water (%)	\dot{D} (Gy ka ⁻¹)
UNIL/NB123	K-feldspar	1.10 ± 0.03	21.90 ± 0.79	2.56 ± 0.04	14.99 ± 0.19	2 ± 2	7.00 ± 0.92
	Na-rich K-feldspar				10.74 ± 0.18		6.10 ± 0.69
UNIL/NB124	K-feldspar	0.80 ± 0.02	5.40 ± 0.19	3.50 ± 0.02	14.32 ± 0.52	2 ± 2	9.87 ± 0.75
	Na-rich K-feldspar				9.46 ± 0.22		7.27 ± 0.47

Table 2: Dosimetry data.

4.2.3 OSL Measurements

Luminescence measurements were done using two Risø TL-DA-20 readers at the University of Lausanne, with dose rates of ~0.1 Gy s⁻¹. The feldspar extracts were analysed using a MET protocol after Li and Li (2011a) which comprised a preheat at 250 °C for 60 s, followed by infra-red stimulation (IRSL) at 50, 100, 150 and 225 °C for 100 s. A high-temperature optical wash at 290 °C was incorporated at the end of each measurement cycle after Buylaert et al. (2009). Luminescence was detected through a BG39 and a BG3 filter and typical luminescence decay curves are shown in Supplementary Figure S.1A. These bedrock feldspar samples have bright luminescence signals and small (2 mm Ø) aliquots were measured using a neutral density filter which reduced the signals by one order of magnitude, dependent on instrument. Signals were integrated over the first 4 s of stimulation, and background signals were integrated over the final 20 s of stimulation. In order to fully characterise the complete sample dose response curve, beta doses were given from 28 to 4,500 Gy in a SAR protocol. The test dose was either 46 or 59 Gy for all measurements, dependent on instrument. Samples were corrected for sensitivity changes relative to a signal measured at the equivalent temperature, i.e. the IRSL₂₂₅ signal was corrected by a test dose signal measured at 225 °C.

Because measured dose response curves, and resultant D_e and D_0 values were similar between aliquots (typical uncertainties 2-6%, Table 1), only three aliquots were measured for each sample. All aliquots fulfilled the sample acceptance criteria of recuperation <5% of the natural signal, recycling ratio within 10% of unity and maximum test dose uncertainty <10%.

The efficacy of the selected protocol was confirmed through a dose-recovery experiment on three aliquots of the K-feldspar extract of sample UNIL/NB124 which were bleached for 4 hours in a SOL2 solar simulator. A dose approximately equal to the D_e of the IRSL₅₀ signal (145 Gy) was administered, and a residual signal measured following the same bleaching conditions was subtracted. All signals recovered dose within 10% of unity with the exception of the IRSL₅₀ signal which had a dose recovery ratio of 0.76 ± 0.01 (Supplementary Figure S.1B). The cause of this dose underestimation for the IRSL₅₀ signal is unclear but may be related to changing charge trapping efficiency (Kars et al., 2014), and is in agreement with the observations of other workers using post-IR IRSL measurement protocols (e.g. Buylaert et al., 2012). Dose response curves were fitted using equation [5] and fits for all samples are shown in Supplementary Figures S.2 and S.3.

4.2.4 Fading measurements & confirmation of thermal signal

After measurement of the natural trapped charge population, fading was measured for each of the aliquots using a SAR MET protocol. Regenerative doses of either 46 or 59 Gy dependent on instrument, equal to the test dose, were used in the fading experiments which were detected using the BG39 and BG3 filters only to ensure good counting statistics. A prompt measurement was repeated after the longest delayed measurement to confirm that sensitivity changes had been appropriately corrected for by the test dose. Fading measurements were made over up to four decades of time and were fitted using equation [6], with t calculated as 250 s (i.e. half the irradiation time), plus the measurement delay time. Individual sample ρ' values are summarised in Table 1. The fading data for both samples are shown in Supplementary Figures S.2 and S.3.

The Kars et al. (2008) approach was used to screen whether the samples were in field steady state, or whether they exhibited disequilibrium (i.e. contained a thermal signal), through comparison of (n/N) values with those predicted for field saturation $((n/N)_{SS}$, see section 2.5 for details).

4.2.5 Measurement of thermal kinetics

Isothermal holding experiments were used to enable calculation of E_t , E_u and s values for one representative aliquot of each of the samples. A dose of either 46 or 59 Gy dependent on instrument was administered and aliquots were held at temperatures ranging from 170 °C to 300 °C for times of 0 to 10,240 s. Luminescence measurements were made using a SAR MET protocol and were fitted

using equation [4], where t^* was estimated from half the irradiation time of 500 s, plus the isothermal holding time. Parameters E_t , E_u and s were fitted simultaneously across all temperatures. The measured isothermal holding data for samples UNIL/NB123 and UNIL/NB124 are shown in the Supplementary Figures S.2 and S.3, and best-fitting parameters are summarised in Table 1.

4.3 Results

4.3.1 Luminescence dose response measurements

The dose response of three aliquots measured for each sample were reproducible with typical relative standard deviations of <6 % (Table 1). Saturation ratios (n/N) and “unfaded” D_0 values (Kars et al., 2008) were directly obtained through fitting of Eq. [5] to the SAR data. This is a significant procedural improvement over Guralnik et al. (2015b), where derivation of (n/N) included an additional (and convoluted) step, avoided here thanks to the φ multiplier. The IRSL₅₀ signals have the smallest (n/N) values, and the IRSL₂₂₅ signals the greatest (n/N) values for all samples. This increase in (n/N) values does not reflect reducing D_0 values for most signals, although D_0 values for the IRSL₂₂₅ signals are always smaller than D_0 measured for the IRSL₁₅₀ signals (Table 1).

4.3.2 Athermal detrapping measurements

The fading measurements used to quantify the rate of athermal detrapping using equation [2] show that the measured ρ' values reduce for all samples with increasing measurement temperature (Table 1). If rather than ρ' values, g_{2days} values are derived following the approach of Auclair et al (2003), then fading rates for the IRSL₅₀ signals are ~6 %/decade, and for the IRSL₂₂₅ signals are ~1.5 %/decade (Table 1); these values are within the range commonly reported for sedimentary samples. The fading model of Kars et al. (2008) was used to calculate the sample (n/N) and signal specific steady-state (n/N)_{SS} ratios in order to screen the samples for the presence of a thermal signal (Fig. 4, after Guralnik et al., 2015b). The calculated (n/N)_{SS} ratios are similar to those reported for granitic rocks in field saturation, for equivalent rates of fading (Huntley and Lian, 2006, their Figure 5). All of the MET signals for both feldspar extracts of samples UNIL/NB123 and UNIL/NB124 are in disequilibrium and exhibit significant thermal signals.

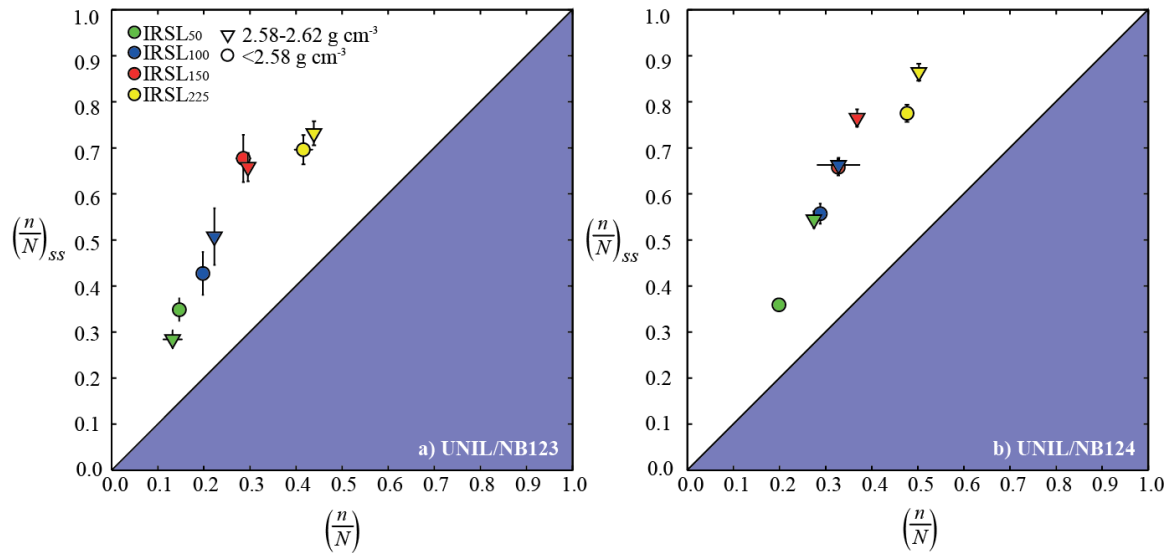


Figure 4: Contrast of (n/N) values for the K-feldspar (<2.58 g cm⁻³) and Na-rich K-feldspar (2.58-2.62 g cm⁻³) extracts of samples (a) UNIL/NB123 and (b) UNIL/NB124 with $(n/N)_{SS}$ calculated using the method described in section 2.5. All samples and signals are in disequilibrium and therefore contain thermal information.

4.3.3 Thermal detrapping measurements

The isothermal holding data for the IRSL₅₀ and IRSL₁₀₀ signals exhibit a misfit with the modelled values for the 300 and 350 °C holding temperatures; this may be explained by enhanced thermal transfer at temperatures greater than the preheat temperature. However, excluding the 300 and 350 °C data does not significantly change the determined E_t , E_u and s values for the IRSL₅₀ and IRSL₁₀₀ signals, but does result in poor constraint of the IRSL₁₅₀ and IRSL₂₂₅ signals, consequently we have chosen to use all data from the different isothermal holding temperatures for model fitting.

The thermal kinetic parameters E_t , E_u and s derived from fitting the isothermal decay curves can be regarded as “unfaded” (cf. Kars et al., 2008), i.e. properly corrected for fading effects (through the φ multiplier). Here too, the present treatment surpasses that of Guralnik et al. (2015b), who assumed no influence of athermal loss upon the high-temperature isothermal data (and thus potentially slightly underestimated the true thermal stability of their IRSL₅₀ system). The best-fitting thermal loss parameters are summarised in Table 1, and show increasing thermal stability for higher temperature stimulations (Figure 5), which is in agreement with the observations of Li and Li (2011b). This may be explained by changes in potential recombination pathways (cf. Jain et al., 2015), or the accessing of different trap populations at higher stimulation temperatures (Li and Li, 2011b).

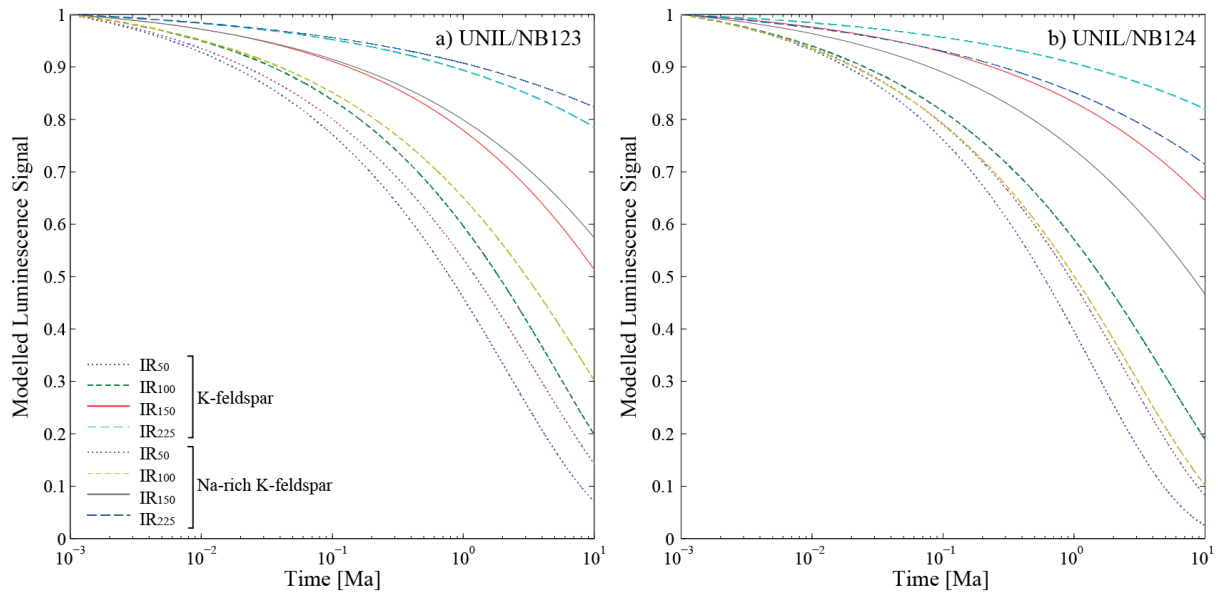


Figure 5: Simulated isothermal decay at 20 °C for 10 Ma using equation [6] and the E_t , E_u and s values reported in Table 1. Infra-red stimulated luminescence signals measured at higher temperatures are more thermally stable.

4.3.4 Extracting a cooling history

To invert the measurements into cooling histories, we used the same Monte Carlo approach described in section 3.2. We randomly prescribed a range of different time-temperature histories, which assumed monotonic cooling from a temperature of 150 °C to 5 ± 5 °C, over a time period of 0.5 Ma. The model was iterated 20,000 times and the randomly generated time-temperature paths were used to calculate synthetic $(n/N)_{mod}$ values, to be tested against the measured (n/N) .

Initially only the IRSL₅₀ signal of the K-feldspar extract of UNIL/NB123 was used for cooling-history constraint (Figure 6a), before using all four IRSL signals for the K-feldspar extract of that sample (Figure 6b) and additionally all four of the Na-rich K-feldspar extract IRSL signals (Figure 6c). Finally all eight IRSL signals for sample UNIL/NB124 (Figure 6d) were inverted.

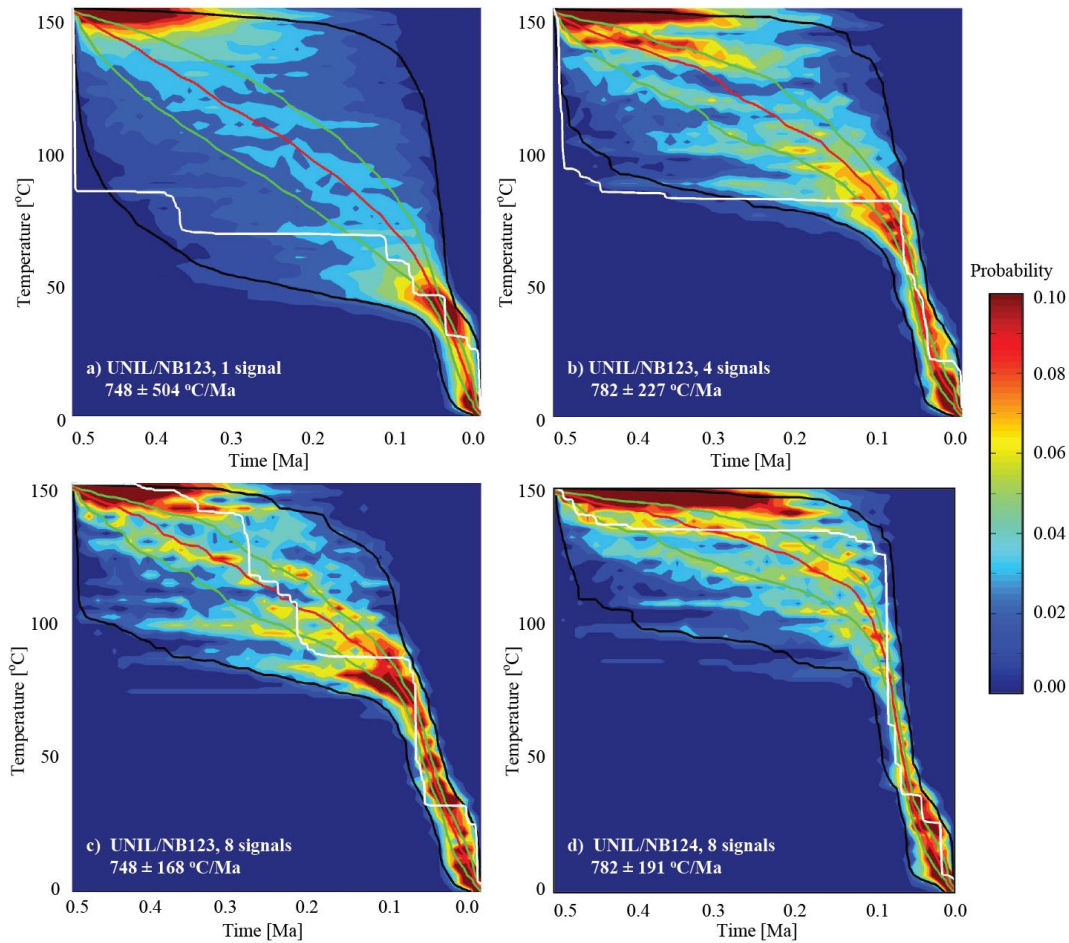


Figure 6: Time-temperature histories for sample UNIL/NB123 constrained (a) with only the $IRSL_{50}$ signal of K-feldspar and (b) with the $IRSL_{50}$, $IRSL_{100}$, $IRSL_{150}$ and $IRSL_{225}$ signals of K-feldspar. (c) UNIL/NB123 and (d) UNIL/NB124 constrained with the $IRSL_{50}$, $IRSL_{100}$, $IRSL_{150}$ and $IRSL_{225}$ signals of both K- and Na-rich K-feldspar extracts. The 60% quantile is shown in green, the 90% quantile is shown in black, the median model is shown in red and the fit with the highest likelihood is shown in white.

5. Discussion

The challenges of athermal signal detrapping and signal saturation have previously been highlighted as major limitations for the application of feldspar OSL-thermochronometry (e.g. Guralnik et al., 2015b). However, testing of all four IRSL signals from both the K-rich and Na-rich K-feldspar feldspar extracts of samples UNIL/NB123 and UNIL/NB124 using the model of Huntley (2006), as modified by Kars et al. (2008), reveals that all of the signals from these two Namche Barwa samples have thermal signals (Figure 4).

Sample specific kinetic parameters E_t , E_u and s were measured for each of the different signals for the different samples, and exhibit increasing stability with increasing measurement temperature (Figure 5, Table 1). The E_u values reported here are similar to those published (Li and Li, 2013; Poolton et al., 2009), although the E_t and s values are notably smaller (cf. Guralnik et al., 2015b;

Murray et al., 2009). To date, only a few studies have reported the kinetic parameters of feldspar MET IRSL signals and so it is not yet possible to comment on the variability of these values between feldspars of different chemical compositions, structures and/or geological provenances. Further research is required to understand the complexity of the feldspar luminescence system and particularly an explanation for the greater misfit of measured high temperature isothermal data to modelled values.

The different thermal and athermal stabilities of the MET SAR luminescence signals, coupled with the possibility of measuring both the K- and Na-feldspar extracts of a single sample, offers the potential for improved constraint of recent cooling histories relative to using a single thermochronometric system. Although the IRSL₅₀ signal failed the dose-recovery test, which forms a fundamental acceptance criterion in luminescence dating approaches, we have explored its potential contribution as a low temperature thermochronometer in this proof of concept multi-thermochronometry study. This is because for different samples, or through using a different measurement protocol (e.g. Guralnik et al., 2015b) it may be possible to measure a robust IRSL₅₀ signal which can be incorporated into a multi-thermochronometry approach. Initially only the IRSL₅₀ signal of the K-feldspar extract of sample UNIL/NB123 was inverted to infer the rock-cooling history (Figure 6a); using this signal only, provides little constraint on cooling histories at temperatures ≥ 40 °C, but better constraint below this temperature (i.e. below the T_c). In contrast, incorporating the higher temperature IRSL signals measured in the MET protocol provides much better constraint of cooling histories for temperatures up to ~ 70 °C (Figures 6b-d), which is a consequence of the higher thermal stability of the higher temperature IRSL signals. These data demonstrate that multi-OSL-thermochronometry is able to provide constraint for low-temperature (and therefore recent) cooling histories. Excluding the IRSL₅₀ signals of the K-feldspar and Na-rich K-feldspar extracts from the multi-signal inversions was also tested and exhibited almost no influence on the resultant inversions (Supplementary Figures S.4A and B).

The advantages offered by OSL-thermochronometry are illustrated when the T_c for other thermochronometric systems utilised in Namche Barwa are considered. In this region, AFT has T_c of between 110 and 140 ± 20 °C, and the closure temperature of ZFT is estimated to be ~ 300 °C (after Rahn et al., 2004, Seward and Burg, 2008). These thermochronometers are therefore unable to resolve changes in cooling histories at lower temperatures (i.e. at $T < T_c$), which have occurred in the more recent past. Although other thermochronometric systems such as apatite (U-Th)/He (AHe), and $^4\text{He}/^3\text{He}$ have the potential to resolve low-temperature cooling histories, very young AHe ages are difficult to measure because of the lack of He (e.g. Herman et al., 2007). Furthermore $^4\text{He}/^3\text{He}$ is

presently challenging for such rapid cooling because the low abundance of radiogenic ^4He may be below current detection limits.

The cooling histories of samples UNIL/NB123 and UNIL/NB124 are similar, with both samples indicating cooling rates of $\sim 750\text{ }^\circ\text{C Ma}^{-1}$ over the past $\sim 0.1\text{ Ma}$. The cooling rate of $\sim 750\text{ }^\circ\text{C Ma}^{-1}$ is greater than, but broadly consistent with the $\sim 500\text{ }^\circ\text{C}$ rates reported by Seward and Burg (2008). Rather than indicating that OSL-thermochronometry samples overestimate cooling rates, these differences may reflect the averaging of OSL-thermochronometry signals over different time periods to other thermochronometric systems, which is a consequence of their lower closure temperatures. Furthermore OSL-thermochronometry records near-surface histories where compression of the geotherm can result in rapid apparent cooling histories (c.f. Braun et al., 2006).

6. Conclusion

Multi-OSL-thermochronometry offers the potential for tight-constraint of cooling histories over recent (0.1-0.2 Ma) timescales, providing high-resolution of cooling histories beyond the range of other thermochronometric systems such as apatite (U-Th)/He. In this study, a series of synthetic cooling histories have been used to explore the potential of multi-OSL-thermochronometry, revealing a sensitivity to temperatures $< 75\text{ }^\circ\text{C}$ and that cooling histories can be constrained over the past 0.1-0.2 Ma. A case study of two samples from the eastern Himalaya syntax showed that different MET IRSL signals from K- and Na-rich K-feldspar extracts of the same sample provide multi-thermochronometric control, resulting in a high-resolution cooling history which is consistent with existing thermochronometric data for this region. Comparison of the cooling history of sample UNIL/NB123 with a second, nearby sample, UNIL/NB124, reveals OSL-thermochronometric data to be both robust and reproducible. Multi-OSL-thermochronometry will potentially contribute to key geomorphological debates, such as the interplay between tectonics and climate over Quaternary timescales, as well as provide insights into recent hydrothermal histories.

Acknowledgements

Sally Lowick is thanked for access to the Bern luminescence laboratory for sample chemical treatment whilst the UNIL lab was being constructed. We are also grateful to Yang Rong and Lena Märki who assisted with sample preparation, and to Olivier Reubi for assistance with EPMA measurements. This research was funded by Swiss National Fund (SNF) grant numbers PP00P2-38956 and 200021-127127 awarded to FH and PZ00P2-148191/1 awarded to PGV. BG acknowledges support from SNF grant 200021-127127, and NWO VENI grant 863.15.026. Jean-Pierre Burg (ETH Zurich) is thanked for providing samples UNIL/NB123 and UNIL/NB124. We are also grateful to David

Huntley for useful discussions on an earlier version of this manuscript, as well as to Bo Li and another, anonymous reviewer.

References

- Auclair, M., Lamothe, M., Huot, S., 2003. Measurement of anomalous fading for feldspar IRSL using SAR. *Radiation Measurements* 37, 487-492.
- Balescu, S., Lamothe, M., 1994. Comparison of TL and IRSL age estimates of feldspar coarse grains from waterlain sediments. *Quaternary Science Reviews* 13, 437-444.
- Bateman, M., Swift, D.A., Piotrowski, J.A., Sanderson, D.C.W., 2012. Investigating the effects of glacial shearing of sediment on luminescence. *Quaternary Geochronology* 10, 230-236.
- Bell, W.T., 1980. Alpha dose attenuation in quartz grains for thermoluminescence dating. *Ancient TL* 12, 4 - 8.
- Braun, J., Van Der Beek, P., Batt, G., 2006. *Quantitative thermochronology: numerical methods for the interpretation of thermochronological data*. Cambridge University Press.
- Braun, J., van Der Beek, P., Valla, P.G., Robert, X., Herman, F., 2012. Quantifying rates of landscape evolution and tectonic processes by thermochronology and numerical modelling of crustal heat transport using PECUBE. *Tectonophysics* 20, 1-28.
- Brennan, B.J., 2003. Beta doses to spherical grains. *Radiation Measurements* 37, 299-303.
- Burg, J.-P., Davy, P., Nievergelt, P., Oberli, F., Seward, D., Diao, Z., Meier, M., 1997. Exhumation during crustal folding in the Namche-Barwa syntaxis. *Terra Nova* 9, 53-56.
- Burg, J.-P., Nievergelt, P., Oberli, F., Seward, D., Davy, P., Maurin, J.-C., Diao, Z., Meier, M., 1998. The Namche Barwa syntaxis: evidence for exhumation related to compressional crustal folding. *Journal of Asian Earth Sciences* 16, 239-252.
- Buscombe, D., 2013. Transferable wavelet method for grain-size distribution from images of sediment surfaces and thin sections, and other natural granular patterns. *Sedimentology* 60(7), 1709-1732.
- Buylaert, J.-P., Jain, M., Murray, A.S., Thomsen, K.J., Thiel, C., Sohbaty, R., 2012. A robust feldspar luminescence dating method for Middle and Late Pleistocene sediments. *Boreas* 41, 435-451.
- Buylaert, J.P., Murray, A.S., Thomsen, K.J., Jain, M., 2009. Testing the potential of an elevated temperature IRSL signal from K-feldspar. *Radiation Measurements* 44, 560-565.
- Christodoulides, C., Ettinger, K.V., Fremlin, J.H., 1971. The use of TL glow peaks at equilibrium in the examination of the thermal and radiation history of materials. *Modern Geology* 2, 275-280.
- De Sarkar, S., Mathew, G., Pande, K., Chauhan, N., Singhvi, A., 2013. Rapid denudation of Higher Himalaya during late Pliocene, evidence from OSL thermochronology. *Geochronometria* 40, 304-310.
- Dodson, M., 1973. Closure temperature in cooling geochronological and petrological systems. *Contrib Mineral Petrol* 40, 259-274.

- Duller, G.A.T., 1992. Luminescence chronology of raised marine terraces, south-west North Island, New Zealand. University of Wales, Aberystwyth.
- Durcan, J.A., King, G.E., Duller, G.A.T., 2015. DRAC: Dose Rate and Age Calculator for trapped charge dating. *Quaternary Geochronology* 28, 54-61.
- Gallagher, K., 1995. Evolving temperature histories from apatite fission track data. *Earth and Planetary Science Letters* 136, 421-435.
- Gallagher, K., 2012. Transdimensional inverse thermal history modeling for quantitative thermochronology. *Journal of Geophysical research* 117, 2156-2202.
- Gorynski, K.E., Walker, J.D., Stockli, D.F., Sabin, A., 2014. Apatite (U–Th)/He thermochronometry as an innovative geothermal exploration tool: A case study from the southern Wassuk Range, Nevada. *Journal of Volcanology and Geothermal Research* 270, 99-114.
- Grün, R., Tani, A., Gurbanov, A., Koshchug, D., Williams, I., Braun, J., 1999. A new method for the estimation of cooling and denudation rates using paramagnetic centers in quartz: a case study on the Eldzhurtinskiy Granite, Caucasus. *Journal of Geophysical Research: Solid Earth (1978–2012)* 104, 17531-17549.
- Guralnik, B., Ankjaergaard, C., Jain, M., Murray, A.S., Muller, A., Walle, M., Lowick, S.E., Preusser, F., Rhodes, E.J., Wu, T.S., Mathew, G., Herman, F., 2015a. OSL-thermochronometry using bedrock quartz: A note of caution. *Quaternary Geochronology* 25, 37-48.
- Guralnik, B., Jain, M., Herman, F., Ankjærgaard, C., Murray, A.S., Valla, P.G., Preusser, F., King, G.E., Chen, R., Lowick, S.E., Kook, M., Rhodes, E.J., 2015b. OSL-thermochronology of feldspar from the KTB Borehole, Germany. *Earth and Planetary Science Letters* 423, 232-243.
- Guralnik, B., Li, B., Jain, M., Chen, R., Paris, R.B., Murray, A., Li, S.H., Pagonis, V., Valla, P.G., Herman, F., 2015c. Radiation-induced growth and isothermal decay of infrared-stimulated luminescence from feldspar. *Radiation Measurements* 81, 224-231.
- Guralnik, B., Jain, M., Herman, F., Paris, R.B., Harrison, T.M., Murray, A.S., Valla, P.G., Rhodes, E.J., 2013. Effective closure temperature in leaky and/or saturating thermochronometers. *Earth and Planetary Science Letters* 384, 209-218.
- Herman, F., Braun, J., Senden, T.J., Dunlap, W.J., 2007. (U–Th)/He thermochronometry: Mapping 3D geometry using micro-X-ray tomography and solving the associated production–diffusion equation. *Chemical Geology* 242, 126-136.
- Herman, F., Rhodes, E.J., Braun, J., Heiniger, L., 2010. Uniform erosion rates and relief amplitude during glacial cycles in the Southern Alps of New Zealand, as revealed from OSL-thermochronology. *Earth and Planetary Science Letters* 297, 183-189.
- Herman, F., Seward, D., Valla, P.G., Carter, A., Kohn, B., Willett, S.D., Ehlers, T.A., 2013. Worldwide acceleration of mountain erosion under a cooling climate. *Nature* 504, 423-426.
- Huntley, D.J., 2006. An explanation of the power-law decay of luminescence. *Journal of Physics: Condensed Matter* 18, 1359.
- Huntley, D.J., Lamothe, M., 2001. Ubiquity of anomalous fading in K-feldspars and the measurement and correction for it in optical dating. *Canadian Journal of Earth Sciences* 38, 1093-1106.

- Huntley, D.J., Lian, O.B., 2006. Some observations on tunnelling of trapped electrons in feldspars and their implications for optical dating. *Quaternary Science Reviews* 25, 2503-2512.
- Jain, M., Sohbati, R., Guralnik, B., Murray, A.S., Kook, M., Lapp, T., Prasad, A.K., Thomsen, K.J., Buylaert, J.P., 2015. Kinetics of infrared stimulated luminescence from feldspars. *Radiation Measurements*.
- Kars, R. H., Wallinga, J., Cohen, K. M., 2008. A new approach towards anomalous fading correction for feldspar IRSL dating - tests on samples in field saturation. *Radiation Measurements* 43(2-6), 786-790.
- Kars, R. H., Wallinga, J., 2009. IRSL dating of K-feldspars: Modelling natural dose response curves to deal with anomalous fading and trap competition. *Radiation Measurements* 44(5-6), 594-599.
- Kars, R. H., Reimann, T., Wallinga, J., 2014. Are feldspar SAR protocols appropriate for post-IR IRSL dating? *Quaternary Geochronology* 22, 126-136.
- Li, B., Li, S.-H., 2008. Investigations of the dose-dependent anomalous fading rate of feldspar from sediments. *Journal of Physics D: Applied Physics* 41(22), 225502.
- Li, B., Li, S.-H., 2011a. Luminescence dating of K-feldspar from sediments: A protocol without anomalous fading correction. *Quaternary Geochronology* 6, 468-479.
- Li, B., Li, S.-H., 2011b. Thermal stability of infrared stimulated luminescence of sedimentary K-feldspar. *Radiation Measurements* 46, 29-36.
- Li, B., Li, S.-H., 2012. Determining the cooling age using luminescence-thermochronology. *Tectonophysics* 580, 242-248.
- Li, B., Li, S.-H., 2013. The effect of band-tail states on the thermal stability of the infrared stimulated luminescence from K-feldspar. *Journal of Luminescence* 136, 5-10.
- Liritzis, I., Stamoulis, K., Papachristodoulou, C., Ioannides, K., 2013. A re-evaluation of radiation dose-rate conversion factors. *Mediterranean Archaeology & Archaeometry* 13, 1-15.
- McDougall, Ian, and T. Mark Harrison. 1999. *Geochronology and Thermochronology by the $^{40}\text{Ar}/^{39}\text{Ar}$ Method*. Oxford University Press.
- McInnes, B.I.A., Evans, N.J., Fu, F.Q., Garwin, S., 2005. Application of Thermochronology to Hydrothermal Ore Deposits. *Reviews in Mineralogy and Geochemistry* 58, 467-498.
- Molnar, P., 2004. Late Cenozoic increase in accumulation rates of terrestrial sediment: How Might Climate Change Have Affected Erosion Rates? *Annual Review of Earth and Planetary Sciences* 32, 67-89.
- Murray, A.S., Buylaert, J.P., Thomsen, K.J., Jain, M., 2009. The effect of preheating on the IRSL signal from feldspar. *Radiation Measurements* 44, 554-559.
- Poolton, N.R.J., Kars, R.H., Wallinga, J., Bos, A.J.J., 2009. Direct evidence for the participation of band-tails and excited-state tunnelling in the luminescence of irradiated feldspars. *Journal of Physics: Condensed Matter* 21, 485505.
- Press, W.H., 2007. *Numerical recipes 3rd edition: The art of scientific computing*. Cambridge University Press.

- Prokein, J., Wagner, G.A., 1994. Analysis of thermoluminescent glow peaks in quartz derived from the KTB-drill hole. *Radiation Measurements* 23, 85-94.
- Qin, J., Chen, J., Valla, P.G., Herman, F., Li, K., 2015. Estimating rock cooling rates by using multiple luminescence thermochronometers. *Radiation Measurements* 79, 13-18.
- Rahn, M.K., Brandon, M.T., Batt, G.E., Garver, J.I., 2004. A zero-damage model for fission-track annealing in zircon. *American Mineralogist* 89 (4), 473–484.
- Reiners, P.W., Brandon, M.T., 2006. Using thermochronology to understand orogenic erosion. *Annual Review of Earth and Planetary Sciences* 34 (1), 419-466.
- Seward, D., Burg, J.-P., 2008. Growth of the Namche Barwa Syntaxis and associated evolution of the Tsangpo Gorge: Constraints from structural and thermochronological data. *Tectonophysics* 451, 282-289.
- Shuster, D.L., Farley, K.A., 2005. *⁴He/³He Thermochronometry: Theory, Practice, and Potential Complications*. *Reviews in Mineralogy and Geochemistry* 58, 181-203.
- Tarantola, A., 2005. *Inverse Problem Theory and Model Parameter Estimation*. SIAM.
- Thomsen, K., Murray, A., Jain, M., 2011. Stability of IRSL signals from sedimentary K-feldspar samples. *Geochronometria* 38, 1-13.
- Thomsen, K.J., Murray, A.S., Jain, M., Bøtter-Jensen, L., 2008. Laboratory fading rates of various luminescence signals from feldspar-rich sediment extracts. *Radiation Measurements* 43, 1474-1486.
- Willenbring, J.K., von Blanckenburg, F., 2010. Long-term stability of global erosion rates and weathering during late-Cenozoic cooling. *Nature* 465, 211-214.
- Zeitler, P.K., Meltzer, A.S., Brown, L., Kidd, W.S.F., Lim, C., Enkelmann, E., 2014. Tectonics and topographic evolution of Namche Barwa and the easternmost Lhasa block, Tibet. *Geological Society of America Special Papers* 507.
- Zhang, P., Molnar, P., Downs, W.R., 2001. Increased sedimentation rates and grain sizes 2–4 Myr ago due to the influence of climate change on erosion rates. *Nature* 410, 891-897.

Thermoluminescence analysis for particle temperature sensing and thermochronometry: Principles and fundamental challenges

E.G. Yukiwara^{a,b}, A.C. Coleman^a, R.H. Biswas^c, R. Lambert^c, F. Herman^c, G.E. King^d

^a Physics Department, Oklahoma State University, Stillwater, OK 74078, USA

^b Department of Radiation Safety and Security, Paul Scherrer Institute, 5232 Villigen PSI, Switzerland

^c Institute of Earth Surface Dynamics, University of Lausanne, Geopolis, 1015 Lausanne, Switzerland

^d Institute of Geological Sciences, University of Bern, Baltzerstrasse 1+3, 3012, Bern, Switzerland

The complete manuscript is in press in Radiation Measurements and published online:

<https://doi.org/10.1016/j.radmeas.2018.05.007>

Highlights

- Fundamentals of temperature sensing using TL are presented.
- Parallels between the applications in thermochronometry and in particle temperature sensing are made.
- Fundamental and practical challenges for the advancement of the technique are discussed.
- Possible solutions to these challenges and future research directions are proposed.

Abstract

Thermoluminescence (TL) has traditionally been used to estimate the depth of trapping centers in luminescence materials and explain the isothermal decay in the case of synthetic dosimeters and natural materials used in luminescence dating. Nevertheless, new fields of application of TL and optically stimulated luminescence (OSL) materials, namely particle temperature sensing and thermochronometry, motivate a need for accurate models for the luminescence processes and estimation of the trapping parameters, in particular activation energy and frequency factor. Although calibration of the TL materials may be possible and recommended in some applications, using for example, microheaters, laser heating or pyroprobes, the procedures can be complicated and time consuming. With TL, however, appropriate models with parameters obtained in laboratory conditions can in principle be used to predict the temperature and time dependence of the stimulation processes in the microsecond to the second timescales (in the case of particle

temperature sensing), and in the tens of thousands years (in the case of thermochronometry). In this paper we present the fundamentals of temperature sensing using TL, tracing parallels between the applications in thermochronometry and in particle temperature sensing, and review the main challenges, both fundamental and practical, for the advancement of the technique. Fundamental challenges are the very wide timescales involved in these applications, the need for better TL models, and the inherent time-temperature ambiguity in the Arrhenius equation, in addition to other practical problems. Possible solutions to these challenges and future research directions are discussed.